Universidad de La Laguna

Departamento de Ingeniería Química y Tecnología Farmacéutica

DESARROLLO DE FOTOBIORREACTORES DE MEMBRANA SUMERGIDA PARA EL TRATAMIENTO DE AGUAS RESIDUALES

Directora: Luisa Mª Vera Peña

Codirector: Enrique González Cabrera

Memoria para optar al grado de

Doctor en Química e Ingeniería Química

Autora: Elisabet Segredo Morales

Mayo 2023

Tesis Doctoral:

Desarrollo de fotobiorreactores de membrana sumergida para el tratamiento de aguas residuales

Elisabet Segredo Morales

Departamento de Ingeniería Química
y Tecnología Farmacéutica

Universidad de La Laguna
2023

Universidad
de La Laguna

Departamento de Ingeniería Química y Tecnología Farmacéutica
Universidad de La Laguna

Luisa Mª Vera Peña y Enrique González Cabrera, profesores Titular de Universidad y Contratado Doctor, respectivamente, del área de Ingeniería Química del Departamento de Ingeniería Química y Tecnología Farmacéutica de la Universidad de La Laguna

Autorizan:

La presentación y defensa de la Memoria titulada "**Desarrollo de fotobiorreactores de membrana sumergida para el tratamiento de aguas residuales**", realizada en el marco del Programa de Doctorado de Química e Ingeniería Química, dado que reúne los requisitos de cantidad y calidad necesarios para constituir la Tesis Doctoral que presenta Dña. Elisabet Segredo Morales para optar al título de Doctora por la Universidad de La Laguna. Para que conste y surta los efectos oportunos, firman el presente certificado en San Cristóbal de La Laguna, a 26 de mayo de 2023.

Dra. Luisa Mª Vera Peña   Dr. Enrique González Cabrera

Directora   Codirector

"Todas las verdades son fáciles de entender una vez que son descubiertas; la cuestión es descubrirlas"

-Galileo Galilei

Agradecimientos

Quisiera agradecer a todo el Departamento de Ingeniería Química y Tecnología Farmacéutica por formar parte de mi aprendizaje a lo largo de todos estos años, especialmente a mis directores, la Dra. Luisa Vera y el Dr. Enrique González por su dedicación durante el desarrollo de esta tesis doctoral.

A la Entidad Pública Balsas de Tenerife (BALTEN) y al Consejo Insular de Aguas de Tenerife por el agua residual que ha sido utilizada como influente en los ensayos de esta tesis doctoral.

A Cristina González por su estupendo trabajo en la identificación de microorganismos de las suspensiones biológicas.

Al Servicio General de Apoyo a la Investigación (SEGAI) de la Universidad de La Laguna, en especial a los Servicios de Análisis Térmico, Análisis Elemental, Espectroscopía Infrarroja y al Laboratorio de Caracterización de Partículas y Microsuperficies en los cuales se han llevado a cabo gran parte de los ensayos que se presentan en los capítulos de esta tesis. En especial a Olmedo, Sergio, Yayi y Judith por su disponibilidad siempre.

Al Laboratorio de Aguas del Departamento de Ingeniería Química y Tecnología Farmacéutica, en especial a Rai por su eterna predisposición a ayudar en lo que sea, gracias por las conversaciones y la música que amenizaba las largas mañanas de analíticas.

A Andrés Figueira por sus discusiones filosóficas, su ayuda en las analíticas, su predisposición y su buen humor, a pesar de todo, la vida no es tan "desastre".

A Margarita de la Rosa, por su apoyo, por su ayuda, por su acogida y por su cariño siempre.

A mis "jefas" de T. F. May y Araceli, por enseñarme tanto en lo personal y en lo profesional, entre otras cosas la importancia de la honestidad y la honradez en muchos aspectos, pero sobre todo en lo que a investigación se refiere.

A Idaira por algo tan simple y a la vez tan complicado como estar para lo que te necesitase.

A Oliver y a Laura nuevamente por formar parte de esto también, por entenderme y cuidarme año tras año. Gracias por alegrarme la vida siempre.

A mis padres y a mi hermano por darme la educación que tengo, enseñarme el valor de esforzarse y trabajar por las cosas que uno quiere y por alegrarse de cada logro.

A Enrique, nada de lo que aquí escriba será suficiente ni resumirá todo lo que te mereces. Gracias por la paciencia, por el apoyo, por la constancia, por el esfuerzo, por tus ideas, por el cariño, por no dejar que me rinda, por la objetividad y la exigencia, por estar dispuesto siempre a escuchar, por los ánimos, por las mañanas y tardes tirados en el suelo del laboratorio montando instalaciones y, por tanto, tanto, tanto…pero, sobre todo, mil gracias por estar aquí.

A ti, que estás, aunque solo te sienta yo, gracias por darme fuerzas y permitirme terminar esta etapa de tanto esfuerzo y dedicación. Me hará ilusión contarte que estuviste presente y formaste parte de esto. Espero estar a la altura.

A todo aquel que se haya sentido parte de esta tesis y que no he mencionado, gracias.

Índice:

Tesis Doctoral:

Desarrollo de fotobiorreactores de membrana sumergida para el tratamiento de aguas residuales

Elisabet Segredo Morales

Departamento de Ingeniería Química
y Tecnología Farmacéutica

Universidad de La Laguna
2023

Universidad
de La Laguna

CAPÍTULO 1

Introducción

1. Introducción

Las emisiones de gases de efecto invernadero, principalmente el dióxido de carbono (CO_2), se han incrementado notablemente desde el inicio de la revolución industrial, teniendo una mayor incidencia desde mediados del siglo pasado. Como es ampliamente conocido, la acumulación de estos gases en la atmósfera tiene efectos nocivos sobre el medioambiente, induciendo el llamado "cambio climático". Dado el impacto global de las emisiones de estos gases, desde 2015 se ha iniciado una estrategia conjunta para reducir las mismas a nivel mundial, teniendo como punto de partida, la firma del Acuerdo de París. En consonancia con este compromiso, los países de la Unión Europea presentaron sus planes climáticos actualizados a finales de 2020, comprometiéndose a una reducción de emisiones como mínimo en un 55% para el año 2030, en relación a los valores registrados en 1990, como etapa intermedia para alcanzar la neutralidad de emisiones en 2050. Estas actuaciones se están implementando de manera integrada junto con otras iniciativas, como los planes de acción para la economía circular y de contaminación cero, dentro de la estrategia de crecimiento sostenible denominada Pacto Verde Europeo [1].

El agua, como recurso fundamental, ha sido objeto de especial protección por parte de las políticas de la Unión Europea. La normativa vigente protege los recursos hídricos, los ecosistemas de agua dulce y salada, y asegura la adecuada calidad del agua potable y de baño. En el contexto del Pacto Verde Europeo, la Directiva Marco del Agua proporciona el marco principal y los objetivos para la política del agua en Europa. En el caso particular del tratamiento de aguas residuales, la Directiva 91/271 actualmente en vigor, supuso un hito en el desarrollo de los sistemas de recolección y tratamiento. No obstante, todavía existen contaminantes que deben abordarse y que serán objeto de la inminente actualización de dicha Directiva, junto con los mencionados aspectos de reducción de emisiones de gases de efecto invernadero, eficiencia energética y mejora de la gestión de recursos. En relación a la regeneración de aguas residuales, para fomentar su uso seguro en el sector agrícola, que es el principal demandante, y reducir el consumo de agua dulce, se ha aprobado el Reglamento (UE 2020/741) que entrará en vigor este año, 2023.

En este contexto, el sector del agua necesita un cambio de paradigma para dejar de centrarse en el tratamiento y suministro de agua, la recogida y el tratamiento

de aguas residuales para alcanzar los límites de vertido, y el procesamiento de los residuos de estas operaciones, y pasar a enfocarse en una gestión integrada que permita una economía circular de aguas con un mínimo de emisiones [2]. Este cambio de visión lleva a que las tradicionales "estaciones de tratamiento de aguas residuales" se consideren ahora, como "centros de recuperación de recursos y regeneración de agua". Desde un punto de vista tecnológico, los nuevos desarrollos deben centrarse en la intensificación de procesos, la recuperación de recursos y el diseño de sistemas que permitan elevadas calidades de los efluentes con un mínimo de emisiones o incluso, alcanzando la neutralidad de emisiones de carbono. Como ejemplos de esas nuevas tecnologías cabría citar los procesos avanzados de digestión anaerobia desarrollados en biorreactores de membrana, la eliminación biológica de nutrientes por medio de biomasa granular (proceso conocido comercialmente como *Nereda*®), la eliminación de amonio mediante la nitrificación parcial seguida un proceso *anammox* o los sistemas fotobiológicos, basados en microalgas y cianobacterias.

Las microalgas han sido ampliamente estudiadas para la captura de CO_2 en sistemas orientados a la producción de materias primas para biocombustibles y bioproductos. Estos microorganismos fototróficos son capaces de convertir energía lumínica y moléculas inorgánicas sencillas en moléculas más complejas como carbohidratos. Las microalgas son un grupo de microorganismos uni- o pluricelulares simples de células eucariotas y procariotas [3] que poseen cualidades como su rápida capacidad de reproducción [4], estando su crecimiento controlado por las condiciones lumínicas [5]. Las microalgas pueden eliminar nitrógeno, fósforo y materia orgánica del agua residual y transformarla en biomasa [6]. En este sentido, la utilización conjunta de bacterias y microalgas para el tratamiento de aguas residuales ha acaparado recientemente la atención de numerosos investigadores [7]. Los tratamientos de aguas residuales basados en las microalgas han emergido en los últimos años como un potencial sustituto de los tratamientos convencionales, debido a su sostenibilidad económica [8] y medioambiental [6].

En concreto, la utilización de fotobiorreactores de membrana, MPBR por sus siglas en inglés, ha experimentado un auge en la investigación desarrollada desde el año 2000, llegando a publicarse un total de 157 artículos científicos en esta temática hasta abril del año 2023, como se aprecia en la Figura 1. Mayoritariamente, la

función que desempeña el MPBR en dichas publicaciones es la retención de biomasa y el tratamiento de agua residual, siendo minoritarios, en este período (2000-2023), los artículos dedicados a la utilización de MPBR para la carbonatación. Además, el uso de efluentes secundarios como influente de los MPBR ha suscitado mayor interés que el uso de otro tipo de efluentes en todos los años, salvo en lo que va de año 2023, en el que se aprecia una mayor aplicación para otro tipo de efluentes.
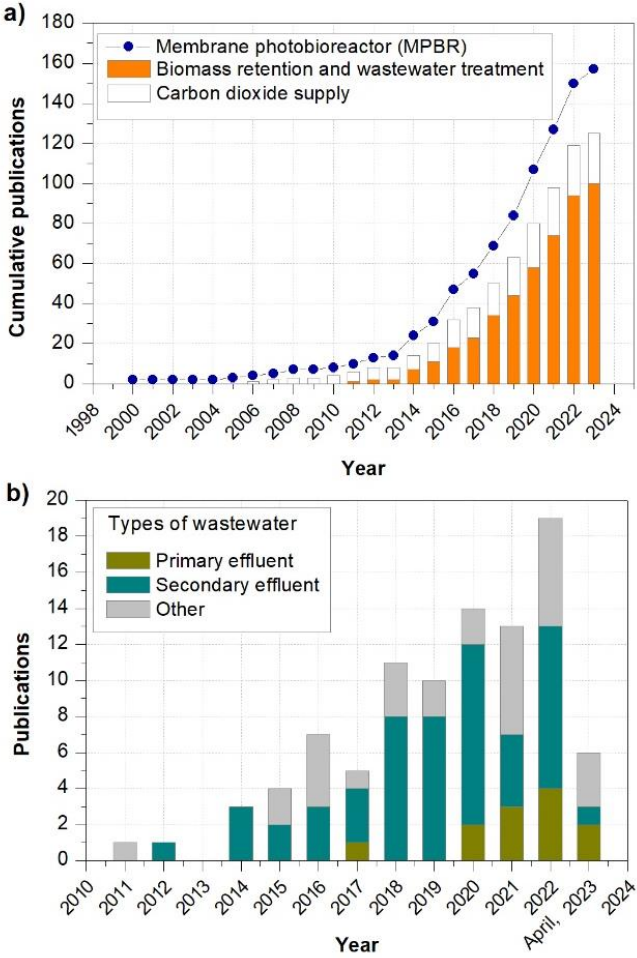
Figura 1. Publicaciones anuales recopiladas en Scopus a) acumulado de publicaciones dedicadas a la operación de un MPBR y según su función y b) publicaciones anuales, según el tipo de agua residual utilizada como alimentación.

2. Consorcios microalgas-bacterias aplicados al tratamiento de aguas residuales

Las bacterias y las microalgas forman una simbiosis compleja que es posible utilizar en el proceso de depuración de aguas residuales [9]. Por un lado, los microorganismos bacterianos pueden descomponer la materia orgánica de las aguas residuales en dióxido de carbono y agua, y el dióxido de carbono generado por descomposición se convierte en una de las fuentes de carbono para las microalgas y favorece su fotosíntesis; además, los metabolitos de bacterias, hongos y otros microorganismos pueden transferirse al citoplasma de las microalgas [10]. Las microalgas, por otro lado, pueden aumentar la eficiencia metabólica de las bacterias u otros microorganismos al producir oxígeno a través de la fotosíntesis. Debe existir un equilibrio entre la producción de O_2 y el consumo de CO_2 o bien entre la degradación de carbono orgánico disuelto y la asimilación de nutrientes [9].

Los beneficios de la aplicación de consorcios microalgas-bacterias en el tratamiento de aguas residuales son ampliamente conocidos y han sido estudiados en los últimos años por numerosos autores [11]. El agua residual utilizada como medio de cultivo presenta muchas ventajas; la principal es el contenido en nutrientes, que es aprovechado por las microalgas y las bacterias para su crecimiento [12]. El nitrógeno y el fósforo presentes en las aguas residuales son utilizados como nutrientes esenciales para el crecimiento de las microalgas que lo asimilan en su estructura, eliminándolo del agua residual. Además, algunas microalgas son capaces de degradar materia orgánica y diferentes contaminantes presentes en diferentes tipos de aguas residuales tanto domésticas, como industriales [13] y agrícolas [14]. El crecimiento de microalgas y bacterias se ve favorecido por la presencia de las otras en la suspensión, ya que entre ellas se produce un intercambio de metabolitos, hecho que favorece la asimilación de nutrientes [15].

El cultivo de microalgas sea para su posterior utilización como materia prima en la obtención de biodiesel o principios activos, o bien para el tratamiento de aguas residuales, presenta una importante desventaja: los elevados costes de separación debido a su pequeño tamaño (3-30 μm) y su baja densidad, cercana a

la densidad del agua [16]. Esta dificultad repercute en gran medida en el coste total del proceso, contribuyendo a un 20-30% del global [17].

Existen diferentes métodos para el cosechado de microalgas: físicos, químicos y biológicos. Sin embargo, los métodos biológicos, como la biofloculación, han demostrado ser efectivos a un menor coste [12]. Por tanto, el establecimiento de consorcios microalgas-bacterias para el tratamiento de aguas residuales, posee otra ventaja, la biofloculación de la suspensión biológica, lo que mejora la separación de los microorganismos, contribuyendo a la disminución de los costes de operación. En este sentido, algunos autores han encontrado reducciones de entre el 58% y el 76% del consumo energético y de la huella de carbono, respectivamente [18]. No obstante, se requiere un adecuado control para obtener una eficaz biofloculación. Entre los factores que influyen en el proceso cabe destacar la intensidad de la luz aplicada [19], el tiempo de retención de sólidos (SRT), debido a que condiciona el contenido en polímeros extracelulares (EPS) [20], el tiempo de residencia hidráulico (HRT), que influye en la carga de nutrientes al sistema y, por tanto, en el crecimiento de microorganismos [21], y la relación C/N, que tiene un papel fundamental en el contenido en carbohidratos y proteínas de los EPS [15,22]. Todo ello sin perjuicio de una eficiencia aceptable de eliminación de nutrientes, por lo que se hace necesario profundizar en la naturaleza de las interacciones que tienen lugar entre las algas y las bacterias para una mejor operación de este tipo de procesos [15].

3. Fotobiorreactores

El diseño del fotobiorreactor debe tener en cuenta múltiples factores. Algunos autores señalan como críticos una adecuada iluminación, una agitación eficiente y un adecuado aporte de nutrientes [23].

El crecimiento de microorganismos fototróficos, como son las microalgas, está íntimamente ligado por el nivel de intensidad lumínica [24]. Sin embargo, existen condiciones en las cuales, si la exposición a la luz es demasiado intensa, resultan dañadas partes de la célula de manera irremediable [3]. Esto puede ocurrir en condiciones de crecimiento en exteriores, en los que la luminosidad natural debida al sol resulte excesiva [5]. Muchos autores han realizado estudios con el fin de establecer modelos empíricos de crecimiento a partir de datos de irradiación locales [25]. En este marco es importante destacar que existen y se distinguen, condiciones de limitación de luz, de saturación y de inhibición [5]. En

un fotobiorreactor, la luz incidente es absorbida por las células situadas en las paredes iluminadas, quedando reducida la cantidad de la misma que es capaz de penetrar a las zonas más internas del fotobiorreactor [23]. Este hecho conlleva que puedan llegar a crearse dos zonas en el fotobiorreactor, con velocidades de crecimiento diferentes [5]. También, en este sentido, se han desarrollado modelos con el fin de predecir la intensidad lumínica que llega a la suspensión biológica en función de la concentración de microorganismos presentes [26] y, en consecuencia, ajustar la luz incidente para tener en cuenta la radiación que se requiere en el interior del reactor [27]. Otra forma de paliar este efecto es utilizar un adecuado sistema de agitación que promueva el establecimiento de ciclos de luz/oscuridad de la misma duración para todos los microorganismos presentes en el fotobiorreactor e incrementar así, su productividad [28].

Además de mejorar el acceso de todos los microorganismos de la suspensión biológica a la luz, la agitación asegura la correcta distribución de los nutrientes [29] y mantiene la biomasa en suspensión [5]. Los sistemas de agitación pueden ser mecánicos (tanque agitado, con agitador de paletas en los reactores tipo *raceways*), o no mecánicos (tipo *air-lift*, donde el fotobiorreactor incorpora una columna de burbujeo, tipo *flat panel* con burbujeo inferior o un fotobiorreactor tubular en el que la circulación del propio fluido actúe como agitador). Sin embargo, se requiere un control de la agitación ya que, si ésta es excesiva, las células pueden sufrir daños [28] e inhibir su actividad metabólica [5].

Entre los otros factores que se han de tener en cuenta para el diseño del fotobiorreactor, se encuentran el pH, la temperatura, la asimilación de CO_2 y el contenido en oxígeno, todos ellos ligados entre sí. Por ejemplo, la asimilación de CO_2 por parte de las microalgas provoca cambios en el pH con el consiguiente efecto que esta variación de pH tiene en el equilibrio $CO_2/HCO_3^-/CO_3^{2-}$ [30]. La temperatura, además de influir en el crecimiento de los microorganismos [31], influye en la cantidad de oxígeno disuelto. A su vez, estos factores son controlados por el diseño del reactor, en tanto que sobre ellos influyen factores como el HRT, el SRT, el régimen y la cantidad de irradiación que recibe el fotobiorreactor, el tipo de influente utilizado y el tipo y el grado de agitación que recibe la suspensión biológica.

Los esfuerzos realizados por la comunidad científica para encontrar las condiciones óptimas de operación, según la función que desempeñe el

fotobiorreactor, han dado como resultado una gran variedad de tipos de fotobiorreactores, que pueden ser clasificados en dos grandes grupos: fotobiorreactores abiertos y cerrados. Los sistemas abiertos tienen como ventaja su bajo coste de operación y producción [24]; sin embargo, están expuestos a la variabilidad de las condiciones ambientales, lo cual dificulta el control de los parámetros clave de operación, además de poder sufrir contaminación [5]. El tipo más común de estos sistemas es el fotobiorreactor tipo *raceway,* en el que las algas se mantienen en suspensión gracias a un agitador de paletas [24]. Los sistemas cerrados son los protagonistas de las últimas investigaciones, y engloban a sistemas que no tienen intercambio gaseoso directo con la atmósfera [5]. Se han diseñado muchos tipos de fotobiorreactores cerrados, clasificados en tres grandes grupos: columnas, tubulares y planos. Dentro de los primeros, podemos encontrar columna de burbujas y tipo *air-lift*. Entre los segundos: fotobiorreactores verticales tubulares, horizontales tubulares y helicoidales. Dentro de los fotobiorreactores planos, el más común es el tipo panel plano. Además, en los últimos años han surgido los fotobiorreactores híbridos que combinan dos tipos convencionales de fotobiorreactores cerrados [24]. La Figura 2 resume los tipos de fotobiorreactores más comunes encontrados en la bibliografía.
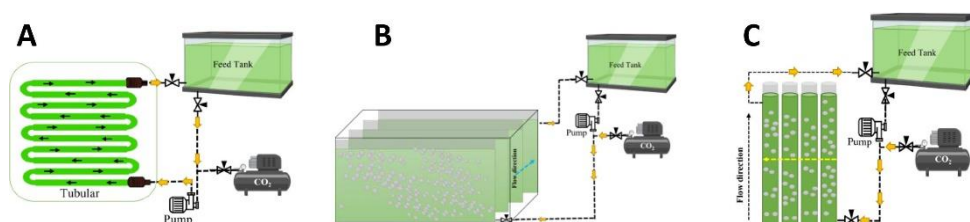
Figura 2. Tipos de fotobiorreactores cerrados. Adaptado de Sirohi et al., 2022 [32].

Los campos de aplicación de los fotobiorreactores son muy diversos. Las microalgas son consideradas como materias primas para la producción de biocombustibles de tercera generación y productos químicos extraídos naturalmente [5]. La obtención de materias primas para las industrias cosmética y farmacéutica, como alimento para animales y humanos en la industria alimentaria, son algunas de las actuales aplicaciones de este tipo de tecnología [33,34]. Además, las microalgas han demostrado su potencial en la eliminación de

nutrientes y otros contaminantes de las aguas residuales, convirtiéndolas en biomasa con un alto valor que puede ser aprovechada en múltiples sectores [35].

4. Fotobiorreactores de membrana para el tratamiento de aguas residuales

Entre los métodos para el cultivo de microalgas, los MPBRs suponen importantes ventajas debido a su versatilidad y la facilidad para escalar la tecnología [36]. Un MPBR es un sistema que opera de manera continua y que combina un fotobiorreactor con un sistema integrado o separado que utiliza una membrana de micro o ultrafiltración para la separación de la biomasa generada [21]. En los últimos años, se han diseñado nuevos fotobiorreactores de membrana que utilizan membranas de ósmosis directa y de intercambio iónico [37].

Estos MPBR surgen como solución a la baja capacidad de sedimentación de la biomasa y su consiguiente pérdida, así como, a las limitaciones que presentan los fotobiorreactores convencionales [21]. Se diseñan para maximizar el acceso a la luz natural o artificial y ofrecer las condiciones necesarias para el crecimiento de las algas [38]. Algunos autores consideran a este tipo de fotobiorreactores como fotobiorreactores híbridos [25,32], ya que combinan un fotobiorreactor con un sistema de panel plano o una columna tipo *air-lift* dentro de los cuales se puede introducir una membrana de microfiltración o ultrafiltración [39].

La membrana permite controlar de manera independiente el HRT y el SRT, manteniendo altas concentraciones de biomasa sin que esta se vea afectada por la carga hidráulica, ni por la velocidad de crecimiento celular [12]. Desvincular el HRT del SRT consigue concentraciones de biomasa, hasta 3,5 veces superiores a las obtenidas en los fotobiorreactores [21]. De esta manera, se alcanzan altas eficiencias de eliminación de nutrientes y elevadas tasas de producción de biomasa, superiores a las obtenidas en un fotobiorreactor convencional [40]. Los MPBRs han demostrado obtener mejores eficiencias de eliminación de nitrógeno y fósforo (N, P) que un sistema convencional de lodos activos [37]. En este tipo de sistemas, se ha obtenido una concentración 9 veces superior de biomasa y una reducción del 77% de la huella de carbono respecto a un fotobiorreactor convencional [39].

En MPBRs, las membranas pueden estar fabricadas en diferentes materiales: poliméricos o cerámicos, aunque las más utilizadas se fabrican con fluoruro de polivinilideno (PVDF) o cloruro de polivinilo (PVC) dado que sus consumos energéticos son bajos [37]. Se fabrican bajo diferentes geometrías: planas, tubulares, multi-tubulares, de fibra hueca, capilares o de arrollamiento en espiral [39]. Según el tamaño de poro, pueden ser de microfiltración (MF, 5 µm-50 nm), ultrafiltración (UF, 2-50 nm), nanofiltración (NF, < 1 nm) y ósmosis inversa (RO, son consideradas membranas no porosas). Las membranas de MF son las recomendadas para una operación prolongada en el tiempo a unos bajos costes de mantenimiento [39].

Varios autores han estudiado la utilidad de este tipo de sistemas para ser aplicados como tratamiento terciario de aguas residuales, en concreto, han ensayado combinaciones de un biorreactor de membrana (MBR) convencional seguido de un MPBR, logrando una total oxidación de la materia orgánica y una completa eliminación de nutrientes [41,42]. Alcanzar estos niveles de eliminación en una planta de tratamiento de aguas residuales que opera con un MBR, hubiera requerido la implementación de un sistema de tratamiento terciario que incluyera, por un lado, un sistema de nitrificación/desnitrificación y por otro, un sistema de coagulación-floculación para la eliminación del fósforo, dando como resultado un proceso global mucho más costoso [39].

Por otra parte, se ha utilizado una amplia variedad de especies de microalgas en el tratamiento de aguas residuales, siendo la especie más utilizada, *Chlorella* sp. La mayoría de los estudios se han llevado a cabo utilizando agua sintética o agua residual municipal como agua de alimentación, pero sólo un par de especies como *Chlorella* sp. y *Scenedesmus* sp. han resultado adecuadas para el tratamiento de agua residual industrial [43].

La eficiencia de los sistemas MPBRs depende de las características del agua residual, principalmente su contenido en nutrientes (relación C/N, N/P) [44], pero también de las condiciones de operación, HRT, SRT, iluminación, aireación, temperatura, pH. Además, desde el punto de vista de la operación, el mayor reto es el ensuciamiento que sufre la membrana debido a sustancias excretadas por las algas [39]. En los próximos apartados se discutirán los principales factores que afectan a la operatividad de este tipo de sistemas, así como las estrategias de mitigación del ensuciamiento de la membrana que pueden ser implementadas.

4.1. Características del agua residual

Los estudios con MPBRs han utilizado principalmente tres tipos de aguas residuales como alimentación: efluente primario, que únicamente ha sido sometida a un proceso de decantación primaria; efluente secundario, que se obtiene tras un proceso de tratamiento mediante lodos activos; y digestato, obtenido de la digestión anaerobia del lodo [44]. Estos tres tipos de aguas residuales presentan diferentes concentraciones de nutrientes.

La mayoría de los estudios encontrados utilizan aguas residuales sintéticas o aguas residuales reales que son sometidas a procesos de esterilización con el fin de desarrollar un único cultivo de microalgas previamente inoculado [45–47]. La complejidad de la matriz de un agua residual real, unida a la variabilidad de concentración de la misma, consecuencia de vertidos o de la climatología local, hace que su utilización como agua de alimentación sea limitada y reducida a unos pocos estudios publicados [48,49]. Debido a las características del agua residual real, sembrar un inóculo parece inadecuado, debido a la tendencia de los microorganismos indígenas de la propia agua residual a desarrollarse y colonizar el sistema. Por otro lado, un cultivo donde la alimentación esté controlada impide valorar posibles interferencias o factores inhibidores para el crecimiento de microalgas. La variabilidad propia del agua residual real puede aportar conocimiento sobre los factores que puedan afectar al equilibrio en el consorcio microalgas-bacterias y con ello, información valiosa para el escalado de esta tecnología.

Entre los pocos trabajos que utilizan agua residual real, la alimentación que se utiliza mayoritariamente es el efluente de un tratamiento secundario, debido a su bajo contenido en materia orgánica en comparación con un efluente primario, lo que inhibe el crecimiento de bacterias heterótrofas, manteniendo alta la ratio microalgas/bacterias [50]. Las aguas residuales sintéticas poseen menor cantidad de nutrientes traza y, por tanto, logran menor productividad de biomasa [51].

El contenido en nitrógeno y fósforo es vital para la producción de biomasa y la relación N/P es crucial, en tanto que el nitrógeno no será eliminado si no existe una cantidad determinada de P [9]. Muchos autores coinciden en que bajos niveles de estos dos nutrientes en las aguas residuales, limitan el crecimiento de biomasa [50]. En un MPBR la membrana logra que, aunque el efluente no contenga cantidades suficientes de nutrientes, como puede ser el caso de efluentes secundarios, la concentración de la suspensión que se consigue

desacoplando el HRT del SRT, sea suficiente para un adecuado crecimiento de las microalgas [50].

Por el contrario, elevadas cantidades de estos nutrientes producen un efecto negativo; una inhibición en el crecimiento de microalgas. Por ejemplo, se han encontrado en las aguas residuales, valores perjudiciales de amonio para algunas especies de microalgas [52]. Por esto, la mayoría de autores coinciden en que un efluente primario no es adecuado para el cultivo de microalgas, si bien otros estudios indican que se obtienen elevadas productividades de biomasa con efluentes con altas concentraciones de nutrientes y un diseño adecuado del reactor [53–55] e incluso, hay autores que señalan a los consorcios microalgas-bacterias que se establecen en fotobiorreactores como un remedio para el tratamiento de aguas residuales ricas en contaminantes tóxicos [11].

En cuanto al contenido en carbono, la mayoría de los estudios incorpora la inyección de CO_2 o de algún tipo de carbono inorgánico, como fuente adicional de carbono que contribuya a una mejor asimilación del N y del P. Aún en aguas en las que la cantidad de carbono es suficiente, se inyecta CO_2 con el fin de controlar el valor del pH [9]. Por otro lado, altas concentraciones de carbono orgánico disuelto (DOC) pueden generar un daño foto-oxidativo en las células de las microalgas y disminuir su eficiencia [56]. Además, los valores de la relación entre carbono y nitrógeno pueden marcar la composición de la biomasa formada, de esta manera, una relación alta de C/N hace que los microorganismos predominantes sean las bacterias heterótrofas, provocando un déficit de oxígeno e impidiendo el acceso a la luz de las microalgas. Para una eliminación de nitrógeno más efectiva, es necesario que exista una sinergia entre las microalgas y las bacterias, que se produce cuando las cantidades de amonio y de carbono son limitados [15].

4.2. Intensidad lumínica y fotoperiodo

Ambos parámetros, la intensidad de la luz y el fotoperiodo con que se aplica son de vital importancia para el crecimiento de microorganismos fototróficos como las microalgas [5,21,43,50]. Como se ha comentado a lo largo de este capítulo, una intensidad lumínica muy elevada puede provocar fenómenos de fotoinhibición, por lo que es un parámetro clave a controlar dado que, generalmente, optimizando la intensidad de la luz, se incrementa la asimilación de CO_2, la productividad de la biomasa [57,58], y con ello, la eliminación de nutrientes del agua residual [21]. Por ello, el fotobiorreactor debe ser diseñado para optimizar el acceso a la luz por parte de las microalgas, impidiendo que se produzcan

fenómenos de fotoinhibición y de atenuación [30]. Generalmente, esto se consigue con una alta relación superficie/volumen del fotobiorreactor [5,21].

De la energía solar, sólo una parte es absorbida por las microalgas, en concreto aquella radiación cuya longitud de onda esté entre los 400 y 700 nm [59], es la llamada radiación fotosintéticamente activa (PAR) [23]. La mayoría de los estudios realizados a escala laboratorio utilizan luz artificial por su estabilidad frente a la luz natural, a pesar del ahorro energético que esta segunda ofrece [60]. Las fuentes de luz artificial preferidas por los autores son sistemas LEDs, y lámparas fluorescentes [60].

La longitud de onda de la luz utilizada también es un factor clave a tener en cuenta, ya que existen especies de microalgas que presentan un mayor crecimiento cuando sobre ellas incide luz cuya longitud de onda se sitúa entre los 600-700 nm, lo que se considera luz roja, y otras, que lo hacen bajo longitudes de onda entre los 400-500 nm, luz azul [5]. Existen otras especies que se desarrollan mejor ante lo que se llama luz verde, 510 nm. Sin embargo, está ampliamente aceptado por la literatura que la mayor productividad se obtiene cuando se aplica luz de las regiones roja y azul [21].

El fotoperiodo, es decir la duración de los periodos de luz/oscuridad que se aplican a las microalgas, también es un parámetro que afecta al crecimiento de la biomasa [15,30,60]. Se han llevado a cabo estudios con el fin de determinar cuál es el fotoperiodo óptimo en fotobiorreactores y algunos autores han encontrado que, aumentando el periodo de iluminación a 24 h, se obtienen altos valores de crecimiento de la biomasa, sin embargo, se reduce la eliminación de nutrientes, como consecuencia, probablemente, de la atenuación de la luz por la alta concentración celular del fotobiorreactor [61]. Otros autores apuntan a la necesidad de un periodo de oscuridad para que tenga lugar una correcta división celular y mejorar la generación de nuevos microorganismos [62], para que éstos acumulen energía que será utilizada posteriormente, para realizar la fotosíntesis [63]. Además del beneficio para las microalgas, la aplicación de un ciclo de luz/oscuridad que contenga ciertas horas sin iluminación, reduce el consumo energético del proceso [21].

4.3. Tiempo de retención hidráulico y tiempo de retención de sólidos

En las lagunas de algas con alta carga, conocidas en inglés como *High-Rate Algal Ponds* (HRAPs), el tiempo de residencia hidráulico típicamente aplicado es de 2-6 días, y resulta insuficiente para que las bacterias nitrificantes se desarrollen, lo que provoca una baja tasa de nitrificación [64]. Generalmente, en este tipo de configuraciones se requieren HRTs superiores a los 8 días [65]. En MPBRs, el HRT utilizado varía entre las 6 horas y los 8 días [60], y por tanto, son generalmente más bajos que los aplicados en los PBRs y en los HRAPs [21]. Los HRTs bajos promueven el crecimiento celular al incrementar la carga de nutrientes que entra al reactor [20], mientras que valores más altos de HRT consiguen mejores eliminaciones de nutrientes, pero pueden conllevar una limitación de sustrato [51].

Se han llevado a cabo numerosos estudios centrados en la evaluación de la influencia de la variación del HRT en la productividad de biomasa, que concluyen que el valor óptimo de HRT varía considerablemente con la especie de microalgas y está altamente relacionado con la velocidad de crecimiento específica, definida como la productividad normalizada con la concentración inicial de células [21]. También se ha estudiado el efecto que tiene el HRT en la eficacia de eliminación de nutrientes, mostrando que se prefieren HRT largos para lograr una adecuada eliminación de contaminantes [66]. En este sentido autores como Honda et al., 2017, han encontrado que un incremento desde 8 a 24 horas en el HRT de un MPBR alimentado con agua sintética, consigue aumentar la eliminación de nitrógeno y fósforo un 3% y un 14%, respectivamente [67]. Aunque la mayoría de autores coinciden en que el aumento del HRT conlleva una pérdida de productividad de biomasa, al disminuir la carga de nutrientes que entra al sistema [60].

Un incremento en el HRT supone una mayor necesidad de espacio, por lo que varios estudios se han enfocado en la búsqueda de alternativas al aumento del HRT como vía para conseguir eficacias de eliminación de nutrientes adecuadas. Una opción que se ha evaluado ha sido aumentar el tiempo de retención celular, o tiempo de retención de sólidos (SRT) para lograr una concentración alta de microorganismos en el reactor y, de esta manera, conseguir una eliminación de nutrientes más rápida y estable que compense la aplicación de un HRT bajo [21]. Sin embargo, hay que tener en cuenta que aumentar la concentración de biomasa en un fotobiorreactor puede llevar a una atenuación de la entrada de luz a la

suspensión biológica, limitando el acceso de luz a los microorganismos y provocando una disminución de la actividad fotosintética [68]. Es por esto que algunos autores señalan que el efecto del SRT en la eliminación de nutrientes es complejo, y no recomiendan la aplicación de SRT demasiado largos al operar los MPBRs, estableciendo el valor óptimo de este parámetro en el rango de los 15-25 días [60].

La posibilidad de separar el HRT del SRT que ofrecen los MPBRs ha permitido la realización de diferentes estudios variando ambos parámetros para establecer la influencia de uno sobre el otro y de ambos en el proceso. En la mayoría de los casos, estos estudios no se han llevado a cabo con HRTs superiores a los 2 días [68–72] ni SRT inferiores, en la mayoría de los casos, a los 30 días [68–70,72,73].

Respecto al SRT, se han encontrado resultados interesantes con valores superiores a los 30 días, como los obtenidos por Valigore *et al*. (2012) que permitieron mejorar la sedimentabilidad de la biomasa gracias a la formación natural de flóculos [20]. Estos autores señalan que la causa de esta mejoría puede ser la liberación sostenida de EPS que se obtiene al tener lugar un crecimiento lento de biomasa. Esta liberación favorece la aglomeración y permite la formación de flóculos [20]. Precisamente la presencia de EPS en la suspensión es un factor limitante cuando se implementa esta tecnología, debido al alto ensuciamiento que generan en las membranas de los MPBRs y que se tratará en apartados posteriores.

4.4. Aireación/agitación

La aireación mecánica supone más del 50% del coste total de energía de un tratamiento aerobio típico de aguas residuales [30]. Las microalgas producen O_2 que puede suplir las necesidades de este por las bacterias heterótrofas. Sin embargo, en un MPBR la aireación debe ser suficiente para mantener a los microorganismos dispersos en suspensión y su función principal es la de proporcionar CO_2 a las microalgas [21]. El carbono es el mayor constituyente de las microalgas, que estas obtienen del CO_2. Sin embargo, la concentración de CO_2 en la atmósfera es baja, por lo que, para incrementar la productividad de biomasa, algunos autores sugieren la inyección de CO_2 puro [74], o proveniente de gases de combustión [75]. A pesar de esto, el bajo coeficiente de transferencia hace que la mayor parte del CO_2 inyectado no se encuentre disuelto [76], y por tanto no sea accesible para las microalgas. Para solventar esto, se han utilizado MPBR en los

que la membrana actúa como contactor o como rociador. Estos reactores se han llamado fotobiorreactores de carbonatación (C-MPBR), y en aquellos en los que la membrana se utiliza como contactor, la membrana permite la recirculación del CO_2 no utilizado a presiones de gas más bajas. En cambio, en los reactores en que la membrana se utiliza como rociador, se utilizan membranas cuyo tamaño de poro es micrométrico, de tal manera que se generan burbujas de aire más pequeñas, aumentando sustancialmente, su superficie [60]. Es un tipo de MPBR en el que la función de la membrana es mejorar el contacto entre el CO_2 y lograr mayores tasas de disolución de este [76].

En un MPBR, la aireación puede tener otras funciones como, por ejemplo, eliminar el oxígeno disuelto sobrante, que resulta en ocasiones, perjudicial ya que interfiere en la eficiencia de la fotosíntesis [77]. Además, mantiene agitada la suspensión biológica, permitiendo que los microorganismos se encuentren dispersos en la suspensión y que el reparto de nutrientes sea el adecuado [78]. Por último, la aireación puede contribuir a la mitigación del ensuciamiento de la membrana [60], que será tratado en el apartado siguiente. Además, el aporte de CO_2 también está relacionado con la regulación del pH de la suspensión biológica [79].

Otro parámetro importante es la agitación, que permite mantener la homogeneidad del cultivo, mejorar la transferencia de gases [80] y prevenir la sedimentación de la biomasa [81]. Además, la agitación consigue que los nutrientes lleguen al conjunto de los microorganismos, además de establecer periodos de luz/oscuridad adecuados, al mejorar la distribución de luz en las células [5,80].

La agitación puede ser neumática o mecánica. La primera consiste en mover el fluido mediante la acción de burbujas de gas que se inyectan mediante rociadores o tubos perforados. La energía cinética que desprenden durante el ascenso a la superficie es comunicada al fluido [81]. Por su parte, la agitación mecánica consiste en la agitación mediante paletas o bombas.

4.5. Estrategias de mitigación del ensuciamiento de la membrana

El principal inconveniente en la implementación de los MPBR es el ensuciamiento que se deposita sobre la membrana, y que disminuye la productividad al disminuir el flujo de permeado y obligar a la realización de paradas para efectuar

operaciones de limpieza física, incrementando el coste del proceso [31,37]. Estudios preliminares de costes indican que el control del ensuciamiento supone más del 57% de los costes de operación y mantenimiento de esta tecnología [82]. El ensuciamiento se produce por acumulación sobre la superficie de la membrana y en los poros de esta, de microalgas, bacterias y sus productos metabólicos [39]. Existe poca información sobre las características del ensuciamiento en MPBRs [83], sin embargo, varios autores asumen los mismos mecanismos de ensuciamiento que los que ocurren en un biorreactor de membrana (MBR) convencional [31].

El ensuciamiento de la membrana puede ser debido a la formación de torta, la formación de una capa de gel, el bloqueo de poros y la adsorción y se debe a la deposición de células sobre la membrana además de materia orgánica, partículas coloidales inorgánicas, materia extracelular, materia extracelular de las algas y productos microbianos solubles [39]. A su vez, las sustancias causantes del ensuciamiento pueden clasificarse en aquellas que generan ensuciamiento interno, por penetración en los poros de la membrana, o bien aquellas que forman una torta, por deposición sobre la superficie de la membrana [76]. El mecanismo por el cual se genera el ensuciamiento ha sido descrito por numerosos autores [84–86] y resumido por Bilad *et al*. (2014) [76] de la siguiente manera:

- En la etapa inicial de la filtración, la materia coloidal y soluble, las bacterias y microalgas se retienen en la superficie de la membrana debido al flujo convectivo del permeado.
- Durante la etapa de filtración, la torta que se ha formado inicialmente crece y las células depositadas se multiplican, de manera que se forma una biopelícula más compleja [76].

La disposición temporal de este mecanismo hace que, si se lleva a cabo una filtración a flujo constante, el perfil de presión transmembrana (TMP) observado sea el que ha descrito Meng et al., 2017 [86] y que se muestra en la Figura 3.

La acumulación de material colmatante sobre la superficie de la membrana se suele llamar torta y está compuesta por numerosas sustancias o microorganismos. Esta capa forma una segunda capa filtrante que puede denominarse membrana dinámica [76].

La afinidad de los materiales colmatantes sobre la membrana afecta a su eliminación [39]. Según su vía de eliminación, el ensuciamiento puede ser reversible, si es eliminado mediante limpiezas físicas (establecimiento de periodos de relax o retrolavados), o irreversible cuando requiere la adición de químicos para su eliminación [76]. La torta depositada sobre la superficie de la membrana puede ser eliminada fácilmente mediante limpiezas físicas [36], mientras que el ensuciamiento que se deposita en los poros de la membrana es causado principalmente por sales, microalgas, restos celulares, y productos metabólicos excretados y se debe a interacciones hidrofóbicas con la membrana [39], por lo que requiere de limpiezas químicas con productos cáusticos, ácidos, surfactantes, etc. para su eliminación. Las limpiezas químicas con agentes oxidantes como el hipoclorito de sodio (NaClO) o ácidos inorgánicos como el ácido cítrico, son ampliamente utilizadas para la eliminación del ensuciamiento orgánico e inorgánico, respectivamente. Sin embargo, el efecto que la aplicación de estos agentes químicos tiene sobre la vida útil de la membrana no debe ser ignorado [37].
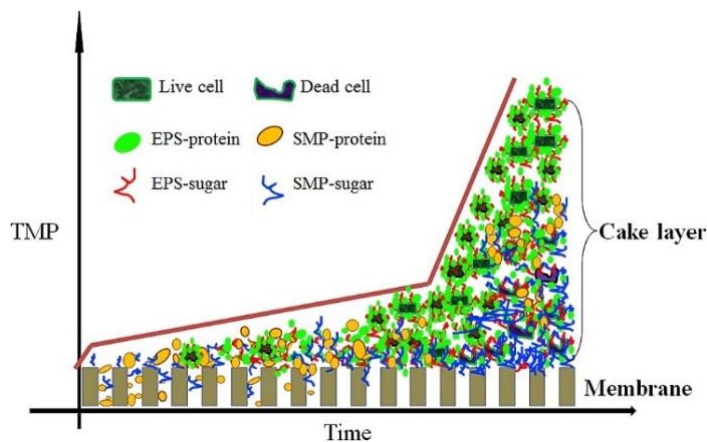
Figura 3. Evolución de la presión transmembrana (TMP) y distribución de los biopolímeros y microorganismos que componen el ensuciamiento que se deposita sobre la membrana. Fuente: Meng *et al.* (2017) [86].

El principal método para la mitigación del ensuciamiento de las membranas es el control de los parámetros de operación y en este sentido se han realizado esfuerzos por establecer las mejores estrategias de operación en MPBRs. Una de estas estrategias puede ser el aumento del esfuerzo cortante sobre la superficie de la membrana mediante la aplicación de un flujo turbulento en un módulo de

flujo cruzado, que se puede conseguir mediante inyección de burbujas de aire que generen el movimiento necesario en el fluido [87]. La aplicación de un burbujeo continuo puede inducir el esfuerzo cortante necesario para reducir significativamente la velocidad de ensuciamiento [39].

Las investigaciones recientes se han centrado en métodos de limpieza no convencionales basados en principios mecánicos. Estos incluyen sistemas que utilizan la rotación o la vibración de las membranas, lo que permite generar altos niveles de turbulencia en las proximidades de la membrana, mejorando el proceso de filtración y aumentando los caudales de permeado obtenidos respecto a los sistemas convencionales, principalmente debido al control de la capa de polarización y formación de torta [88–90]. Estos sistemas de filtración se basan en el movimiento de la propia membrana o de cualquier componente más cercano a su superficie, con el fin de generar esfuerzos cortantes independientes del flujo de alimentación (a diferencia de los sistemas de filtración tangencial). Por lo tanto, la energía suministrada a estos sistemas se concentra principalmente en la superficie de la membrana en lugar de en la circulación de la suspensión [91,92].

Otra estrategia evaluada es operar a flujos de permeado por debajo del denominado flujo crítico o umbral, que es aquel por debajo del cual el ensuciamiento de la membrana es prácticamente imperceptible, y por encima del cual la operación no resulta viable debido al alto ensuciamiento que sufre la membrana [93]. El conocimiento del valor de este flujo crítico en las condiciones de operación es clave para prevenir el depósito de material colmatante sobre la membrana y mantener una operación sostenible en el tiempo [94].

La utilización de materiales anti-ensuciamiento o baja propensión al ensuciamiento para la fabricación de membranas o bien, establecer modificaciones estructurales de las mismas pueden ser soluciones para mitigar el grado de ensuciamiento de la membrana en este tipo de procesos [39].

La modificación de parámetros de operación como el SRT y el HRT, ha sido ampliamente estudiada y aquellos autores que lo han explorado, han encontrado importantes hallazgos que parecen indicar que son parámetros influyentes en el ensuciamiento de la membrana. Así, por ejemplo, el SRT afecta a la estructura de la biomasa, con lo cual, tiene influencia sobre la materia orgánica que ésta genera y su biofloculación [73]. Por tanto, se requieren valores altos de SRT que permitan

el adecuado crecimiento de las microalgas [36], mejorar la biodiversidad microbiana y su biofloculación [15].

Por su parte, el HRT influye sobre la carga orgánica que ingresa al sistema y con ello, la cantidad de nutrientes. Un incremento del mismo disminuye la cantidad de nutrientes, y con ello se minimiza la formación de torta en la membrana. Además, cuando un MPBR trabaja a altos valores de HRT, la biomasa es capaz de hidrolizar materia orgánica compleja y convertirla en materia orgánica de menor peso molecular, reduciendo el ensuciamiento de la membrana [36].

A pesar de que, según lo anterior, cabría pensar que lo más conveniente sería trabajar a altos valores de ambos parámetros, como ya se ha mencionado, varios investigadores recomiendan valores de SRT entre 2 y 25 días para evitar la inhibición del crecimiento de las microalgas por fenómenos de atenuación de luz en suspensiones muy concentradas [21,60] y no se suelen encontrar trabajos que apliquen HRTs superiores a los 5 días. Sin embargo, recientemente, algunos autores han encontrado que aumentando el SRT desde los 10 días hasta los 30 días se disminuye notablemente el ensuciamiento de la membrana debido a cambios en el tamaño y morfología de los flóculos formados [73]. Incluso hay autores que han conseguido productividades importantes y eliminaciones de nutrientes óptimas utilizando SRTs superiores a los 200 días [95].

Algunos autores han demostrado que el tamaño del flóculo afecta al ensuciamiento, aunque no es la única causa del mismo. En estudios previos con un biorreactor de membrana terciario se demostró que el contenido en biopolímeros de las suspensiones era un factor que limitaba la operatividad del sistema por su influencia en el ensuciamiento de la membrana [96]. En este sentido, la optimización del HRT y del SRT puede contribuir a la disminución de este tipo de sustancias en suspensión [97,98], y con ello, mitigar el ensuciamiento de la membrana.

Aunque se han llevado a cabo numerosos estudios para definir las condiciones óptimas de iluminación que mejoren el crecimiento de microalgas, se han encontrado pocos trabajos enfocados al estudio de la influencia de estas condiciones de iluminación sobre la producción de sustancias orgánicas excretadas por las microalgas y su influencia en el ensuciamiento de la membrana en un MPBR [21,99]. El tipo y la cantidad de sustancias poliméricas extracelulares (EPS) que son excretadas por las microalgas dependen del fotoperiodo y algunos autores han establecido que son la causa principal del ensuciamiento en

fotobiorreactores de membrana [100]. Otros han encontrado variaciones en la cantidad de EPS y de productos microbianos solubles (SMP) cuando se varía el fotoperiodo en cultivos de *Chlorella vulgaris* en un fotobiorreactor de membrana recíproco*,* observando, además, una variación de este tipo de sustancias al inicio y al final de cada uno de los ciclos de luz/oscuridad inducidos, demostrando la necesidad de un periodo de oscuridad [101].

5. Estructura y justificación de la unidad temática de la tesis doctoral

La presente tesis doctoral se presenta bajo la modalidad de compendio de publicaciones con 3 capítulos correspondientes cada uno de ellos, con una de estas publicaciones.

La presente tesis, atendiendo al Reglamento de Enseñanzas oficiales de Doctorado de la Universidad de La Laguna establecido según el Artículo 13 del Real Decreto 99/2011, de 28 de enero, por el que se regulan las enseñanzas oficiales de doctorado y recogido en el Acuerdo 2/CG 25-07-2017, incluye en su estructura: una introducción general (en este capítulo), un resumen global de los objetivos (Capítulo 2), de la metodología empleada (Capítulo 3), de los resultados obtenidos, así como, la discusión de los resultados (Capítulo 7) y conclusiones finales. Entre el Capítulo 3 y el Capítulo 7 se encuentran los capítulos correspondientes a los trabajos publicados (Capítulos 4, 5 y 6).

Las tres publicaciones que compendian esta tesis doctoral versan sobre la aplicación de fotobiorreactores de membrana para el tratamiento de aguas residuales domésticas. En concreto, los Capítulos 5 y 6 se dedican al tratamiento de aguas residuales parcialmente depuradas y el Capítulo 7 al tratamiento de un agua residual bruta. Se ha utilizado, en los tres capítulos, la misma metodología y se han establecido los parámetros óptimos de operación en cada caso, atendiendo en todos ellos a la adecuada eliminación de nutrientes para conseguir efluentes que cumplan con la normativa europea para reutilización de aguas [102] y permitan una operación sostenible, en cuanto a ensuciamiento de la membrana se refiere.

La instalación MPBR a escala laboratorio que se ha utilizado en el desarrollo de esta tesis doctoral se probó, en primer lugar, para el establecimiento de los valores

óptimos de SRT y HRT necesarios para alcanzar un efluente con una calidad adecuada para ser reutilizado en riego agrícola, bajo un régimen de operación continuo, sin limpiezas químicas, durante al menos 1000 horas de operación (Capítulo 5). Una vez establecidos estos valores, se optimizó el fotoperiodo manteniendo unas condiciones preestablecidas de SRT y HRT basadas en el estudio previo que se describe en el Capítulo 5 (Capítulo 6).

El siguiente paso fue modificar el agua de alimentación al sistema sustituyendo el agua parcialmente depurada que se había utilizado en los Capítulos 5 y 6, por agua residual bruta, intentando establecer la viabilidad de la utilización de un MPBR como tratamiento secundario de dichas aguas residuales. En este caso, además, para mitigar el mayor ensuciamiento sobre la membrana que cabía esperar que se produjese al alimentar un efluente con una carga orgánica y de nutrientes mayor, se utilizó un protocolo de limpieza física de la membrana diferente al retrolavado con burbujeo de aire utilizado en los Capítulos 5 y 6, el giro de la membrana durante el retrolavado y semanalmente, estableciendo un periodo de relax de 5 minutos.

En todos los capítulos se han determinado las eficacias de eliminación de contaminantes de las aguas residuales, se ha profundizado en la naturaleza del ensuciamiento de las membranas e incluso, se han identificado los microorganismos presentes en cada una de las suspensiones biológicas.

Como se puede apreciar, todos los artículos que compendian esta tesis doctoral siguen la misma unidad temática que es el desarrollo y optimización de las condiciones de operación de fotobiorreactores de membrana aplicados al tratamiento de aguas residuales domésticas.

Las copias de los artículos ya publicados se encuentran, además, como anexos de la presente Tesis Doctoral y en cada uno de los Capítulos 5, 6 y 7 se encuentran manuscritos, siguiendo el formato de la tesis.

Referencias

[1]   European Union, European Green Deal, Https://Commission.Europa.Eu/Strategy-and-Policy/Priorities-2019-2024/European-Green-Deal_es. (2023).

[2]   Z.J. Ren, K. Pagilla, Pathways to Water Sector Decarbonization, Carbon Capture and Utilization, IWA Publishing, London, 2022.

[3]   S.K. Wang, A.R. Stiles, C. Guo, C.Z. Liu, Microalgae cultivation in photobioreactors: An overview of light characteristics, Eng Life Sci. 14 (2014) 550–559. https://doi.org/10.1002/elsc.201300170.

[4]   X. ya Liu, Y. Hong, Microalgae-Based Wastewater Treatment and Recovery with Biomass and Value-Added Products: a Brief Review, Curr Pollut Rep. 7 (2021) 227–245. https://doi.org/10.1007/s40726-021-00184-6.

[5]   J.S. Chang, P.L. Show, T.C. Ling, C.Y. Chen, S.H. Ho, C.H. Tan, D. Nagarajan, W.N. Phong, Photobioreactors, in: Current Developments in Biotechnology and Bioengineering: Bioprocesses, Bioreactors and Controls, Elsevier Inc., 2017: pp. 313–352. https://doi.org/10.1016/B978-0-444-63663-8.00011-2.

[6]   K.X. Huang, A. Vadiveloo, J.L. Zhou, L. Yang, D.Z. Chen, F. Gao, Integrated culture and harvest systems for improved microalgal biomass production and wastewater treatment, Bioresour Technol. 376 (2023). https://doi.org/10.1016/j.biortech.2023.128941.

[7]   L. Aditya, T.M.I. Mahlia, L.N. Nguyen, H.P. Vu, L.D. Nghiem, Microalgae-bacteria consortium for wastewater treatment and biomass production, Science of the Total Environment. 838 (2022). https://doi.org/10.1016/j.scitotenv.2022.155871.

[8]   M. Ma, Z. Yu, L. Jiang, Q. Hou, Z. Xie, M. Liu, S. Yu, H. Pei, Alga-based dairy wastewater treatment scheme: Candidates screening, process advancement, and economic analysis, J Clean Prod. 390 (2023). https://doi.org/10.1016/j.jclepro.2023.136105.

[9]   F.G. Acién, C. Gómez-Serrano, M.M. Morales-Amaral, J.M. Fernández-Sevilla, E. Molina-Grima, Wastewater treatment using microalgae: how realistic a contribution might it be to significant urban wastewater treatment?, Appl Microbiol Biotechnol. 100 (2016) 9013–9022. https://doi.org/10.1007/s00253-016-7835-7.

[10]   B. Zhang, W. Li, Y. Guo, Z. Zhang, W. Shi, F. Cui, P.N.L. Lens, J.H. Tay, Microalgal-bacterial consortia: From interspecies interactions to biotechnological applications, Renewable and Sustainable Energy Reviews. 118 (2020). https://doi.org/10.1016/j.rser.2019.109563.

[11]   D. Nagarajan, D.J. Lee, S. Varjani, S.S. Lam, S.I. Allakhverdiev, J.S. Chang, Microalgae-based wastewater treatment – Microalgae-bacteria consortia, multi-omics approaches and algal stress response, Science of the Total Environment. 845 (2022). https://doi.org/10.1016/j.scitotenv.2022.157110.

[12]   K.X. Huang, A. Vadiveloo, J.L. Zhou, L. Yang, D.Z. Chen, F. Gao, Integrated culture and harvest systems for improved microalgal biomass production

and wastewater treatment, Bioresour Technol. 376 (2023). https://doi.org/10.1016/j.biortech.2023.128941.

[13]   G. Goswami, B.B. Makut, D. Das, Sustainable production of bio-crude oil via hydrothermal liquefaction of symbiotically grown biomass of microalgae-bacteria coupled with effective wastewater treatment, Sci Rep. 9 (2019). https://doi.org/10.1038/s41598-019-51315-5.

[14]   G. Goswami, B.B. Makut, D. Das, Sustainable production of bio-crude oil via hydrothermal liquefaction of symbiotically grown biomass of microalgae-bacteria coupled with effective wastewater treatment, Sci Rep. 9 (2019). https://doi.org/10.1038/s41598-019-51315-5.

[15]   A. Fallahi, F. Rezvani, H. Asgharnejad, E. Khorshidi, N. Hajinajaf, B. Higgins, Interactions of microalgae-bacteria consortia for nutrient removal from wastewater: A review, Chemosphere. 272 (2021) 129878. https://doi.org/10.1016/j.chemosphere.2021.129878.

[16]   D. Hernández, B. Riaño, M. Coca, M. Solana, A. Bertucco, M.C. García-González, Microalgae cultivation in high rate algal ponds using slaughterhouse wastewater for biofuel applications, Chemical Engineering Journal. 285 (2016) 449–458. https://doi.org/10.1016/j.cej.2015.09.072.

[17]   R. Chu, S. Li, L. Zhu, Z. Yin, D. Hu, C. Liu, F. Mo, A review on co-cultivation of microalgae with filamentous fungi: Efficient harvesting, wastewater treatment and biofuel production, Renewable and Sustainable Energy Reviews. 139 (2021). https://doi.org/10.1016/j.rser.2020.110689.

[18]   Q. Wang, H. Li, Q. Shen, J. Wang, X. Chen, Z. Zhang, Z. Lei, T. Yuan, K. Shimizu, Y. Liu, D.J. Lee, Biogranulation process facilitates cost-efficient resources recovery from microalgae-based wastewater treatment systems and the creation of a circular bioeconomy, Science of the Total Environment. 828 (2022). https://doi.org/10.1016/j.scitotenv.2022.154471.

[19]   J.S. Arcila, G. Buitrón, Influence of solar irradiance levels on the formation of microalgae-bacteria aggregates for municipal wastewater treatment, Algal Res. 27 (2017) 190–197. https://doi.org/10.1016/j.algal.2017.09.011.

[20]   J.M. Valigore, P.A. Gostomski, D.G. Wareham, A.D. O'Sullivan, Effects of hydraulic and solids retention times on productivity and settleability of microbial (microalgal-bacterial) biomass grown on primary treated wastewater as a biofuel feedstock, Water Res. 46 (2012) 2957–2964. https://doi.org/10.1016/j.watres.2012.03.023.

[21]   Y. Luo, P. Le-Clech, R.K. Henderson, Simultaneous microalgae cultivation and wastewater treatment in submerged membrane photobioreactors: A

review, Algal Res. 24 (2017) 425–437. https://doi.org/10.1016/j.algal.2016.10.026.

[22] F. Ye, Y. Ye, Y. Li, Effect of C/N ratio on extracellular polymeric substances (EPS) and physicochemical properties of activated sludge flocs, J Hazard Mater. 188 (2011) 37–43. https://doi.org/10.1016/j.jhazmat.2011.01.043.

[23] P. Sathinathan, H.M. Parab, R. Yusoff, S. Ibrahim, V. Vello, G.C. Ngoh, Photobioreactor design and parameters essential for algal cultivation using industrial wastewater: A review, Renewable and Sustainable Energy Reviews. 173 (2023). https://doi.org/10.1016/j.rser.2022.113096.

[24] R.N. Singh, S. Sharma, Development of suitable photobioreactor for algae production - A review, Renewable and Sustainable Energy Reviews. 16 (2012) 2347–2353. https://doi.org/10.1016/j.rser.2012.01.026.

[25] H.N.P. Vo, H.H. Ngo, W. Guo, T.M.H. Nguyen, Y. Liu, Y. Liu, D.D. Nguyen, S.W. Chang, A critical review on designs and applications of microalgae-based photobioreactors for pollutants treatment, Science of the Total Environment. 651 (2019) 1549–1568. https://doi.org/10.1016/j.scitotenv.2018.09.282.

[26] E. Molina Grima, J.A. Sanchez Prez, F. Garcia Camacho, J.M. FernAndez Sevilla, F.G. Aci, Productivity analysis of outdoor chemostat culture in tubular air-lift photobioreactors, Kluwer Academic Publishers, 1996.

[27] B. Brzychczyk, T. Hebda, J. Fitas, J. Giełżecki, The follow-up photobioreactor illumination system for the cultivation of photosynthetic microorganisms, Energies (Basel). 13 (2020). https://doi.org/10.3390/en13051143.

[28] H. Yan, C. Guan, Y. Jia, X. Huang, W. Yang, Mixing characteristics, cell trajectories, pressure loss and shear stress of tubular photobioreactor with inserted self-rotating helical rotors, Journal of Chemical Technology and Biotechnology. 93 (2018) 1261–1269. https://doi.org/10.1002/jctb.5484.

[29] K. Weck, S. Calvo, A. Delafosse, D. Toye, Hydrodynamic Characterization of a Non-conventional Photobioreactor, Chem Eng Technol. 44 (2021) 1803–1813. https://doi.org/10.1002/ceat.202100076.

[30] R. Muñoz, B. Guieysse, Algal-bacterial processes for the treatment of hazardous contaminants: A review, Water Res. 40 (2006) 2799–2815. https://doi.org/10.1016/j.watres.2006.06.011.

[31] Y. Liao, A. Bokhary, E. Maleki, B. Liao, A review of membrane fouling and its control in algal-related membrane processes, Bioresour Technol. 264 (2018) 343–358. https://doi.org/10.1016/j.biortech.2018.06.102.

[32] R. Sirohi, A. Kumar Pandey, P. Ranganathan, S. Singh, A. Udayan, M. Kumar Awasthi, A.T. Hoang, C.R. Chilakamarry, S.H. Kim, S.J. Sim, Design and

applications of photobioreactors- a review, Bioresour Technol. 349 (2022). https://doi.org/10.1016/j.biortech.2022.126858.

[33]   Y. Chisti, Biodiesel from microalgae, Biotechnol Adv. 25 (2007) 294–306. https://doi.org/10.1016/j.biotechadv.2007.02.001.

[34]   S.D. Ríos, J. Castañeda, C. Torras, X. Farriol, J. Salvadó, Lipid extraction methods from microalgal biomass harvested by two different paths: Screening studies toward biodiesel production, Bioresour Technol. 133 (2013) 378–388. https://doi.org/10.1016/j.biortech.2013.01.093.

[35]   Y. Luo, P. Le-Clech, R.K. Henderson, Assessment of membrane photobioreactor (MPBR) performance parameters and operating conditions, Water Res. 138 (2018) 169–180. https://doi.org/10.1016/j.watres.2018.03.050.

[36]   Y. Liao, A. Bokhary, E. Maleki, B. Liao, A review of membrane fouling and its control in algal-related membrane processes, Bioresour Technol. 264 (2018) 343–358. https://doi.org/10.1016/j.biortech.2018.06.102.

[37]   Z. Zhao, K. Muylaert, I. F.J. Vankelecom, Applying membrane technology in microalgae industry: A comprehensive review, Renewable and Sustainable Energy Reviews. 172 (2023). https://doi.org/10.1016/j.rser.2022.113041.

[38]   C. Alcántara, E. Posadas, B. Guieysse, R. Muñoz, Microalgae-based Wastewater Treatment, in: Handbook of Marine Microalgae: Biotechnology Advances, Elsevier Inc., 2015: pp. 439–455. https://doi.org/10.1016/B978-0-12-800776-1.00029-7.

[39]   R. Kumar, A.K. Ghosh, P. Pal, Synergy of biofuel production with waste remediation along with value-added co-products recovery through microalgae cultivation: A review of membrane-integrated green approach, Science of the Total Environment. 698 (2020). https://doi.org/10.1016/j.scitotenv.2019.134169.

[40]   F. Gao, Z.H. Yang, C. Li, Y. jie Wang, W. hong Jin, Y. bing Deng, Concentrated microalgae cultivation in treated sewage by membrane photobioreactor operated in batch flow mode, Bioresour Technol. 167 (2014) 441–446. https://doi.org/10.1016/j.biortech.2014.06.042.

[41]   L. Marbelia, M.R. Bilad, I. Passaris, V. Discart, D. Vandamme, A. Beuckels, K. Muylaert, I.F.J. Vankelecom, Membrane photobioreactors for integrated microalgae cultivation and nutrient remediation of membrane bioreactors effluent, Bioresour Technol. 163 (2014) 228–235. https://doi.org/10.1016/j.biortech.2014.04.012.

[42]   G. Singh, P.B. Thomas, Nutrient removal from membrane bioreactor permeate using microalgae and in a microalgae membrane photoreactor,

Bioresour Technol. 117 (2012) 80–85. https://doi.org/10.1016/j.biortech.2012.03.125.

[43] K. Li, Q. Liu, F. Fang, R. Luo, Q. Lu, W. Zhou, S. Huo, P. Cheng, J. Liu, M. Addy, P. Chen, D. Chen, R. Ruan, Microalgae-based wastewater treatment for nutrients recovery: A review, Bioresour Technol. 291 (2019) 121934. https://doi.org/10.1016/j.biortech.2019.121934.

[44] K. Li, Q. Liu, F. Fang, R. Luo, Q. Lu, W. Zhou, S. Huo, P. Cheng, J. Liu, M. Addy, P. Chen, D. Chen, R. Ruan, Microalgae-based wastewater treatment for nutrients recovery: A review, Bioresour Technol. 291 (2019). https://doi.org/10.1016/j.biortech.2019.121934.

[45] A.L. Gonçalves, J.C.M. Pires, M. Simões, A review on the use of microalgal consortia for wastewater treatment, Algal Res. 24 (2017) 403–415. https://doi.org/10.1016/j.algal.2016.11.008.

[46] D. García, E. Posadas, S. Blanco, G. Acién, P. García-Encina, S. Bolado, R. Muñoz, Evaluation of the dynamics of microalgae population structure and process performance during piggery wastewater treatment in algal-bacterial photobioreactors, Bioresour Technol. 248 (2018) 120–126. https://doi.org/10.1016/j.biortech.2017.06.079.

[47] A. Solmaz, M. Işık, Polishing the secondary effluent and biomass production by microalgae submerged membrane photo bioreactor, Sustainable Energy Technologies and Assessments. 34 (2019) 1–8. https://doi.org/10.1016/j.seta.2019.04.002.

[48] A.L.K. Sheng, M.R. Bilad, N.B. Osman, N. Arahman, Sequencing batch membrane photobioreactor for real secondary effluent polishing using native microalgae: Process performance and full-scale projection, J Clean Prod. 168 (2017) 708–715. https://doi.org/10.1016/j.jclepro.2017.09.083.

[49] C. Haixing, F. Qian, H. Yun, X. Ao, L. Qiang, Z. Xun, Improvement of microalgae lipid productivity and quality in an ion-exchange-membrane photobioreactor using real municipal wastewater, International Journal of Agricultural and Biological Engineering. 10 (2017) 97–106. https://doi.org/10.3965/j.ijabe.20171001.2706.

[50] M. Zhang, L. Yao, E. Maleki, B.Q. Liao, H. Lin, Membrane technologies for microalgal cultivation and dewatering: Recent progress and challenges, Algal Res. 44 (2019). https://doi.org/10.1016/j.algal.2019.101686.

[51] M. Xu, P. Li, T. Tang, Z. Hu, Roles of SRT and HRT of an algal membrane bioreactor system with a tanks-in-series configuration for secondary wastewater effluent polishing, Ecol Eng. 85 (2015) 257–264. https://doi.org/10.1016/j.ecoleng.2015.09.064.

[52] X. Chen, Z. Li, N. He, Y. Zheng, H. Li, H. Wang, Y. Wang, Y. Lu, Q. Li, Y. Peng, Nitrogen and phosphorus removal from anaerobically digested wastewater by microalgae cultured in a novel membrane photobioreactor, Biotechnol Biofuels. 11 (2018). https://doi.org/10.1186/s13068-018-1190-0.

[53] H. Chang, X. Quan, N. Zhong, Z. Zhang, C. Lu, G. Li, Z. Cheng, L. Yang, High-efficiency nutrients reclamation from landfill leachate by microalgae Chlorella vulgaris in membrane photobioreactor for bio-lipid production, Bioresour Technol. 266 (2018) 374–381. https://doi.org/10.1016/j.biortech.2018.06.077.

[54] I. De Godos, C. González, E. Becares, P.A. García-Encina, R. Muñoz, Simultaneous nutrients and carbon removal during pretreated swine slurry degradation in a tubular biofilm photobioreactor, Appl Microbiol Biotechnol. 82 (2009) 187–194. https://doi.org/10.1007/s00253-008-1825-3.

[55] C. González, J. Marciniak, S. Villaverde, C. León, P.A. García, R. Muñoz, Efficient nutrient removal from swine manure in a tubular biofilm photo-bioreactor using algae-bacteria consortia, Water Science and Technology. 58 (2008) 95–102. https://doi.org/10.2166/wst.2008.655.

[56] I. Suh, C.G. Lee, Photobioreactor engineering design and performance, Biotechnology and Bioprocess Engineering . 8 (2003) 313–321.

[57] E. Sforza, D. Simionato, G.M. Giacometti, A. Bertucco, T. Morosinotto, Adjusted light and dark cycles can optimize photosynthetic efficiency in algae growing in photobioreactors, PLoS One. 7 (2012). https://doi.org/10.1371/journal.pone.0038975.

[58] D. Simionato, S. Basso, G.M. Giacometti, T. Morosinotto, Optimization of light use efficiency for biofuel production in algae, Biophys Chem. 182 (2013) 71–78. https://doi.org/10.1016/j.bpc.2013.06.017.

[59] A. Mehrabadi, R. Craggs, M.M. Farid, Wastewater treatment high rate algal ponds (WWT HRAP) for low-cost biofuel production, Bioresour Technol. 184 (2015) 202–214. https://doi.org/10.1016/j.biortech.2014.11.004.

[60] M. Zhang, L. Yao, E. Maleki, B.Q. Liao, H. Lin, Membrane technologies for microalgal cultivation and dewatering: Recent progress and challenges, Algal Res. 44 (2019) 101686. https://doi.org/10.1016/j.algal.2019.101686.

[61] H. Jia, Q. Yuan, Nitrogen removal in photo sequence batch reactor using algae-bacteria consortium, Journal of Water Process Engineering. 26 (2018) 108–115. https://doi.org/10.1016/j.jwpe.2018.10.003.

[62] L. Hollis, C.G. Trick, N.P.A. Hüner, Continuous monitoring of growth detects photoperiod-dependent oscillations in growth rates of chlorella vulgaris, Botany. 98 (2020) 103–115. https://doi.org/10.1139/cjb-2019-0116.

[63]   J. González-Camejo, A. Viruela, M. V. Ruano, R. Barat, A. Seco, J. Ferrer, Effect of light intensity, light duration and photoperiods in the performance of an outdoor photobioreactor for urban wastewater treatment, Algal Res. 40 (2019) 101511. https://doi.org/10.1016/j.algal.2019.101511.

[64]   A. Toledo-Cervantes, E. Posadas, I. Bertol, S. Turiel, A. Alcoceba, R. Muñoz, Assessing the influence of the hydraulic retention time and carbon/nitrogen ratio on urban wastewater treatment in a new anoxic-aerobic algal-bacterial photobioreactor configuration, Algal Res. 44 (2019) 101672. https://doi.org/10.1016/j.algal.2019.101672.

[65]   D. García, C. Alcántara, S. Blanco, R. Pérez, S. Bolado, R. Muñoz, Enhanced carbon, nitrogen and phosphorus removal from domestic wastewater in a novel anoxic-aerobic photobioreactor coupled with biogas upgrading, Chemical Engineering Journal. 313 (2017) 424–434. https://doi.org/10.1016/j.cej.2016.12.054.

[66]   M. Xu, P. Li, T. Tang, Z. Hu, Roles of SRT and HRT of an algal membrane bioreactor system with a tanks-in-series configuration for secondary wastewater effluent polishing, Ecol Eng. 85 (2015) 257–264. https://doi.org/10.1016/j.ecoleng.2015.09.064.

[67]   R. Honda, Y. Teraoka, M. Noguchi, S. Yang, Optimization of Hydraulic Retention Time and Biomass Concentration in Microalgae Biomass Production from Treated Sewage with a Membrane Photobioreactor, J Water Environ Technol. 15 (2017) 1–11. https://doi.org/10.2965/jwet.15-085.

[68]   A. Solmaz, M. Işık, Optimization of membrane photobioreactor; the effect of hydraulic retention time on biomass production and nutrient removal by mixed microalgae culture, Biomass Bioenergy. 142 (2020). https://doi.org/10.1016/j.biombioe.2020.105809.

[69]   J. González-Camejo, A. Jiménez-Benítez, M. V. Ruano, A. Robles, R. Barat, J. Ferrer, Optimising an outdoor membrane photobioreactor for tertiary sewage treatment, J Environ Manage. 245 (2019) 76–85. https://doi.org/10.1016/j.jenvman.2019.05.010.

[70]   A.F. Novoa, L. Fortunato, Z.U. Rehman, T.O. Leiknes, Evaluating the effect of hydraulic retention time on fouling development and biomass characteristics in an algal membrane photobioreactor treating a secondary wastewater effluent, Bioresour Technol. 309 (2020) 123348. https://doi.org/10.1016/j.biortech.2020.123348.

[71]   J. González-Camejo, S. Aparicio, A. Jiménez-Benítez, M. Pachés, M. V. Ruano, L. Borrás, R. Barat, A. Seco, Improving membrane photobioreactor

performance by reducing light path: operating conditions and key performance indicators, Water Res. 172 (2020). https://doi.org/10.1016/j.watres.2020.115518.

[72] E. Barbera, E. Sforza, A. Grandi, A. Bertucco, Uncoupling solid and hydraulic retention time in photobioreactors for microalgae mass production: A model-based analysis, Chem Eng Sci. 218 (2020) 115578. https://doi.org/10.1016/j.ces.2020.115578.

[73] A.M. Rada-Ariza, D. Fredy, C.M. Lopez-Vazquez, N.P. Van der Steen, P.N.L. Lens, A. Toledo-Cervantes, E. Posadas, I. Bertol, S. Turiel, A. Alcoceba, R. Muñoz, M. Zhang, K.T. Leung, H. Lin, B. Liao, J. González-Camejo, S. Aparicio, A. Jiménez-Benítez, M. Pachés, M. V. Ruano, L. Borrás, R. Barat, A. Seco, Effects of solids retention time on the biological performance of a novel microalgal-bacterial membrane photobioreactor for industrial wastewater treatment, J Environ Chem Eng. 9 (2021) 105500. https://doi.org/10.1016/j.jece.2021.105500.

[74] F. Gao, W. Cui, J.P. Xu, C. Li, W.H. Jin, H.L. Yang, Lipid accumulation properties of Chlorella vulgaris and Scenedesmus obliquus in membrane photobioreactor (MPBR) fed with secondary effluent from municipal wastewater treatment plant, Renew Energy. 136 (2019) 671–676. https://doi.org/10.1016/j.renene.2019.01.038.

[75] P. Kandimalla, S. Desi, H. Vurimindi, Mixotrophic cultivation of microalgae using industrial flue gases for biodiesel production, Environmental Science and Pollution Research. 23 (2016) 9345–9354. https://doi.org/10.1007/s11356-015-5264-2.

[76] M.R. Bilad, H.A. Arafat, I.F.J. Vankelecom, Membrane technology in microalgae cultivation and harvesting: A review, Biotechnol Adv. 32 (2014) 1283–1300. https://doi.org/10.1016/j.biotechadv.2014.07.008.

[77] L. Christenson, R. Sims, Production and harvesting of microalgae for wastewater treatment, biofuels, and bioproducts, Biotechnol Adv. 29 (2011) 686–702. https://doi.org/10.1016/j.biotechadv.2011.05.015.

[78] P. Chawla, D. Gola, V. Dalvi, T.R. Sreekrishnan, T.U. Ariyadasa, A. Malik, Design and development of mini-photobioreactor system for strategic high throughput selection of optimum microalgae-wastewater combination, Bioresour Technol Rep. 17 (2022). https://doi.org/10.1016/j.biteb.2022.100967.

[79] Z. Arbib, J. Ruiz, P. Álvarez-Díaz, C. Garrido-Pérez, J. Barragan, J.A. Perales, Effect of pH control by means of flue gas addition on three different photo-bioreactors treating urban wastewater in long-term operation, Ecol Eng. 57 (2013) 226–235. https://doi.org/10.1016/j.ecoleng.2013.04.040.

[80] Q. Huang, F. Jiang, L. Wang, C. Yang, Design of Photobioreactors for Mass Cultivation of Photosynthetic Organisms, Engineering. 3 (2017) 318–329. https://doi.org/10.1016/J.ENG.2017.03.020.

[81] P.C. de Souza Kirnev, L.P. de Souza Vandenberghe, C.R. Soccol, J.C. de Carvalho, Mixing and agitation in photobioreactors, in: Innovations in Fermentation and Phytopharmaceutical Technologies, Elsevier, 2022: pp. 13–35. https://doi.org/10.1016/B978-0-12-821877-8.00005-1.

[82] A.L.K. Sheng, M.R. Bilad, N.B. Osman, N. Arahman, Sequencing batch membrane photobioreactor for real secondary effluent polishing using native microalgae: Process performance and full-scale projection, J Clean Prod. 168 (2017) 708–715. https://doi.org/10.1016/j.jclepro.2017.09.083.

[83] A. Babaei, M.R. Mehrnia, Fouling in microalgal membrane bioreactor containing nitrate-enriched wastewater under different trophic conditions, Algal Res. 36 (2018) 167–174. https://doi.org/10.1016/j.algal.2018.10.017.

[84] P. Le-Clech, V. Chen, T.A.G. Fane, Fouling in membrane bioreactors used in wastewater treatment, J Memb Sci. 284 (2006) 17–53. https://doi.org/10.1016/j.memsci.2006.08.019.

[85] A. Drews, Membrane fouling in membrane bioreactors-Characterisation, contradictions, cause and cures, J Memb Sci. 363 (2010) 1–28. https://doi.org/10.1016/j.memsci.2010.06.046.

[86] F. Meng, S. Zhang, Y. Oh, Z. Zhou, H.S. Shin, S.R. Chae, Fouling in membrane bioreactors: An updated review, Water Res. 114 (2017) 151–180. https://doi.org/10.1016/j.watres.2017.02.006.

[87] F. Wicaksana, A.G. Fane, P. Pongpairoj, R. Field, Microfiltration of algae (Chlorella sorokiniana): Critical flux, fouling and transmission, J Memb Sci. 387–388 (2012) 83–92. https://doi.org/10.1016/j.memsci.2011.10.013.

[88] W. Zhang, J. Luo, L. Ding, M.Y. Jaffrin, A review on flux decline control strategies in pressure-driven membrane processes, Ind Eng Chem Res. 54 (2015) 2843–2861. https://doi.org/10.1021/ie504848m.

[89] C. Shin, J. Bae, Current status of the pilot-scale anaerobic membrane bioreactor treatments of domestic wastewaters: A critical review, Bioresour Technol. 247 (2018) 1038–1046. https://doi.org/10.1016/j.biortech.2017.09.002.

[90] Z. Wang, J. Ma, C.Y. Tang, K. Kimura, Q. Wang, X. Han, Membrane cleaning in membrane bioreactors: A review, J Memb Sci. 468 (2014) 276–307. https://doi.org/10.1016/j.memsci.2014.05.060.

[91]   M.Y. Jaffrin, Dynamic shear-enhanced membrane filtration: A review of rotating disks, rotating membranes and vibrating systems, J Memb Sci. 324 (2008) 7–25. https://doi.org/10.1016/j.memsci.2008.06.050.

[92]   A. Kola, Y. Ye, P. Le-Clech, V. Chen, Transverse vibration as novel membrane fouling mitigation strategy in anaerobic membrane bioreactor applications, J Memb Sci. 455 (2014) 320–329. https://doi.org/10.1016/j.memsci.2013.12.078.

[93]   R.W. Field, D. Wu, J.A. Howell, B.B. Gupta, Critical flux concept for microfiltration fouling, 1995.

[94]   H. Elcik, M. Cakmakci, Harvesting microalgal biomass using crossflow membrane filtration: critical flux, filtration performance, and fouling characterization, Environmental Technology (United Kingdom). 38 (2017) 1585–1596. https://doi.org/10.1080/09593330.2016.1237560.

[95]   P. Praveen, Y. Guo, H. Kang, C. Lefebvre, K.-C.K.C. Loh, Enhancing microalgae cultivation in anaerobic digestate through nitrification, Chemical Engineering Journal. 354 (2018) 905–912. https://doi.org/10.1016/j.cej.2018.08.099.

[96]   L. Vera, E. González, O. Díaz, R. Sánchez, R. Bohorque, J. Rodríguez-Sevilla, Fouling analysis of a tertiary submerged membrane bioreactor operated in dead-end mode at high-fluxes, J Memb Sci. 493 (2015) 8–18. https://doi.org/10.1016/j.memsci.2015.06.014.

[97]   S.L. Low, S.L. Ong, H.Y. Ng, Characterization of membrane fouling in submerged ceramic membrane photobioreactors fed with effluent from membrane bioreactors, Chemical Engineering Journal. 290 (2016) 91–102. https://doi.org/10.1016/j.cej.2016.01.005.

[98]   E. Segredo-Morales, E. González, C. González-Martín, L. Vera, Secondary wastewater effluent treatment by microalgal-bacterial membrane photobioreactor at long solid retention times, Journal of Water Process Engineering. 49 (2022). https://doi.org/10.1016/j.jwpe.2022.103200.

[99]   E. Segredo-Morales, E. González, C. González-Martín, L. Vera, Evaluation of membrane fouling in a microalgal-bacterial membrane photobioreactor treating secondary wastewater effluent: effect of photoperiod conditions, Environ Sci (Camb). (2023). https://doi.org/10.1039/d3ew00138e.

[100] A. Keramati, S. Azizi, A. Hashemi, F. Pajoum Shariati, Effects of flashing light–emitting diodes (LEDs) on membrane fouling in a reciprocal membrane photobioreactor (RMPBR) to assess nitrate and phosphate removal from whey wastewater, J Appl Phycol. 33 (2021) 1513–1524. https://doi.org/10.1007/s10811-021-02388-1.

[101] S. Azizi, A. Hashemi, F. Pajoum Shariati, H. Tayebati, A. Keramati, B. Bonakdarpour, M.M. Mohammad, Effect of different light-dark cycles on the membrane fouling, EPS and SMP production in a novel reciprocal membrane photobioreactor (RMPBR) by C. vulgaris species, Journal of Water Process Engineering. 43 (2021) 102256. https://doi.org/10.1016/j.jwpe.2021.102256.

[102] European Parliament and of the Council 2020/741, Regulation (EU) 2020/741 of 25 May 2020 on minimum requirements for water reuse, 2020.

CAPÍTULO 2

Objetivos

En la presente tesis se ha analizado la influencia de los principales parámetros de operación (tiempos de residencia hidráulico y de retención de sólidos) y ambientales (frecuencia de luz) sobre el comportamiento de un fotobiorreactor de membrana aplicado a la depuración de aguas residuales domésticas. Se investigó la capacidad de depuración, la productividad de biomasa y el ensuciamiento de la membrana cuando el proceso se aplicó al tratamiento de aguas residuales con diferentes composiciones (de nutrientes y de materia orgánica) en escenarios de bajo consumo energético. Además, se investigó el efecto del diseño y la operación del módulo de membrana (particularmente la intensidad de la turbulencia generada en las inmediaciones de la membrana) en las condiciones estudiadas.

Finalmente, se estudió la naturaleza de las suspensiones generadas, se identificaron tanto las especies de microalgas presentes como otros microorganismos. También se llevó a cabo un estudio termogravimétrico y un análisis elemental de la biomasa tras un proceso de secado.

Objetivos específicos

- Evaluación de la capacidad de la tecnología MPBR para la eliminación de nutrientes en dos tipos de afluentes. Efecto de las condiciones óptimas de funcionamiento (tiempos hidráulicos y de retención de sólidos) sobre el crecimiento de la biomasa y la tasa de eliminación de nutrientes. Caracterización de las especies microbianas desarrolladas en cada condición.
- Identificación de los mecanismos predominantes de ensuciamiento de la membrana implicados y su relación con las principales propiedades de la suspensión. Efecto de las condiciones de filtración (flujo de permeado, turbulencia y limpieza física) sobre el fenómeno de ensuciamiento.
- Exploración de la idoneidad de un módulo rotativo en el MPBR en términos de actividad de la biomasa, biofloculación y reducción de ensuciamiento.

CAPÍTULO 3

Materiales y métodos

1. Instalaciones experimentales

1.1.   Módulo de membrana estática

La instalación experimental, cuyo esquema se muestra en la Figura 3.1, consiste en un depósito de proceso cilíndrico de 3 L de capacidad, con un diámetro de 14 cm, elaborado en polietileno de alta densidad. En este depósito se dispone de un módulo sumergido de membrana de fibra hueca *ZeeWeed*®-1 (ZW-1) (*Veolia Water Technologies & Solutions*, Saint-Maurice, Francia). El módulo está constituido por 97 fibras de fluoruro de polivinilideno (*PVDF*) con una longitud de 80 mm y un tamaño de poro nominal de 0,04 μm. El diámetro externo de las fibras es de 1,9 mm y proporciona una superficie de filtración de 0,047 m^2. El permeado se extrae del cabezal superior aplicando un ligero vacío mediante una microbomba de engranajes de accionamiento magnético y doble sentido *Micropump*®-*GA-V21.PFS.M* accionada por un motor *I-drive* (P-2) (*Micropump*, Estocolmo, Suecia). La presión transmembrana (*TMP*) se mide mediante un transductor de presión (PI-1) (*Sensotech*, Barcelona, España) y la señal se registra en el sistema de control. El módulo dispone de un tubo central con varios orificios situados en la base, que permiten la salida del aire de limpieza. El aire se introduce mediante un compresor MK-10 (B-1) (*Secoh*, Shanghái, Japón). Tanto el caudal como la frecuencia de aireación se regulan a través de un controlador de flujo másico *Bronkhorst*® *El-Flow* (EV-1) (*Bronkhorst*® *High-Tech*, Ruurlo, Holanda) conectado al sistema de control. Para homogeneizar la suspensión y mantener las condiciones aerobias, se suministra aire mediante un segundo compresor *MK-10* (B-2) (*Secoh*, Shanghái, Japón). El aire se introduce en el fondo del depósito a través de difusores dispuestos de tal manera que abarcan todo el diámetro. El caudal se regula mediante una válvula manual (HV-1) y un rotámetro (FI-2).

El agua residual de alimentación se bombea hasta el depósito de proceso a través de una bomba peristáltica *Masterflex Easy-Load L/S 7518–00* (P-1) (*Cole-Parmer Instrument Co.,* Vernon Hills, IL, EE. UU.). Esta bomba se acciona mediante un controlador de nivel *HSE-20987* (LC-1) (Aeman, España).

La instalación dispone de un depósito de permeado de 0,5 L, de vidrio, necesario para la realización de los retrolavados. Este depósito tiene un rebose lateral, que permite recircular el exceso del permeado al depósito de proceso. Asimismo, del depósito se extrae la cantidad específica de permeado para mantener el tiempo de retención hidráulico (*HRT*) en los valores preestablecidos. Para ello se utiliza

una bomba peristáltica *Masterflex L/S 7518-00* (P-3) (*Cole-Parmer Instrument Co.*, Vernon Hills, IL, EE. UU.).

El depósito de proceso se ilumina bajo una irradiación de 300 µmol/(m^2·s), medida en la superficie del depósito de proceso (irradiancia PAR usando un medidor de irradiancia, *QSP2150A, Biospherical Instrument Inc.*, EE. UU.). Las fases de luz y oscuridad se controlan mediante un temporizador.

Para el control de la unidad de filtración se utiliza el software *DAQ Factory* (*AzeoTech® Inc.*, Ashland, OR, EE. UU.), el cual permite procesar la información para la visualización y controlar las variables de filtración.
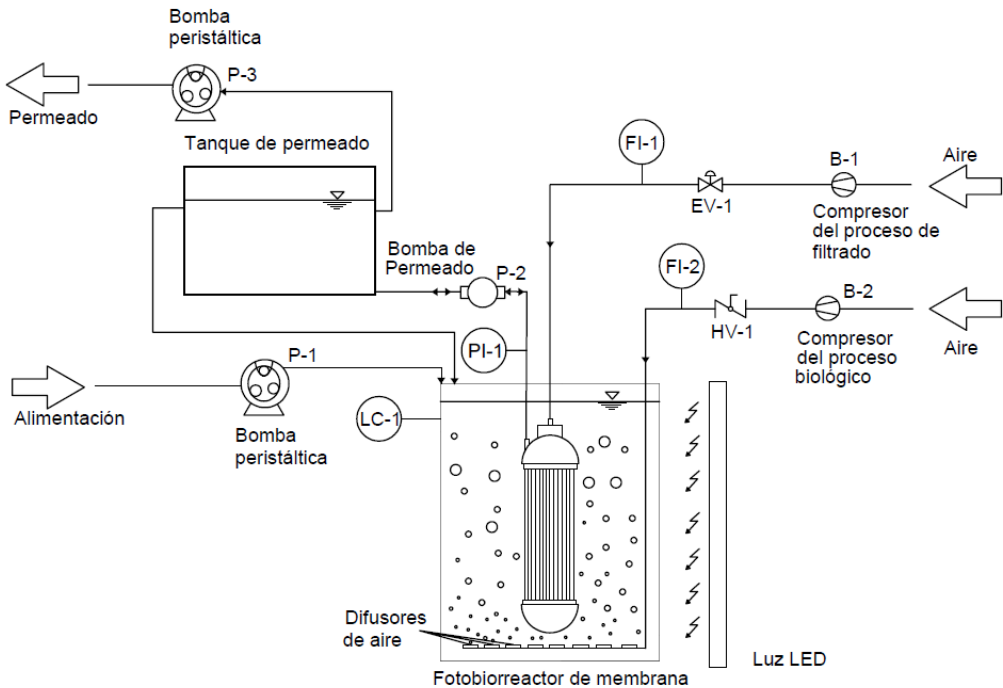
Figura 3.1. Instalación experimental del módulo de membrana estática.

1.2. Módulo de membrana rotativa

La instalación experimental ha sido la misma que la utilizada en los ensayos con la membrana estática, pero con una modificación del módulo empleado (Figura 3.2). En este caso, se incorpora un tubo de cobre de 10 mm que se une al cabezal superior y por cuyo interior se hace circular el permeado. El tubo va conectado a un agitador *Heidolph RZR 2020* (M-1) (*Heidolph Instruments GmbH & Co.,* Schwabach, Alemania) que permite el giro del conjunto. El resto de características básicas de la unidad experimental se mantienen. En estos ensayos no se suministra aire para la homogeneización de la suspensión.
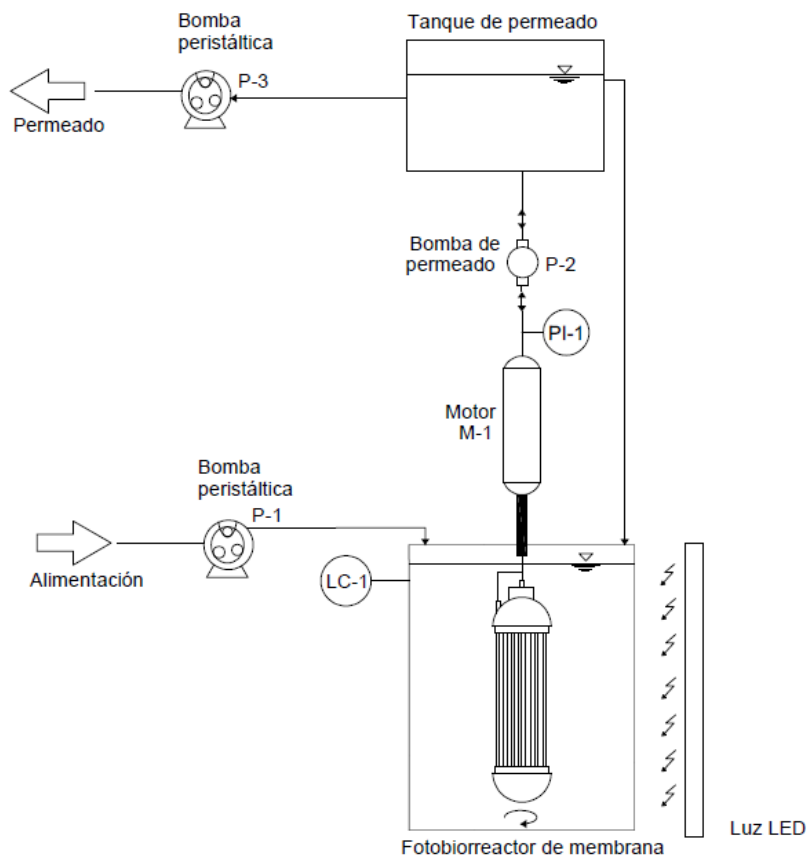
Figura 3.2. Instalación experimental del módulo de membrana rotativa.

2. Metodología experimental

2.1. Procedimiento experimental

En las series experimentales que se llevaron a cabo durante el desarrollo de la presente tesis doctoral se variaron los siguientes parámetros:

Condiciones de operación
- Tiempo de residencia hidráulico (HRT)
- Tiempo de retención de solidos (SRT)
- Fotoperiodo

Agua de alimentación
- Efluente secundario
- Efluente primario

Módulo de membrana
- Estática
- Rotativa

En la Tabla 3.1 se resumen los valores de las condiciones experimentales estudiadas en los diferentes capítulos de esta tesis.

Asimismo, durante cada ensayo se han medido los siguientes parámetros:

Alimentación y permeado
- Demanda química de oxígeno (COD)
- Carbono orgánico total (DOC)
- Compuestos nitrogenados: nitrógeno amonio ($N-NH_4^+$), nitrógeno nitrito ($N-NO_2^-$) y nitrógeno nitrato ($N-NO_3^-$)
- Fósforo fosfato ($P-PO_4^{3-}$)
- pH
- Turbidez
- Concentración de sólidos suspendidos totales (SST)*
- Determinación de *Escherichia coli* y *Legionella spp.***

*solo se miden la alimentación; **solo se determinan en el permeado

Suspensión biológica
- Concentración de sólidos suspendidos totales (MLSS)
- Carbono orgánico total en filtrado (DOC)

- Distribución de tamaño de partículas
- Solidos suspendidos en el sobrenadante ($(MLSS)_s$)
- Turbidez en el sobrenadante

Adicionalmente, la suspensión biológica se caracterizó mediante las siguientes técnicas analíticas:

- Análisis elemental (C, N, H y S)
- Análisis termogravimétrico
- Espectroscopia infrarroja por Transformada de Fourier
- Identificación de las especies microorganismos fotosintéticos y superiores

Para el análisis del proceso de filtración, se utilizaron dos tipos de ensayos: escalonados de corta duración y ensayos de larga duración. Además, al final de cada ensayo de larga duración se aplicó un protocolo específico de limpieza para caracterizar el ensuciamiento obtenido.

Tabla 3.1. Condiciones experimentales de los ensayos realizados en los capítulos 4, 5 y 6 de la presente tesis doctoral.

Capítulo	Experimento	Módulo	Alimentación	HRT (d)	SRT (d)	Fotoperiodo (h / h)
4	Control	Estática	ES	0,75	40	0/24
	MPBR-1	Estática	ES	0,75	20	12/12
	MPBR-2	Estática	ES	0,75	40	12/12
	MPBR-3	Estática	ES	0,75	80	12/12
	MPBR-4	Estática	ES	2	80	12/12
	MPBR-5	Estática	ES	5	80	12/12
5	Control	Estática	ES	0,75	80	0/24
	12/12	Estática	ES	0,75	80	12/12
	16/8	Estática	ES	0,75	80	16/8
	24/0	Estática	ES	0,75	80	24/0
6	R-Control	Rotativa	EP	2	80	0/24
	R-MPBR-1	Rotativa	EP	2	80	12/12
	R-MPBR-2	Rotativa	EP	5	80	12/12
	R-MPBR-3	Rotativa	EP	3,5	80	12/12

Nota: ES: Efluente procedente de un tratamiento secundario de aguas residuales; EP: efluente procedente de un tratamiento primario de aguas residuales.

2.2.   *Fase de desarrollo inicial de la biomasa*

Al inicio de cada ensayo, se rellena la instalación experimental con agua de alimentación y se inicia la fase de desarrollo de la biomasa. Se opera de manera continua bajo el HRT preestablecido según la serie experimental. Una vez transcurrido un tiempo igual al seleccionado como tiempo de retención de sólidos (*SRT*), se considera finalizada la fase de desarrollo inicial. Durante este periodo, se realizan analíticas completas de alimentación, suspensión y permeado tres veces por semana. Posteriormente, el sistema se purga de manera manual para mantener el SRT en el valor seleccionado.

Al no utilizar inóculo, se permite el crecimiento de las especies indígenas para las diferentes condiciones de operación utilizadas.

2.3.   *Ensayos de filtración escalonados de corta duración*

Los ensayos de filtración escalonados se realizaron en las unidades experimentales previamente descritas. Se utilizaron las suspensiones biológicas desarrolladas en cada condición experimental. Adicionalmente, se analizaron los respectivos sobrenadantes obtenidos tras 30 minutos de decantación de las suspensiones.

2.3.1.   Módulo de membrana estática

El flujo de permeado se incrementó desde 8 L/(h·m^2) hasta 40 L/(h·m^2) en incrementos de 2 L/(h·m^2). El tiempo de filtración en cada escalón fue de 15 minutos. Entre cada escalón se aplicó un retrolavado durante 30 s a un flujo de 30 L/(h·m^2). Durante la fase de filtración se aplicó aireación intermitente con ciclos de encendido/parada de 10 s/30 s a un caudal de 5 NL/min, y durante el retrolavado, aireación continua a 5 NL/min. Tras la finalización de cada ensayo, la membrana fue sometida a una limpieza química con NaClO (500 mg/L) durante 24 h.

Se midió el ensuciamiento reversible como velocidad de ensuciamiento (r_f), dado como la variación de la presión transmembrana (TMP) con el tiempo, (*dTMP/dt*).

2.3.2.   Módulo de membrana rotativa

Los ensayos se realizaron con valores de flujo desde 6 L/(h·m^2) hasta 30 L/(h·m^2), en escalones de flujo de 1 L/(h·m^2). El tiempo de filtración de cada escalón fue de

15 minutos. Entre cada escalón se aplicó un retrolavado durante 30 s a un flujo de 30 L/(h·m²). La unidad operó sin giro durante la fase de filtración y con giro continuo a 260 rpm durante el retrolavado.

De la misma manera que en el módulo estático, el ensuciamiento se analizó mediante la velocidad de ensuciamiento.

2.4. *Ensayos de filtración de larga duración*

Como en los ensayos escalonados, estos experimentos se realizaron en las unidades previamente descritas. También se utilizaron las suspensiones biológicas obtenidas después del periodo inicial de desarrollo.

2.4.1. Módulo de membrana estática

Los ensayos se realizaron a un flujo de permeado constante de 10 L/(h·m²). La instalación operó mediante ciclos consecutivos de filtración y retrolavado, con duraciones de 450 s y 30 s, respectivamente. El flujo de retrolavado se fijó en 30 L/(h·m²). Para la limpieza del módulo, se aplicó un caudal intermitente de aire con ciclos de encendido/parada de 10 s/30 s a 5 NL/min. El caudal de homogenización se fijó en 1 L/min y los ensayos se realizaron a temperatura ambiente (20 ± 2 °C).

El ensuciamiento de la membrana se determinó por medio de la evolución de la presión transmembrana tras los ciclos de filtración/retrolavado. Durante la fase de filtración, esta evolución puede ser descrita mediante la ecuación 1:

$$TMP = \ TMP_i + \ r_f \cdot t \ (1)$$

donde TMP_i es la presión transmembrana al inicio de cada ciclo de filtración, r_f es la velocidad de ensuciamiento reversible y t es el tiempo transcurrido.

El ensuciamiento residual que no es eliminado mediante el retrolavado se mide mediante el seguimiento de la TMP_i a lo largo de los ciclos de filtración. La ecuación [1] asume que la velocidad de ensuciamiento es constante a lo largo de un ciclo de filtración, lo que implica la formación de una torta incompresible en la pared de la membrana.

2.4.2. Módulo de membrana rotativa

Las condiciones de filtración y retrolavado fueron las mismas que las utilizadas con el módulo de membrana estática: flujo de permeado de 10 L/(h·m²), flujo de retrolavado de 30 L/(h·m²) y ciclos de filtración/retrolavado de 450 s/30 s,

respectivamente. En este caso, la unidad operó sin giro durante la fase de filtración y el agitador solo era accionado durante la fase de retrolavado, con un giro continuo a 260 rpm. Adicionalmente, se realizaron limpiezas físicas una vez por semana, llevando a cabo un periodo de relajación (cese de filtración) durante 5 minutos con agitación continua del módulo a 260 rpm. No se aplicó aireación para la homogeneización y los ensayos se realizaron a temperatura ambiente (20 ± 2 °C).

El seguimiento del ensuciamiento se efectuó siguiendo el mismo método que en el estudio con módulo estático.

2.5.   Protocolo de limpieza de la membrana

2.5.1. Módulo de membrana estática

Tras la finalización de cada ensayo de filtración, la membrana fue sometida a un protocolo de limpieza con el fin de caracterizar las diferentes fracciones del ensuciamiento depositado sobre ella. En primer lugar, se aplicó agua a presión sobre la membrana. Tras esto, la membrana fue sumergida en una solución de NaClO (500 mg/L) durante 24 h y, por último, se volvía a sumergir en una disolución de ácido cítrico (6 g/L) durante 2 h. Al inicio y tras cada uno de estos pasos, la membrana era sumergida en agua limpia y se medía la presión transmembrana filtrando a 10 L/(h·m^2). De esta manera, se obtenía inicialmente, la presión transmembrana de la membrana sucia (TMP_f), tras el primer paso, la TMP tras limpieza con agua a presión (TMP_{rinse}), tras el segundo, la $TMP_{oxidant}$ y tras el último, TMP_{acid}, respectivamente. Todas las medidas de presión transmembrana se tomaron transcurridos 4 minutos de filtración.

La resistencia hidráulica de cada fracción se calculó mediante el modelo de resistencias en serie:

$$TMP_{ci} = J \cdot \mu \cdot (R_m + R_{ci})   \quad (2)$$

donde J es el flujo de permeado, μ es la viscosidad del permeado, R_m es la resistencia de la membrana y TMP_{ci} y R_{ci} son la presión transmembrana y la resistencia del ensuciamiento de cada etapa de limpieza, respectivamente.

2.5.2. Módulo de membrana rotativa

El protocolo de limpieza de la membrana rotativa contempló un primer paso en el que se sumergió la membrana en un recipiente con agua limpia y se hizo girar a 260 rpm durante 5 minutos. El resto de los pasos a seguir en el protocolo de limpieza para la membrana rotatoria fue similar a los seguidos para la limpieza de membrana estática.

2.6. *Métodos analíticos*

Demanda Química de Oxígeno (COD): se ha realizado mediante el método 5220 D [1]. Para la medida por colorimetría se utilizó un espectrofotómetro *DR-5000 Hach* (*Hach*, EE. UU.)*.

Carbono orgánico disuelto (DOC): se llevó a cabo mediante el método 5310 B [1], de combustión-infrarrojo, en el que la muestra es inyectada en una cámara de reacción donde se encuentra un catalizador oxidante. Para evitar las interferencias ocasionadas por la presencia de carbonatos y bicarbonatos de la muestra, esta fue ligeramente acidificada antes de la combustión. El medidor que se utilizó es el medidor *TOC-5000A* (*Shimadzu*, Japón). Las muestras de alimentación y de las suspensiones biológicas eran previamente filtradas por un filtro de nitrocelulosa (*Millipore*, Alemania) de 0,45 µm de diámetro nominal de poro.

Agregados biopoliméricos (BPCs): el contenido en BPCs de las suspensiones se obtuvo por diferencia entre el valor del DOC entre la suspensión biológica y el permeado.

Nitrógeno amoniacal: se realizó mediante el método Nessler (8038, Hach) utilizando un espectrofotómetro *DR-5000 Hach* (*Hach*, EE. UU.)*.

Determinación aniónica (N-NO$_2^-$, N-NO$_3^-$ y P-PO$_4^{3-}$): se realizó en un cromatógrafo iónico (*Metrohm Compact IC 882, Metrohm*, Suiza) siguiendo el método 4110 C [1].

Determinación del contenido en sólidos suspendidos totales en el licor mezcla (MLSS): se realizó filtrando la muestra a través de filtros de nitrocelulosa de diámetro nominal de poro de 0,45 µm (*Millipore*, Alemania) según lo establecido en el método 2540 D [1].

Determinación del contenido en materia volátil: se llevó a cabo por análisis termogravimétrico utilizando el Analizador Térmico Simultáneo *TG/DSC Discovery SDT 650* (*TA Instruments*, EE. UU.) disponible en el Servicio de Análisis Térmico del Servicio General de Apoyo a la Investigación de la Universidad de La Laguna (SEGAI-ULL) y se obtuvo como el porcentaje de materia que se había volatilizado tras el calentamiento de la muestra hasta los 550 °C.

Turbidez de la alimentación y del permeado: se llevó a cabo mediante el método 2130 [1], utilizando el turbidímetro *Hach 2100D* (*Hach*, EE. UU.) expresando el resultado en unidades nefelométricas de turbidez (NTU).

Turbidez del sobrenadante de las suspensiones biológicas: se realizó por el mismo método que la medida de la turbidez del permeado y de la alimentación, pero, en este caso, se midió la turbidez del sobrenadante de la suspensión biológica obtenido tras decantación durante 30 minutos.

Distribución de tamaño de partículas: se llevó a cabo mediante difracción de luz láser utilizando para ello el equipo disponible en el Laboratorio de Caracterización de Partículas y Microsuperficies perteneciente al SEGAI-ULL, *Mastersizer 2000* (*Malvern Instruments Ldt.*, Reino Unido), haciendo uso del accesorio *Hydro SM* que permite realizar la medida mediante vía húmeda.

Concentración de oxígeno disuelto (DO) en el biorreactor: se llevó a cabo mediante el uso del oxímetro *Hach HQ40d* (*Hach*, EE. UU.).

Temperatura en el fotobiorreactor: se tomó el valor aportado por el oxímetro *Hach HQ40d* (*Hach*, EE. UU.).

Análisis elemental: el contenido en carbono, hidrógeno, nitrógeno y azufre de las muestras de suspensiones biológicas se llevó a cabo mediante el Analizador Elemental *Flash EA 1112* (*ThermoFisher Scientific*, EE. UU.) disponible en el Servicio de Análisis Elemental perteneciente al SEGAI-ULL, que oxida por completo la muestra, generando gases de combustión que son transportados por un gas portador (Helio) hasta un tubo de reducción y posteriormente separados en columnas cromatográficas. Se realiza una desorción térmica y los gases ya separados, pasan por un detector de conductividad térmica. Previamente, las muestras fueron secadas al aire a temperatura ambiente, durante al menos una semana y sometidas a un secado posterior a 100 °C durante 1 hora para eliminar cualquier resto de humedad que pudiera interferir en la medida.

Análisis termogravimétrico/calorimetría diferencial de barrido: el análisis termogravimétrico se realizó de manera simultánea a la calorimetría diferencial de barrido en el Analizador Térmico Simultáneo *TG/DSC Discovery SDT 650* (*TA Instruments*, EE. UU.) disponible en el Servicio de Análisis Térmico perteneciente al SEGAI-ULL. Este equipo permite analizar de manera simultánea la pérdida de masa por descomposición cuando una muestra se va calentando y el cambio de entalpía de una muestra en función de la temperatura, consiguiendo, de esta manera distinguir eventos térmicos que sufra la muestra sean dependientes o no de la temperatura. Para llevar a cabo el análisis, las muestras fueron previamente secadas al aire a temperatura ambiente durante al menos una semana y secadas posteriormente a 100 °C durante al menos 1 hora. Cierta cantidad de muestra fue depositada en un crisol de platino y calentada desde los 25 °C hasta los 600 °C con una velocidad de calentamiento de 15 °C/min utilizando como gas portador nitrógeno (*Alphagaz nitrogen gas*, *Air Liquid*, Francia) que se hizo circular a un caudal de 50 mL/min.

Espectroscopía Infrarroja por Transformada de Fourier (FTIR): se llevó a cabo en el Espectrómetro *Bruker IFS 66/S* (*Bruker*, EE. UU.) disponible en el Servicio de Espectroscopía Infrarroja perteneciente al SEGAI-ULL mediante reflectancia total atenuada (ATR) que midió la transmitancia de las muestras en el intervalo de longitudes de onda entre los 900 cm^{-1} y los 4000 cm^{-1}.

Identificación de las especies de microalgas presentes en las suspensiones biológicas: se realizó en un microscopio óptico (*DM750*, *Leica*, Alemania) y se compararon las imágenes obtenidas con el *Water Organisms Atlas Manual* [2].

Determinación de *Escherichia coli* y *Legionella spp.* en el permeado: se llevó a cabo por el método establecido en la Norma UNE-EN ISO 9308 y UNE-EN ISO 11731, respectivamente, de acuerdo con la legislación vigente.

Referencias

[1]   APHA, Standard Methods for the Examination of Water and Wastewater, 21st ed., Washington DC, USA, DC, USA, 2005.

[2]   S.G. Berk, J.H. Gunderson, Wastewater Organisms A Color Atlas, 1st Editio, CRC Press, Florida, USA, 1993.

CAPÍTULO 4

Tratamiento de un efluente secundario con un fotobiorreactor de membrana a altos tiempos de retención de sólidos

ÍNDICE:

Tratamiento de un efluente secundario con un fotobiorreactor de membrana a altos tiempos de retención de sólidos

E. Segredo-Morales, E. González, C. González-Martín, L. Vera

HIGHLIGHTS

- Long solid retention times avoid biopolymer clusters accumulation.
- Moderate nutrient removal affected by influent fluctuations was reported.
- Reversible and residual fouling are related to biopolymer clusters.
- Membrane fouling has been effectively controlled at long solid retention times.
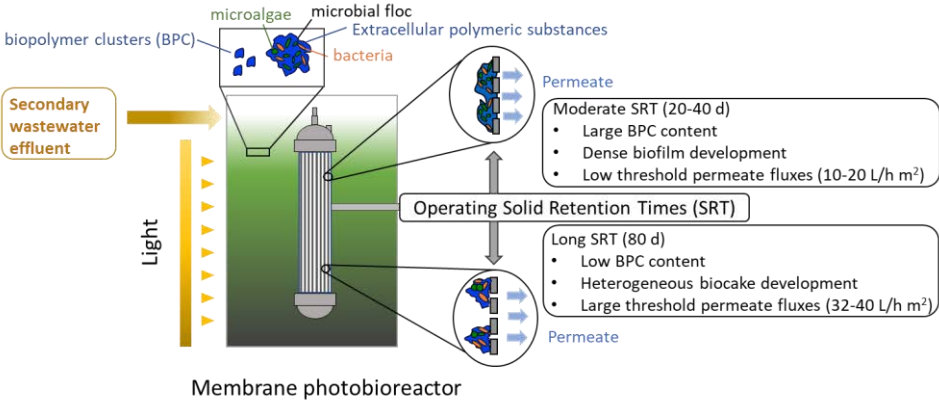
RESUMEN

De manera similar a otros procesos con membranas, el ensuciamiento es el factor limitante en la aplicación generalizada de la tecnología de fotobiorreactores de membrana (MPBR), siendo la principal causa de los costes de inversión y operación. Entre las variables que determinan el ensuciamiento, los parámetros de la suspensión juegan un papel fundamental. Entre estos, los más estudiados en la literatura son las sustancias solubles microbianas (SMP), los agregados biopoliméricos (BPC) y las bacterias o microalgas dispersas. Una estrategia para reducir el impacto de estos parámetros es operar a elevados tiempos de retención se sólidos (SRT), permitiendo el desarrollo de un cultivo mixto de microalgas-bacterias adecuado para la biofloculación. Al mismo tiempo, al permitir el crecimiento de bacterias heterótrofas, se reduce la acumulación de SMPs y, en consecuencia, de BPCs. En la literatura, son escasos los estudios en estas condiciones, debido a que el desarrollo de la tecnología se ha centrado principalmente en optimizar la productividad de biomasa y el rendimiento de eliminación de nutrientes. Por ello, los valores habituales de SRT en la operación de estos sistemas se encuentran entre 2 y 25 días.

En este capítulo se analizó el efecto de operar a valores elevados de SRT (20, 40 y 80 días) sobre el comportamiento de un MPBR. El objetivo fue establecer un valor óptimo para la biofloculación, impidiendo la acumulación de biopolímeros y minimizando el ensuciamiento de la membrana. El estudio se realizó sin inóculo, permitiendo el crecimiento de un cultivo mixto algas-bacterias indígenas. Con el objeto de optimizar la eliminación de nutrientes, se modificó el tiempo de retención hidráulico (HRT) entre 0,75 y 5 días en las condiciones óptimas de SRT. Asimismo, los resultados se compararon con los obtenidos en un ensayo control, en el que se evitó el crecimiento de microalgas mediante la ausencia de luz. Para analizar el ensuciamiento de la membrana, se realizaron estudios de determinación de flujo umbral, así como, ensayos de larga duración. Estos últimos resultan clave en el análisis de la operatividad del proceso. La información obtenida se complementó con el seguimiento de la eficacia en la eliminación de nutrientes, la productividad de la biomasa, las principales características de la suspensión biológica y la estructura de la comunidad de microalgas.

Los resultados experimentales mostraron un aumento significativo de la productividad de la biomasa en el MPBR frente a la condición control (aproximadamente 11 veces), lo que se debe al adecuado crecimiento de microrganismos fotosintéticos (principalmente microalgas) en las condiciones de operación. Tanto el SRT como el HRT determinaron la producción y concentración de biomasa en el sistema. La producción disminuyó significativamente de 43,7 a 22,1 mg/(L·d) al aumentar el SRT desde 20 a 80 días. Al mismo tiempo, un incremento del HRT desde 0,75 a 5 días aumentó un 27% la producción de biomasa. Cabe destacar que para el valor de SRT de 80 días se obtuvieron las mayores concentraciones de biomasa (en el rango 1770-2250 mg/L, de acuerdo con el HRT seleccionado). Estos valores son sensiblemente superiores a los encontrados en estudios previos (< 1000 mg/L), lo que supone una ventaja de las condiciones de operación utilizadas, al disminuir los costes de gestión de la biomasa.

Por otra parte, las condiciones de operación también afectaron a las características de la suspensión. Los análisis termogravimétrico y elemental confirmaron el mayor contenido en sustancias poliméricas extracelulares en la biomasa procedente del MPBR en relación al ensayo control, reflejando la obtención de una mejor y más amplia biofloculación. Estos resultados fueron confirmados por los análisis de distribución de tamaño de partículas, donde el tamaño medio de los flóculos en MPBR estuvo comprendido entre 75,3 y 129,8 µm frente al valor de 40,2 µm obtenido en el ensayo control. Además, el análisis por espectroscopía infrarroja mostró una mayor relación de carbohidratos-proteínas en las suspensiones procedentes del MPBR.

En relación al rendimiento de depuración, analizado principalmente en términos de eliminación de nutrientes, se observó una mejora apreciable en el MPBR respecto al ensayo control. Al analizar la influencia de las diferentes condiciones, se concluyó que se requiere un valor de HRT entre 2 y 5 días para obtener una moderada eliminación de nutrientes (40,6-48,7% y 18,5-34,7% para el nitrógeno inorgánico soluble y los fosfatos, respectivamente).

Cuando se analizó el ensuciamiento de la membrana, tanto en ensayos de determinación de flujo umbral como en los de larga duración, de manera general, el MPBR mostró menor grado de ensuciamiento, salvo en el ensayo a HRT de 0,75 días y SRT de 40 días, en la que el contenido en BPCs fue especialmente alto (32,4

mg/L). Las condiciones óptimas de filtración se obtuvieron para un SRT de 80 días y un HRT de 5 días.

En todas las condiciones se observaron microalgas verdes pertenecientes a los géneros *Chorella* y *Scenedesmus* y diatomeas de los géneros *Nitzschia* y *Navicula*, lo que confirmó una alta productividad de estas especies, así como una adecuada tolerancia a los contaminantes presentes en las aguas residuales. En menor proporción y sólo en algunas condiciones, aparecieron cianobacterias del género *Oscillatoria*.

Abstract

Microalgal-bacterial membrane photobioreactors (MPBRs) have recently emerged as a new sustainable technology in wastewater treatment. For advanced treatment of domestic secondary effluents, selecting long solids retention times (SRTs) may be crucial to achieve optimal community structure and therefore, process performance. This study assesses the effects of operating conditions on nutrient removal, biomass productivity, suspension characteristics and membrane fouling. A lab-scale MPBR was run during long-term tests to assess process stability. Indigenous microalgae-bacteria consortia were developed for each condition. Conventional membrane bioreactor was used for tested control condition. Experimental results showed the crucial role of extending SRT to 80 d to enhance bioflocculation, avoid biopolymer clusters accumulation and minimize membrane fouling rates. Despite influent fluctuations, optimal hydraulic retention time value between 2 and 5 d was necessary to achieve moderate nutrient removal (40.6-48.7% and 18.5-34.7% for nitrogen and phosphorus, respectively). A mixed microalgal structure of green microalgae, cyanobacteria and diatoms was also achieved.

Keywords: Biopolymer clusters, membrane fouling, membrane photobioreactor, microalgae-bacteria consortia, nutrient removal.

1.   Introduction

Integration of microalgae-bacteria consortia into membrane photobioreactors (MPBRs) has recently been explored as a sustainable technology for nutrient

removal from wastewater [1]. The use of microalgae-bacteria systems offers remarkable reductions in nutrient removal costs associated with wastewater treatment [2]. It is well recognized that symbiotic interactions between microalgae and bacteria exhibit better performance with low C/N ratio wastewaters [1,3]. This includes greater nitrifying bacteria population, lower external oxygen demand and direct bioflocculation [4,5]. Consequently, nutrient removal through an algae-bacteria consortium is especially suitable for the treatment of secondary wastewater effluents. Furthermore, the residual biomass produced can be reused for production of bioenergy, animal feedstock or other high-value products [6].

Although the advantages offered by microalgae-bacteria consortia have been demonstrated, there are few studies that have cultured native consortia for real wastewater treatment purposes. Most studies have been performed with inoculated mixed cultures, which may not be representative of native wastewater microbial communities [7]. Another issue to be considered is process stability over long periods with variable wastewater compositions. In this sense, several studies have demonstrated the difficulty to maintain inoculated cultures during wastewater treatment [8,9].

As stated, MPBRs have been considered an emerging option capable of achieving high nutrient removal, complete biomass retention and high-quality permeate [10]. One of the main advantages of the technology is decoupling hydraulic and solid retention times (HRT and SRT, respectively), which allows higher biomass concentration and nutrient load, and thus reduces process footprint [11]. Typical HRT values reported in the literature range between 1 and 5 d, where the optimum mainly depends on nutrient load [12,13]. Another essential parameter that affects process performance is SRT. While short times enhance biomass growth, longer SRTs generally increase microbial diversity, biomass concentration and bioflocculation [1]. Due to self-shading effect and possible nutrient limitation at large biomass concentration, SRT is typically limited to low to moderate values (2-25 d) to avoid microalgae growth inhibition [10,11]. Nevertheless, although studies at longer SRT are limited, some authors have reported an efficient process performance. Sheng et al. observed low biomass productivity (11-17 mg·L^{-1}·d^{-1}) and high nutrient removal (>95% and >70%, for nitrogen and phosphorus, respectively) at SRT of 60 d [14]. Another study showed a considerable

productivity (50-167 mg·L^{-1}·d^{-1}) and also optimal nutrient removal at very large SRT (> 200 d) [15].

However, a major constraint to this technology's development on a large scale is membrane fouling, which decreases permeate productivity and raises treatment costs [16]. Preliminary cost analysis indicates that fouling control accounts for up to 57% of operating and maintenance costs [14]. The rate and extent of fouling is influenced by the microbial suspension properties, mainly composed of organic biopolymers, inorganic colloids, cells, cell debris and microbial flocs [17]. In pure microalgae MPBRs, large biopolymers (often associated with algal-derived organic matter, AOM) and small size flocs have been related to severe membrane fouling [18,19]. This can be partially overcome by symbiotic systems, where bacteria can use AOM as carbon source for growth and also promote microalgae aggregation [20]. Membrane fouling is crucially affected by SRT due to its influence over microbial structure, AOM production and bioflocculation. Recent research has shown that increasing SRT from 10 to 30 d decreased membrane fouling as a consequence of changes on the floc size and micromorphology of the microalgal-bacterial flocs [21]. However, as most of MPBR literature is mainly limited to low to moderate SRT values, filtration performance at long SRT is yet to be investigated.

Based on the above considerations, this study prime novelty contribution is the evaluation of the performance of an MPBR operated at long SRT (> 20 d). This is higher than that typically adopted, with the aim to define favourable conditions for improving bioflocculation, avoiding biopolymers accumulation and minimizing membrane fouling. Moreover, there are only a few studies that have cultured native consortia from real secondary effluents, which determines the stability of the microbial consortia and therefore, the technical feasibility of the treatment process. Additionally, deep studies assessing membrane fouling, particularly residual fouling during long-term tests, are scarce. This study provides fundamental information of process performance by monitoring nutrient removal efficiency, biomass productivity and main suspension characteristics, microalgae community structure and membrane fouling rates.

2. Materials and methods

2.1. Feedwater

Experimental unit was fed with an effluent from a conventional activated sludge domestic wastewater treatment plant (Santa Cruz de Tenerife, Canary Island, Spain). This plant was designed for only carbon removal forty years ago. Values measured for the different parameters were the chemical oxygen demand (COD), dissolved organic carbon (DOC), ammonium-nitrogen (NH_4^+-N), total nitrogen (TN) and phosphate-phosphorus (PO_4^{3-}-P): 30-109 mg/L, 12.55-48.10 mg/L, 2.18-39.98 mg/L, 6.82-43.61 mg/L and 0.13-13.59 mg/L, respectively. Finally, it presented an average pH of 8.1 with a medium salinity (1390 $\mu S \cdot cm^{-1}$).

2.2. Experimental unit

The laboratory unit consisted of a 3.0 L capacity tank equipped with a ZeeWeed® ZW-1 hollow fiber membrane module (Suez Water Technologies & Solutions, Ontario, ON, Canada) (Figure 1). ZW-1 was made of PVDF with a nominal pore size of 0.04 μm and a filtration surface of 0.047 m^2. The permeate was extracted by a magnetic drive gear pump (Micropump-GA Series, Stockholm, Sweden) applying a slight vacuum. The experiments were carried out at a constant permeate flux of 10 $L \cdot h^{-1} \cdot m^{-2}$, measuring the transmembrane pressure (TMP) with a pressure sensor (Sensotech, Barcelona, Spain). This permeate flux value was within the typical range reported in the literature (2.6-15 $L \cdot h^{-1} . m^{-2}$) [11]. The unit operated with intermittent aeration 10/30 s on/off at 5 $NL \cdot min^{-1}$. For mixing and to maintain similar aerobic conditions in all the tests, air was supplied at a flow rate of 1 $NL \cdot min^{-1}$ injected at the bottom of the tank. The filtration was conducted under temporized mode, with filtration/backwashing cycles of 450/30 s. The backwash flux was set at 30 $L \cdot h^{-1} \cdot m^{-2}$. During backwashing, air was continuously applied at 5 $NL \cdot min^{-1}$. To control the laboratory unit, DAQ Factory software (AzeoTech® Inc., Ashland, OR, USA) was used, which allows the information to be processed for visualization and control filtration variables. The permeate was collected in a tank from which the specific amount of permeate was extracted by a peristaltic pump (Cole-Parmer Instrument Co., USA) to maintain the HRT at the pre-established values. Tests were carried out at room temperature (20±2 °C) and the duration of the experimental tests was 1000 h. All experimental tests were carried out under

constant irradiation of 300 µmol/m²s measured at the surface of the photobioreactor (PAR irradiance using an irradiance meter, QSP2150A, Biospherical Instrument Inc., USA) in 12/12 h light/dark cycles, except for the control condition in which 0/24 h light/dark was imposed.
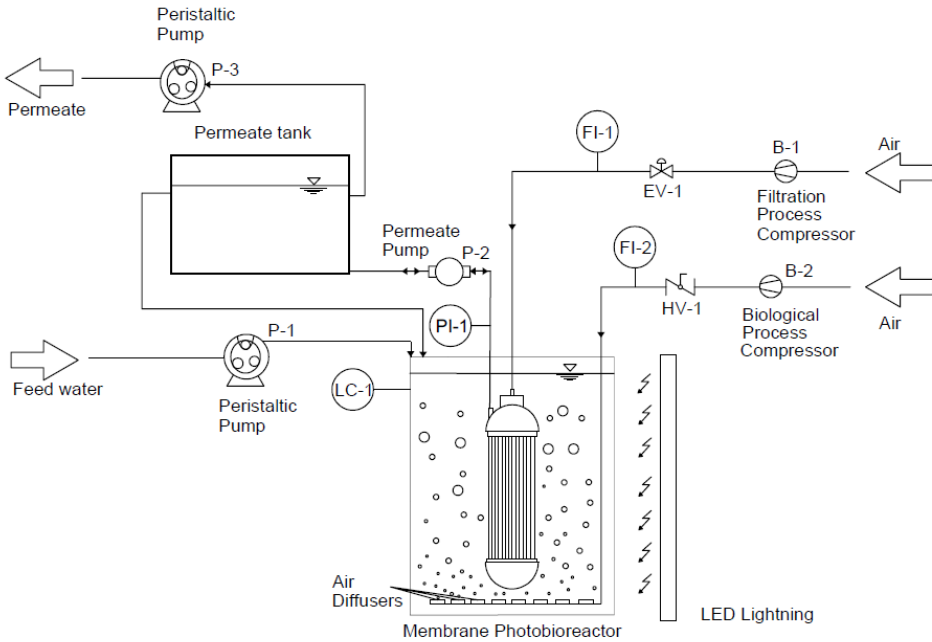
Figura 1. Experimental setup of the MPBR system.

2.3. Experimental conditions

As previously stated, values typically adopted for SRT and HRT in the literature are between 5 and 30 d, and between 6 h and 8 d, respectively [10,11]. In accordance with the main objective of the study, longer SRTs were selected (20-80 d), based in a previous study with a conventional MBR treating the same secondary effluent [22]. For each condition, the unit started without any inoculum and the biomass developed from the indigenous microorganisms existing in the influent. Starting (i.e. acclimation) period lasted for a minimum of the design sludge retention times (20, 40 and 80 d), during which the system operated without biomass purge. Then,

the amount of suspension necessary to maintain SRT values at the desired levels was periodically purged manually. Biomass concentration reached after each start-up phase was close to that maintained during the tests.

Different combinations of SRTs (20, 40 and 80 d) and HRTs (0.75, 2 and 5 d) were assayed in the MPBR unit: MPBR 1 (HRT=0.75 d, SRT=20 d), MPBR 2 (HRT=0.75 d, SRT=40 d), MPBR 3 (HRT=0.75 d, SRT=80 d), MPBR 4 (HRT=2 d, SRT=80 d) and MPBR 5 (HRT=5 d, SRT=80 d). As control condition, SRT of 40 d and HRT of 0.75 d were applied. Samples of feedwater, suspension and permeate were withdrawn three times per week. Suspensions were characterized in terms of mixed liquor suspended solid (MLSS), particle size distribution, supernatant DOC, elemental analysis, thermogravimetric analysis (TGA) and Fourier-transform infrared spectroscopy (FTIR).

The biomass productivity was estimated according to Eq. (1):

$$r_x = \frac{MLSS}{SRT} \qquad (1)$$

2.4. Short-term flux step trials

Short-term flux step experiments were performed by the flux-step method. Parameters were selected according to previous studies [23]. For these experiments, the flux was increased from 8 L·h^{-1}·m^{-2} to a maximum of 40 L·h^{-1}·m^{-2} in steps of 2 L·h^{-1}·m^{-2}. Each step lasted 15 minutes. Aeration and backwashing conditions were the same as those applied in the experimental phases. The filtration time was set at 900 s. After each flux-step run, the membrane was chemically cleaned using a 500 mg·L^{-1} sodium hypochlorite solution. The experiments were carried out on all the suspensions of the experimental phases and on the supernatant obtained after 30 min of decantation.

Results were related to reversible fouling rate (r_f), given by the derivative of the transmembrane pressure (*dTMP/dt*).

2.5. Membrane cleaning protocol

After each experimental phase, the membrane was subjected to a cleaning protocol to characterize the fouling produced during the experiments [24]. Firstly, the fouled membrane module was immersed in tap water to measure the

transmembrane pressure (TMP_f), then the membrane was rinsed with pressurized water and the transmembrane pressure was measured again with tap water (TMP_{rinse}). After this, the membrane was immersed in a 500 mg·L^{-1} sodium hypochlorite solution for 24 h. Then, the transmembrane pressure was measured again with clean water ($TMP_{oxidant}$). Finally, it was immersed in a 6 g·L^{-1} citric acid solution for 2 h. The transmembrane pressure measured after this step was called TMP_{acid}. Each of the transmembrane pressure measurements were made after 4 min of filtration. Resistances were calculated from TMP data according to the resistance in a series model (Eq. (2)):

$$TMP_{ci} = J \cdot \mu \cdot (R_m + R_{ci}) \qquad (2)$$

Where J is the permeate flux, μ is the permeate viscosity, R_m is membrane resistance and TMP_{ci} and R_{ci} are the corresponding post-cleaning step transmembrane pressure and resistance, respectively.

2.6. Membrane fouling characterization

TMP evolution under consecutive cycles of filtration was used to characterize membrane fouling. Reversible fouling was evaluated from the fouling rate data (r_f). Meanwhile, the residual fouling phenomena, which was not removed by backwashing, was measured by the initial transmembrane pressure TMP_i at the beginning of the filtration cycle. Therefore, TMP evolution during the filtration phase can be described by the following equation [23]:

$$TPM = TMP_i + r_f \cdot t \qquad (3)$$

where t is the elapsed time.

2.7. Analytical methods

Chemical oxygen demand (COD) and mixed liquor suspended solids (MLSS) were measured by standard methods [25]. Turbidity was measured using a turbidimeter HACH 2100 N (Hach, USA). DOC was measured by a TOC-meter (TOC-5000A, Shimadzu, Japan). The difference in DOC concentration between the filtered supernatant from the suspension (0.45 µm nitrocellulose membrane filter, HA, Millipore, Germany) and the permeate was considered as biopolymer cluster

(BPC) concentration. The Nessler method was used for NH_4^+-N measurement using a DR-5000 Hach spectrophotometer (Hach, USA). Nitrate-nitrogen (NO_3^--N), nitrite-nitrogen (NO_2^--N), PO_4^{3-}-P were measured through ion chromatography using a Compact IC plus 882 device supplied by Metrohm (Metrohm Switzerland). Particle size distribution was measured using a Malvern Mastersizer 2000 instrument (Malvern Instruments Ltd., UK). For elemental analysis, a FLASH EA 1112 Elemental Analyzer (ThermoFisher Scientific, USA) was used. Thermogravimetric analysis (TGA) was performed using a simultaneous thermal analyzer (TG/DSC): Discovery SDT 650 (TA Instruments, USA). A quantity of biomass was loaded in a platinum crucible and heated between 25 and 600 °C at a heating rate of 15 °C/min under a nitrogen flow of 50 mL/min (Alphagaz nitrogen gas, Air Liquid, France). Fourier-transform infrared spectrometry was performed using an IFS 66/S spectrometer (Bruker, USA) equipped with an ATR accessory that measured the transmittance of the samples in a wavelength range between 900 and 4000 cm^{-1}. Dissolved oxygen and temperature in the bioreactor were measured with an on-line Hach HQ40d oximeter (Hach, USA). Microalgae identification and quantification were carried out by optical microscopy (DM750, Leica, Germany), according to Wastewater Organisms Atlas Manual [26].

3. Results and discussion

3.1. Biomass concentration and productivity

Figure 2 shows biomass concentration and productivity for the control condition, and the MPBR at the different SRTs and HRTs. There was a substantial improvement in biomass productivity (about 11 times) in the MPBR compared with the control one at the same conditions (SRT of 40 d and HRT of 0.75 d). It should be considered that the only difference between both reactors is the lighting regime, therefore, the different productivity should be associated with the presence of microalgae. Due to the characteristics of the feedwater, characterized by a low C/N ratio, severe organic carbon limitation was imposed. Under this condition, heterotrophic bacteria should preferentially meet their maintenance energy requirements instead of producing additional biomass [27]. This can justify the low biomass productivity in control condition. In the MPBRs, microalgae can fix CO_2 during autotrophic growth while secreting organic carbon, mainly as polysaccharides and proteins, which can be used as a carbon source by the

heterotrophs [28]. Accordingly, the synergistic support of bacteria and microalgae enhanced the consortium growth, as previously reported [7].

As can be seen in Figure 2, both SRT and HRT effectively controlled biomass concentration and productivity in the MPBR. Biomass concentration increased with SRT, since the biomass disposal rate decreased to a greater extent than biomass productivity. The decrease in productivity can be attributed to slight attenuation at high biomass concentrations, as reported in a similar study at moderate SRTs [29]. Nevertheless, productivity values varied between 43.7 and 22.1 mg·L^{-1}·d^{-1}, which are comparable with those typically reported in an MPBR at moderate SRTs (4.5-30 d) (20-52 mg·L^{-1}·d^{-1}) [29,30] but higher than those observed at SRT of 60 d (10-17 mg·L^{-1}·d^{-1}) [14]. Results also showed an increase in biomass concentration and productivity by extending HRT. Specifically, an increase in HRT from 0.75 to 5 d resulted in a productivity increase of 27%. This trend seems to contradict some previous studies that reported biomass production is inversely proportional to HRT due to nutrient limitation [12,31]. By contrast, other studies have found a positive effect [14] or only slight differences [13]. In the present study, the symbiotic relationship between microalga and bacteria seems to be enhanced at large HRT.

3.2. Biomass characteristics

Many researchers have highlighted the relevance of free-biopolymers secreted by microalgae-bacteria consortia in biomass flocculation [1] and also in membrane fouling [11]. For this reason, DOC was routinely determined in feedwater, suspension supernatant and permeate. The colloidal fraction of the biopolymers (often called biopolymer clusters, BPC) was estimated from the difference between DOC concentration of the supernatant and the permeate. As showed in Figure 3, there was significant BPC accumulation in the control condition, which was reduced in the MPBR at moderate SRTs (20-40 d) and reached very low concentrations at SRT of 80 d. This clearly indicates that the joint development of microalgae and bacteria enhances the degradation of biopolymers, decreasing the colloidal fraction in the liquid phase. In the range studied, HRT did not have a significant effect. The positive effect microalgae-bacteria consortia in bioflocculation was confirmed by analysis of particle size distribution. Mean value was 40.2 µm for the control condition and ranged between 75.3 and 129.8 µm in

the MPBR (Supplementary data, Table S1). Due to the crucial role of BPC and floc size distribution in membrane fouling, the selection of a long SRT will be essential for the sustainable operation of an MPBR.

Figure 2. Biomass concentration and productivity for the control condition and the MPBR at different HRTs and SRTs. Control: HRT=0.75 d, SRT=40 d; MPBR 1: HRT=0.75 d, SRT=20 d; MPBR 2: HRT=0.75 d, SRT=40 d; MPBR 3: HRT=0.75 d, SRT=80 d; MPBR 4: HRT=2 d, SRT=80 d; MPBR 5: HRT=5 d, SRT=80 d.

A basic biomass characterization was also performed by thermogravimetric and elemental analysis. The former has been used to investigate devolatilization process of biomass samples between 150 °C and 600 °C [32]. Analysis of derivative weight curves (Figure 4) showed significant differences between the samples from the MPBR and the control condition. The curves of the MPBR were wider, covering a range of temperature between 200 and 450 °C, which has been attributed to the thermal degradation of significant amounts of the three main components of the biomass: carbohydrates, proteins and lipids [32]. However, the curve for the control condition was narrower, with a maximum rate of reaction at approximately 275 °C, which could be due to a higher content of proteins compared to carbohydrates [33]. The elemental analysis also seems to support this approach according to the lower C/N ratio observed in the control condition (Table 1). At the same time, the addition of microalgae to the bacteria community

clearly seems to enhance CO_2 fixation, achieving a higher carbon content in the biomass. Consistently, greater volatile matter in the MPBR biomass was obtained (38.3-48.9%) (Table 1). In general, the volatile content is lower than that typically reported in other studies using a synthetic growth medium, but similar to microalgae biomass cultivated in wastewater [34]. This is probably explained by the characteristics of the feedwater used: a secondary effluent water with a medium saline content (average electrical conductivity of 1390 $\mu S \cdot cm^{-1}$). Therefore, thermal degradation and elemental analysis showed a higher biopolymer content in the MPBR biomass, confirming higher bioflocculation ability, which was enhanced at long SRTs.

Figure 3. Dissolved organic carbon (DOC) in feedwater, suspension supernatant and permeate, and biopolymer clusters (BPC) at different operating conditions. Control: HRT=0.75 d, SRT=40 d; MPBR 1: HRT=0.75 d, SRT=20 d; MPBR 2: HRT=0.75 d, SRT=40 d; MPBR 3: HRT=0.75 d, SRT=80 d; MPBR 4: HRT=2 d, SRT=80 d; MPBR 5: HRT=5 d, SRT=80 d.
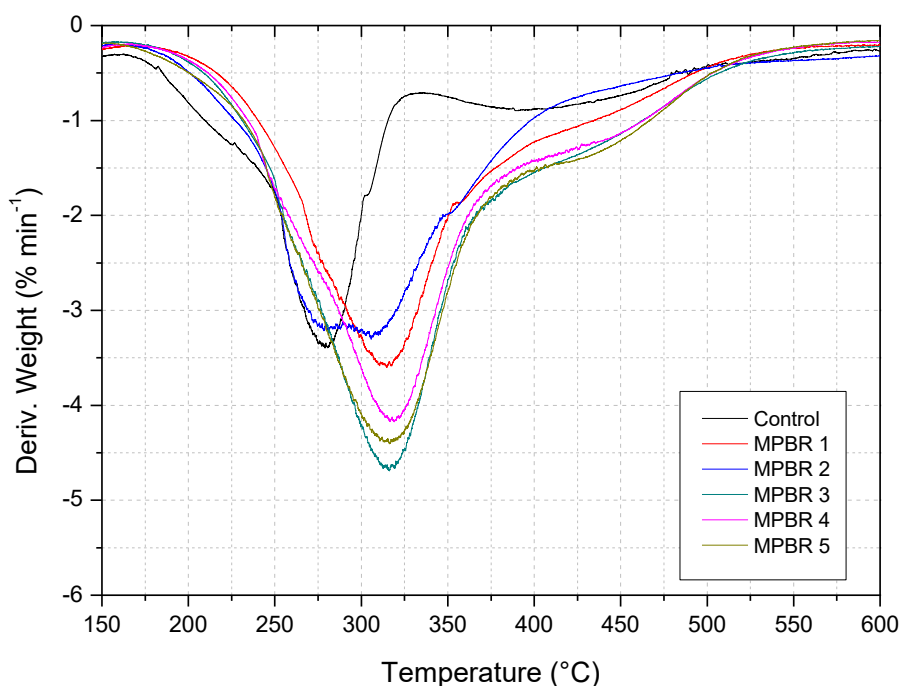
Figure 4. Derivative weight loss curve for the control condition and the MPBR samples. Control: HRT=0.75 d, SRT=40 d; MPBR 1: HRT=0.75 d, SRT=20 d; MPBR 2: HRT=0.75 d, SRT=40 d; MPBR 3: HRT=0.75 d, SRT=80 d; MPBR 4: HRT=2 d, SRT=80 d; MPBR 5: HRT=5 d, SRT=80 d.

Table 1. Volatile matter and elemental composition of MPBR and control condition biomass samples.

	MPBR 1	MPBR 2	MPBR 3	MPBR 4	MPBR 5	Control
Volatile matter[a]						
	38.3 ± 0.8	38.7 ± 1.5	48.9 ± 1.0	43.6 ± 0.6	48.2 ± 0.4	33.8 ± 2.1
Elemental analysis[a]						
C	22.8 ± 0.8	24.9 ± 1.4	26.4 ± 1.0	26.4 ± 0.3	28.3 ± 0.3	5.8 ± 1.5
H	3.6 ± 0.1	3.7 ± 0.2	4.2 ± 0.6	3.7 ± 0.1	4.4 ± 0.1	0.9 ± 0.2
N	4.5 ± 0.3	4.7± 0.7	4.9 ± 0.4	4.5 ± 0.1	5.6 ± 0.2	3.1 ± 0.8

Note: The data are expressed as mean ± standard deviation. [a] (%wt, dry basis)

Biochemical composition has been also studied by analyzing FTIR spectra of biomass samples from the MPBR and the control condition (Figure 5).

Characteristic bands are observed in all cases, presenting peaks of carbohydrates (980-1174 cm^{-1}), nucleic acids (1072-1099 cm^{-1} and 1191-1356 cm^{-1}), proteins (1357-1709 cm^{-1} and 3029-3639 cm^{-1}) and hydrocarbons from lipids (2809-3012 cm^{-1}), comparable with those reported in the literature [35–37]. In particular, a broad region around a peak at 1052 cm^{-1} can be seen, which is attributed to the υ(C-O-C) stretching of carbohydrates [35]. Nucleic acids also have a specific band in this region (υ$_s$(>P=O) stretching of phosphodiesters) and another at 1230 cm^{-1} (υ$_{as}$(>P=O) stretching of phosphodiesters), which can be observed in the spectra of the samples. The presence of proteins was confirmed by peaks at 1643 and 1546 cm^{-1}, representative of υ(C=O) stretching vibrations, and combined δ(N-H) bending and υ(C-N) stretching vibrations, corresponding to protein-associated amides I and II, respectively [36]. Similarly, the characteristic broad band at around 3286 cm^{-1} associated with water υ(O-H) stretching and protein υ(N-H) stretching can also be seen [38]. The proteins have also characteristic bands at 1425-1477 cm^{-1} (δ$_{as}$(CH$_3$) and δ$_{as}$(CH$_2$) bending of methyl) and 1357-1423 cm^{-1} (δ$_s$(CH$_3$) and δ$_s$(CH$_2$) bending of methyl) [35]. This protein specific pattern appeared in all samples, but band intensities significantly decreased in the MPBR samples compared with the control condition, which was especially obvious at regions around 1400 cm^{-1} and 3286 cm^{-1}. This fact, together with the lower intensity of the carbohydrate-associated band in the control, was probably a result of a higher carbohydrate-to-protein ratio in the MPBR biomass, as previously observed in thermogravimetric and elemental analyses. Finally, a weak peak at 2927 cm^{-1}, assigned to υ$_{as}$(CH$_2$) and υ$_s$(CH$_2$) stretching, was observed in all samples, which has been attributed to the presence of lipid-associated hydrocarbons [38].

3.3. Organic matter and nutrient removal

Table 2 shows the organic matter and nutrient removal efficiencies reported in the MPBR at different SRT and HRT conditions. As a result of the nature of the secondary effluent treated, there was a large variation in the concentration of influent pollutants fed to the MPBR under different tested operating conditions. Nevertheless, a significant improvement was observed in all parameters with respect to the control condition (i.e. aerobic MBR). Average COD concentrations of 34.9-50.9 mg·L^{-1} and 61.9 mg·L^{-1} were reported in the permeate of the MPBR and of the control condition, leading to COD removals of 23.2-44.8% and 17.8%,

respectively. Regarding nutrient removal, the MPBR also showed a better performance. A complete nitrification (effluent NH_4^+-N<1 mg·L^{-1}) was also observed in both conditions, but total nitrogen and phosphorus removal increased by 80% and 97%, respectively. This is explained by higher biomass growth rate in the MPBR (Figure 2), where nutrient removal is expected to be mainly achieved through microalgae biomass assimilation [21]. It should be noted that external aeration was supplied for both conditions and dissolved oxygen was always maintained at high levels (9.2 ± 0.7 mg·L^{-1} and 9.1 ± 0.3 mg·L^{-1} for control condition and MPBR, respectively), which prevails over the indirect nitrogen remediation process. An example of the dissolved oxygen profiles is showed in Figure S1. In addition, similar pH values (8.4-8.6) were recorded for both conditions, reflecting a similar effect of the indirect removal methods of ammonia volatilization and phosphate precipitation [39].

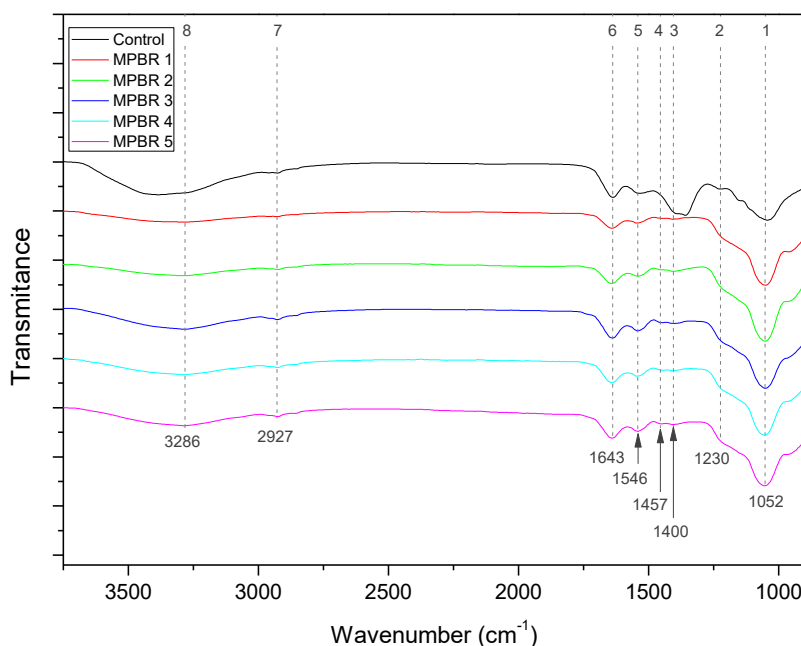**Figure 5.** FTIR spectra of biomass samples from the MPBR and the control condition. Characteristics bands were identified from carbohydrates (band 1), nucleic acids (band 2), proteins (bands 3-6 and 8) and lipids (band 7). Control: HRT=0.75 d, SRT=40 d; MPBR 1: HRT=0.75 d, SRT=20 d; MPBR 2: HRT=0.75 d, SRT=40 d; MPBR 3: HRT=0.75 d, SRT=80 d; MPBR 4: HRT=2 d, SRT=80 d; MPBR 5: HRT=5 d, SRT=80 d.

TN removal efficiency decreased with longer SRTs in the MPBR (Table 2), which can be related to lower growth rates. These results are in agreement with other MPBR studies treating synthetic secondary effluents for pure [29] and mixed cultures [21], in which a deterioration was observed of nitrogen removal when increasing SRTs above 20 d. By contrast, no appreciable effect was found on PO_4^{3-}-P removal, which ranged between 5.2 and 14.8% and seems to be very sensitive to influent fluctuation. Therefore, to improve nutrient removal at the optimum SRT of 80 d, HRT was extended for effective bioflocculation. At values of 2 and 5 d, the system increased TN removal efficiencies up to 48.7 and 40.6%, respectively, while PO_4^{3-}-P removal achieved values of 18.5 and 34.7%, respectively. In these conditions, removal rates varied between 2.0 and 3.4 $mg \cdot L^{-1} \cdot d^{-1}$ for nitrogen and between 0.1 and 0.4 $mg \cdot L^{-1} \cdot d^{-1}$ for phosphorus, which are within the typical range reported in MPBRs [12]. In the present study, despite influent fluctuations, establishing an optimal HRT value between 2 and 5 d seems necessary to achieve moderate nutrient removal, consistent with previous studies [13]. Nevertheless, the system does not meet the legal treatment requirements (10 mg $TN \cdot L^{-1}$ and 1 mg $P \cdot L^{-1}$, stipulated by EU) [40] (Table 2).

3.4. Membrane fouling

3.4.1. Threshold flux determination

Threshold fluxes were evaluated using the widely used flux-step method [41]. These values are used to describe the permeate flux before reversible fouling (i.e. $r_f=dTMP/dt$) increases to unsustainable rates. Although the selection of sustainable fouling rates is indeed quite subjective, a reference of 1 mbar/min was used in the present study, based on operative values reported in full-scale MBRs [42]. In all cases, a power relationship between the fouling rates and the permeate fluxes was observed, where the MPBR clearly showed better performance than the control condition, excluding for SRT of 40 d and HRT of 0.75 d (MPBR 2) (Figure 6). It should be noted that under these conditions, the MPBR was characterized by a high level of BCPs, even higher than the control condition. Therefore, there was a significant impact of SRT on the threshold flux, which firstly decreased, reaching a minimum at 40 d, and then sharply increased with increasing SRT. As consequence, compared to value of 20 d, typically adopted in the literature [10],

an operation at 80 d increased the threshold flux from 22 to 32-40 $L \cdot h^{-1} \cdot m^{-2}$. In the tested conditions, there was no significant impact of HRT. Results also showed an evident relationship between reversible fouling rate and BPC content. Similar results were reported in a previous study of an MBR applied to a secondary effluent treatment [22]. In addition, this is consistent with many studies in the literature, which have identified algal organic matter as the main contributor to the membrane fouling in MPBRs [11,17]. This type of fouling is usually associated with gel/cake layer formation on the membrane surface by colloidal and particulate matter. In order to confirm the impact of the colloidal fraction of the biopolymers and fine particles on membrane fouling, results were compared with those obtained under the same conditions by removing sedimentable solids (through 30 min of sedimentation, obtaining suspended solid removal of 71-95%).

Table 2. Biological performance of MPBR and control condition.

Parameters	MPBR 1	MPBR 2	MPBR 3	MPBR 4	MPBR 5	Control
	SRT=20 d	SRT=40 d	SRT=80 d	SRT=80 d	SRT=80 d	SRT=40 d
	HRT=0.75 d	HRT=0.75 d	HRT=0.75 d	HRT=2 d	HRT=5 d	HRT=0.75 d
Effluent concentration (mg·L^{-1})						
COD	50.9 ±10.1	48.8 ±10.5	46.9 ±10.0	34.9 ±10.3	36.4 ±10.1	61.9 ±8.2
NH_4^+-N	0.5 ± 0.1	0.9 ± 0.9	0.4 ± 0.1	0.4 ± 0.1	0.4 ± 0.1	0.6 ± 0.4
TN	8.7 ± 2.5	23.7 ± 7.0	9.9 ± 1.8	7.4 ± 3.5	14.5 ± 2.5	20.4 ± 5.2
PO_4^{3-}-P	5.4 ± 2.8	4.8 ± 2.2	5.0 ± 1.7	4.2 ± 1.6	1.5 ± 0.4	4.3 ± 1.5
Removal Efficiency (%)						
COD	23.2 ± 4.3	24.7 ± 14.2	26.7 ±14.0	35.0 ± 9.7	44.8 ± 14.5	17.8 ± 9.4
NH_4^+-N	90.8 ± 3.7	95.7 ± 2.7	92.2 ±4.1	93.9 ± 2.8	94.9 ± 8.0	95.3 ± 2.2
TN	30.0 ± 12.3	22.2 ± 9.1	5.6 ±4.9	48.7 ± 13.1	40.6 ± 12.9	4.5 ± 5.9
PO_4^{3-}-P	6.4 ± 3.3	14.8 ± 7.2	5.2 ±3.3	18.5 ± 18.9	34.7 ± 13.4	0.5 ± 1.3

Note: The data are expressed as mean ± standard deviation.

Mean characteristics of the supernatants are displayed in Supplementary data, Table S2. Similar behavior was observed (Supplementary data, Figure S2), confirming the crucial role of BPCs. This was probably due to shear conditions in the membrane vicinity due to intermittent air-sparging, which induces back-transport of large suspended solids resulting from shear-induced particle diffusion and inertial lift forces and therefore colloids are selectively deposited [43]. In the present study, optimum conditions involve BPCs below ~5 mg·L^{-1}, which were achieved at SRT of 80 d.

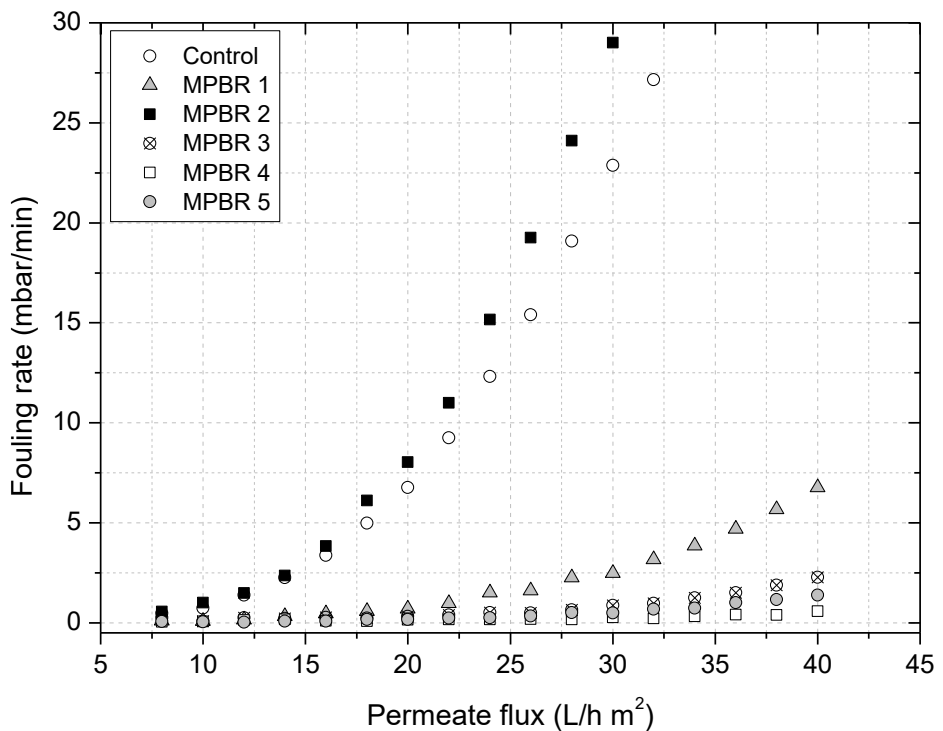**Figure 6.** Fouling rate against permeate flux for MPBR and control condition. Control: HRT=0.75 d, SRT=40 d; MPBR 1: HRT=0.75 d, SRT=20 d; MPBR 2: HRT=0.75 d, SRT=40 d; MPBR 3: HRT=0.75 d, SRT=80 d; MPBR 4: HRT=2 d, SRT=80 d; MPBR 5: HRT=5 d, SRT=80 d.

3.4.2. Residual fouling evolution

Figure 7 shows the *TMP$_i$* evolution at the operating conditions, and Table 3 displays average residual and reversible fouling rates.

Since residual fouling refers to the fouling that cannot be removed by frequent physical cleanings (i.e. backwashing) [42], this type of fouling might be related with reversible fouling rates. Therefore, as expected from the flux-steps results, SRT clearly decreased residual fouling rate $dTMP_i/dt$ (Figure 7d, e, f and Table 3). Furthermore, under these conditions, a significant effect of HRT on both fouling rates were observed, revealing optimal filtration conditions at 5 d. These results are consistent with those reported by Low *et al.* [19] who reported a decrease in membrane fouling with an increase in HRT in a ceramic MPBR, which was attributed to lower production of supernatant biopolymers. Nevertheless, specific behavior was observed in the MPBR at SRT of 40 d and HRT of 0.75 d (MPBR 2) (Figure 7c and Table 3), characterized by a sudden TMP_i increase after ~500 h. This sharp increase is commonly observed in MBRs, where different explanations based on pore/area loss, cake-layer porosity decrease and osmotic pressure increase have been provided [44]. All these mechanisms are increased at larger biopolymer content in the supernatant. In addition, once a cake layer (often named biocake in MBRs) is formed, increasing TMP up to a critical value might induce cake compaction, resulting in a higher specific cake resistance and thus requiring further TMP increases to maintain a constant permeate flux [45]. A simple visual inspection of the fouled membranes at the end of the tests showed appreciable biocake development in all cases, but with different structure and heterogeneity. An apparent flat layer was formed in the control condition, while a heterogeneous biocake is observed in the MPBR, that apparently tended to decrease at the higher SRT of 80 d (MPBR 3-5) (Figure 8). This is consistent with BPC content, since the development of organic coating by biopolymers on the membrane allows the attachment of microalgae and bacteria [17]. Therefore, the notable biocake development together with high concentrations of biopolymers in the supernatant could explain the sudden TMP increase in MPBR 2**.**

Regarding r_f, average values followed a similar trend observed for the flux-step trials, though increasing according to the residual fouling development (Table 3). This can be related to a reduction in the available membrane filtration area due to pore/area loss, where the resulting local flux increased [46].
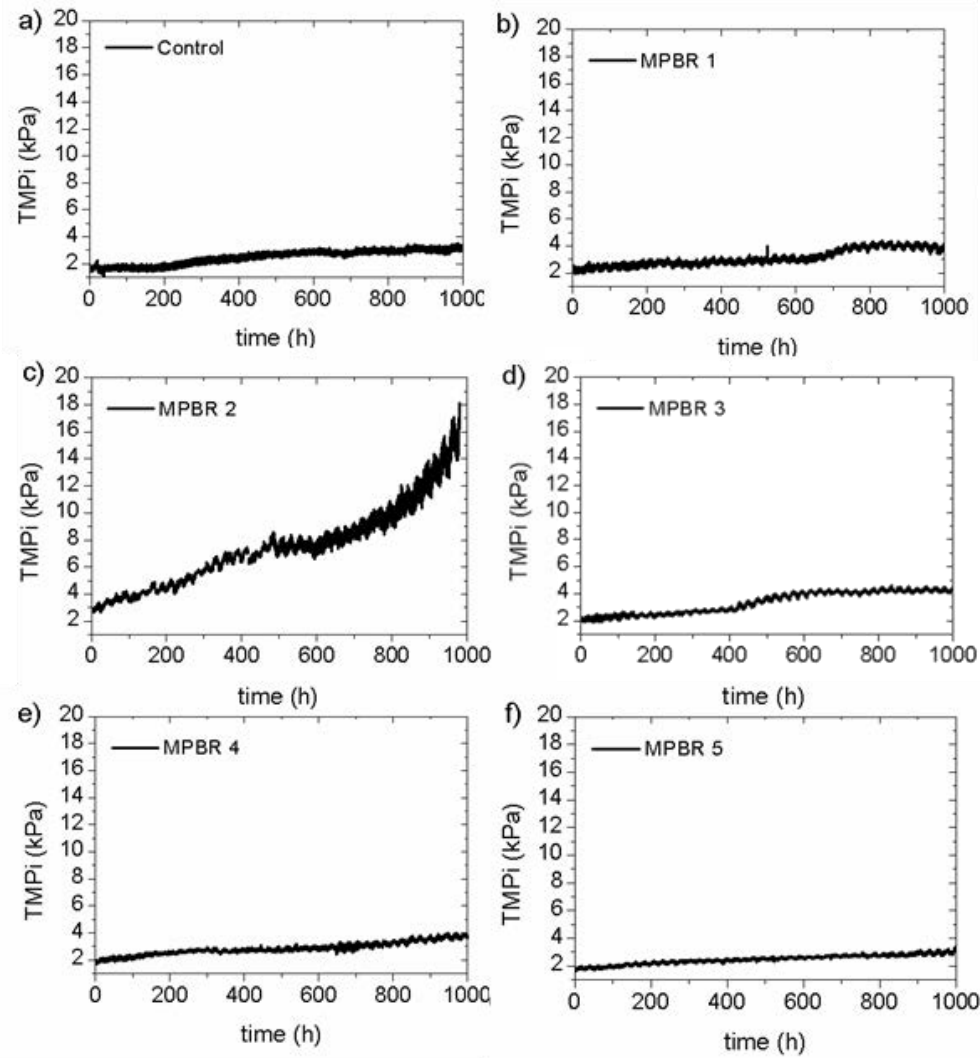
Figure 7. Initial transmembrane pressure *(TMPᵢ)* for MPBR and control condition. Control: HRT=0.75 d, SRT=40 d; MPBR 1: HRT=0.75 d, SRT=20 d; MPBR 2: HRT=0.75 d, SRT=40 d; MPBR 3: HRT=0.75 d, SRT=80 d; MPBR 4: HRT=2 d, SRT=80 d; MPBR 5: HRT=5 d, SRT=80 d.

Figure 8. Fouled membranes. Control: HRT=0.75 d, SRT=40 d; MPBR 1: HRT=0.75 d, SRT=20 d; MPBR 2: HRT=0.75 d, SRT=40 d; MPBR 3: HRT=0.75 d, SRT=80 d; MPBR 4: HRT=2 d, SRT=80 d; MPBR 5: HRT=5 d, SRT=80 d.

3.4.3. Residual fouling characterization

To investigate biocake organic foulants, samples were collected at the end of the test and analyzed using FTIR (Figure 9). Characteristic biomass bands were observed, similar to those found in the suspension samples. Nevertheless, specific peaks of carbohydrates (980-1174 cm^{-1}) showed a higher intensity for the MPBR samples at SRT of 80 d (MPBR 3-5) compared to those observed at lower SRTs (MPBR 1 and 2) and the control condition. The opposite trend was found for proteins bands (3-6). It seems that by extending SRT to 80 d, there was a shift in biocake organic composition towards a higher carbohydrate to protein ratio. It was previously reported that carbohydrates represent the main component of the biocake during the slight TMP rise phase, while an increase in protein content is associated with TMP's sharp increase in the MBR [47]. This agrees with the results obtained in the present study for the MPBR 2 condition.

In addition, a fouling resistance analysis was conducted at the end of the tests by using a cleaning protocol. Thus, residual fouling was separated into three main types of foulants: biocake (removed by physical means: rinse with tap water), organic fouling (removed by an oxidant) and inorganic fouling (removed by an acid). As can be seen in Figure 10, in all cases, most of the residual fouling was removed by physical means, which is consistent with the significant biocake development, as previously stated. This resistance removal accounted for 62% in the control condition and increased to 70-87% in the MPBR, probably due to the lower biomass concentration in the control condition. The significant role of

organic biopolymer fouling was also confirmed by the resistance to removal by the oxidant, while a minor significance was observed for inorganic foulants.
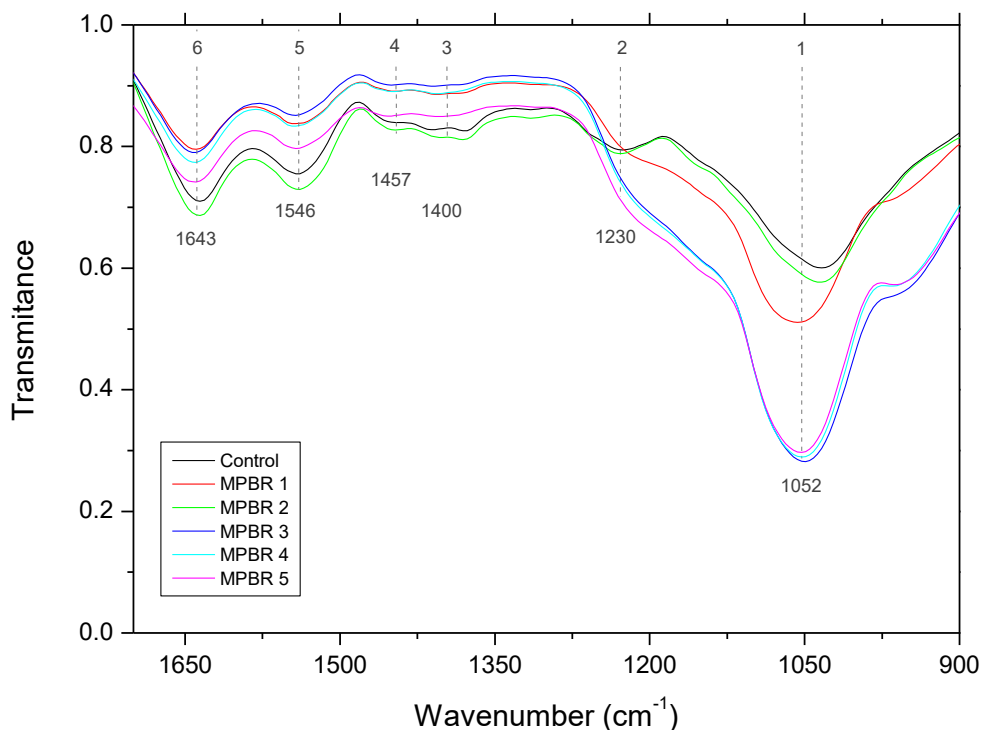
Figure 9. FTIR spectra of biocake samples from the MPBR and the control condition. Characteristics bands were identified from carbohydrates (band 1), nucleic acids (band 2), proteins (bands 3-6). Control: HRT=0.75 d, SRT=40 d; MPBR 1: HRT=0.75 d, SRT=20 d; MPBR 2: HRT=0.75 d, SRT=40 d; MPBR 3: HRT=0.75 d, SRT=80 d; MPBR 4: HRT=2 d, SRT=80 d; MPBR 5: HRT=5 d, SRT=80 d.

3.5. Microalgal community structure

Indigenous growth of microalgae was successfully achieved in the MPBR under all tested conditions, where a mixed population of green algae, cyanobacteria and diatoms was observed (Table 4). Green microalgae belonging to the genera *Chorella* and *Scenedesmus* and diatoms *Nitzschia* and *Navicula* were observed under all conditions, which confirmed their high productivity and tolerance to secondary effluent pollutants. Nevertheless, the variability in microalgae structure between the different operating conditions revealed the sensitivity of mixed culture to influent fluctuations and the difficulty to maintain a specific microalgae

culture over long periods. Dominant species reported here are commonly observed in microalgal consortia applied to wastewater treatment [7,9]. Although less abundant, green microalgae belonging to the genus *Chaetophora* were observed, whose presence was significant in MPBR 2 and 4 conditions. This is in agreement with several studies that have reported effective growth of *Chaetophora sp.* in a mixed microalgae culture in an MPBR applied to secondary effluent treatment [9,12]. As stated, the cyanobacteria population was also representative of the mixed culture in several conditions (MPBR 1, 2 and 4), where species belonging to the order *Oscillatoriales* were observed.
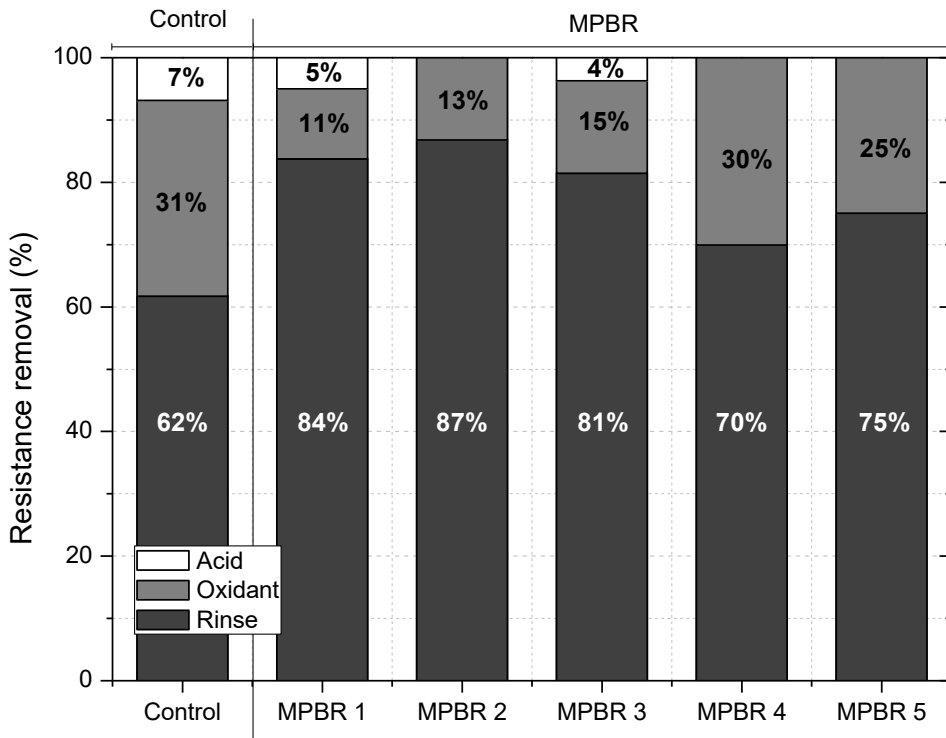
Figure 10. Resistance removed by rinse, oxidant, and acid at different operating conditions for MPBR and control condition. Control: HRT=0.75 d, SRT=40 d; MPBR 1: HRT=0.75 d, SRT=20 d; MPBR 2: HRT=0.75 d, SRT=40 d; MPBR 3: HRT=0.75 d, SRT=80 d; MPBR 4: HRT=2 d, SRT=80 d; MPBR 5: HRT=5 d, SRT=80 d.

Table 3. Average residual and reversible fouling rates for the control and the MPBR at different operating conditions.

Parameters	MPBR 1	MPBR 2	MPBR 3	MPBR 4	MPBR 5	Control
	SRT=20 d	SRT=40 d	SRT=80 d	SRT=80 d	SRT=80 d	SRT=40 d
	HRT=0.75 d	HRT=0.75 d	HRT=0.75 d	HRT=2 d	HRT=5 d	HRT=0.75 d
$dTMPi/dt \cdot 10^3$ (kPa/h)	1.5	9.87a	2.51	1.58	1.14	1.73
r_f (mbar/min)	1.02	6.90a	0.12	0.03	0.01	2.49

a Data obtained from the first 500 h of operation

Table 4. Relative abundance of the microalgal community.

Phylum	Family	Genus	MPBR 1	MPBR 2	MPBR 3	MPBR 4	MPBR 5
Chlorophyta	Trebouxiophyceae	Chlorella	12%	6%	28%	8%	56%
	Chlorophyceae	Scenedesmus	12%	39%	3%	8%	39%
	Chlorophyceae	Chaetophora	1%	15%		4%	1%
Cyanocbacteria	Cyanophyceae	Oscillatoriales	7%		8%	6%	
	Microcoleaceae	Microcoelus				10%	
Ochrophyta	Bacillariaceae	Nitzschia	17%	9%	13%	16%	1%
	Naviculaceae	Navicula	50%	32%	49%	49%	4%

4. Conclusions

Microalgal-bacterial membrane photobioreactors (MPBR) for secondary wastewater effluent treatment were investigated. For this purpose, the performance of a MPBR with indigenous microalgae-bacteria consortia was assessed under different SRT and HRT conditions. From this study, the following may be concluded:

- Due to the low C/N ratio in the secondary effluent, the MPBR showed better process performance than a conventional MBR. There was a substantial improvement in biomass productivity, nutrient removal and bioflocculation.
- Extending SRT to 80 d in the MPBR enhanced bioflocculation and effectively prevented biopolymer clusters (BPC) accumulation in the suspension. Despite influent fluctuations, optimal HRT value between 2 and 5 d was necessary to achieve moderate nutrient removal (40.6-48.7% and 18.5-34.7% for nitrogen and phosphorus, respectively).
- Reversible fouling was mainly caused by the supernatant fraction of the suspension, particularly by the BPC content. Residual fouling was associated to a biocake development onto the membrane, which could be enhanced at large BPC concentration. Consequently, optimal filtration conditions were obtained at SRT of 80 d and HRT of 5 d.
- Indigenous growth of microalgae was successfully achieved in the MPBR under all tested conditions. Green microalgae belonging to the genera *Chorella* and *Scenedesmus* and diatoms *Nitzschia* and *Navicula* were identified at high abundance.

References

[1]   A. Fallahi, F. Rezvani, H. Asgharnejad, E. Khorshidi, N. Hajinajaf, B. Higgins, Interactions of microalgae-bacteria consortia for nutrient removal from wastewater: A review, Chemosphere. 272 (2021) 129878. https://doi.org/10.1016/j.chemosphere.2021.129878.

[2]   A. Morillas-España, T. Lafarga, A. Sánchez-Zurano, F.G. Acién-Fernández, C. González-López, Microalgae based wastewater treatment coupled to the production of high value agricultural products: Current needs and challenges, Chemosphere. 291 (2022). https://doi.org/10.1016/j.chemosphere.2021.132968.

[3] S.S. Chan, K.S. Khoo, K.W. Chew, T.C. Ling, P.L. Show, Recent advances biodegradation and biosorption of organic compounds from wastewater: Microalgae-bacteria consortium - A review, Bioresour. Technol. 344 (2022) 126159. https://doi.org/10.1016/j.biortech.2021.126159.

[4] S. Li, Y. Chu, P. Xie, Y. Xie, H. Chang, S.H. Ho, Insights into the microalgae-bacteria consortia treating swine wastewater: Symbiotic mechanism and resistance genes analysis, Bioresour. Technol. 349 (2022) 126892. https://doi.org/10.1016/j.biortech.2022.126892.

[5] C. Zhang, S. Li, S.H. Ho, Converting nitrogen and phosphorus wastewater into bioenergy using microalgae-bacteria consortia: A critical review, Bioresour. Technol. 342 (2021) 126056. https://doi.org/10.1016/j.biortech.2021.126056.

[6] S. Judd, L.J.P. van den Broeke, M. Shurair, Y. Kuti, H. Znad, Algal remediation of CO2 and nutrient discharges: A review, Water Res. 87 (2015) 356–366. https://doi.org/10.1016/j.watres.2015.08.021.

[7] A.L. Gonçalves, J.C.M. Pires, M. Simões, A review on the use of microalgal consortia for wastewater treatment, Algal Res. 24 (2017) 403–415. https://doi.org/10.1016/j.algal.2016.11.008.

[8] D. García, E. Posadas, S. Blanco, G. Acién, P. García-Encina, S. Bolado, R. Muñoz, Evaluation of the dynamics of microalgae population structure and process performance during piggery wastewater treatment in algal-bacterial photobioreactors, Bioresour. Technol. 248 (2018) 120–126. https://doi.org/10.1016/j.biortech.2017.06.079.

[9] A. Solmaz, M. Işık, Polishing the secondary effluent and biomass production by microalgae submerged membrane photo bioreactor, Sustain. Energy Technol. Assessments. 34 (2019) 1–8. https://doi.org/10.1016/j.seta.2019.04.002.

[10] M. Zhang, L. Yao, E. Maleki, B.Q. Liao, H. Lin, Membrane technologies for microalgal cultivation and dewatering: Recent progress and challenges, Algal Res. 44 (2019) 101686. https://doi.org/10.1016/j.algal.2019.101686.

[11] Y. Luo, P. Le-Clech, R.K. Henderson, Simultaneous microalgae cultivation and wastewater treatment in submerged membrane photobioreactors: A review, Algal Res. 24 (2017) 425–437. https://doi.org/10.1016/j.algal.2016.10.026.

[12] A. Solmaz, M. Işık, Optimization of membrane photobioreactor; the effect of hydraulic retention time on biomass production and nutrient removal by mixed microalgae culture, Biomass and Bioenergy. 142 (2020). https://doi.org/10.1016/j.biombioe.2020.105809.

[13] J. González-Camejo, A. Jiménez-Benítez, M. V. Ruano, A. Robles, R. Barat, J. Ferrer, Optimising an outdoor membrane photobioreactor for tertiary sewage treatment, J. Environ. Manage. 245 (2019) 76–85. https://doi.org/10.1016/j.jenvman.2019.05.010.

[14] A.L.K. Sheng, M.R. Bilad, N.B. Osman, N. Arahman, Sequencing batch membrane photobioreactor for real secondary effluent polishing using native microalgae: Process performance and full-scale projection, J. Clean. Prod. 168 (2017) 708–715. https://doi.org/10.1016/j.jclepro.2017.09.083.

[15] P. Praveen, Y. Guo, H. Kang, C. Lefebvre, K.C. Loh, Enhancing microalgae cultivation in anaerobic digestate through nitrification, Chem. Eng. J. 354 (2018) 905–912. https://doi.org/10.1016/j.cej.2018.08.099.

[16] Y. Zhang, Q. Fu, Algal fouling of microfiltration and ultrafiltration membranes and control strategies: A review, Sep. Purif. Technol. 203 (2018) 193–208. https://doi.org/10.1016/j.seppur.2018.04.040.

[17] Y. Liao, A. Bokhary, E. Maleki, B. Liao, A review of membrane fouling and its control in algal-related membrane processes, Bioresour. Technol. 264 (2018) 343–358. https://doi.org/10.1016/j.biortech.2018.06.102.

[18] A.F. Novoa, L. Fortunato, Z.U. Rehman, T.O. Leiknes, Evaluating the effect of hydraulic retention time on fouling development and biomass characteristics in an algal membrane photobioreactor treating a secondary wastewater effluent, Bioresour. Technol. 309 (2020) 123348. https://doi.org/10.1016/j.biortech.2020.123348.

[19] S.L. Low, S.L. Ong, H.Y. Ng, Characterization of membrane fouling in submerged ceramic membrane photobioreactors fed with effluent from membrane bioreactors, Chem. Eng. J. 290 (2016) 91–102. https://doi.org/10.1016/j.cej.2016.01.005.

[20] S.-N. Li, C. Zhang, F. Li, N.-Q. Ren, S.-H. Ho, Recent advances of algae-bacteria consortia in aquatic remediation, Crit. Rev. Environ. Sci. Technol. (2022). https://doi.org/10.1080/10643389.2022.2052704.

[21] M. Zhang, K.T. Leung, H. Lin, B. Liao, Effects of solids retention time on the biological performance of a novel microalgal-bacterial membrane photobioreactor for industrial wastewater treatment, J. Environ. Chem. Eng. 9 (2021) 105500. https://doi.org/10.1016/j.jece.2021.105500.

[22] O. Díaz, L. Vera, E. González, E. García, J. Rodríguez-Sevilla, Effect of sludge characteristics on membrane fouling during start-up of a tertiary submerged membrane bioreactor, Environ. Sci. Pollut. Res. 23 (2016) 8951–8962. https://doi.org/10.1007/s11356-016-6138-y.

[23] E. González, O. Díaz, E. Segredo-Morales, L.E. Rodríguez-Gómez, L. Vera, Enhancement of Peak Flux Capacity in Membrane Bioreactors for Wastewater Reuse by Controlling the Backwashing Strategy, Ind. Eng. Chem. Res. 58 (2019) 1373–1381. https://doi.org/10.1021/acs.iecr.8b05650.

[24] L. Vera, E. González, O. Díaz, R. Sánchez, R. Bohorque, J. Rodríguez-Sevilla, Fouling analysis of a tertiary submerged membrane bioreactor operated in dead-end mode at high-fluxes, J. Memb. Sci. 493 (2015) 8–18.

https://doi.org/10.1016/j.memsci.2015.06.014.

[25] APHA, Standard Methods for the Examination of Water and Wastewater, 21st ed., Washington, DC, USA, 2005.

[26] S.G. Berk, J.H. Gunderson, Wastewater Organisms A Color Atlas, 1st Editio, CRC Press, Florida, USA, 1993.

[27] A. Pollice, G. Laera, D. Saturno, C. Giordano, Effects of sludge retention time on the performance of a membrane bioreactor treating municipal sewage, J. Memb. Sci. 317 (2008) 65–70. https://doi.org/10.1016/j.memsci.2007.08.051.

[28] G. Padmaperuma, R.V. Kapoore, D.J. Gilmour, S. Vaidyanathan, Microbial consortia: a critical look at microalgae co-cultures for enhanced biomanufacturing, Crit. Rev. Biotechnol. 38 (2018) 690–703. https://doi.org/10.1080/07388551.2017.1390728.

[29] Y. Luo, P. Le-Clech, R.K. Henderson, Assessment of membrane photobioreactor (MPBR) performance parameters and operating conditions, Water Res. 138 (2018) 169–180. https://doi.org/10.1016/j.watres.2018.03.050.

[30] A. Viruela, Á. Robles, F. Durán, M.V. Ruano, R. Barat, J. Ferrer, A. Seco, Performance of an outdoor membrane photobioreactor for resource recovery from anaerobically treated sewage, J. Clean. Prod. 178 (2018) 665–674. https://doi.org/10.1016/j.jclepro.2017.12.223.

[31] M. Xu, P. Li, T. Tang, Z. Hu, Roles of SRT and HRT of an algal membrane bioreactor system with a tanks-in-series configuration for secondary wastewater effluent polishing, Ecol. Eng. 85 (2015) 257–264. https://doi.org/10.1016/j.ecoleng.2015.09.064.

[32] Q.V. Bach, W.H. Chen, Pyrolysis characteristics and kinetics of microalgae via thermogravimetric analysis (TGA): A state-of-the-art review, Bioresour. Technol. 246 (2017) 88–100. https://doi.org/10.1016/j.biortech.2017.06.087.

[33] A. Soria-Verdugo, E. Goos, N. García-Hernando, U. Riedel, Analyzing the pyrolysis kinetics of several microalgae species by various differential and integral isoconversional kinetic methods and the Distributed Activation Energy Model, Algal Res. 32 (2018) 11–29. https://doi.org/10.1016/j.algal.2018.03.005.

[34] R.B. Carpio, Y. Zhang, C.T. Kuo, W.T. Chen, L.C. Schideman, R.L. de Leon, Characterization and thermal decomposition of demineralized wastewater algae biomass, Algal Res. 38 (2019) 101399. https://doi.org/10.1016/j.algal.2018.101399.

[35] D.Y. Duygu, A.U. Udoh, T. Ozer, A. Akbulut, I. Erkaya, K. Yildiz, D. Guler, Fourier transform infrared (FTIR) spectroscopy for identification of Chlorella vulgaris Beijerinck 1890 and Scenedesmus obliquus (Turpin) Kützing 1833, African J. Biotechnol. 11 (2012) 3817–3824.

https://doi.org/10.5897/ajb11.1863.

[36] A.P. Dean, M.C. Martin, D.C. Sigee, Resolution of codominant phytoplankton species in a eutrophic lake using synchrotron-based Fourier transform infrared spectroscopy, Phycologia. 46 (2007) 151–159. https://doi.org/10.2216/06-27.1.

[37] M. Arif, Y. Li, M.M. El-Dalatony, C. Zhang, X. Li, E.S. Salama, A complete characterization of microalgal biomass through FTIR/TGA/CHNS analysis: An approach for biofuel generation and nutrients removal, Renew. Energy. 163 (2021) 1973–1982. https://doi.org/10.1016/j.renene.2020.10.066.

[38] Y. Liu, S. Chang, F.M. Defersha, Characterization of the proton binding sites of extracellular polymeric substances in an anaerobic membrane bioreactor, Water Res. 78 (2015) 133–143. https://doi.org/10.1016/j.watres.2015.04.007.

[39] R. Whitton, F. Ometto, M. Pidou, P. Jarvis, R. Villa, B. Jefferson, Microalgae for municipal wastewater nutrient remediation: mechanisms, reactors and outlook for tertiary treatment, Environ. Technol. Rev. 4 (2015) 133–148. https://doi.org/10.1080/21622515.2015.1105308.

[40] Commission Directive 98/15/EC, Commission Directive 98/15/EC of 27 February 1998 amending Council Directive 91/271/EEC, OJ L 67. (1998) 29.

[41] M.C. Martí-Calatayud, S. Schneider, S. Yüce, M. Wessling, Interplay between physical cleaning, membrane pore size and fluid rheology during the evolution of fouling in membrane bioreactors, Water Res. 147 (2018) 393–402. https://doi.org/10.1016/j.watres.2018.10.017.

[42] A. Drews, Membrane fouling in membrane bioreactors-Characterisation, contradictions, cause and cures, J. Memb. Sci. 363 (2010) 1–28. https://doi.org/10.1016/j.memsci.2010.06.046.

[43] L.J. Zeman, A.L. Zydney, Microfiltration and Ultrafiltration: Principles and Applications, 1st Editio, Marcel Dekker, New York, 1996. https://doi.org/https://doi.org/10.1201/9780203747223.

[44] Seong-Hoon Yoon, Membrane Bioreactor Processes Principles and Applications, 1st Editio, CRC Press, New York, 2016.

[45] E. Poorasgari, T.V. Bugge, M.L. Christensen, M.K. Jørgensen, Compressibility of fouling layers in membrane bioreactors, J. Memb. Sci. 475 (2015) 65–70. https://doi.org/10.1016/j.memsci.2014.09.056.

[46] P. van der Marel, A. Zwijnenburg, A. Kemperman, M. Wessling, H. Temmink, W. van der Meer, An improved flux-step method to determine the critical flux and the critical flux for irreversibility in a membrane bioreactor, J. Memb. Sci. 332 (2009) 24–29. https://doi.org/10.1016/j.memsci.2009.01.046.

[47] J. Luo, J. Zhang, X. Tan, D. McDougald, G. Zhuang, A.G. Fane, S. Kjelleberg, Y. Cohen, S.A. Rice, The correlation between biofilm biopolymer

composition and membrane fouling in submerged membrane bioreactors, Biofouling. 30 (2014) 1093–1110. https://doi.org/10.1080/08927014.2014.971238.

Supplementary data

Table S1. Particle size distribution for the control condition and MPBR samples. Average values of 3 measurements.

Characteristics	MPBR 1	MPBR 2	MPBR 3	MPBR 4	MPBR 5	Control
	SRT=20 d	SRT=40 d	SRT=80 d	SRT=80 d	SRT=80 d	SRT=40d
	HRT=0.75 d	HRT=0.75 d	HRT=0.75 d	HRT=2 d	HRT=5 d	HRT=0.75 d
d(0.1) (µm)	15.1	10.8	14.4	14.0	12.5	7.2
d(0.5) (µm)	52.2	45.2	59.5	46.0	41.0	30.9
d(0.9) (µm)	364.8	164.8	270.6	188.7	158.4	122.8
vol. Weighted Mean (µm)	129.8	75.3	104.9	83.9	79.2	40.2

Table S2. Supernatant main characteristics. Average values of 3 measurements.

Characteristics	MPBR 1	MPBR 2	MPBR 3	MPBR 4	MPBR 5	Control
	SRT=20 d	SRT=40 d	SRT=80 d	SRT=80 d	SRT=80 d	SRT=40d
	HRT=0.75 d	HRT=0.75 d	HRT=0.75 d	HRT=2 d	HRT=5 d	HRT=0.75 d
Suspended solids (mg·L^{-1})	115	378	147	132	119	96
Turbidity (NTU)	46.0	248	61.9	55.8	52.1	41.1
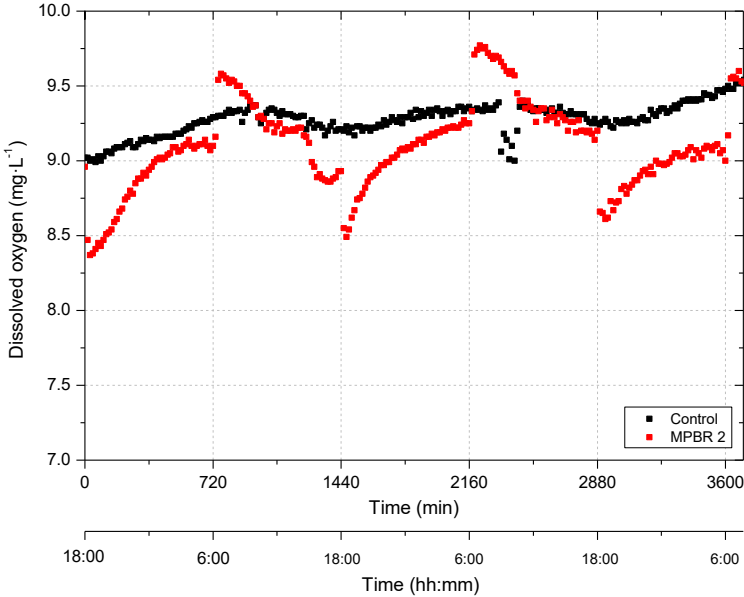
Figure S1. Dissolved oxygen profiles during operation time for control condition and MPBR. Control: HRT=0,75 d, SRT=40 d; MPBR 2: HRT=0,75 d, SRT=40 d. Light/dark cycle of 12/12h (light period started at 6:00).
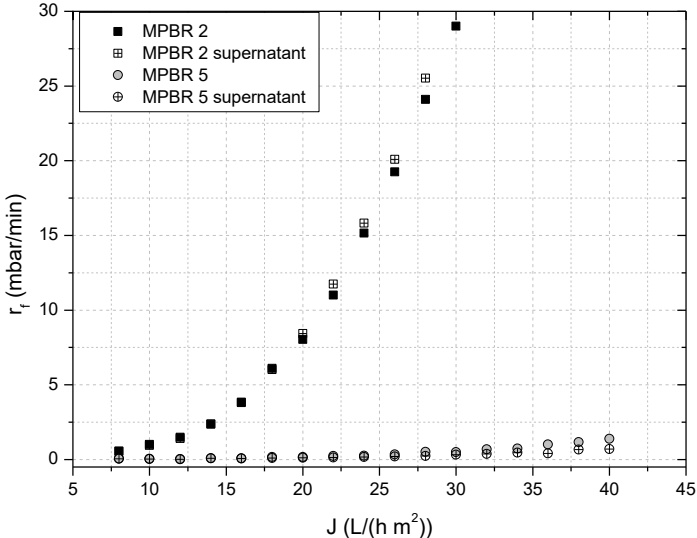
Figure S2. Fouling rate (r_f) against permeate flux (J) for MPBR. Comparison between the whole suspension and the supernatant. MPBR 2: HRT=0.75 d, SRT=40 d; MPBR 5: HRT=5 d, SRT=80 d.

CAPÍTULO 5

Evaluación del ensuciamiento en un fotobiorreactor de membrana para el tratamiento de un efluente procedente de un tratamiento secundario: efecto del fotoperiodo

ÍNDICE:

Evaluación del ensuciamiento en un fotobiorreactor de membrana para el tratamiento de un efluente procedente de un tratamiento secundario: efecto del fotoperiodo

Evaluation of membrane fouling in a microalgal-bacterial membrane photobioreactor treating secondary wastewater effluent: effect of photoperiod conditions

E. Segredo-Morales, E. González, C. González-Martín, L. Vera

Water Impact

Microalgal-bacterial membrane photobioreactor is a promising approach for sustainable wastewater reclamation. However, its widespread application is limited by the high costs associated with membrane fouling. Due to complex interactions among indigenous consortia, selecting optimal conditions is challenging. This study demonstrated that long-term fouling is minimized at intermediate light/dark photoperiods, which also allows high biomass concentration and effective nutrient removal.
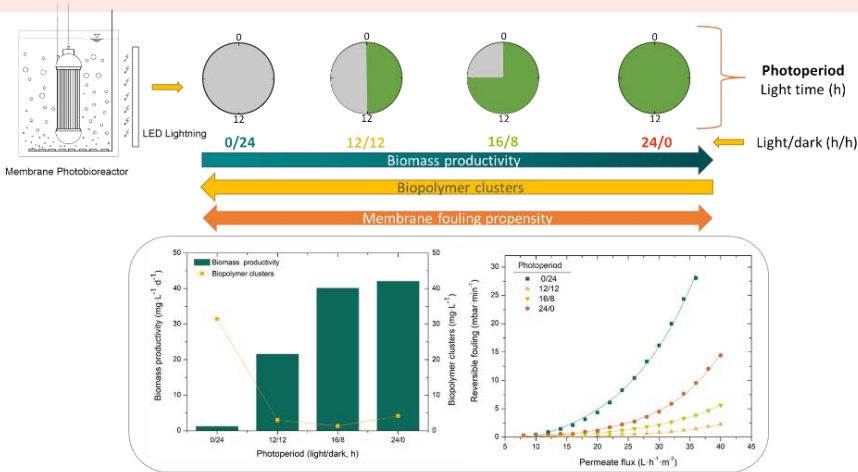
RESUMEN

Los fotobiorreactores de membrana (MPBRs) han surgido en los últimos años como una tecnología viable para el tratamiento de aguas residuales. Su potencial de tratamiento se basa en las relaciones simbióticas que se establecen entre las microalgas y las bacterias, donde las microalgas producen el oxígeno que necesitan las bacterias en su respiración celular, reduciendo los costes de aireación respecto a un tratamiento convencional de lodos activos. Al mismo tiempo, el dióxido de carbono que generan las bacterias es utilizado en el anabolismo de las microalgas. El equilibrio entre ambos microorganismos depende de numerosos factores, entre los que cabe destacar las condiciones de iluminación que se aplica al sistema. Generalmente, la actividad de las microalgas se incrementa cuando lo hace la intensidad de la luz, pero existen condiciones en las que se produce saturación (~200-540 $\mu mol \cdot m^{-2} \cdot s^{-1}$, dependiendo de la especie). Asimismo, se han descrito comportamientos similares en bacterias nitrificantes, en las cuales se han encontrado fenómenos de fotoinhibición a irradiancias próximas a los 500 $\mu mol \cdot m^{-2} \cdot s^{-1}$. De la misma manera, el crecimiento de microalgas generalmente se mejora extendiendo el período de luz de 12/12 a 24/0 h, pero varios estudios no han encontrado ningún efecto apreciable o incluso, una disminución en la tasa de crecimiento. Este hecho se debe a la existencia de otros factores que condicionan el efecto de la intensidad de luz o del fotoperiodo, como pueden ser el diseño del reactor o la concentración de biomasa.

Por todo lo indicado, el establecimiento de un fotoperiodo adecuado, además de la optimización de parámetros clave en el diseño del reactor como son el tiempo de retención hidráulico (HRT) y el tiempo de retención de sólidos (SRT), resulta de vital importancia en la operatividad de este tipo de fotobiorreactores.

Además de los parámetros ya mencionados, se han llevado a cabo investigaciones destinadas a dilucidar el mecanismo que controla el ensuciamiento de la membrana; un parámetro clave en la operatividad de este tipo de tecnologías. Un elevado ensuciamiento de la membrana provoca una disminución de la productividad del proceso.

En este capítulo se presentan los estudios relativos al efecto del fotoperiodo aplicado en la operación de un MPBR, en concreto, su influencia en el ensuciamiento de la membrana. Para ello, se caracterizó la biomasa de un MPBR

alimentado con agua procedente de un tratamiento secundario de aguas residuales y que operó a un HRT de 0,75 días y un SRT de 80 días, en términos de concentración, análisis elemental, distribución de tamaño de partículas y presencia de biopolímeros en el sobrenadante de la misma. Se llevaron a cabo ensayos de corta y de larga duración con el fin de establecer las condiciones óptimas de operación en cuanto al fotoperiodo se refiere. De hecho, se probaron 4 fotoperiodos diferentes: 12 horas de luz/ 12 horas de oscuridad (12/12), 16 horas de luz/ 8 horas de oscuridad (16/8), 24 horas de luz/ 0 horas de oscuridad (24/0) y una condición control en la que el reactor no se iluminó en ningún momento, 0 horas de luz/ 24 horas de oscuridad (0/24).

Los resultados mostraron que la concentración máxima de biomasa se alcanzó en el fotoperiodo 16/8 h, con un valor de $3,21 \pm 0,45$ $g \cdot L^{-1}$ y que no aumentó significativamente cuando el fotoperiodo aplicado fue el de irradiación continua, 24/0 h, probablemente debido a que la concentración de biomasa del reactor era tal que impedía el paso de la luz. Esto supuso una producción de biomasa de 40,1 $mg \cdot L^{-1} \cdot d^{-1}$, valores por encima de los encontrados en la literatura para MPBRs que operan a altos valores de SRT. Las especies mayoritarias presentes en las suspensiones biológicas pertenecían a los géneros *Scenedesmus* y *Chorella*.

Se encontraron diferencias en la composición elemental y en el contenido en materia orgánica volátil de las suspensiones biológicas dependiendo del fotoperiodo aplicado. Así, por ejemplo, el contenido en materia orgánica volátil del experimento sin irradiación (0/24 h) se situó por debajo del 26%, mientras que para el fotoperiodo 16/8 h superó el 37%, probablemente debido a la fijación de CO_2 por la actividad fotosintética de las microalgas.

El análisis por espectroscopía infrarroja por transformada de Fourier muestra un mayor contenido en sustancias poliméricas extracelulares en las suspensiones irradiadas respecto a la suspensión control. Estos datos, junto con los obtenidos con el análisis de la distribución de tamaño de partículas indican una mejor biofloculación de las suspensiones biológicas de los MPBRs frente al experimento control.

En cuanto a la eliminación de nutrientes, tal y como se vio en el anterior capítulo, la eliminación de contaminantes se ve mejorada por la presencia de microalgas en las suspensiones biológicas, así, los MPBRs obtienen mejores eliminaciones de carbono orgánico disuelto (DOC), de nitrógeno amoniacal, de nitrógeno

inorgánico disuelto (DIN), y de fósforo como fosfato respecto al experimento control (0/24 h). Entre los MPBRs destaca las elevadas eliminaciones de DOC y DIN obtenidas con el fotoperiodo 16/8 h, debido a la alta productividad de esta condición, y la mejora en la eliminación de fósforo como fosfato en aquellos MPBRs cuyo fotoperiodo contiene más de 12 horas de luz, es decir, en las condiciones 16/8 y 24/0 h.

Los experimentos de corta duración mostraron que el ensuciamiento está altamente relacionado con el contenido en agregados biopoliméricos (BPCs) de las suspensiones, pero no mostraron una clara correlación entre el fotoperiodo y flujo umbral. Sin embargo, las diferencias observadas en el flujo umbral y en el tamaño de flóculo entre las condiciones 16/8 y 24/0 h, indican que si bien el consorcio microalgas-bacterias supone un efecto positivo en la biofloculación de la suspensión biológica, una proporción excesiva de microalgas respecto a bacterias provoca una disminución del tamaño de flóculo, y una mayor tendencia al ensuciamiento de la membrana. Este hecho se comprobó cuando se realizaron ensayos de filtración de larga duración, en los que se obtuvo una operación estable con el tiempo en la condición 16/8 h, mientras que el fotoperiodo 24/0 h mostró un aumento significativo del ensuciamiento residual con el tiempo. La mejor operatividad a largo plazo, del fotoperiodo 16/8 h coincide con un menor contenido en BPCs de la suspensión biológica.

Abstract

Microalgal-bacterial membrane photobioreactors (MPBRs) have emerged as a transformative wastewater treatment technology for reducing carbon emissions whilst achieving high quality effluent. However, membrane fouling negatively affects process performance by increasing energy consumption and reducing membrane lifespan. In this study, light/dark photoperiods were varied to optimize treatment performance, biomass properties and reduce membrane fouling. Increasing the length of the light period favored higher production of biomass but decreased bioflocculation. An intermediate photoperiod of 16/8 h achieved high values of biomass concentration (3.21 ± 0.45 g·L^{-1}) and nutrient removal rates (4.71 mg N·L^{-1}·d^{-1} and 0.67 mg P·L^{-1}·d^{-1}, respectively), while preventing accumulation of biopolymer clusters (≤ 5.5 mg DOC·L^{-1}) in the suspension. In addition, short-term fouling—associated with floc deposition forming a cake layer—was minimized at

intermediate photoperiods, thus increasing the sustainable (i.e., threshold) permeate flux. At these sustainable flux conditions, membrane fouling was mainly determined by the biopolymer cluster content, with best performance being attained at 16/8 h. The above results reveal that the photoperiod is a crucial parameter for controlling membrane fouling in microalgal-bacterial membrane photobioreactors.

Keywords: Light/dark cycle, membrane fouling, membrane photobioreactor, microalgal-bacterial consortia, photoperiod, wastewater treatment.

1. Introduction

Progressive decarbonization is prompting the wastewater treatment sector to search for transformative technologies that can increase energy efficiency, recover resources and prevent greenhouse gases emissions [1,2]. Recently, novel treatment technologies, such as photocatalysis [3], microwave catalysis [4,5] or zero-valent iron nanoparticles [6] have been proposed. Nevertheless, although these are promising technologies, there are several disadvantages that have to be addressed to ensure their safe and effective use in wastewater treatment. Further investigation on catalysis deactivation, safety hazards due to microwave radiation or release of nanoparticles into the environment, are needed before practical use. Alternatively, a photobioreactor system based on microalgae-bacteria consortia is a promising approach to achieve sustainable wastewater technologies [7–9]. In a symbiotic relationship, microalgae produce dissolved oxygen, which can be used for bacterial respiration (oxidizing organic matter, ammonium and nitrite), reducing operating costs resulting from mechanical aeration. In turn, the carbon dioxide generated is used by the microalgae for carbon anabolism. Additionally, microalgae-bacteria consortia recover nutrients from wastewater through biomass synthesis. Produced biomass can be further valorized into added-value products, such as biogas or agricultural products [10,11]. Likewise, the move to a circular economy needs to be accomplished through the consistent promotion of safe water re-use [12]. Current advanced systems combine biological treatment with microfiltration or ultrafiltration membranes to produce high-quality effluents that are suitable for most industrial applications, including highly demanding agriculture irrigation [13,14].

A technology now actively being investigated is a microalgal-bacterial membrane photobioreactor (MPBR), which combines suspended biomass with immersed microfiltration or ultrafiltration membranes [15,16]. This technology has demonstrated the capability to efficiently treat municipal wastewaters [17] or secondary effluents [18,19]. Hydraulic and solid retention times (HRT and SRT, respectively) are commonly studied parameters, mainly focused on nutrient removal and biomass productivity [15,20]. Another important factor affecting microalgal-bacterial processes is light availability, mainly determined by light intensity and photoperiods [21,22]. Typically, microalgae activity increases with light intensity up to a saturation point (~200-540 $\mu mol \cdot m^{-2} \cdot s^{-1}$), which is species dependent, above which the effect becomes insignificant [23]. Indeed, in many species, increasing intensity results in photoinhibition thus reducing microalgae growth rate [24]. A similar behaviour has been reported for nitrifying bacteria, particularly nitrite oxidizers, which show significant photoinhibition above 500 $\mu mol \cdot m^{-2} \cdot s^{-1}$ [25]. Nevertheless, several strategies can be applied to control light intensity by modifying reactor design (i.e. culture depth) or biomass concentration (affecting light shading effect) [8]. Regarding the photoperiod, microalgae growth rate is generally enhanced by extending the light period from 12/12 to 24/0 h (continuous illumination) [26,27], but several studies have reported no appreciable effect [28] or even a decrease in the growth rate [29]. These contradictory findings suggest that photoperiod, light intensity and light shading may be interrelated.

A critical constraint of MBPR technology development at an industrial scale is the inherent membrane fouling [30,31]. In general, the extent of fouling is a complex function of biomass characteristics, operating conditions and membrane properties [20]. To alleviate membrane fouling, common practices in MPBRs are the use of moderate permeate fluxes, membrane air scouring, physical cleaning methods (relaxation and backwashing) and chemical cleanings [19,32]. Fouling can be classified into two main categories based on membrane permeability recovery by physical methods. The first is reversible fouling, which can be removed by physical means and is mainly attributed to cake layer development and possibly to pore blocking. The second category is residual fouling (also called physically irreversible fouling), which mainly refers to adsorption of foulants and gel formation and is only removed by chemical means [33]. These phenomena lead to a loss in membrane permeability, higher energy consumption and more

frequent chemical cleanings, which can reduce the membrane's lifespan [34]. Most previous studies assessing membrane fouling in MPBR have focused on biomass characteristics, particularly biomass concentration, particle size distribution and supernatant biopolymers content [30,35–39]. Main influencing factors assessed in these studies are hydraulic and solid retention times, feedwater characteristics (nitrogen source and ratio of N/P) and alga/activated sludge inoculation ratios. Nevertheless, although light is a key parameter in microalgae-bacteria consortia growth and biomass properties, it has been less studied. In fact, a previous study revealed a trade-off between biomass productivity/nutrient removal and membrane fouling [40]. In this work it is reported that reducing the light path in a photobioreactor (i.e. increasing photosynthetic efficiency) significantly increases the membrane fouling rate. Therefore, finding optimal illumination conditions (intensity and/or photoperiod) would considerably improve operational feasibility and reduce the cost of MPBR technology.

This study focuses on assessing the effect of the photoperiod on the performance of a MPBR, particularly on membrane fouling. The assessment was conducted by analyzing treatment performance and main biomass properties, such as concentration, elemental composition, particle size distribution and supernatant biopolymers content. Using a flux-step method, fouling propensity and sustainable flux conditions were investigated. Finally, long-term fouling tests verified sustainable membrane performance by assessing residual fouling evolution.

2. Materials and methods

2.1. Feedwater

The MPBR unit was fed with a secondary effluent obtained from a conventional activated sludge wastewater treatment plant (Santa Cruz de Tenerife, Canary Island, Spain), which was designed for organic matter removal. Main physical-chemical characteristics are given in Table 1.

Table 1. Main physical-chemical characteristics of the feedwater (n = 55)

Parameters	Units	Mean	Range
COD	mg·L^{-1}	67.2	39-113
DOC	mg·L^{-1}	17.9	12.7-45.7
pH	-	8.2	7.9-8.4
N-NH$_4^+$	mg·L^{-1}	25.8	2.5-41.9
N-NO$_3^-$	mg·L^{-1}	2.0	0-12.9
N-NO$_2^-$	mg·L^{-1}	1.7	0-9.5
P-PO$_4^{3-}$	mg·L^{-1}	4.1	0.8-7.9
CO$_3^{2-}$	mg·L^{-1}	8.5	0-21.6
HCO$_3^-$	mg·L^{-1}	552.6	414.0-698.7
Turbidity	NTU	2.0	1.1-5.0
TSS	mg·L^{-1}	4.5	0-22

2.2. MPBR set-up

The experimental unit consisted of a cylindrical 3.0 L (diameter = 14 cm) MPBR equipped with ZeeWeed® ZW-1 (Suez Water Technologies & Solutions, Ontario, ON, Canada) hollow fiber membranes with a nominal pore size of 0.04 µm and 1.9 mm outer diameter, assembled vertically, which provide 0.047 m^2 of filtering surface area (Fig. 1). ZeeWeed® consists of a woven reinforcing braid on which a PVDF membrane is cast. The permeate was extracted by a magnetic drive gear pump (Micropump-GA Series, Stockholm, Sweden) applying a slight vacuum. All the experiments were conducted at a permeate flux (J) of 10 L·h^{-1}·m^{-2}, measuring transmembrane pressure (TMP) with a pressure sensor (Sensotech, Barcelona, Spain). To prevent severe membrane fouling, the system operated under consecutive filtration/backwashing cycles of 450/30 s combined with intermittent air scouring (10/30 s on/off) at 5 NL·min^{-1} during the filtration. The backwash flux was set at 30 L·h^{-1}·m^{-2} with continuous aeration at 5 NL·min^{-1}. DAQ Factory software (AzeoTech® Inc., Ashland, OR, USA) was used for visualization and control of the filtration variables.

Air was also injected at the bottom of the MPBR at 1 NL·min^{-1} to provide aerobic conditions and mix the biological suspension. Dissolved oxygen concentration and pH were within the ranges of 6.9-9.6 mg·L^{-1} and 8.1-8.9, respectively, throughout

all experiments. The system was run at HRT and SRT values of 0.75 d and 80 d, respectively. The former was within the typical range of operating values in MPBRs [41] and the latter was selected according to a previous study on enhancing bioflocculation and avoiding biopolymer cluster accumulation [42]. The effluent was extracted from the permeate tank by a peristaltic pump (Cole-Parmer Instrument Co., USA) according to the selected HRT. To maintain a constant HRT regardless of permeate flux, excess permeate was returned to the MPBR. Experiments were carried out at room temperature (19 ± 1 °C) under constant irradiation of 300 $\mu mol \cdot m^{-2} s^{-1}$ measured at the surface of the photobioreactor (PAR irradiance using an irradiance meter, QSP2150A, Biospherical Instrument Inc., USA). The aim of the experiments was to assess the impact of photoperiods on the MPBR performance. To do this, four long-term experiments of 900 h were carried out under different light/dark photoperiods (0/24, 12/12, 16/8 and 24/0 h).

Before starting each experiment, the system was initially filled only with feedwater. Then, it was operated at 0.75 d of HRT for a minimum of 80 d without biomass purge. Thus, the system started without inoculum and the biomass developed from indigenous microorganisms. After the acclimation period, the biomass was manually purged to maintain the desired SRT. This procedure allowed the biomass concentration to remain stable during the experiments.
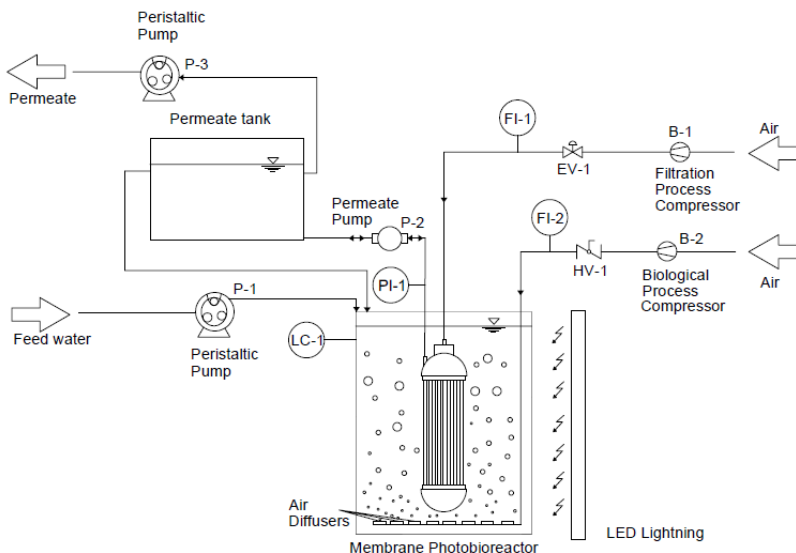

Figure 1. Schematic diagram of the R-MPBR system.

Samples of feedwater, suspension and permeate were analyzed three times per week. Suspensions were characterized by particles size, mixed liquor suspended solids (MLSS), volatile matter, elemental composition (C, N and H), supernatant dissolved organic carbon (DOC) and suspended solids (SS), and Fourier-transform infrared spectroscopy (FTIR). The average biomass productivity (r_x) was estimated following equation (1):

$$r_x = \frac{MLSS}{SRT} \qquad (1)$$

2.3. Short-term flux step trials

A flux-step method with intermediate backwashing cycles was applied [43]. Main parameters were: flux range of 8-40 L·h^{-1}·m^{-2}, flux increment of 2 L·h^{-1}·m^{-2} and step duration of 15 min. Air scouring and backwashing conditions were the same as those applied in the long-term experiments. The flux-step trials were carried out with the suspensions and supernatants (obtained after 30 min of decantation and transferred into a clean vessel). Before each run, the membrane was chemically cleaned using a 500 mg·L^{-1} of NaClO for 24 h. Reversible fouling was assessed by the fouling rate (r_f), given by the change in transmembrane pressure with time (dTMP/dt).

2.4. Membrane cleaning protocol

After the long-term fouling tests, the fouled membrane was subjected to a cleaning protocol that included the following steps [44]: (1) rinsing with tap water, (2) chemical cleaning with NaClO (500 mg·L^{-1}) for 24 h, and (3) chemical cleaning with citric acid (6 g·L^{-1}) for 2 h. After each step, the hydraulic resistance was calculated using a tap water filtration test.

2.5. Membrane fouling characterization

During the long-term tests, TMP evolution with consecutive filtration/backwashing was used to assess membrane fouling. It can be described by the following equation [43]:

$$TMP = TMP_0 + r_f \cdot t \qquad (2)$$

where TMP_i is the initial transmembrane pressure at the beginning of each filtration cycle, r_f is the reversible fouling rate and t is the elapsed time.

Equation (2) assumes a constant r_f during the filtration phases, describing an incompressible cake development mechanism on the membrane wall. On the other hand, TMP_i is related to residual fouling, which cannot be removed by physical means. Both parameters have been widely used to describe membrane fouling in conventional membrane bioreactors (MBRs) [33].

2.6. Analytical methods

Dissolved oxygen was measured using an oximeter Hach Lange LDO (USA). Total suspended solids (TSS), mixed liquor suspended solids (MLSS) and chemical oxygen demand (COD) were analyzed according to the Standard Methods [45]. Nitrogen-ammonium (N-NH$_4^+$) was analyzed by the Nessler method using a DR-5000 Hach spectrophotometer (USA). Nitrogen-nitrite (N-NO$_2^-$), nitrogen-nitrate (N-NO$_3^-$) and phosphorus-phosphate (P-PO$_4^{3-}$) were analyzed by ion chromatography using a Compact IC plus 882 device, supplied by Metrohm. Total dissolved inorganic nitrogen (DIN) was obtained by adding N-NH$_4^+$, N-NO$_2^-$ and N-NO$_3^-$. Dissolved organic carbon (DOC) concentration was measured with a TOC-meter (TOC-5000A, Shimadzu, Japan). The DOC difference between the filtered supernatant (through a filter of glass-fiber with a nominal pore size of 1.2 μm) and the permeate was assigned as biopolymers clusters (BPC) concentration. Particle size distribution was analyzed using Malvern Mastersizer 2000 (UK) laser diffraction particle size analyzer with a detection range of 0.02-2000 μm. FLASH EA 1112 Elemental Analyzer (ThermoFisher Scientific, USA) was used for the elemental analysis. Samples were previously dried in an oven at 100 °C for 1 h. Volatile matter was measured by a thermal analyzer (TG/DSC): Discovery SDT 650 (TA Instruments, USA). Fourier-transform infrared spectrometry was performed using an IFS 66/S spectrometer (Bruker, USA) equipped with an ATR accessory that measured the transmittance of the samples in a wavelength range between 900 and 4000 cm^{-1}. Microalgae identification was conducted by optical microscopy (DM750, Leica, Germany) according to Wastewater Organisms Atlas Manual [46]. Detection of *Escherichia coli* and *Legionella spp*. was performed in the permeate according to ISO 9308 and ISO 11731, respectively, as recommended by the legislation.

2.7. Statistical analysis

The results were analyzed by OriginPro (OriginLab Corporation, MA, USA). Analysis of variance (one-way ANOVA) and Tukey´s test was used to assess differences between photoperiods. Significance was assumed when p-values < 0.05.

3. Results and discussion

3.1. Biomass productivity and characteristics

As shown in Fig. 2a, longer lighting periods significantly influenced biomass concentration and productivity. Maximum biomass concentration (3.21 ± 0.45 g·L^1) was obtained at 16/8 h photoperiod (light/dark), which did not increase at continuous illumination (p > 0.05). Compared to operation at 0/24 h (control condition), the results revealed a significant growth of microalgae in the mixed consortia (representing approximately a 30-fold increase), which achieved a productivity value of 40.1 mg·L^{-1}·d^{-1}. Indeed, microalgae belonging to the genera *Scenedesmus* and *Chorella* were identified in abundance. This is consistent with those productivities usually reported for MBPRs operated at long SRTs with secondary effluents (28-41 mg·L^{-1}·d^{-1}) [22]. Nevertheless, the fact that productivity did not increase by extending the photoperiod from 16/8 h to continuous illumination seems to contradict previous results obtained in photo sequencing batch reactors [27,47]. Probably, this behavior can be attributed to an interplay between light penetration and biomass concentration, which may have a relevant role in MPBRs at long SRTs [48]. Therefore, results suggest that it may be difficult to increase biomass concentration up to 3.0-3.5 g·L^{-1} due to self-shading effect, as previously reported in MPBR studies [49,50].

As the nature of the biomass varies with the microbial community, volatile matter and elemental composition were analyzed at the different photoperiods (Fig. 2b). Volatile fraction increased from 25.9 to 37.3% when extending the lighting period from the control condition (0/24 h) to the 16/8 h photoperiod. Again, no further increment was obtained with the continuous illumination (p > 0.05). This volatile content was mainly attributed to microalgae growth, where CO2 fixation was expected due to photosynthetic activity. Indeed, consistent C/N mass ratios (5.0-5.4) for microalgae biomass [51] were only detected for the MPBR under lighting

conditions (Fig. 2c). Nevertheless, it should be noted that no significant variations were observed in the C/N ratios for the different photoperiods, so this parameter could not be related to the ratio of microalgae to bacteria in the biomass. In contrast, the low ratio at 0/24 h can be attributed to low organic carbon in the feedwater (Table 1). Moreover, the ratios of the intensity of the peak assigned to carbohydrate (C-O-C) bonds to the intensity of the specific peaks assigned to proteins (N-H and C=O) in the Fourier transform infrared (FTIR) spectra were probably a result of a higher carbohydrate-to-protein ratio for the MPBR at lighting conditions (Fig. 2c), consistent with the result of the elemental analysis. As reported in the literature, carbohydrates and proteins are major components of the bound extracellular polymeric substances (EPS), which are key in bioflocculation [8]. Since carbohydrate facilitate cell adhesion [52], a consistent carbohydrate-to-protein ratio can be related to efficient flocculation. This is in accordance with the higher mean particle size obtained in the MPBR under lighting conditions (Fig. 2d). Apparently, microalgal-bacterial consortia enhanced the formation of larger flocs, which agrees with previous studies [36]. However, mean floc size decreased from 104.9 to 38.9 μm while extending the lighting period from 12/12 h to continuous illumination. Particle size distribution has been attributed to microalgae/bacteria proportion, where partial inhibition of microalgae growth results in larger flocs [31]. In this study, results showed smaller flocs at continuous illumination, which can be justified by the increased microalgae growth (reflected by the higher biomass concentration) associated with the extension of the lighting period.

Due to the biological activity in the MPBR, hydrolysis of EPS and decay products generate soluble microbial products (SMP) and biopolymer clusters (BPC) [53]. Due to their larger size, BPC were retained by the membrane and can lead to severe membrane fouling [38]. It was observed that the photoperiod had a significant impact on BPC content (Fig. 2d). Under the control condition, BPC accumulated the most significantly (31.1 ± 6.6 mg·L^{-1}), which can be related to the low biomass concentration due to carbon-limited conditions imposed (i.e. low influent COD and long HRT). A previous study has demonstrated that endogenous conditions may induce cells lysis and biopolymer release in a MBR fed with a secondary effluent [54]. By contrast, very low BPC contents were found in the MPBR, which achieved a minimum at 16/8 h photoperiod ($p < 0.05$). This is probably due to favorable growth conditions for the microalgal-bacterial consortia, where cells lysis and biopolymers release were minimized. In addition,

due to a probable higher abundance of heterotrophic bacteria (see section 3.2), biopolymers are expected to be degraded into smaller compounds [38]. A similar trend was also observed for supernatant suspended solids, which decreased at the 16/8 h photoperiod ($p < 0.05$).

Figure 2. Effect of the photoperiod on biomass concentration and productivity (n = 15) (a), volatile matter and elemental analysis (n = 3) (b), FTIR spectra (n = 3) (c), and BPC (n = 15), supernatant suspended solids (SS) (n = 3) and mean particle size (n = 3) (d). Elemental analysis data are provided as % wt and dry basis.

3.2. Treatment performance

In order to assess treatment performance, feedwater and permeate concentration of dissolved organic carbon (DOC), nitrogen-ammonium ($N-NH_4^+$), total dissolved inorganic nitrogen (DIN) and phosphorus-phosphate ($P-PO_4^{3-}$) were analyzed. Inherent parameter fluctuation in feedwater can be observed, which was particularly evident in the low nitrogen content at 12/12 h photoperiod run (Fig. 3b). As showed in Fig. 3a, DOC removal was significantly increased (approximately 9-fold increase) in the MPBR under lighting conditions, suggesting

significant activity of heterotrophic bacteria in the mixed consortia. As stated, this affects process performance positively by decreasing BPC content. In addition, significant DOC permeate concentration has a negative effect on subsequent processes, such as disinfection byproducts [55].

The ammonium in feedwater varied between 23.0 and 6.3 mg·L^{-1} for the different conditions (Fig. 3b). A complete nitrification was achieved in all cases, obtaining a nitrogen-ammonium content in the permeate below 0.7 mg·L^{-1}, where DIN in the permeate was mainly in form of nitrate (> 96%), revealing the presence of nitrifying bacteria. In addition, DIN removal significantly increased from 3.5% to 18.1% with increasing photoperiods from control condition (0/24 h) to 16/8 h ($p < 0.05$) (Fig. 3c). However, no further improvement was observed at continuous illumination ($p > 0.05$). At 16/8 h, the average removal rate was 4.71 mg N·L^{-1}·d^{-1}, consistent with previous studies with similar biomass productivities [56,57]. Since pH was always maintained at similar values (8.1-8.9) under all conditions, the observed increment of nutrient removal was mainly associated with biomass assimilation. As recently reviewed [58], feedwater ammonium leads to microalgae-nitrifying bacteria competition, which negatively affects nitrogen removal rate. To overcome this issue, operation at short to moderate SRTs has been proposed [16,37]. Nevertheless, a lower SRT would lead to significantly lower biomass concentration and thus increase harvest costs [8]. In addition, long SRTs can decrease BPC and therefore, minimize membrane fouling [42].

The phosphate concentration in the feedwater and the permeate are showed in Fig. 3d. A similar trend as that observed for nitrogen removal was found, where photoperiod increased the phosphate removal. A maximum value of 12.1% was obtained for 16/8 h photoperiod, which did not significantly increase at continuous illumination ($p > 0.05$). This can be attributed to a higher biomass productivity when compared with the control condition or the 12/12 h photoperiod. The calculated phosphate removal rate was 0.67 mg·L^{-1}·d^{-1}, comparable with those reported in previous studies [48,57].

Finally, it is important to note that the membrane provided a high quality effluent in terms of microbial (absence of *E. Coli* and *Legionella spp.*) and physical (turbidity <0.5 NTU) parameters, which complied with the new European regulation of minimum requirements for the use of reclaimed water quality for agricultural irrigation [59].

In summary, results demonstrate consistent organic matter and nutrient removal rates in MPBR under lighting conditions. Removal rates were influenced by the photoperiod, where maximum values were obtained at 16/8 h, mainly due to greater biomass productivity. No further improvement was attained at continuous illumination, probably due to self-shading caused by the high biomass concentration at long SRTs. Therefore, future work should focus on improving MPBR design to optimize light utilization by reducing culture depth and allow biomass productivities and nutrient removal rates comparable to those obtained at short SRTs.

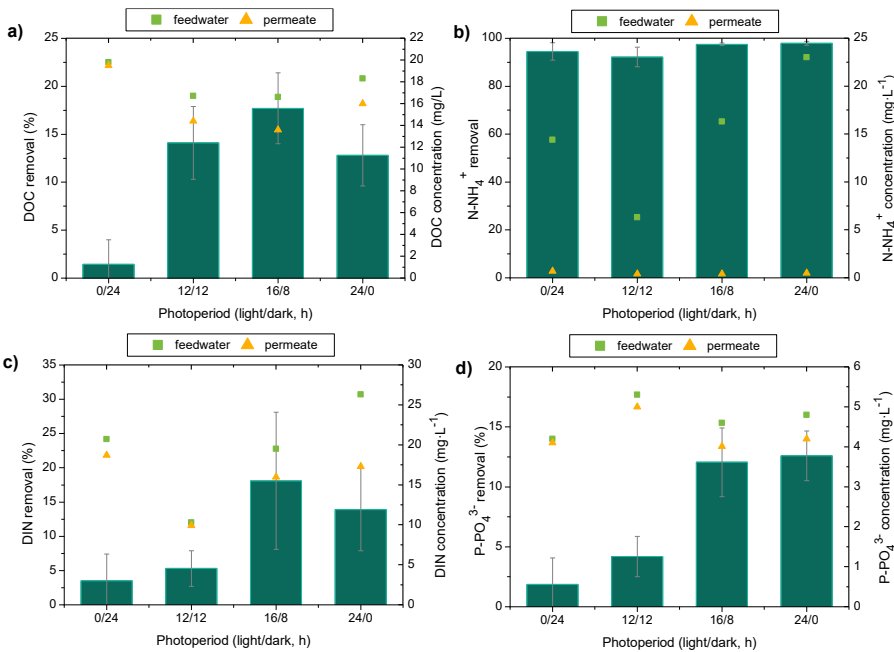**Figure 3.** Influence of the photoperiod on the removal of DOC (a), N-NH$_4^+$ (b), DIN (c) and P-PO$_4^{3-}$ (d). Error bars represent the standard deviation (n = 15).

3.3. Membrane fouling

3.3.1. Reversible fouling characterization: flux step experiments

The effect of the photoperiod on fouling propensity was investigated by conducting the flux-step method [43], using the reversible fouling rate (r$_f$

=d*TMP*/d*t*) as the fouling parameter (Fig. 4). It should be noted that applying lab-scale results to full-scale plant operation may be limited due to certain differences in hydrodynamics [60]. Nevertheless, despite these limitations, lab-scale experiments are useful for elucidating fouling propensity for the different conditions tested, mainly based on the effect of different light/dark photoperiods on biomass properties and biopolymer accumulation. Given the importance of dispersed cells and BPC in the fouling process [61], the results were compared, under the same experimental conditions, with those obtained while filtering the non-settleable fraction of the suspension. It should be noted that there was no appreciable sedimentation in the control suspension, therefore fractionation could not be carried out. In all cases, an exponential relationship was observed, in accordance with most studies of fouling rate trends in MBRs [62,63]. Therefore, a threshold flux (J_{th}) that separates low and high fouling regions can be identified [64]. A reference value for the fouling rate of 0.2 mbar·min^{-1} was assumed which is within the typical range (0.1-1 mbar·min^{-1}) reported for reversible fouling rates occurring in full-scale MBRs [33]. Results did not show a linear correlation between the photoperiod and J_{th}, which varied within the range of 8-18 L·h^{-1}·m^{-2}. Such variation can be explained by the different suspension characteristics. Many previous studies have emphasized the importance of biomass concentration, supernatant biopolymers content and floc size distribution on fouling propensity in MPBRs [30,35–37,65]. Consistently, the lower J_{th} obtained for the control condition (0/24 h) may be attributed to significant BPC accumulation (Fig. 2d). Under lighting conditions, due to lower BPC content, the non-settleable fraction showed a low fouling propensity in all cases (Fig. 4b-d). Therefore, differences in J_{th} may be related to the variations in settleable solid concentration and size. In the case of the suspension at 12/12 h photoperiod, due to its lower biomass concentration, the contribution of settleable solids was negligible and the r_f curve was similar to that obtained for the non-settleable fraction (Fig. 4b). Consequently, the highest J_{th} was attained. This can be explained by the effect of shear conditions associated with air scouring in preventing solids deposition onto the membrane [66]. However, this efficiency declines with increasing solids concentration, resulting in cake layer development [63]. This may explain the relevant contribution of settleable solids at fluxes above the J_{th} and photoperiods of 16/8 and 24/0 h. The increasing trend of fouling rates with the permeate flux also supports the cake development mechanism [67]. Therefore, due to the similar biomass concentrations of the 16/8 and 24/0 h photoperiods, lower fouling

rates at the former were consistent with the higher mean floc size. In accordance with previous studies [31,39], these results suggest that although there is a positive effect of microalgae growth in the mixed culture bioflocculation (BPC decrease and floc size increase), an excessive microalgae/bacteria proportion led to a floc size decrease and higher fouling propensity.

Figure 4. Fouling characterization by flux stepping experiments: reversible fouling rate (rf) of the suspension and non-settleable fraction against permeate flux (J) for the different photoperiods. Threshold fluxes (Jth) are determined at each condition.

3.3.2. Long-term fouling evolution

To assess residual fouling evolution, long-term tests were conducted under temporized filtration/backwashing cycles (Fig. 5). As previously reported, the residual fouling was characterized by the transmembrane pressure after each backwashing [43]. A permeate flux of 10 $L \cdot h^{-1} \cdot m^{-2}$ was selected, which according to previously determined threshold values, appeared reasonable to achieve long-term sustainable conditions [64]. This value was comparable with those typically reported in MPBR studies, generally in the range 1.5-17 $L \cdot h^{-1} \cdot m^{-2}$ [31,35,39].

Throughout the assays, TMP_i increases as a consequence of residual fouling, regardless of the low permeate flux applied (below the threshold one for 12/12, 16/8 and 24/0 h photoperiods). As expected, the high fouling rates obtained for the control condition (0.6-4.8 mbar·min^{-1}) led to rapid residual fouling development (Fig. 4a). However, values higher than 4.3 kPa were not reached, observing some fluctuations that seem to correspond to variations in BPC over experimentation time. This reflects an effective control of residual fouling due to the physical cleaning applied. By contrast, under lighting conditions, TMP_i tended to increase continuously at a low rate (0.9·10-3-2.2·10-3 kPa·h^{-1}, equivalent to 1.5·10-4-3.7·10-4 mbar·min^{-1}), consistent with the very low fouling rates observed (0.1-0.3 mbar·min^{-1}) and BPC content. Optimal performance was achieved at 16/8 h photoperiod, corresponding to the minimal BPC accumulation. Again, results suggest that excessive light irradiation may negatively affect filtration performance.

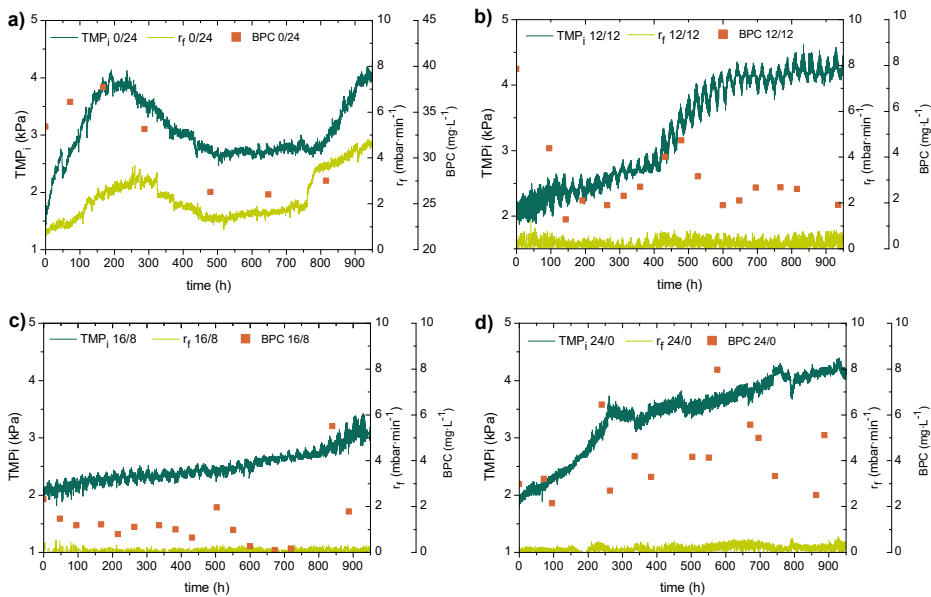**Figure 5.** Fouling evolution during long-term tests: initial transmembrane pressure (TMP_i), reversible fouling rate (r_f) and BPC for the different photoperiods.

In addition, membrane recovery by physical and cleaning methods was analyzed. Most residual fouling was removed by physical means (rinsing with tap water), revealing external biocake development (Fig. 6a). This was supported by images

of the membrane (Fig. 6b-e), in which significant differences in biocake morphology were observed. A dense and compact layer was found for the control condition (Fig. 6b) in contrast to the porous and heterogeneous biocake formed under lighting conditions (Figs. 6c-e). As reported in previous studies, slight biocake formation is inevitable regardless of the physical cleaning (i.e. air scouring and backwashing) applied [2,3]. Nevertheless, the results obtained in this study showed a less attached and non-homogeneous biocake layer for the MPBR under lighting conditions, probably due to low BPC accumulation in the supernatant at the tested conditions. Generally, it is reported that biofouling development begins after the formation of an organic conditioning layer on the support [4]. This is corroborated by the hydraulic resistances obtained after rising, which declined when cleaning with an oxidant (Fig. 6a). Also, this organic film was clearly observed in membrane images (Fig. 6f-i), which disappeared after cleaning (Fig. 6j-m). In addition, some level of inorganic fouling was obtained, but the membrane was completely recovered by the acid cleaning (Fig. 6a).
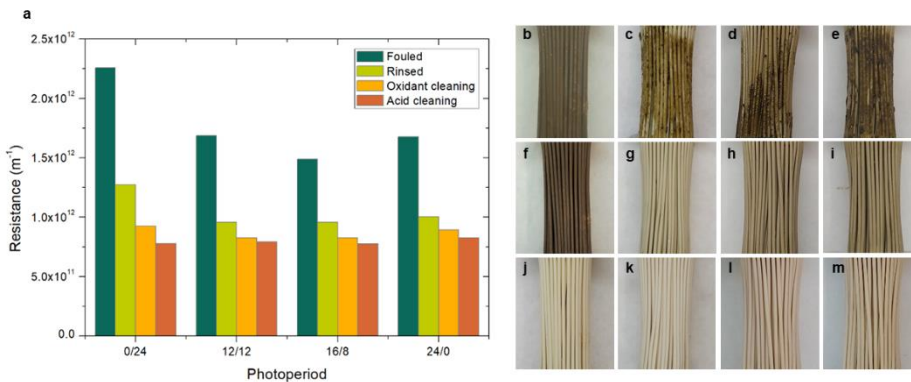
Figure 6. (a) Recovery of long-term fouled membranes after cleaning protocol: hydraulic resistances of fouled, rinsed and chemical cleaned (oxidant and acid) membranes for the different photoperiods. Images of the fouled membranes for 0/24 h (b), 12/12 h (c), 16/8 h (d) and 24/0 h (e); after rising for 0/24 h (f), 12/12 h (g), 16/8 h (h) and 24/0 h (i); and after cleaning with an oxidant for 0/24 h (j), 12/12 h (k), 16/8 h (l) and 24/0 h (m).

4. Conclusions

This study has demonstrated the significant effect of photoperiod on the performance of a microalgal-bacterial membrane photobioreactor (MPBR) treating real secondary wastewater effluent. Under the long SRT applied (80 d), biomass productivity and nutrient removal increased with the length of the light period up to a saturation point at 16/8 h (light/dark), above which the effect became insignificant. Subsequently, increasing illumination above saturation deteriorated bioflocculation, decreasing particle size and increasing biopolymer cluster content. This negatively impacted membrane performance by decreasing the sustainable (i.e., threshold) permeate flux and enhancing biocake layer growth during long-term operation.

Development of MPBR technology requires appropriate values of operating parameters, which can maximize biomass productivity and nutrient removal without worsening membrane performance. This work has revealed that the photoperiod is a crucial parameter to be considered.

References

[1]   Z.J. Ren, K. Pagilla, Pathway to water sector decarbonization, carbon capture and utilization, IWA Publishing, London, UK, 2022.

[2]   A. Soares, Wastewater treatment in 2050: Challenges ahead and future vision in a European context, Environ. Sci. Ecotechnology. 2 (2020) 100030. https://doi.org/10.1016/j.ese.2020.100030.

[3]   N. Liu, Y. Dang, B. Hu, M. Tian, H. Jiang, G. Quan, R. Qiao, J. Lei, X. Zhang, BN/Fe3O4/MIL-53(Fe) ternary nanocomposite for boosted ibuprofen degradation by visible light assisted photocatalytic activation of persulfate, Surfaces and Interfaces. 35 (2022).

[4]   H. Li, J. Yu, Y. Gong, N. Lin, Q. Yang, X. Zhang, Y. Wang, Perovskite catalysts with different dimensionalities for environmental and energy applications: A review, Sep. Purif. Technol. 307 (2023) 122716. https://doi.org/10.1016/j.seppur.2022.122716.

[5]   J. Yu, H. Li, N. Lin, Y. Gong, H. Jiang, J. Chen, Y. Wang, X. Zhang, Oxygen-Deficient Engineering for Perovskite Oxides in the Application of AOPs: Regulation, Detection, and Reduction Mechanism, Catalysts. 13 (2023).

[6]   Y. Wang, Y. Gong, N. Lin, L. Yu, B. Du, X. Zhang, Enhanced removal of Cr(VI) from aqueous solution by stabilized nanoscale zero valent iron and copper bimetal intercalated montmorillonite, J. Colloid Interface Sci. 606 (2022) 941–952. https://doi.org/10.1016/j.jcis.2021.08.075.

[7]   J.J.J.Y. Yong, K.W. Chew, K.S. Khoo, P.L. Show, J.S. Chang, Prospects and

development of algal-bacterial biotechnology in environmental management and protection, Biotechnol. Adv. 47 (2021) 107684. https://doi.org/10.1016/j.biotechadv.2020.107684.

[8] A. Fallahi, F. Rezvani, H. Asgharnejad, E. Khorshidi, N. Hajinajaf, B. Higgins, Interactions of microalgae-bacteria consortia for nutrient removal from wastewater: A review, Chemosphere. 272 (2021) 129878. https://doi.org/10.1016/j.chemosphere.2021.129878.

[9] R. Mu, Y. Jia, G. Ma, L. Liu, K. Hao, F. Qi, Y. Shao, Advances in the use of microalgal–bacterial consortia for wastewater treatment: Community structures, interactions, economic resource reclamation, and study techniques, Water Environ. Res. 93 (2021) 1217–1230. https://doi.org/10.1002/wer.1496.

[10] A. Morillas-España, T. Lafarga, A. Sánchez-Zurano, F.G. Acién-Fernández, C. González-López, Microalgae based wastewater treatment coupled to the production of high value agricultural products: Current needs and challenges, Chemosphere. 291 (2022). https://doi.org/10.1016/j.chemosphere.2021.132968.

[11] C. Zhang, S. Li, S.H. Ho, Converting nitrogen and phosphorus wastewater into bioenergy using microalgae-bacteria consortia: A critical review, Bioresour. Technol. 342 (2021) 126056. https://doi.org/10.1016/j.biortech.2021.126056.

[12] G. Mannina, H. Gulhan, B.J. Ni, Water reuse from wastewater treatment: The transition towards circular economy in the water sector, Bioresour. Technol. 363 (2022) 127951. https://doi.org/10.1016/j.biortech.2022.127951.

[13] J.R. Werber, C.O. Osuji, M. Elimelech, Materials for next-generation desalination and water purification membranes, Nat. Rev. Mater. 1 (2016). https://doi.org/10.1038/natrevmats.2016.18.

[14] P. Kehrein, M. Jafari, M. Slagt, E. Cornelissen, P. Osseweijer, J. Posada, M. van Loosdrecht, A techno-economic analysis of membrane-based advanced treatment processes for the reuse of municipal wastewater, Water Reuse. 11 (2021) 705–725. https://doi.org/10.2166/wrd.2021.016.

[15] M. Zhang, L. Yao, E. Maleki, B.Q. Liao, H. Lin, Membrane technologies for microalgal cultivation and dewatering: Recent progress and challenges, Algal Res. 44 (2019) 101686. https://doi.org/10.1016/j.algal.2019.101686.

[16] J. González-Camejo, P. Montero, S. Aparicio, M. V. Ruano, L. Borrás, A. Seco, R. Barat, Nitrite inhibition of microalgae induced by the competition between microalgae and nitrifying bacteria, Water Res. 172 (2020). https://doi.org/10.1016/j.watres.2020.115499.

[17] M. Zhang, K.T. Leung, H. Lin, B. Liao, The biological performance of a novel microalgal-bacterial membrane photobioreactor: Effects of HRT and N/P ratio, Chemosphere. 261 (2020) 128199. https://doi.org/10.1016/j.chemosphere.2020.128199.

[18] A.F. Novoa, L. Fortunato, Z.U. Rehman, T.O. Leiknes, Evaluating the effect of hydraulic retention time on fouling development and biomass characteristics in an algal membrane photobioreactor treating a secondary

wastewater effluent, Bioresour. Technol. 309 (2020) 123348. https://doi.org/10.1016/j.biortech.2020.123348.

[19]   E. González, O. Díaz, I. Ruigómez, C.R. de Vera, L.E. Rodríguez-Gómez, J. Rodríguez-Sevilla, L. Vera, Photosynthetic bacteria-based membrane bioreactor as post-treatment of an anaerobic membrane bioreactor effluent, Bioresour. Technol. 239 (2017) 528–532. https://doi.org/10.1016/j.biortech.2017.05.042.

[20]   Y. Liao, A. Bokhary, E. Maleki, B. Liao, A review of membrane fouling and its control in algal-related membrane processes, Bioresour. Technol. 264 (2018) 343–358. https://doi.org/10.1016/j.biortech.2018.06.102.

[21]   K. Li, Q. Liu, F. Fang, R. Luo, Q. Lu, W. Zhou, S. Huo, P. Cheng, J. Liu, M. Addy, P. Chen, D. Chen, R. Ruan, Microalgae-based wastewater treatment for nutrients recovery: A review, Bioresour. Technol. 291 (2019) 121934. https://doi.org/10.1016/j.biortech.2019.121934.

[22]   Y. Luo, P. Le-Clech, R.K. Henderson, Assessment of membrane photobioreactor (MPBR) performance parameters and operating conditions, Water Res. 138 (2018) 169–180. https://doi.org/10.1016/j.watres.2018.03.050.

[23]   M. Wang, R. Keeley, N. Zalivina, T. Halfhide, K. Scott, Q. Zhang, P. van der Steen, S.J. Ergas, Advances in algal-prokaryotic wastewater treatment: A review of nitrogen transformations, reactor configurations and molecular tools, J. Environ. Manage. 217 (2018) 845–857. https://doi.org/10.1016/j.jenvman.2018.04.021.

[24]   M. Raeisossadati, N.R. Moheimani, D. Parlevliet, Luminescent solar concentrator panels for increasing the efficiency of mass microalgal production, Renew. Sustain. Energy Rev. 101 (2019) 47–59. https://doi.org/10.1016/j.rser.2018.10.029.

[25]   C. Vergara, R. Muñoz, J.L. Campos, M. Seeger, D. Jeison, Influence of light intensity on bacterial nitrifying activity in algal-bacterial photobioreactors and its implications for microalgae-based wastewater treatment, Int. Biodeterior. Biodegrad. 114 (2016) 116–121. https://doi.org/10.1016/j.ibiod.2016.06.006.

[26]   M.M. Maroneze, S.F. Siqueira, R.G. Vendruscolo, R. Wagner, C.R. de Menezes, L.Q. Zepka, E. Jacob-Lopes, The role of photoperiods on photobioreactors – A potential strategy to reduce costs, Bioresour. Technol. 219 (2016) 493–499. https://doi.org/10.1016/j.biortech.2016.08.003.

[27]   H. Jia, Q. Yuan, Nitrogen removal in photo sequence batch reactor using algae-bacteria consortium, J. Water Process Eng. 26 (2018) 108–115. https://doi.org/10.1016/j.jwpe.2018.10.003.

[28]   J. González-Camejo, A. Viruela, M. V. Ruano, R. Barat, A. Seco, J. Ferrer, Effect of light intensity, light duration and photoperiods in the performance of an outdoor photobioreactor for urban wastewater treatment, Algal Res. 40 (2019) 101511. https://doi.org/10.1016/j.algal.2019.101511.

[29]   M. Atta, A. Idris, A. Bukhari, S. Wahidin, Intensity of blue LED light: A potential stimulus for biomass and lipid content in fresh water microalgae

Chlorella vulgaris, Bioresour. Technol. 148 (2013) 373–378. https://doi.org/10.1016/j.biortech.2013.08.162.

[30]   J. González-Camejo, A. Jiménez-Benítez, M. V. Ruano, A. Robles, R. Barat, J. Ferrer, Optimising an outdoor membrane photobioreactor for tertiary sewage treatment, J. Environ. Manage. 245 (2019) 76–85. https://doi.org/10.1016/j.jenvman.2019.05.010.

[31]   M. Zhang, K.T. Leung, H. Lin, B. Liao, Membrane fouling in a microalgal-bacterial membrane photobioreactor: Effects of P-availability controlled by N:P ratio, Chemosphere. 282 (2021) 131015. https://doi.org/10.1016/j.chemosphere.2021.131015.

[32]   L. Fortunato, A.F. Lamprea, T.O. Leiknes, Evaluation of membrane fouling mitigation strategies in an algal membrane photobioreactor (AMPBR) treating secondary wastewater effluent, Sci. Total Environ. 708 (2020) 134548. https://doi.org/10.1016/j.scitotenv.2019.134548.

[33]   A. Drews, Membrane fouling in membrane bioreactors-Characterisation, contradictions, cause and cures, J. Memb. Sci. 363 (2010) 1–28. https://doi.org/10.1016/j.memsci.2010.06.046.

[34]   A.L.K. Sheng, M.R. Bilad, N.B. Osman, N. Arahman, Sequencing batch membrane photobioreactor for real secondary effluent polishing using native microalgae: Process performance and full-scale projection, J. Clean. Prod. 168 (2017) 708–715. https://doi.org/10.1016/j.jclepro.2017.09.083.

[35]   S.L. Low, S.L. Ong, H.Y. Ng, Characterization of membrane fouling in submerged ceramic membrane photobioreactors fed with effluent from membrane bioreactors, Chem. Eng. J. 290 (2016) 91–102. https://doi.org/10.1016/j.cej.2016.01.005.

[36]   M. Zhang, K.T. Leung, H. Lin, B. Liao, Effects of solids retention time on the biological performance of a novel microalgal-bacterial membrane photobioreactor for industrial wastewater treatment, J. Environ. Chem. Eng. 9 (2021) 105500. https://doi.org/10.1016/j.jece.2021.105500.

[37]   Y. Luo, P. Le-Clech, R.K. Henderson, Assessing the performance of membrane photobioreactors (MPBR) for polishing effluents containing different types of nitrogen, Algal Res. 50 (2020) 102013. https://doi.org/10.1016/j.algal.2020.102013.

[38]   Y. Luo, R.K. Henderson, P. Le-Clech, Characterisation of organic matter in membrane photobioreactors (MPBRs) and its impact on membrane performance, Algal Res. 44 (2019) 101682. https://doi.org/10.1016/j.algal.2019.101682.

[39]   L. Sun, Y. Tian, J. Zhang, H. Li, C. Tang, J. Li, Wastewater treatment and membrane fouling with algal-activated sludge culture in a novel membrane bioreactor: Influence of inoculation ratios, Chem. Eng. J. 343 (2018) 455–459. https://doi.org/10.1016/j.cej.2018.03.022.

[40]   J. González-Camejo, S. Aparicio, A. Jiménez-Benítez, M. Pachés, M. V. Ruano, L. Borrás, R. Barat, A. Seco, Improving membrane photobioreactor performance by reducing light path: operating conditions and key performance indicators, Water Res. 172 (2020). https://doi.org/10.1016/j.watres.2020.115518.

[41]   Y. Luo, P. Le-Clech, R.K. Henderson, Simultaneous microalgae cultivation and wastewater treatment in submerged membrane photobioreactors: A review, Algal Res. 24 (2017) 425–437. https://doi.org/10.1016/j.algal.2016.10.026.

[42]   E. Segredo-Morales, E. González, C. González-Martín, L. Vera, Secondary wastewater effluent treatment by microalgal-bacterial membrane photobioreactor at long solid retention times, J. Water Process Eng. 49 (2022) 0–11. https://doi.org/10.1016/j.jwpe.2022.103200.

[43]   E. González, O. Díaz, E. Segredo-Morales, L.E. Rodríguez-Gómez, L. Vera, Enhancement of Peak Flux Capacity in Membrane Bioreactors for Wastewater Reuse by Controlling the Backwashing Strategy, Ind. Eng. Chem. Res. 58 (2019) 1373–1381. https://doi.org/10.1021/acs.iecr.8b05650.

[44]   L. Vera, E. González, O. Díaz, R. Sánchez, R. Bohorque, J. Rodríguez-Sevilla, Fouling analysis of a tertiary submerged membrane bioreactor operated in dead-end mode at high-fluxes, J. Memb. Sci. 493 (2015) 8–18. https://doi.org/10.1016/j.memsci.2015.06.014.

[45]   APHA, Standard Methods for the Examination of Water and Wastewater, 21st ed., Washington, DC, USA, 2005.

[46]   S.G. Berk, J.H. Gunderson, Wastewater Organisms A Color Atlas, 1st Editio, CRC Press, Florida, USA, 1993.

[47]   C.S. Lee, H.S. Oh, H.M. Oh, H.S. Kim, C.Y. Ahn, Two-phase photoperiodic cultivation of algal-bacterial consortia for high biomass production and efficient nutrient removal from municipal wastewater, Bioresour. Technol. 200 (2016) 867–875. https://doi.org/10.1016/j.biortech.2015.11.007.

[48]   A. Solmaz, M. Işık, Effect of Sludge Retention Time on Biomass Production and Nutrient Removal at an Algal Membrane Photobioreactor, Bioenergy Res. 12 (2019) 197–204. https://doi.org/10.1007/s12155-019-9961-4.

[49]   S.K. Parakh, P. Praveen, K.C. Loh, Y.W. Tong, Integrating gravity settler with an algal membrane photobioreactor for in situ biomass concentration and harvesting, Bioresour. Technol. 315 (2020) 123822. https://doi.org/10.1016/j.biortech.2020.123822.

[50]   P. Praveen, W. Xiao, B. Lamba, K.C. Loh, Low-retention operation to enhance biomass productivity in an algal membrane photobioreactor, Algal Res. 40 (2019) 101487. https://doi.org/10.1016/j.algal.2019.101487.

[51]   P.E.A. Debiagi, M. Trinchera, A. Frassoldati, T. Faravelli, R. Vinu, E. Ranzi, Algae characterization and multistep pyrolysis mechanism, J. Anal. Appl. Pyrolysis. 128 (2017) 423–436. https://doi.org/10.1016/j.jaap.2017.08.007.

[52]   O. Orgad, Y. Oren, S.L. Walker, M. Herzberg, The role of alginate in Pseudomonas aeruginosa EPS adherence, viscoelastic properties and cell attachment, Biofouling. 27 (2011) 787–798. https://doi.org/10.1080/08927014.2011.603145.

[53]   Y. Shi, J. Huang, G. Zeng, Y. Gu, Y. Hu, B. Tang, J. Zhou, Y. Yang, L. Shi, Evaluation of soluble microbial products (SMP) on membrane fouling in membrane bioreactors (MBRs) at the fractional and overall level: a review, Rev. Environ. Sci. Biotechnol. 17 (2018) 71–85.

https://doi.org/10.1007/s11157-017-9455-9.

[54]   O. Díaz, L. Vera, E. González, E. García, J. Rodríguez-Sevilla, Effect of sludge characteristics on membrane fouling during start-up of a tertiary submerged membrane bioreactor, Environ. Sci. Pollut. Res. 23 (2016) 8951–8962. https://doi.org/10.1007/s11356-016-6138-y.

[55]   H.Y. He, W. Qiu, Y.L. Liu, H.R. Yu, L. Wang, J. Ma, Effect of ferrate pre-oxidation on algae-laden water ultrafiltration: Attenuating membrane fouling and decreasing formation potential of disinfection byproducts, Water Res. 190 (2021) 116690. https://doi.org/10.1016/j.watres.2020.116690.

[56]   A. Solmaz, M. Işık, Polishing the secondary effluent and biomass production by microalgae submerged membrane photo bioreactor, Sustain. Energy Technol. Assessments. 34 (2019) 1–8. https://doi.org/10.1016/j.seta.2019.04.002.

[57]   A. Solmaz, M. Işık, Optimization of membrane photobioreactor; the effect of hydraulic retention time on biomass production and nutrient removal by mixed microalgae culture, Biomass and Bioenergy. 142 (2020). https://doi.org/10.1016/j.biombioe.2020.105809.

[58]   J. González-Camejo, S. Aparicio, M. Pachés, L. Borrás, A. Seco, Comprehensive assessment of the microalgae-nitrifying bacteria competition in microalgae-based wastewater treatment systems: Relevant factors, evaluation methods and control strategies, Algal Res. 61 (2022). https://doi.org/10.1016/j.algal.2021.102563.

[59]   European Parliament and the Council 2020/741, Regulation (EU) 2020/741, Minimum requirements for water reuse, Off. J. Eur. Union. 177/33 (2020) 32–55. https://eur-lex.europa.eu/legal-content/EN/TXT/PDF/?uri=CELEX:32020R0741&from=EN.

[60]   M. Kraume, D. Wedi, J. Schaller, V. Iversen, A. Drews, Fouling in MBR: What use are lab investigations for full scale operation?, Desalination. 236 (2009) 94–103. https://doi.org/10.1016/j.desal.2007.10.055.

[61]   Y. Zhang, Q. Fu, Algal fouling of microfiltration and ultrafiltration membranes and control strategies: A review, Sep. Purif. Technol. 203 (2018) 193–208. https://doi.org/10.1016/j.seppur.2018.04.040.

[62]   P. Buzatu, H. Qiblawey, A. Odai, J. Jamaleddin, M. Nasser, S.J. Judd, Clogging vs. fouling in immersed membrane bioreactors, Water Res. 144 (2018) 46–54. https://doi.org/10.1016/j.watres.2018.07.019.

[63]   A. Robles, M. V. Ruano, J. Ribes, A. Seco, J. Ferrer, A filtration model applied to submerged anaerobic MBRs (SAnMBRs), J. Memb. Sci. 444 (2013) 139–147. https://doi.org/10.1016/j.memsci.2013.05.021.

[64]   R.W. Field, G.K. Pearce, Critical, sustainable and threshold fluxes for membrane filtration with water industry applications, Adv. Colloid Interface Sci. 164 (2011) 38–44. https://doi.org/10.1016/j.cis.2010.12.008.

[65]   L. Sun, Y. Tian, J. Zhang, L. Li, J. Zhang, J. Li, A novel membrane bioreactor inoculated with symbiotic sludge bacteria and algae: Performance and microbial community analysis, Bioresour. Technol. 251 (2018) 311–319. https://doi.org/10.1016/j.biortech.2017.12.048.

[66]   M. Bagheri, S.A. Mirbagheri, Critical review of fouling mitigation strategies in membrane bioreactors treating water and wastewater, Bioresour. Technol. 258 (2018) 318–334. https://doi.org/10.1016/j.biortech.2018.03.026.

[67]   Y. Jang, H.S. Kim, J.H. Lee, S.Y. Ham, J.H. Park, H.D. Park, Development of a new method to evaluate critical flux and system reliability based on particle properties in a membrane bioreactor, Chemosphere. 280 (2021) 130763. https://doi.org/10.1016/j.chemosphere.2021.130763.

[68]   C. Thobie, W. Blel, C. Dupré, H. Marec, J. Pruvost, C. Gentric, Different types of bubbly flows in a confined channel with the aim of limiting microalgae biofilm development – Part II: Study of the development and removal of microalgae biofilm, Chem. Eng. Process. - Process Intensif. 175 (2022). https://doi.org/10.1016/j.cep.2022.108899.

CAPÍTULO 6

Operación de un fotobiorreactor de membrana rotativa basado en un consorcio microalgas-bacterias indígenas para la regeneración de aguas residuales

Índice:

Operación de un fotobiorreactor de membrana rotativa basado en un consorcio microalgas-bacterias indígenas para la regeneración de aguas residuales

Performance of a novel rotating membrane photobioreactor based on indigenous microalgae-bacteria consortia for wastewater reclamation

E. Segredo-Morales, C. González-Martín, L. Vera, E. González

HIGHLIGHTS

- Carbon loading rate (CLR) determines bioflocculation.
- Nitrogen removal rates can be enhanced at high CLRs.
- Reversible and residual fouling are related to biopolymer clusters content.
- Effective long-term fouling control by the rotating membrane photobioreactor.
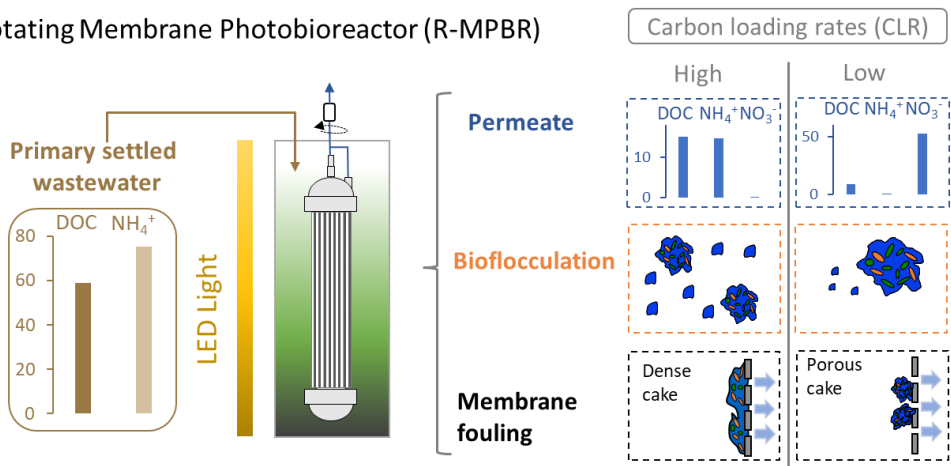
RESUMEN

Como se ha descrito en estudios recientes, los fotobiorreactores de membrana basados en consorcios de microalgas y bacterias son capaces de eliminar de manera conjunta, la materia orgánica y los nutrientes del agua residual. No obstante, la aplicación a aguas residuales con alta carga orgánica, como es el caso del efluente de un tratamiento primario, ha sido muy poco estudiada en la literatura. En este caso, el proceso de depuración está influenciado por varias condiciones de operación, particularmente por la carga volumétrica, el oxígeno disuelto y el tiempo de retención de sólidos. Estas condiciones deben ser seleccionadas con el fin de optimizar la estructura del consorcio microalgas-bacterias formado. La carga orgánica volumétrica (CLR) es un parámetro crucial en la operación, debido a que determina la concentración de oxígeno disuelto, mediante el balance que se establece con la producción de oxígeno fotosintético. En relación a los tiempos de retención de sólidos, en los capítulos anteriores se ha visto que la utilización de un valor de 80 días mejora significativamente la biofloculación de la suspensión biológica.

Con el objeto de mejorar el control del ensuciamiento de la membrana, en los últimos años se han desarrollado diferentes configuraciones basadas en la generación de turbulencia en las inmediaciones de la membrana mediante métodos mecánicos. La configuración convencional en los MPBRs se basa en la aplicación de aireación intermitente como una forma de inducir un esfuerzo cortante y con ello provocar el desprendimiento de la torta formada. En suspensiones biológicas concentradas o con un bajo nivel de floculación, los costes de aireación se incrementan por la necesidad de una mayor potencia para producir la misma eficacia de limpieza, lo que obliga a adoptar otras estrategias. En este sentido, la aplicación de métodos mecánicos sobre la membrana creando un esfuerzo cortante de alta intensidad provocado por la vibración o rotación de la propia membrana, puede ser una opción prometedora. La alta eficacia de estos métodos, particularmente la rotación, permite que solo sea necesario aplicarlos durante los periodos cortos de limpiezas físicas (relax o retrolavados).

En este capítulo se estudió la operación de un fotobiorreactor de membrana rotativa (R-MPBR) con una suspensión de microalgas y bacterias indígenas para la depuración de un efluente procedente de un tratamiento primario de aguas

residuales. La operación se analizó en términos de capacidad de tratamiento, características de la biomasa y control del ensuciamiento a largo plazo, en función de la carga orgánica volumétrica introducida en el sistema como procedimento para optimizar las condiciones de operación.

Los resultados mostraron una elevada eliminación de materia orgánica (82,6-85,6%), independientemente de las condiciones de operación, lo que puede deberse a la retención que ejerce la membrana sobre la materia orgánica coloidal y particulada. Además, se encontró un valor límite de carga orgánica (11,4 g DOC/(m^3·d)), por debajo del cual se incrementó sensiblemente la concentración de oxígeno disuelto en la suspensión. En la eliminación de nutrientes, se observaron mejoras significativas en el R-MPBR respecto al ensayo control. Los mejores resultados se obtuvieron en condiciones de alta carga orgánica, obteniéndose tasas específicas de eliminación de 37,2 mg/(L·d) de nitrógeno y 1,6 mg/(L·d) de fósforo. Esta tasa de eliminación de nitrógeno es mayor que la estimada por asimilación de la biomasa, por lo que los resultados parecen sugerir—solo en estas condiciones de alta carga—un proceso adicional de nitrificación-desnitrificación simultánea.

Cuando se analizaron las características de la suspensión biológica, se observó un incremento notable en el tamaño de flóculo de los R-MPBR respecto al experimento control, indicando una adecuada biofloculación en el consorcio microalgas-bacterias. Asimismo, se observó un efecto positivo al descender el CLR, aumentando el tamaño de los flóculos y disminuyendo el contenido en sólidos en suspensión en el sobrenadante (MLSS)$_s$. Además, se encontró un descenso en el contenido de los agregados biopoliméricos (BPC) en la suspensión, posiblemente asociado a una mayor actividad bacteriana en condiciones aerobias.

Los ensayos de flujo escalonado permitieron identificar los mecanismos de ensuciamiento y las condiciones óptimas de operación. Los resultados mostraron que el ensuciamiento ocurría fundamentalmente mediante un mecanismo de filtración por torta, en el que la relación entre la velocidad de ensuciamiento y el flujo se expresa en función de la viscosidad del soluto y el producto de la resistencia específica de la torta y la concentración de la torta ($\alpha\omega$). Este producto se utilizó para analizar el efecto de las condiciones fluidodinámicas sobre el ensuciamiento. En el ensayo control, se observó la existencia de un flujo crítico a partir del cual se produce una consolidación de la torta con el correspondiente aumento significativo del ensuciamiento. Este comportamiento es coherente con

el alto contenido en BPCs de la suspensión control, lo que puede llevar a una progresiva colmatación de los espacios vacíos de la torta, el descenso de la porosidad y la consolidación. En cambio, no se observó este fenómeno en el R-MPBR donde $\alpha\omega$ se mantuvo en valores relativamente bajos, con una tendencia decreciente al aumentar CLR. Al realizar ensayos adicionales con los sobrenadantes de las suspensiones, se observaron valores similares de $\alpha\omega$, confirmando el papel fundamental de la biofloculación sobre el ensuciamiento de la membrana.

La evolución del ensuciamiento residual, medido como la evolución de la presión transmembrana al inicio de cada ciclo de filtración (TMP_0) en ensayos de larga duración, mostró un comportamiento coherente con lo observado en los experimentos de flujo escalonado, confirmando que el ensuciamiento se minimiza a los menores valores de CLR ($\leq$ 11,4 g DOC/($m^3 \cdot$d)). Asimismo, el análisis del ensuciamiento residual mediante fraccionamiento confirmó el ensuciamiento producido por una torta no consolidada en periodos largos de operación.

En el análisis de las especies de microalgas presentes en el agua residual, se observó la presencia, en todos los casos, de especies pertenecientes al género *Chlorella* incorporadas formando flóculos densos y diatomeas del género *Nitzschia* y *Navicula*. Estas especies, por su versatilidad y tolerancia a un amplio rango de condiciones ambientales, son las que cabría esperar en este tipo de suspensiones. Además, el análisis microscópico mostró varias especies de ciliados típicamente encontrados en aguas residuales como *Vorticella* sp., *Epistylis* sp., *Paramecium* sp., *Euplotes* sp., *Aspidisca* sp., *Coleps* sp. Se observó, además, un cambio en la estructura de estos ciliados conforme se disminuía la CLR. Finalmente, sólo a bajos valores de CLR se encontraron rotíferos, probablemente debido a la baja disponibilidad de oxígeno existentes en las condiciones con alto CLR, factor que limita su crecimiento.

Abstract

Performance of a novel a rotating membrane photobioreactor (R-MPBR) for wastewater reclamation under photosynthetic oxygenation was investigated. The unit was operated in dead-end mode with an alternative physical cleaning strategy based in membrane module rotation. It was found that the carbon loading rate applied (CLR) (9.1-36.6 g DOC·m^{-3}·d^{-1}) determined the dissolved oxygen

concentration, affecting nutrient removal, bioflocculation and membrane fouling. Indigenous microalgae-bacteria consortia were effectively developed under each condition. At high CLR values, the dissolved inorganic nitrogen removal was significantly enhanced (81.2 ± 13.9%), probably due to a simultaneous nitrification-denitrification process as a result of the negligible dissolved oxygen concentration. Decreasing CLR from 36.6 to 9.1 g $DOC \cdot m^{-3} \cdot d^{-1}$, increased particle size ($D_{(0.5)}$ from 61.9 to 92.8 µm) and decreased biopolymer clusters content (from 50.0 to 2.3 mg $DOC \cdot L^{-1}$). It also revealed that membrane rotation does not compromise bioflocculation. Cake filtration model showed that fouling was associated to the supernatant fraction, particularly to the biopolymer clusters. Sustainable long-term operation was achieved at a permeate flux of 10 $L \cdot h^{-1} \cdot m^{-2}$ and CLR ≤ 11.4 g $DOC \cdot m^{-3} \cdot d^{-1}$. The proposed configuration effectively controlled membrane fouling, allowing to further process optimization.

Keywords: Bioflocculation, biopolymer cluster, microalgal-bacterial consortia, rotating hollow fibre, water reuse.

1. Introduction

Climate change is pushing the water sector towards a new paradigm of circular water economy, where the focus is on water reuse, carbon neutral operations, resource recovery and system level planning [1]. For wastewater treatment and reuse, there is a need for technologies that promote process intensification, low energy consumption and reduced chemical demand. Among such technologies, the use of photobiological systems, particularly microalgal-bacterial based processes, have emerged as efficient technologies for combined carbon and nutrient removal from wastewater. These systems also assimilate ambient CO_2 to provide residual biomass that can be further converted into added-value products [2]. The ongoing technology evolution to overcome challenges (i.e. poor biomass settling and harvesting limitations) and strict legislation affecting reclaimed wastewater reuse has led to the incorporation of micro- or ultrafiltration membranes, resulting in the membrane photobioreactor (MPBR) concept [3,4].

Several configurations of the MPBR technology have been proposed, generally including a closed or semi-closed photobioreactor (bubble columns, flat panel and tubular reactors) combined with a submerged or side stream membrane (hollow fibre or flat sheet modules) [5]. As described in the literature, the MPBR has demonstrated its treatment capabilities for synthetic or real secondary effluents

[6–8]. In addition, MPBRs are also capable of removing organics and nutrients from high organic loading influents, such as anaerobically digested wastewater and primary settled wastewater, although these applications have been less studied [5]. These influents promote microalgae-bacteria consortia to remove simultaneously carbon and nutrients, which can reduce the carbon footprint of the overall wastewater treatment process [1]. Nevertheless, as these consortia are easily affected by several factors such as light restriction, dissolved oxygen and influent characteristics, operating conditions should be carefully selected for avoiding negative impacts on the community structure [3]. Hydraulic retention time (HRT) is a crucial parameter affecting MPBR performance, and while short values typically enhance microbial growth, long HRTs improve nutrient removal efficiency [3]. In addition, HRT (i.e. organic and ammonia loading rates) regulates dissolved oxygen concentration due to the balance between aerobic bacteria consumption and photosynthetic oxygen production by microalgae [9]. Another widely studied parameter is solid retention time (SRT), which can be decoupled from the HRT in MBPRs, and therefore represents a significant advantage over conventional photobioreactors [5]. SRT is related to biomass concentration, growth rate and microbial community. Among these, biomass concentration is critical, since high values can induce photolimitation due to shelf-shading, which negatively impacts on microalgae growth [10]. Typical values reported in the literature for HRTs and SRTs are 0.25-8 d and 5-25 d, respectively [3,5]. Nevertheless, these values are mainly based on studies with pure microalgae cultures and synthetic wastewater, which may not be representative of native microalgae-bacteria consortia performance applied to real wastewater treatment [11].

For all membrane processes, membrane fouling is a major challenge limiting their wide application [5,12–14]. Fouling is caused by specific chemical and physical interactions between the membrane and the microbial components of the suspension, which lead to decreases in membrane permeability. Similar to conventional membrane bioreactors, several mechanisms have been proposed to describe this complex phenomenon, including pore clogging, foulant adsorption and gel o cake layer formation [4]. According to many MPBR studies, extracellular organic matter and small suspension particles have been identified as the main foulants [8,10,15]. Additionally, the rate of fouling is not only governed by

membrane characteristics and suspension foulants, but also by permeate flux, hydrodynamic conditions and any physical-chemical cleaning strategies applied [16–18]. Based on its reversibility by physical means (i.e. backwashing or relaxation), fouling can be classified into two main categories: reversible and residual fouling. The former is generally associated with an external cake deposit which can be removed by physical cleaning. Residual fouling (also called physically irreversible fouling) refers to the fouling that can be only removed by chemical cleaning and is related to gel formation, adsorption and probably to consolidated cake layer [16].

Alleviating membrane fouling by modifying hydrodynamic conditions has been extensively proven as an efficient means of promoting foulant back-transport from the cake layer by inducing shear stress [4]. In submerged MPBRs, intermittent air scouring is generally applied to produce a wall shear rate [6]. However, this operation strategy becomes energy intensive, exceeding 50% of overall O&M costs [19]. Therefore, alternative operation modes with lower energy demands are required. Dead-end filtration (i.e. without shear conditions during the filtration phase) can be an attractive option, and it has been widely used in direct membrane filtration of secondary effluents [20]. However, higher suspended solids in microbial suspension of MPBRs can lead to lower permeate fluxes and more efficient physical cleaning to maintain operative fouling rates is needed. In this sense, to enhance cleaning efficiency, dynamic shear-enhanced membranes, which create a high shear rate by a moving part such as vibrating or rotating systems, are a promising approach. Disc membranes (vibrating or rotating) and vibrating hollow fibre membranes have been extensively applied for the filtration of very concentrated suspensions [21]. More recently, the concept of a rotating hollow fibre module in the submerged configuration has been developed [22]. With the aim of decreasing energy demand for less concentrated matrices, subsequent studies have demonstrated its effectiveness in combination with traditional physical cleaning techniques (i.e. relaxation and backwashing) at dead-end filtration mode [23]. Considering the great concern of membrane fouling in MPBRs, it is hypothesized that the rotating module may enhance backwashing efficiency, achieving a sustainable operation with a low energy demand.

In this study, the performance of a rotating membrane photobioreactor (R-MPBR) with indigenous microalgae-bacteria consortia was investigated for wastewater

reclamation. Performance was assessed in terms of treatment capability, biomass characteristics, microalgae community and long-term fouling control as a function of several organic carbon loadings applied in order to optimise operating conditions.

2. Materials and methods

2.1. Feedwater

The lab-scale unit was fed with primary settled wastewater collected from a municipal wastewater treatment plant (Valle de Guerra, Canary Islands, Spain). Average and standard deviation values for dissolved organic carbon (DOC), chemical oxygen demand (COD), total suspended solids (TSS), ammonium-nitrogen (NH_4^+-N), dissolved inorganic nitrogen (DIN) and phosphate-phosphorus (PO_4^{3-}-P) were: 59.0 ± 26.3 mg·L^{-1}, 331 ± 135 mg·L^{-1}, 65.2 ± 35.6 mg·L^{-1}, 75.5 ± 13.8 mg·L^{-1}, 75.6 ± 13.7 mg·L^{-1} and 8.5 ± 2.4 mg·L^{-1}, respectively. As can be seen, the primary effluent was characterized by a low COD/N mass ratio (4.5) and low organic particulate content (COD/SST = 4.8) [24]. Also, average N/P ratio was 9.0, which was within the typical range reported for adequate microalgae growth [11]. Likewise, it presented an average pH of 8.1 with high alkalinity (12.7 meq·L^{-1}).

2.2. Experimental unit

The photobioreactor consisted of a tubular tank of 3.0 L made of acrylic plastic illuminated by a LED lamp (20W, Aquatlantis Easy LED, Portugal) at 300 µmol·m^{-2}·s^{-1} measured at the outer surface of the photobioreactor, in the area closest to the source (PAR irradiance using QSP2150A, Biospherical Instrument Inc., USA) (Figure 1). A photoperiod of 12/12 h light/dark was applied, except for the control condition, which operated without illumination. A PVDF ultrafiltration hollow fibre (Zeeweed® ZW-1, SUEZ Water Technologies and Solutions, Ontario, ON, Canada) with an average pore size of 0.04 µm and a nominal membrane surface area of 0.047 m^2 was used. A magnetic drive pump (Micropump-GA Series, AxFlow, Stockholm, Sweden) was used to withdraw permeate from the module. Membrane fouling was monitored by an increase in the transmembrane pressure which was measured by a pressure sensor (Sensotech, Barcelona, Spain). A

mechanical stirrer (Heidolph-RZR2020, Heidolph Instruments GmbH & CO., Schwabach, Germany) connected to the permeate line, acted as the impeller of membrane rotation and provided turbulence. During the long-term tests (35 days), the unit operated at dead-mode (i.e. without membrane rotation during the filtration phase) with a filtration flux of 10 $L \cdot h^{-1} \cdot m^{-2}$ at filtration/backwashing cycles of 450/30 s. During the backwashing phase, backwashing flux was fixed at 30 $L \cdot h^{-1} \cdot m^{-2}$ and membrane rotation was applied at 260 rpm in order to improve cleaning effectiveness. Additional physical cleanings were applied once a week by conducting a relaxation phase (i.e. ceasing filtration) during 5 min with continuous module rotation at 260 rpm. The system was equipped with on-line sensors of temperature and dissolved oxygen for process performance monitoring (Hach HQ40d oximeter, Hach, USA). The control system was integrated using a personal computer which allowed implementing programs (DAQ Factory software, AzeoTech®, Inc., Ashland, OR, USA) to control the process and collate data. Further details can be found in a previous study [22]. A level controller HSE-20987 (Aeman, Spain) and two peristaltic pumps Masterflex Easy-Load L/S 7518–00 (Cole-Parmer Instrument Co., USA) controlled influent and permeate flow rates to achieve the selected carbon loading rates (CLR). To maintain a CLR independent of the filtration flux, a fraction of the permeate was returned to the tank.

2.3. Experimental conditions

The unit started without any inoculum, thus, the biomass developed from the indigenous microorganisms existing in the influent. Acclimation period lasted the equivalent of the solids retention time, during which the system operated without biomass purge. Then, the microbial suspension was periodically and manually purged to maintain the selected SRT, which was 80 d in all the tests. The selection of this value was based on a previous study, where an effective fouling control was achieved [25]. Three experiments were conducted to assess the effect of the CLR on the R-MPBR performance: R-MPBR 1 at 36.6 ± 9.5, R-MPBR 2 at 11.4 ± 3.1, and R-MPBR 3 at 9.1 ± 2.1 g $DOC \cdot m^{-3} \cdot d^{-1}$, while operating at HRT of 2, 5 and 3.5 days, respectively. An additional test, with the filtration unit operating under control conditions (i.e. without illumination), was conducted at CLR of 36.9 ± 13.7 $DOC \cdot m^{-3} \cdot d^{-1}$ (HRT = 2 d). Suspension was characterized according to mixed liquor suspended solid (MLSS), supernatant dissolved organic matter (DOC) and suspended solids $(MLSS)_s$, particle size distribution, elemental analysis,

thermogravimetric analysis (TGA) and Fourier-transform infrared spectroscopy (FTIR). The biomass productivity was estimated according to Eq. (1):

$$r_x = \frac{MLSS}{SRT} \qquad (1)$$

Figure 1. Experimental setup of the R-MPBR system.
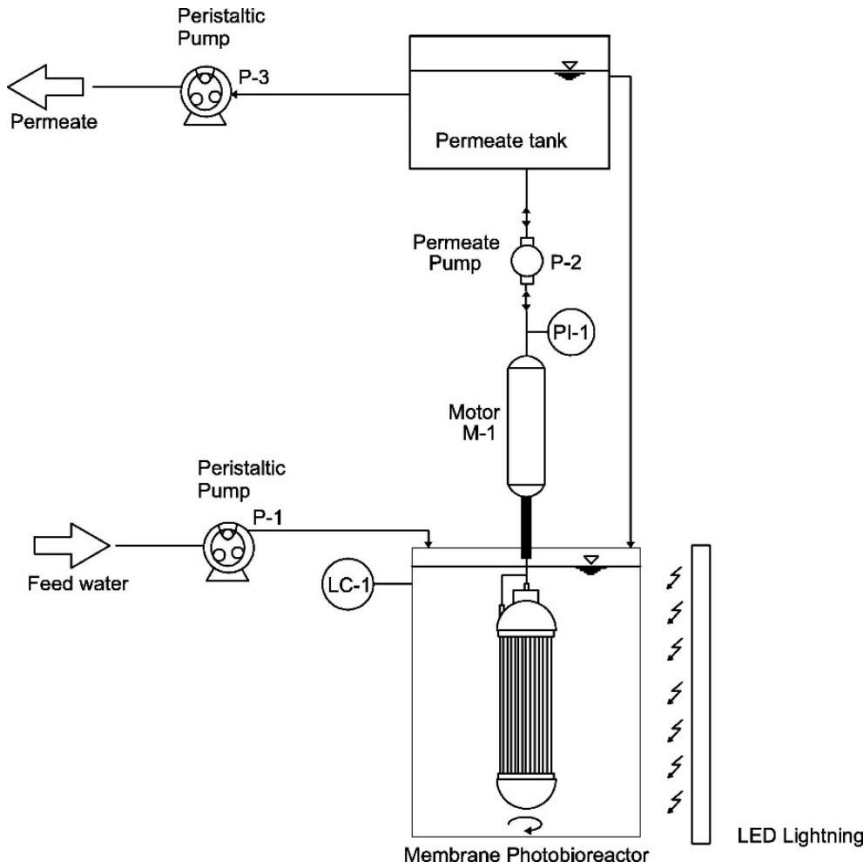
2.4. Short-term flux step trials

After each acclimation period, flux-steps trials were conducted to assess reversible fouling tendency and to establish sustainable conditions for conducting long-term tests, according to previous studies [23]. Selected parameters were a filtration flux range of 6-30 L·h^{-1}·m^{-2}, flux step increment of 1 L·h^{-1}·m^{-2}, step

duration of 15 min, backwashing flux of 30 $L \cdot h^{-1} \cdot m^{-2}$ and backwashing duration of 30 s. Also, membrane rotation at 260 rpm was applied during backwashing.

2.5. Membrane cleaning protocol

After each long-term test, the membrane was cleaned according to a specific "ex situ" protocol, which included three steps: (1) extended rotation, (2) rinsing with tap water and (3) chemical cleaning with sodium hypochlorite (500 $mg \cdot L^{-1}$) for 24 h [26]. At the beginning of the protocol and after each step, a tap water filtration test was conducted to determine the remaining hydraulic resistance.

2.6. Membrane fouling characterization

Transmembrane pressure (*TMP*) evolution under consecutive cycles of filtration/backwashing was used to characterize membrane fouling. Reversible fouling rate (r_f) was evaluated using the slope of the straight line *TMP* against filtration time (*t*). Meanwhile, the residual fouling phenomena, which was not removed by backwashing, was measured by the initial transmembrane pressure TMP_0 at the beginning of the filtration cycle. Therefore, *TMP* evolution during the filtration phase can be described by the following equation:

$$TMP = TMP_0 + r_f \cdot t \quad (2)$$

2.7. Analytical methods

Total suspended solids (TSS), mixed liquor suspended solids (MLSS) and chemical oxygen demand (COD) were analyzed according to the Standard Methods [27]. Turbidity was measured using a turbidimeter HACH 2100 N (Hach, USA). Ammonium-nitrogen (NH_4^+-N) was analyzed by the Nessler method using a DR-5000 Hach spectrophotometer (USA). Nitrite-nitrogen (NO_2^--N), nitrate-nitrogen (NO_3^--N) and phosphate-phosphorus (PO_4^{3-}-P) were analyzed by ion chromatography using a Compact IC plus 882 device, supplied by Metrohm. Total dissolved inorganic nitrogen (DIN) was obtained by adding NH_4^+-N, NO_2^--N and NO_3^--N. Dissolved organic carbon (DOC) concentration was measured with a TOC-meter (TOC-5000A, Shimadzu, Japan). The DOC difference between the filtered supernatant (through a filter of glass-fiber with a nominal pore size of 1.2 µm) and

the permeate was assigned as biopolymer cluster (BPC) concentration [28]. Microbial floc size distribution was measured using a Malvern Mastersizer 2000 instrument (UK) with a detection range of 0.02-2000 µm. For the elemental analysis, a FLASH EA 1112 Elemental Analyzer (ThermoFisher Scientific, USA) was used. Thermogravimetric analysis (TGA) was performed using a simultaneous thermal analyzer (TG/DSC): Discovery SDT 650 (TA Instruments, USA). A quantity of biomass was loaded in a platinum crucible and heated between 25 and 600 ºC at a heating rate of 15 °C/min under a nitrogen flow of 50 mL/min (Alphagaz nitrogen gas, Air Liquid, France). Fourier-transform infrared spectrometry was performed using an IFS 66/S spectrometer (Bruker, USA) equipped with an ATR accessory that measured the transmittance of the samples in a wavelength range between 900 and 4000 cm^{-1}. Microscopic observation of microalgae community and grazers was done following a protocol previously described by Madoni, with modifications [29]. Briefly, three preparations of each sample were analyzed using an aliquot (100 µl) of each one deposited in a glass slide after a gentle homogenization. After covering with a coverslip, they were visualized with an optical microscopy (DM750, Leica, Germany) using objectives 10x, 40x and 100x. Microorganisms were identified according to Wastewater Organisms Atlas Manual [30]. Microalgae community and grazers counts were obtained as the average value of 10 counts per preparation and objective.

Detection of *Escherichia coli* and *Legionella* spp. was performed in the permeate according to ISO 9308 and ISO 11731, respectively, as recommended by the legislation. These methodologies are based in the filtration of the water using 0.45µm pore size nitrocellulose filters that are placed on specific culture media. After the incubation period at 36±2 ºC (21±3 h for E. *coli* and 7-10 days for *Legionella* spp.), bacteria can be identified and quantify, if needed, and results expressed as CFU (Colony Forming Units) per 100 ml (E. *coli*) or 1 L (*Legionella* spp.).

3. Results and discussion

3.1. Treatment performance and biomass productivity

Table 1 shows the removal efficiencies of the main pollutants. Comparable organic matter removal was achieved for the R-MPBR 1 and the control condition,

operated at similar CLR. Average concentrations ranging from 50.4 to 59.9 mg COD·L^{-1}, and from 13.7 to 15.2 mg DOC·L^{-1} were observed in the permeate of both systems, resulting in removal efficiencies of 82.6-85.6% and 78.4-79.5%, respectively. It should be noted that the observed variability was mainly due to the inherent fluctuation of the feedwater. The high efficiencies achieved might be explained by the membrane retention, since no appreciable biological degradation is expected in the control condition. In fact, these results are in agreement with those previously reported in a direct membrane ultrafiltration process applied to the same feedwater [23]. In addition, decreasing CLR in the R-MPBR below 11.4 g DOC·m^{-3}·d^{-1} (57.7 g COD·m^{-3}·d^{-1}) caused a significant increment of dissolved oxygen concentration (DO), as can be seen in Figure 2, revealing that photosynthetic oxygenation potential was enough to provide aerobic conditions below this CLR. It should be noted that average ammonia loading at this condition was 10.2 g N·m^{-3}·d^{-1}, which might increase the theoretical oxygen demand in 46.6 g O$_2$·m^{-3}·d^{-1} (assuming 4.57 g O$_2$·g^{-1} N for complete nitrification [24]), resulting in a global theoretical value of oxygen demand of 104.3 g O$_2$·m^{-3}·d^{-1}. This oxygenation potential was comparable with that reported in a previous study of degradation of piggery wastewater (116 to 133 g O$_2$·m^{-3}·d^{-1}) [9]. Nevertheless, despite the aerobic conditions achieved, no further organic matter removal was obtained (Table 1), which confirmed the main role of membrane retention.

Table 1 also shows biomass concentration and productivity under the different conditions. By comparing the results obtained for the R-MPBR 1 and the control condition, it is evident that the introduction of microalgae significantly increased (2.8 times) biomass productivity.
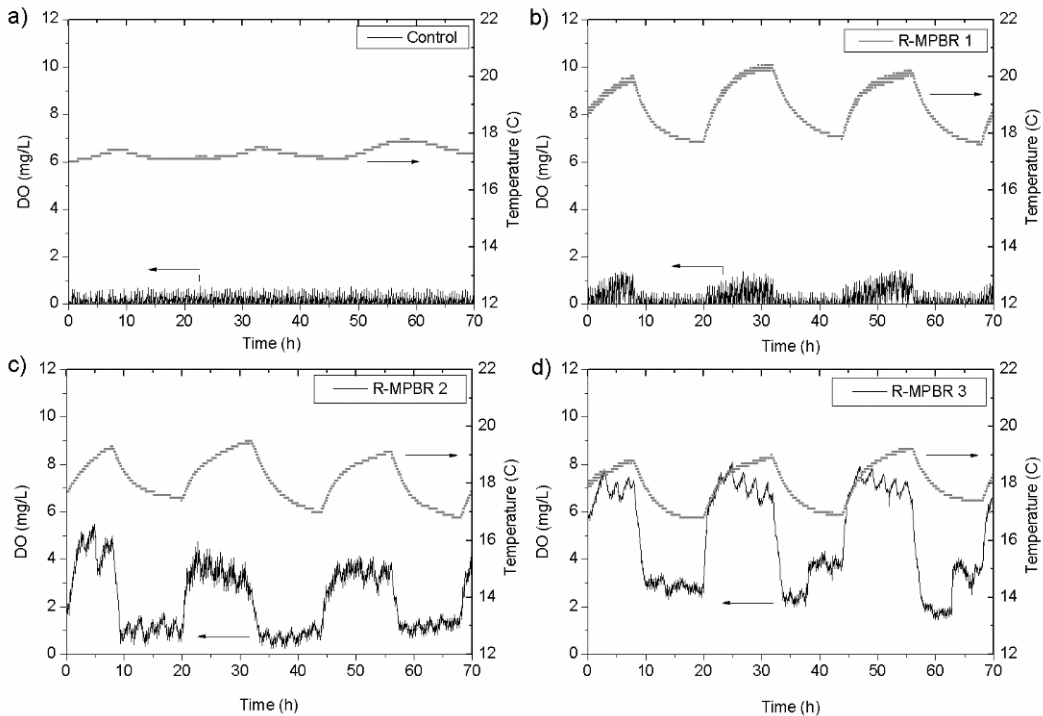
Figure 2. Dissolved oxygen (DO) and temperature profiles of (a) control condition, (b) R-MPBR 1, (c) R-MPBR 2 and (d)R-MPBR 3.

Previous studies have reported the influence of organic matter, more than other environmental factors, on microalgae population in mixed consortia, enhancing the dominance of species with a high tolerance [31]. Nevertheless, very high organic carbon concentrations (> 231 mg DOC·L^{-1}) were found to inhibit the growth of microalgae due to a competitive interaction with heterotrophic bacteria, as noted by He *et al*. [32]. Consistently, the obtained results confirmed the effective growth of native microalgae species in the tested conditions. In this sense, several microalgae, such as *Chlorella* and *Scenedesmus*, have demonstrated their tolerance and/or ability to acclimatize to primary settled wastewater [33]. This is in agreement with a synergistic support between microalgae and bacteria, where microalgae can provide photosynthetic dissolved oxygen and extracellular metabolites and bacteria can release inorganic carbon, vitamins or other substances that can enhance the growth of microalgae in return [2,34]. In fact,

biomass productivities reported here are comparable to those typically found in MPBRs applied to secondary effluents treatment (10-60 mg·L^{-1}·d^{-1}) [35]. Additionally, decreasing CLR should decrease bacterial growth due to lower organic substrate loading. Also, low CLRs promote zooplankton grazers, which mainly consume dispersed bacteria and microalgae [36]. Consistently, biomass productivity decreased from 47.4 ± 3.3 mg·L^{-1}·d^{-1} to 22.0 ± 2.9 mg·L^{-1}·d^{-1}.

Table 1. Biological performance of MPBR and control condition.

Parameters	R-MPBR 1	R-MPBR 2	R-MPBR 3	Control
CLR (g DOC·m^{-3}·d^{-1})	36.6	11.4	9.1	36.9
Permeate concentration (mg·L^{-1})				
COD	50.4 ± 16.0	43.9 ± 15.4	31.0 ± 15.2	59.9 ± 21.4
DOC	15.2 ± 2.0	10.9 ± 1.7	8.6 ± 1.0	13.7 ± 4.8
NH$_4^+$-N	14.7 ± 12.9	0.6 ± 0.3	0.6 ± 0.6	62.4 ± 8.0
NO$_3^-$-N	0.2 ± 0.3	53.2 ± 9.8	52.8 ± 10.6	0.2 ± 0.2
NO$_2^-$-N	2.6 ± 1.9	2.0 ± 2.2	0.4 ± 0.6	0.3 ± 0.3
DIN	17.5 ± 12.9	55.8 ± 8.1	58.8 ± 9.3	62.9 ± 8.0
PO$_4^{3-}$-P	6.8 ± 1.2	6.8 ± 0.7	9.9 ± 1.4	10.4 ± 0.2
Removal efficiency (%)				
COD	85.6 ± 5.2	84.8 ± 6.8	89.2 ± 5.6	82.6 ± 8.9
DOC	78.4 ± 4.0	73.0 ± 19.1	55.4 ± 1.7	79.5 ± 8.8
NH$_4^+$-N	84.3 ± 14.7	98.8 ± 0.6	99.1 ± 1.2	28.4 ± 14.6
DIN	81.2 ± 13.9	20.7 ± 7.9	21.2 ± 10.1	27.9 ± 14.7
PO$_4^{3-}$-P	25.4 ± 12.0	11.0 ± 4.1	12.2 ± 10.6	7.1 ± 4.8
Biomass concentration (mg·L^{-1})	3788 ± 261	2378 ± 427	1759 ± 232	1333 ± 125
Biomass productivity (mg·L^{-1}·d^{-1})	47.4 ± 3.3	29.7 ± 5.3	22.0 ± 2.9	16.7 ± 3.3

Note: The data are expressed as mean ± standard deviation.

Regarding nutrient removal, significant differences were found between the R-MPBR 1 and the control condition (Table 1). At similar CLR, average nitrogen and phosphorus removal efficiencies increased 2.9 and 3.6 times, respectively. This might be attributed to the presence of microalgae growth and the associated nutrient needs, as previously stated. Concentrations of 17.5 ± 12.9 mg DIN·L^{-1} and

6.8 ± 1.2 mg PO_4^{3-}-P·L^{-1} were recorded in the R-MBPR permeate. Calculated removal rates were 37.2 mg·L^{-1}·d^{-1} and 1.6 mg·L^{-1}·d^{-1} for nitrogen and phosphorus, respectively. The DIN removal rate was much higher than those typically found (1.6-12.5 mg·L^{-1}·d^{-1}) in other MPBR studies [10,37]. Also, much more than expected by biomass assimilation (3.8 mg·L^{-1}·d^{-1}, assuming a ratio of nitrogen to increased biomass of 8% [38]), which suggest an additional removal mechanism. It should be noted that recorded pH values (7.8 ± 0.1) made ammonia volatilization negligible. In addition, a slight NO_2^--N concentration was also detected (Table 1), revealing an apparent simultaneous nitrification-denitrification process, consistent with the slightly aerobic conditions (Figure 2b) and the significant nitrogen removal decrease observed at lower CLR (Table 1). This removal mechanism has also been reported in a previous study of a photo-sequencing batch reactor [39]. Regarding phosphorus removal, the obtained rate (1.2 mg·L^{-1}·d^{-1}) was consistent with a biomass assimilation mechanism [40].

Different performance was obtained at CLR bellow 11.4 g DOC·m^{-3}·d^{-1}, since the photosynthetic oxygenation rate was sufficient to provide aerobic conditions, which prevented the denitrification process. Dissolved oxygen profiles showed average values of about 3.5/0.8 mg·L^{-1} and 7/3 mg·L^{-1} during the light/dark periods, for 11.4 and 9.1 g DOC·m^{-3}·d^{-1}, respectively (Figures 2c and d). Consequently, nitrogen removal was mainly due to biomass assimilation. Removal efficiencies decreased to 20.7 ± 7.9% and 21.2 ± 10.1% corresponding to DIN concentrations of 55.8 ± 8.1 mg·L^{-1} and 58.8 ± 9.3 mg·L^{-1} in the permeate, mainly in the form of nitrate-nitrogen, for CLR of 11.4 and 9.1 g DOC·m^{-3}·d^{-1}, respectively (Table 1). Calculated DIN removal rates were 2.1 and 4.5 mg·L^{-1}·d^{-1}, respectively. Additionally, phosphorus removal rates were also lower (0.1 and 0.3 mg·L^{-1}·d^{-1}, respectively) than those obtained at CLR of 36.6 g DOC·m^{-3}·d^{-1}, consistent with a lower biomass productivity.

Finally, microbial (absence of *E. coli* and *Legionella spp.*) and physical (turbidity < 0.5 NTU) quality of the permeate generated in the R-MPBRs complied with the new European regulation of reclaimed water quality for agricultural irrigation [41].

3.2. Biomass suspension characteristics

FTIR spectra of the biomass samples showed the typical biochemical composition, with the presence of specific peaks of carbohydrates, nucleic acids, proteins and lipids [42] (Figure 3). Nevertheless, thermogravimetric analysis revealed different proportions of components according to devolatilization profiles (Figure 4). Control and R-MPBR 1 samples showed a narrow degradation profile with a main peak at about 315 °C (Figure 4a). However, while decreasing the CLR applied (from R-MPBR 2 to R-MPBR 3), the peak intensity progressively decreased and an additional peak appeared at around 275 °C, revealing a wider degradation profile. This could be due to higher protein content, which typically decomposes at a lower temperature than carbohydrates and lipids. Indeed, it has been reported main degradation peaks in the range 275-295 °C for some high-protein microalgae [43].Therefore, it seems that decreasing CLR may induce a more complex biomass structure, which can be related to higher bioflocculation. Nevertheless, no significant differences of total biomass volatile matter were found (57.7-61.8%) (Figure 4b), whose values were within the typical range reported for microalgae biomass [44]. Additionally, elemental analysis showed that all biomass samples had carbon, hydrogen, nitrogen and sulfur content of 36.5-37.8%, 4.4-5.7%, 6.5-8.4% and 0-0.8%, respectively (Table 2). These values are comparable to those reported for microalgal biomass [38]. In agreement with the thermogravimetric analysis, N content increased with decreasing CLR in R-MPBRs, consistent with higher amounts of protein.

Due to its impact on membrane performance, bioflocculation has been assessed by analyzing particle size distribution and biopolymer cluster content in the supernatant (Table 2). A significant increase in floc size was observed in the R-MPBR samples, revealing efficient bioflocculation by the microalgae-bacteria consortium. In R-MPBR 1, medium-size flocs were observed ($D_{(0.5)} = 61.9 \pm 5.9$ µm) with narrow distribution (spread index of 1.17 ± 0.04). Also, decreasing CLR to 11.4 and 9.1 DOC·m^{-3}·d^{-1} increased the median value up to 70.5 ± 8.6 µm (1.15 ± 0.03) and 92.8 ± 3.0 µm (0.95 ± 0.03), respectively. These values are higher than those reported in a microalgal-bacterial MPBR treating a secondary effluent [35], confirming the efficient flocculation achieved in the test conditions. It should be noted that an increase in floc size (with a narrow distribution) may reduce membrane fouling due to formation of a porous cake layer with low filtration resistance. On the other hand, previous studies have highlighted the role of

extracellular polymeric substances (EPS) released by the microalgae and bacteria on the bioflocculation [2]. Several bioflocculation mechanisms have been reported, including charge neutralization and bridging, both due to the adsorption of charged biopolymers [45]. Therefore, it is expected that supernatant biopolymers may be related to the bioflocculation process. This is consistent with the current study, where the biopolymer clusters (BPC), which represented the colloidal fraction of biopolymers, was significantly reduced in the R-MPBR (Table 2). In addition, it has been argued that BPC, which are apparently formed by affinity clustering of soluble EPS, can be degraded by heterotrophic bacteria [46]. This can justify the lower BPC content in the R-MPBR when decreasing the CLR, which, as already indicated, enhances aerobic degradation. It should be noted the impact of BPC in membrane fouling, which can reduce cake layer porosity, and thus enhance floc attachment to the membrane [47]. The enhancement of bioflocculation at low CLR was also confirmed by the low values of suspended solids in the supernatant (MLSS)$_s$ and the corresponding ratios to the solid concentration in the suspension (MLSS)$_s$/MLSS (Table 2).
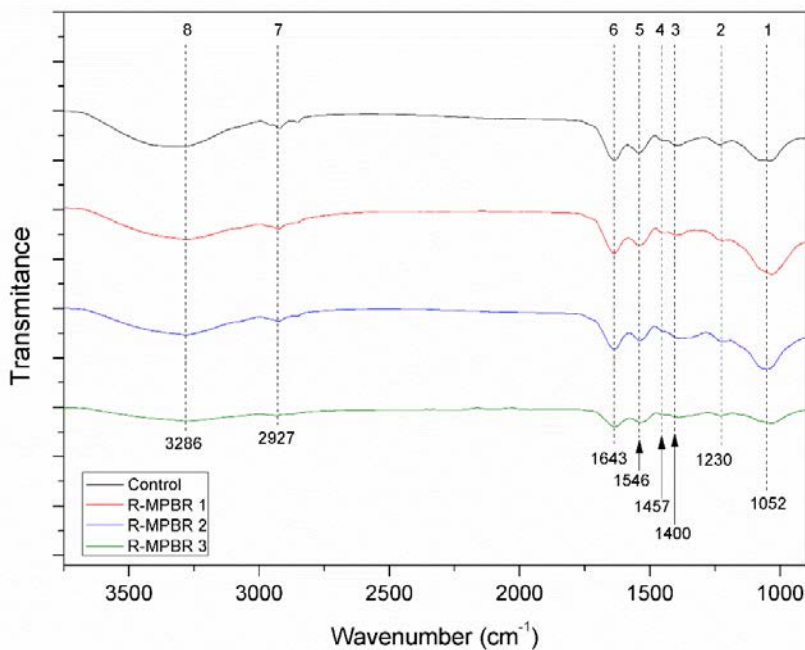

Figure 3. FTIR spectra of biomass samples from the R-MPBRs and the control one. Characteristics bands were identified from carbohydrates (band 1), nucleic acids (band 2), proteins (bands 3-6 and 8) and lipids (band 7).
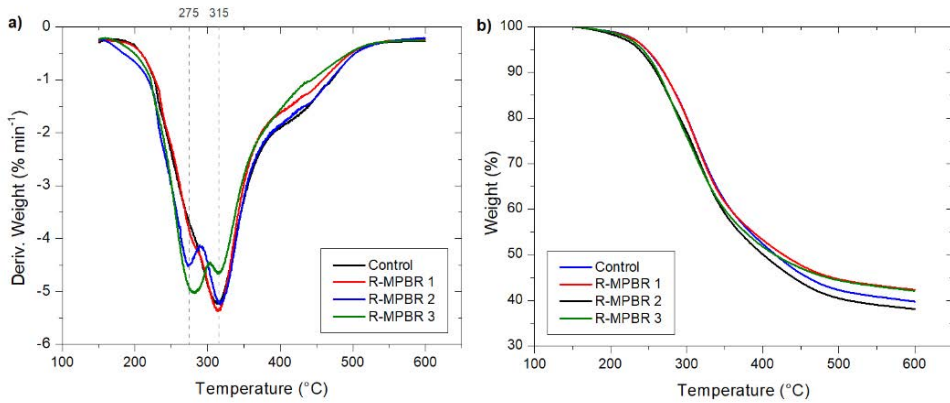
Figure 4. Differential thermogravimetric (DTG) (a) and thermogravimetric analysis (TGA) (b) dataset of the control condition and the R-MPBR samples.

Table 2. Main suspension characteristics of the MPBR and the control condition.

Parameters	R-MPBR 1	R-MPBR 2	R-MPBR 3	Control
CLR (g DOC·m^{-3}·d^{-1})	36.6	11.4	9.1	36.9
Elemental analysis (%wt, dry basis)				
C	36.5 ± 1.2	37.7 ± 0.4	37.8 ± 2.2	37.0 ± 1.8
H	4.4 ± 1.2	5.5 ± 0.1	5.4 ± 0.2	5.7 ± 0.1
N	6.5 ± 0.2	8.2 ± 0.1	8.4 ± 0.2	6.9 ± 0.4
S	0.8 ± 0.3	nd	nd	0.8 ± 0.1
Particle size distribution				
$D_{(0.1)}$ (μm)	17.6 ± 3.0	22.5 ± 4.7	31.4 ± 3.8	13.2 ± 1.2
$D_{(0.5)}$ (μm)	61.9 ± 5.9	70.5± 8.6	92.8 ± 3.0	38.4 ± 5.0
$D_{(0.9)}$ (μm)	162.9 ± 12.1	184.3 ± 20.5	207.9 ± 3.6	81.9 ± 10.9
Supernatant				
BPC (mg DOC·L^{-1})	50.0 ± 14.8	24.3± 7.4	2.3± 0.8	78.2 ± 27.4
$(MLSS)_s$ (mg·L^{-1})	317 ± 66	179 ± 21	65 ± 14	994 ± 63
$(MLSS)_s$/MLSS (%)	8.4	7.5	3.7	74.6

Note: The data are expressed as mean ± standard deviation. nd: not-detected.

3.3. Membrane fouling

3.3.1. Analysis of reversible fouling rate in flux-steps trials

As stated, many MPBR studies have reported similarities in the fouling mechanisms with those typically observed in MBRs [3,4]. Therefore, flux-step trials have been conducted to assess the effect of the suspension characteristics on fouling rates (r_f) under different permeate flux (J) conditions. Additionally, the results were compared to those achieved with the corresponding supernatants, which were obtained by removing sedimentable solids from the suspension (see main characteristics in Table 2). For all the experiments performed, r_f continuously increased with J (Figure 5a). Nevertheless, the control condition and the R-MPBRs behaved differently. In the former, a sharp increase of r_f was observed at moderate fluxes. Specifically, r_f increased from 1.0 to 76.3 mbar·min^{-1} when increasing J from 6 to 29 L·h^{-1}·m^{-2}. By contrast, the fouling trend of the R-MPBR under the same conditions (R-MPBR 1) followed a linear increase. In this case, r_f values were between 1.5 and 32.5 mbar·min^{-1}, which was a substantially lower fouling sensitivity. In addition, an evident effect of decreasing CLR was also observed in R-MPBR 2 and R-MPBR 3, where the r_f ranges were 0.6-12.1 mbar·min^{-1} and 0.2-4.5 mbar·min^{-1}, respectively. Regarding supernatant fractions, similar behaviours were observed, where only slightly lower fouling rates were achieved compared with those obtained by the suspensions. Consequently, results showed that the fouling was mainly determined by supernatant fractions for all the tested conditions.

The results were analysed using the cake filtration model, where the fouling rate is expressed in terms of solvent viscosity (μ), specific cake resistance (α), cake concentration (ω) and permeate flux, as showed in Eq. (3):

$$r_f = \mu \cdot \alpha \cdot \omega \cdot J^2 \qquad (3)$$

According to the model, the product $\alpha\omega$ depends on the cake properties and, consequently, on suspension characteristics. Calculated values for the control condition showed two different regions above and below a critical flux (J^*) of 11 L·h^{-1}·m^{-2}. At subcritical fluxes, constant $\alpha\omega$ was achieved (4.9·10^{14} ± 5.2·10^{13} m^{-2}). By increasing flux above J^*, $\alpha\omega$ linearly increased (4.9·10^{14} + 6.6·10^{13}· ($J - J^*$), R^2 = 0.98). Provided that ω is proportional to the solids concentration in the

suspension, then α should increase with J at supra-critical conditions. For dead-end filtration, the existence of a critical flux has been related to a consolidation of the cake layer [28]. It is expected that in the control condition, characterized by a high BPC content, the internal void spaces of the cake layer become clogged with the biopolymers, reaching an "overclogging situation" [47], where cake porosity substantially decreased. According to the Carman-Kozeny equation, α gradually increases with decreasing cake layer porosity until a threshold value is achieved, from which it increases abruptly [48]. The impact of BPCs was confirmed when filtering the supernatant of the control condition, where the αw values accounted for 75 ± 6% of that obtained for the suspension (Figure 5b).

As stated, R-MPBRs followed a different behaviour. Figure 5b shows nearly constant αw values of $8.6 \cdot 10^{14} \pm 6.3 \cdot 10^{13}$ m^{-2}, $3.1 \cdot 10^{14} \pm 3.4 \cdot 10^{13}$ m^{-2} and $7.8 \cdot 10^{13} \pm 2.2 \cdot 10^{13}$ m^{-2} for R-MPBR 1, R-MPBR 2 and R-MPBR 3, respectively. In addition to the effect of the solid concentration, results also showed that αw decreased with increasing particle size and decreasing BPCs. This is consistent with the crucial role of both parameters in regulating cake porosity. Also, these results are in agreement with those reported in previous MPBR studies culturing *C. Vulgaris*, where significant supernatant biopolymer retention by membrane and a large fraction of smaller particles were found to induce severe fouling [8,15]. Similar to that observed for the control condition, the filtration tests with the supernatants resulted in αw values comparable to those obtained for the suspensions (79%, 77% and 59% for R-MPBR 1, R-MPBR 2 and R-MPBR 3, respectively).
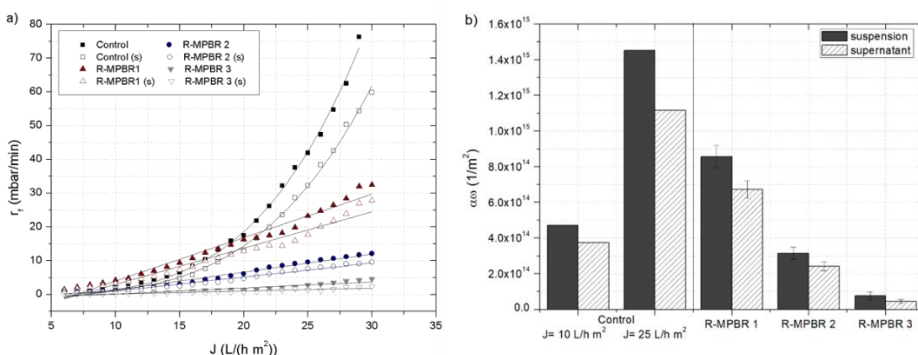

Figure 5. Fouling rate (a) against permeate flux during the flux-step trials and calculated αw values (b) for the suspension and supernatant (s) of the control condition and the R-MPBRs. For the R-MPBRs, αw is expressed as average and standard deviation values at the flux range 6-30 L·h^{-1}·m^{-2}.

3.3.2. Effect of the physical cleaning strategy on residual and reversible *fouling during long term operation*

Process sustainability was analysed by assessing the cleaning efficiency of the proposed strategy. The permeate flux was fixed at 10 $L·h^{-1}·m^{-2}$ to achieve reasonable process productivity, in agreement with most MPBR studies, where operating fluxes were typically within the range of 2.6-15 $L·h^{-1}·m^{-2}$ [3]. In addition, according to the previous flux-steps trials (Figure 5a), this flux should avoid initial non-operative fouling rates (< 5 $mbar·min^{-1}$) for the tested suspensions [6]. Also, additional physical cleanings were applied once a week by conducting a relaxation (RX) phase with continuous module rotation, as described in section 2.

Figure 6 shows the residual fouling evolution, described by the initial transmembrane pressure (TMP_0) at the beginning of the filtration cycles, for the control condition and the R-MPBRs. The results showed the pattern predicted by the flux-steps tests, revealing the relationship between reversible and residual fouling. As physical cleaning cannot completely remove fouling, residual fouling progressively grows with the operation time. For the control condition, TMP_0 increased at a slow rate of 5.9 $mbar·d^{-1}$ for the first 8 days, but then sharply increased up to 200 mbar by day 15. This profile is commonly observed in submerged MBRs and has been mainly associated to a cake layer compaction which accelerates fouling rate [48]. Therefore, similarities can be observed with the effect of increasing permeate flux in the flux-step trials conducted for the control condition. During long-term operation, due to the low flux applied, fouling rates were initially maintained at low values, but some residual fouling was observed (Figure 6a). With increasing operating time, this residual fouling may decrease the available membrane filtration area, leading to a progressive increase of the actual flux, which finally results in a cake layer consolidation. In addition, consolidated cakes are reported to be less reversible by backwashing [49] and probably contributed to the rapid residual fouling (i.e. TMP_0) increase observed. Low fouling reversibility can also be observed in the inefficiency of the relaxing phases conducted after 7 and 14 days (Figure 6a). Moreover, a recent work by Vroman *et al*. [50] has introduced the critical inter cake-membrane concept (i.e. minimal pressure force to detach the cake), which links both cake and membrane hydraulic resistances to the critical backwashing pressure to achieve maximal cleaning efficiency.

A different fouling behaviour was observed for the R-MPBRs. In all cases, a roughly linear TMP_0 increase was found, whose rate of increase declined with CLR (from R-MPBR 1 to R-MPBR 3) (Figures 6b-d). In agreement with a previous MPBR study [7], a noticeable effect of light pattern on TMP_0 profile can be observed, where a reduction of residual fouling was typically recorded during light hours. This can be attributed to the temperature profile (from 17 to 20 °C) and its effect on permeate viscosity. When operated at the same conditions of the control test (R-MPBR 1), TMP_0 continuously increased at an average rate of 6.66 ± 0.02 mbar·d^{-1} (R^2 = 0.95), reaching 200 mbar on day 25. An evident improvement of the filtration performance was achieved as a consequence of avoiding the cake consolidation, but the large r_f values reached throughout the test (> 5 mbar·min^{-1}) (Figure 6b) induced a non-operative residual fouling rate. As stated, this is related to a larger proportion of small flocs and higher BPC obtained at these conditions. Additionally, significant fouling sensitivity (within the range of 5-22 mbar·min^{-1}) to influent fluctuations, particularly the nitrogen organic load and the resulting variable ammonia removal rates (see Table 1) were observed. This positive effect of ammonia nitrification is frequently reported in many MBR studies [51]. Regarding the cleaning efficiency of the relaxation phases, an instantaneous TMP_0 decrease was observed after each event, although it rapidly increased until reaching the previous values. This behaviour suggests that cleaning parameters (mainly backwashing duration) can be improved to achieve better residual fouling control. Hence, although non-operative residual fouling rates were found in R-MPBR 1, the results also revealed the reversibility of a significant part of this type of fouling in contrast with the behaviour obtained in the control condition.

Sustainable operation can be maintained in R-MPBR 2 and R-MPBR 3, where TMP_0 increased at rates of 1.80 ± 0.01 mbar·d^{-1} (R^2 = 0.88) and 0.42 ± 0.01 mbar·d^{-1} (R^2 = 0.86), respectively (Figures 6c and d). Comparable values have been reported for full-scale MBRs [16]. This behaviour can be attributed to the low and stable fouling rates achieved through the tests (3.63 ± 0.90 mbar·min^{-1} and 0.16 ± 0.13 mbar·min^{-1} for R-MPBR 2 and R-MPBR 3, respectively). Compared with the corresponding values found during the flux-steps trials (Figure 5a) at the same flux (10 L·h^{-1}·m^{-2}) with a clean membrane, r_f increased about 3 times in R-MPBR 2 and remained at the same value in R-MPBR 3, consistent with the residual fouling trends for each condition. In addition, due to the low fouling loads at these conditions, relaxation phases did not induce significant fouling removal, revealing that the cleaning parameters were optimal.
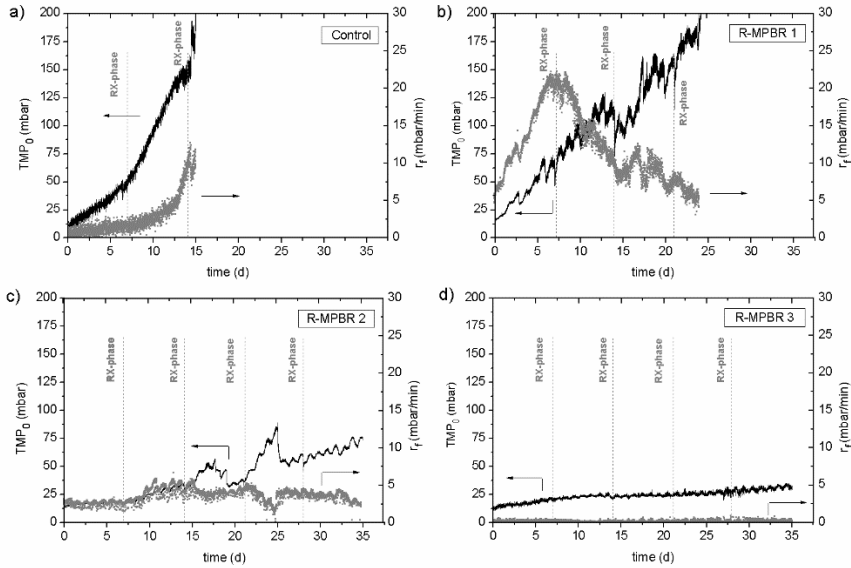
Figure 6. Initial transmembrane pressure (TMP_0) and reversible fouling rate (r_f) evolution of (a) control condition, (b) R-MPBR 1, (c) R-MPBR 2 and (d) R-MPBR 3.

In summary, the long-term behaviour revealed the efficiency of the proposed cleaning strategy at moderate CLR, suggesting that the system can be operated during long periods. Nevertheless, further studies should focus on improving process productivity by increasing permeate flux.

After the long-term tests, a simplified analysis of the residual fouling layer was conducted. A specific "ex situ" cleaning protocol (described in section 2) separated the layers in three main fractions: loose cake (removed by extended rotation), consolidated cake (removed by rinsing in tap water) and adsorbed material (removed by NaClO). Assessing the individual contribution of each layer in terms of resistance, the loose cake accounted for 0%, 68.7%, 11.8% and 1.1% of total fouling resistance, for the control condition, R-MPBR 1, R-MPBR 2 and R-MPBR 3, respectively. As expected, these results are consistent with those obtained by conducting relaxation events in the filtration tests. An opposite trend was found for consolidated cake, achieving values of 98%, 19.6%, 14.2% and 9.1%, respectively. A minor influence of adsorbed material (1-4.4%) was found in all cases, confirming that the cake filtration is the main fouling mechanism.

3.4. Microalgal composition and zooplankton grazers in the R-MPBRs

As stated, the R-MPBR was started-up without inoculum and the feedwater was used to fill the photobioreactor the first day. After the corresponding acclimation period at each condition, a combination of species belonging to *Chlorella* genera embedded in dense flocs and diatoms (*Nitzschia* and *Navicula* genera) were observed in all conditions (Figures 7a-c). Due to their versatility and tolerance to a wide range of environmental conditions, these species are commonly observed in microalgal consortia applied to wastewater treatment [11]. In fact, species of *Chlorella* developed at high COD concentration, probably due to its dual phototrophic and heterotrophic metabolism [52]. However, filamentous species of microalgae (*Chaetophora* sp.) and cyanobacteria (*Oscillatoria* sp.) were only found at higher CLR (Figures 7b and c). Although less studied, *Chaetophora* sp. has been previously observed in MPBRs treating secondary effluents [53]. Moreover, species of *Oscillatoria* were reported as organic pollution-tolerant [54]. Additionally, the development of cyanobacteria can be related to the negligible dissolved oxygen concentration at higher CLR, as reported in a PBR fed with a synthetic wastewater operated at comparable CLR (44.5 g DOC·m^{-3}·d^{-1}), where simultaneous nitrification-denitrification process was also achieved [55].

Microscopic examination also showed several species of ciliates (*Vorticella* sp., *Epistylis* sp., *Paramecium* sp., *Euplotes* sp., *Aspidisca* sp., *Coleps* sp.) (representative species are showed in Figures 7d-g). These protozoan microbes have been frequently recorded in biological wastewater treatments [56], and have a crucial role in bioflocculation by consuming dispersed bacteria and microalgae [36]. In this regard, free-swimming ciliates predominated in all conditions. Additionally, a change in species structure from attached to crawling ciliates (Figures 7e-g) was observed with decreasing CLR, in accordance with previous studies [56]. Moreover, apart from testate amoebae and ciliates, metazoans were also observed. Large nematodes were found in all conditions. By contrast, rotifers (Bdelloidea Order and *Lecane* sp.) were only observed at low CLR (Figures 7h and i). This situation was probably due to the oxygen depletion at high CLR, which has been identified as a significant factor limiting rotifers growth [57]. This seems to be related to the observed trend of decreasing biomass concentration and, particularly, suspended solids in supernatant, with decreasing CLR. Furthermore, it has been stated that bdelloid rotifers enhance bioflocculation due to secreted

substances [58], which is consistent with what was observed in the present study. Hence, results showed that the density and diversity of grazers, mainly crawling ciliates and rotifers, seems to be related to better R-MPBR performance.
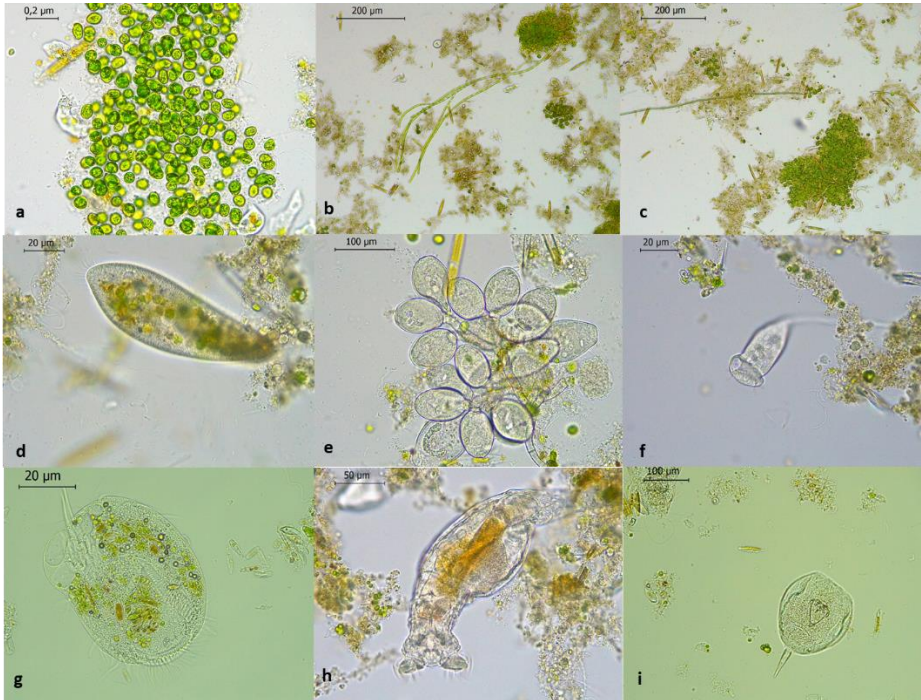

Figure 7. Representative microscopic view of microalgae community and zooplankton grazers developed. (a) *Chlorella* sp. (R-MPBR 1); (b) *Chlorella* sp., *Chaetophora* sp. and *Nitzshia* sp. (R-MPBR 1); (c) *Chlorella* sp., *Oscillatoria* sp. and *Nitzshia* sp. (R-MPBR 1); (d) *Paramecium* sp. (R-MPBR 1), (e) *Epistylis* sp. (R-MPBR 1); (f) *Vorticella* sp. (R-MPBR 2); (g) *Euplotes* sp. (R-MPBR 2); (h) Bdelloid rotifer (R-MPBR 2) and (i) *Lecane* sp. (R-MPBR 2).

4. Conclusions

The rotating membrane photobioreactor with indigenous microalgae-bacteria consortia demonstrated its capability in the treatment of primary settled wastewater under photosynthetic oxygenation. It was observed that the carbon loading rates (CLR) determined the dissolved oxygen concentration, affecting nutrient removal, bioflocculation and membrane fouling. At the higher value (36.6 g DOC·m^{-3}·d^{-1}), dissolved inorganic nitrogen removal was significantly enhanced

(81.2 ± 13.9%), which was about 2.5-2.6 times of those obtained at lower CLRs, revealing a simultaneous nitrification-denitrification process. Decreasing CLR from 36.6 to 9.1 g DOC·m^{-3}·d^{-1} led to complete nitrification, increased particle size (D$_{(0.5)}$ from 61.9 to 92.8 μm) and decreased biopolymer clusters content (from 50.0 to 2.3 mg DOC·L^{-1}). Cake filtration model showed that the fouling was mainly caused by the supernatant fraction of the suspension, particularly by the biopolymer clusters content. Consequently, optimal filtration conditions were obtained at low to moderate CLRs (≤ 11.4 g DOC·m^{-3}·d^{-1}), where a sustainable long-term operation at a filtration flux of 10 L·h^{-1}·m^{-2} was observed. Microalgae species belonging to the genera *Chlorella* and diatoms (*Nitzschia* and *Navicula* genera) were identified in all conditions, while filamentous microalgae (*Chaetophora* sp.) and cyanobacteria (*Oscillatoria* sp.) were only found at high CLR. Meanwhile, crawling ciliates and rotifers were only observed at low CLR, which seems to be related to the lower biomass concentration and, particularly, suspended solids in the supernatant. The new proposed configuration effectively controlled membrane fouling, allowing to further process optimization.

References

[1]   Z.J. Ren, K. Pagilla, Pathway to water sector decarbonization, carbon capture and utilization, IWA Publishing, London, UK, 2022.

[2]   A. Fallahi, F. Rezvani, H. Asgharnejad, E. Khorshidi, N. Hajinajaf, B. Higgins, Interactions of microalgae-bacteria consortia for nutrient removal from wastewater: A review, Chemosphere. 272 (2021) 129878. https://doi.org/10.1016/j.chemosphere.2021.129878.

[3]   Y. Luo, P. Le-Clech, R.K. Henderson, Simultaneous microalgae cultivation and wastewater treatment in submerged membrane photobioreactors: A review, Algal Res. 24 (2017) 425–437. https://doi.org/10.1016/j.algal.2016.10.026.

[4]   Y. Liao, A. Bokhary, E. Maleki, B. Liao, A review of membrane fouling and its control in algal-related membrane processes, Bioresour. Technol. 264 (2018) 343–358. https://doi.org/10.1016/j.biortech.2018.06.102.

[5]   M. Zhang, L. Yao, E. Maleki, B.Q. Liao, H. Lin, Membrane technologies for microalgal cultivation and dewatering: Recent progress and challenges, Algal Res. 44 (2019) 101686. https://doi.org/10.1016/j.algal.2019.101686.

[6]   J. González-Camejo, A. Jiménez-Benítez, M. V. Ruano, A. Robles, R. Barat, J. Ferrer, Optimising an outdoor membrane photobioreactor for tertiary sewage treatment, J. Environ. Manage. 245 (2019) 76–85. https://doi.org/10.1016/j.jenvman.2019.05.010.

[7]   E. González, O. Díaz, I. Ruigómez, C.R. de Vera, L.E. Rodríguez-Gómez, J. Rodríguez-Sevilla, L. Vera, Photosynthetic bacteria-based membrane bioreactor as post-treatment of an anaerobic membrane bioreactor effluent, Bioresour. Technol. 239 (2017). https://doi.org/10.1016/j.biortech.2017.05.042.

[8]   A.F. Novoa, L. Fortunato, Z.U. Rehman, T.O. Leiknes, Evaluating the effect of hydraulic retention time on fouling development and biomass characteristics in an algal membrane photobioreactor treating a secondary wastewater effluent, Bioresour. Technol. 309 (2020) 123348. https://doi.org/10.1016/j.biortech.2020.123348.

[9]   I. de Godos, V.A. Vargas, S. Blanco, M.C.G. González, R. Soto, P.A. García-Encina, E. Becares, R. Muñoz, A comparative evaluation of microalgae for the degradation of piggery wastewater under photosynthetic oxygenation, Bioresour. Technol. 101 (2010) 5150–5158. https://doi.org/10.1016/j.biortech.2010.02.010.

[10]   M. Zhang, K.T. Leung, H. Lin, B. Liao, Effects of solids retention time on the biological performance of a novel microalgal-bacterial membrane photobioreactor for industrial wastewater treatment, J. Environ. Chem. Eng. 9 (2021) 105500. https://doi.org/10.1016/j.jece.2021.105500.

[11]   A.L. Gonçalves, J.C.M. Pires, M. Simões, A review on the use of microalgal consortia for wastewater treatment, Algal Res. 24 (2017) 403–415. https://doi.org/10.1016/j.algal.2016.11.008.

[12]   M. Wu, Y. Chen, H. Lin, L. Zhao, L. Shen, R. Li, Y. Xu, H. Hong, Y. He, Membrane fouling caused by biological foams in a submerged membrane bioreactor: Mechanism insights, Water Res. 181 (2020) 115932. https://doi.org/10.1016/j.watres.2020.115932.

[13]   Y. Long, G. Yu, L. Dong, Y. Xu, H. Lin, Y. Deng, X. You, L. Yang, B.Q. Liao, Synergistic fouling behaviors and mechanisms of calcium ions and polyaluminum chloride associated with alginate solution in coagulation-ultrafiltration (UF) process, Water Res. 189 (2021) 116665. https://doi.org/10.1016/j.watres.2020.116665.

[14]   J. Teng, M. Zhang, K.T. Leung, J. Chen, H. Hong, H. Lin, B.Q. Liao, A unified thermodynamic mechanism underlying fouling behaviors of soluble microbial products (SMPs) in a membrane bioreactor, Water Res. 149 (2019) 477–487. https://doi.org/10.1016/j.watres.2018.11.043.

[15]   S.L. Low, S.L. Ong, H.Y. Ng, Characterization of membrane fouling in submerged ceramic membrane photobioreactors fed with effluent from membrane bioreactors, Chem. Eng. J. 290 (2016) 91–102. https://doi.org/10.1016/j.cej.2016.01.005.

[16]   A. Drews, Membrane fouling in membrane bioreactors-Characterisation, contradictions, cause and cures, J. Memb. Sci. 363 (2010) 1–28.

https://doi.org/10.1016/j.memsci.2010.06.046.

[17] H. Lin, M. Zhang, F. Wang, F. Meng, B.Q. Liao, H. Hong, J. Chen, W. Gao, A critical review of extracellular polymeric substances (EPSs) in membrane bioreactors: Characteristics, roles in membrane fouling and control strategies, J. Memb. Sci. 460 (2014) 110–125. https://doi.org/10.1016/j.memsci.2014.02.034.

[18] H. Lin, W. Peng, M. Zhang, J. Chen, H. Hong, Y. Zhang, A review on anaerobic membrane bioreactors: Applications, membrane fouling and future perspectives, Desalination. 314 (2013) 169–188. https://doi.org/10.1016/j.desal.2013.01.019.

[19] A.L.K. Sheng, M.R. Bilad, N.B. Osman, N. Arahman, Sequencing batch membrane photobioreactor for real secondary effluent polishing using native microalgae: Process performance and full-scale projection, J. Clean. Prod. 168 (2017) 708–715. https://doi.org/10.1016/j.jclepro.2017.09.083.

[20] T. Asano, F.L. Burton, H.L. Leverenz, R. Tsuchihashi, G. Tchobanoglous, Water Reuse: Issues, Technologies, and Applications, 1st editio, Metcalf & Eddy, 2007.

[21] T. Zsirai, H. Qiblawey, M.J. A-Marri, S. Judd, The impact of mechanical shear on membrane flux and energy demand, J. Memb. Sci. 516 (2016) 56–63. https://doi.org/10.1016/j.memsci.2016.06.010.

[22] I. Ruigómez, L. Vera, E. González, G. González, J. Rodríguez-Sevilla, A novel rotating HF membrane to control fouling on anaerobic membrane bioreactors treating wastewater, J. Memb. Sci. 501 (2016). https://doi.org/10.1016/j.memsci.2015.12.011.

[23] I. Ruigómez, E. González, L. Rodríguez-Gómez, L. Vera, Fouling control strategies for direct membrane ultrafiltration: Physical cleanings assisted by membrane rotational movement, Chem. Eng. J. 436 (2022) 135161. https://doi.org/10.1016/j.cej.2022.135161.

[24] G.H. Chen, M.C.M. van Loosdrecht, G.A. Ekama, D. Brdjanovic, Biological Wastewater Treatment, 2nd Editio, IWA Publishing, London, UK, 2020.

[25] E. Segredo-Morales, E. González, C. González-Martín, L. Vera, Secondary wastewater effluent treatment by microalgal-bacterial membrane photobioreactor at long solid retention times, J. Water Process Eng. 49 (2022) 0–11. https://doi.org/10.1016/j.jwpe.2022.103200.

[26] L. Vera, E. González, O. Díaz, R. Sánchez, R. Bohorque, J. Rodríguez-Sevilla, Fouling analysis of a tertiary submerged membrane bioreactor operated in dead-end mode at high-fluxes, J. Memb. Sci. 493 (2015) 8–18. https://doi.org/10.1016/j.memsci.2015.06.014.

[27] APHA, Standard Methods for the Examination of Water and Wastewater, 21st ed., Washington, DC, USA, 2005.

[28] O. Díaz, E. González, L. Vera, J.J. Macías-Hernández, J. Rodríguez-Sevilla, Fouling analysis and mitigation in a tertiary MBR operated under restricted

151

aeration, J. Memb. Sci. 525 (2017) 368–377. https://doi.org/10.1016/j.memsci.2016.12.014.

[29]   P. Madoni, A sludge biotic index (SBI) for the evaluation of the biological performance of activated sludge plants based on the microfauna analysis, Water Res. 28 (1994) 67–75. https://doi.org/10.1016/0043-1354(94)90120-1.

[30]   S.G. Berk, J.H. Gunderson, Wastewater Organisms A Color Atlas, 1st Edition, CRC Press, Florida, USA, 1993.

[31]   D. García, E. Posadas, S. Blanco, G. Acién, P. García-Encina, S. Bolado, R. Muñoz, Evaluation of the dynamics of microalgae population structure and process performance during piggery wastewater treatment in algal-bacterial photobioreactors, Bioresour. Technol. 248 (2018) 120–126. https://doi.org/10.1016/j.biortech.2017.06.079.

[32]   P.J. He, B. Mao, F. L-, L.M. Shao, D.J. Lee, J.S. Chang, The combined effect of bacteria and Chlorella vulgaris on the treatment of municipal wastewaters, Bioresour. Technol. 146 (2013) 562–568. https://doi.org/10.1016/j.biortech.2013.07.111.

[33]   P. Bohutskyi, D.C. Kligerman, N. Byers, L.K. Nasr, C. Cua, S. Chow, C. Su, Y. Tang, M.J. Betenbaugh, E.J. Bouwer, Effects of inoculum size, light intensity, and dose of anaerobic digestion centrate on growth and productivity of Chlorella and Scenedesmus microalgae and their poly-culture in primary and secondary wastewater, Algal Res. 19 (2016) 278–290. https://doi.org/10.1016/j.algal.2016.09.010.

[34]   R. Mu, Y. Jia, G. Ma, L. Liu, K. Hao, F. Qi, Y. Shao, Advances in the use of microalgal–bacterial consortia for wastewater treatment: Community structures, interactions, economic resource reclamation, and study techniques, Water Environ. Res. 93 (2021) 1217–1230. https://doi.org/10.1002/wer.1496.

[35]   Y. Luo, P. Le-Clech, R.K. Henderson, Assessment of membrane photobioreactor (MPBR) performance parameters and operating conditions, Water Res. 138 (2018) 169–180. https://doi.org/10.1016/j.watres.2018.03.050.

[36]   V. Montemezzani, I.C. Duggan, I.D. Hogg, R.J. Craggs, A review of potential methods for zooplankton control in wastewater treatment High Rate Algal Ponds and algal production raceways, Algal Res. 11 (2015) 211–226. https://doi.org/10.1016/j.algal.2015.06.024.

[37]   J. González-Camejo, R. Barat, M. V. Ruano, A. Seco, J. Ferrer, Outdoor flat-panel membrane photobioreactor to treat the effluent of an anaerobic membrane bioreactor. Influence of operating, design, and environmental conditions, Water Sci. Technol. 78 (2018) 195–206. https://doi.org/10.2166/wst.2018.259.

[38]   P.E.A. Debiagi, M. Trinchera, A. Frassoldati, T. Faravelli, R. Vinu, E. Ranzi, Algae characterization and multistep pyrolysis mechanism, J. Anal. Appl. Pyrolysis. 128 (2017) 423–436. https://doi.org/10.1016/j.jaap.2017.08.007.

[39]   M. Wang, H. Yang, S.J. Ergas, P. van der Steen, A novel shortcut nitrogen removal process using an algal-bacterial consortium in a photo-sequencing batch reactor (PSBR), Water Res. 87 (2015) 38–48. https://doi.org/10.1016/j.watres.2015.09.016.

[40]   N. Powell, A. Shilton, Y. Chisti, S. Pratt, Towards a luxury uptake process via microalgae - Defining the polyphosphate dynamics, Water Res. 43 (2009) 4207–4213. https://doi.org/10.1016/j.watres.2009.06.011.

[41]   The European Parliament and the Council, Regulation (EU) 2020/741, Minimum requirements for water reuse, Off. J. Eur. Union. 177/33 (2020) 32–55. https://eur-lex.europa.eu/legal-content/EN/TXT/PDF/?uri=CELEX:32020R0741&from=EN.

[42]   D.Y. Duygu, A.U. Udoh, T. Ozer, A. Akbulut, I. Erkaya, K. Yildiz, D. Guler, Fourier transform infrared (FTIR) spectroscopy for identification of Chlorella vulgaris Beijerinck 1890 and Scenedesmus obliquus (Turpin) Kützing 1833, African J. Biotechnol. 11 (2012) 3817–3824. https://doi.org/10.5897/ajb11.1863.

[43]   C. Gai, Y. Zhang, W.T. Chen, P. Zhang, Y. Dong, Thermogravimetric and kinetic analysis of thermal decomposition characteristics of low-lipid microalgae, Bioresour. Technol. 150 (2013) 139–148. https://doi.org/10.1016/j.biortech.2013.09.137.

[44]   R.B. Carpio, Y. Zhang, C.T. Kuo, W.T. Chen, L.C. Schideman, R.L. de Leon, Characterization and thermal decomposition of demineralized wastewater algae biomass, Algal Res. 38 (2019) 101399. https://doi.org/10.1016/j.algal.2018.101399.

[45]   C.H.T. Vu, S.J. Chun, S.H. Seo, Y. Cui, C.Y. Ahn, H.M. Oh, Bacterial community enhances flocculation efficiency of Ettlia sp. by altering extracellular polymeric substances profile, Bioresour. Technol. 281 (2019) 56–65. https://doi.org/10.1016/j.biortech.2019.02.062.

[46]   D.J. Barker, D.C. Stuckey, A review of soluble microbial products (SMP) in wastewater treatment systems, Water Res. 33 (1999) 3063–3082. https://doi.org/10.1016/S0043-1354(99)00022-6.

[47]   A. Charfi, Y. Yang, J. Harmand, N. Ben Amar, M. Heran, A. Grasmick, Soluble microbial products and suspended solids influence in membrane fouling dynamics and interest of punctual relaxation and/or backwashing, J. Memb. Sci. 475 (2015) 156–166. https://doi.org/10.1016/j.memsci.2014.09.059.

[48]   Seong-Hoon Yoon, Membrane Bioreactor Processes Principles and Applications, 1st Editio, CRC Press, New York, 2016.

[49]   D. Jeison, J.B. van Lier, Cake formation and consolidation: Main factors governing the applicable flux in anaerobic submerged membrane bioreactors (AnSMBR) treating acidified wastewaters, Sep. Purif. Technol. 56 (2007) 71–78. https://doi.org/10.1016/j.seppur.2007.01.022.

[50]   T. Vroman, F. Beaume, V. Armanges, E. Gout, J.C. Remigy, Critical backwash flux for high backwash efficiency: Case of ultrafiltration of bentonite suspensions, J. Memb. Sci. 620 (2021) 118836. https://doi.org/10.1016/j.memsci.2020.118836.

[51]   A. Sepehri, M.H. Sarrafzadeh, Effect of nitrifiers community on fouling mitigation and nitrification efficiency in a membrane bioreactor, Chem. Eng. Process. - Process Intensif. 128 (2018) 10–18. https://doi.org/10.1016/j.cep.2018.04.006.

[52]   E. Spennati, S. Mirizadeh, A.A. Casazza, C. Solisio, A. Converti, Chlorella vulgaris and Arthrospira platensis growth in a continuous membrane photobioreactor using industrial winery wastewater, Algal Res. 60 (2021) 102519. https://doi.org/10.1016/j.algal.2021.102519.

[53]   A. Solmaz, M. Işık, Optimization of membrane photobioreactor; the effect of hydraulic retention time on biomass production and nutrient removal by mixed microalgae culture, Biomass and Bioenergy. 142 (2020). https://doi.org/10.1016/j.biombioe.2020.105809.

[54]   H.O. Tighiri, E.A. Erkurt, Biotreatment of landfill leachate by microalgae-bacteria consortium in sequencing batch mode and product utilization, Bioresour. Technol. 286 (2019) 121396. https://doi.org/10.1016/j.biortech.2019.121396.

[55]   I. de Godos, V.A. Vargas, H.O. Guzmán, R. Soto, B. García, P.A. García, R. Muñoz, Assessing carbon and nitrogen removal in a novel anoxic-aerobic cyanobacterial-bacterial photobioreactor configuration with enhanced biomass sedimentation, Water Res. 61 (2014) 77–85. https://doi.org/10.1016/j.watres.2014.04.050.

[56]   P. Madoni, Protozoa in wastewater treatment processes: A minireview, Ital. J. Zool. 78 (2011) 3–11. https://doi.org/10.1080/11250000903373797.

[57]   B. Deruyck, K.H. Thi Nguyen, E. Decaestecker, K. Muylaert, Modeling the impact of rotifer contamination on microalgal production in open pond, photobioreactor and thin layer cultivation systems, Algal Res. 38 (2019) 101398. https://doi.org/10.1016/j.algal.2018.101398.

[58]   G. Ding, X. Li, W. Lin, Y. Kimochi, R. Sudo, Enhanced flocculation of two bioflocculation-producing bacteria by secretion of Philodina erythrophthalma, Water Res. 112 (2017) 208–216. https://doi.org/10.1016/j.watres.2017.01.044.

CAPÍTULO 7

Discusión general

1. Producción de biomasa: influencia de las condiciones de operación y las características del agua residual

Uno de los principales objetivos de la presente tesis es analizar el adecuado crecimiento de una suspensión mixta de microalgas y bacterias a partir de diferentes tipos de aguas residuales, sin utilizar ningún tipo de inóculo previo. De esta manera, se permite el crecimiento de las especies indígenas para las diferentes condiciones de operación utilizadas. Es necesario indicar que en la mayor parte de la literatura se encuentran estudios con inóculos de microalgas puros. Además, en muchos de estos estudios, se analiza el crecimiento a partir de aguas residuales sintéticas. Esta metodología limita la representatividad de los resultados alcanzados y dificulta el posterior escalado del proceso, como ha sido descrito en numerosos trabajos previos [1–3].

En los capítulos previos se han mostrado valores de productividad de biomasa comprendidos entre 22 y 48 mg/L·d, comparables a los publicados para cultivos puros con influentes sintéticos [4–6]. Tanto en aguas residuales procedentes de un tratamiento secundario (Capítulo 4) como de un primario (Capítulo 6), se observó que el crecimiento de biomasa en el sistema estaba principalmente asociado al metabolismo de microorganismos fotosintéticos (Figura 7.1). En el primer caso, la productividad de la biomasa se incrementó 11 veces respecto al ensayo control (Figura 7.2) y en el segundo, aproximadamente 3 veces (Figura 7.3). El desigual incremento respecto a las condiciones de control se debe principalmente, a las diferentes composiciones de las aguas residuales alimentadas en cada caso, siendo la concentración de materia orgánica en el influente primario sensiblemente superior (331 frente a 69 mg/L, en valores promedio), lo que favorece el crecimiento de bacterias heterótrofas en el ensayo control [7].

En relación a la influencia de las condiciones de operación, se observó un efecto significativo tanto del tiempo de retención de sólidos (SRT) como del tiempo de residencia hidráulico (HRT) en la productividad de biomasa. Con respecto al primero—que sólo se estudió en el influente secundario—, se observó un descenso acusado de la productividad desde 43,7 hasta 22,1 mg/L d al aumentar el SRT desde 20 a 80 días (Figura 7.2a). Este descenso puede estar asociado a una

atenuación en la intensidad de luz disponible para los microorganismos fotosintéticos y su crecimiento, como consecuencia de la disminución exponencial de ésta con la concentración de biomasa [8,9].
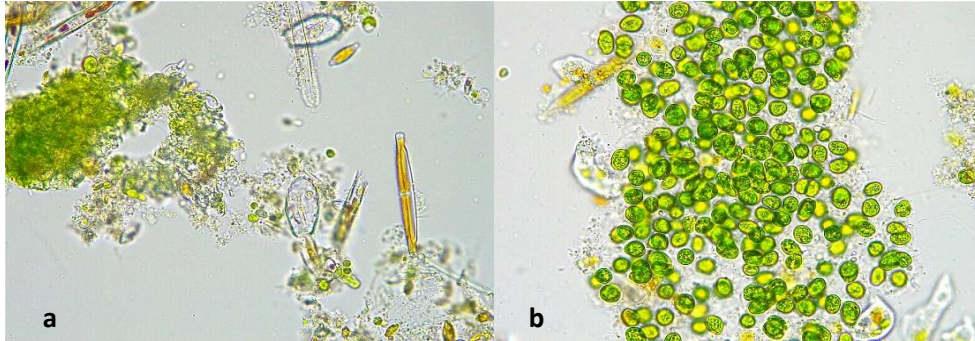

Figura 7.1. Imagen por microscopio óptico de la comunidad de microorganismos fotosintéticos presentes: a) *Scenedesmus* sp. y diatomeas (MPBR 1: HRT = 0,75 días, SRT = 20 días, influente secundario); b) *Chlorella* sp. (R-MPBR 1: HRT = 2 días, SRT = 80 días, influente primario). Observación bajo objetivo 40x.

Este efecto de la disponibilidad de luz sobre la productividad se observó en el estudio presentado en el Capítulo 5, donde la productividad aumentó desde 22,1 hasta 42,1 mg/L·d al extender el fotoperiodo desde 12/12 h (luz/oscuridad) a 16/8 h (Figura 7.2b). No obstante, el hecho de que la productividad de biomasa sea similar en el fotoperiodo de 16/8 h y en el caso de iluminación completa (24/0 h), sugiere que, la concentración de biomasa máxima que se puede obtener en el fotobiorreactor utilizado está comprendida entre 3,0 y 3,8 g/L. Esta concentración límite posiblemente sea debida al mencionado efecto de atenuación por concentración, de acuerdo con estudios previos [10,11]. En relación al HRT, su efecto es diferente según el tipo de influente, lo que puede deberse a la diferente estructura de la comunidad microbiana. Para el influente secundario, la productividad aumentó un 27% al incrementarse el HRT desde 0,75 hasta 5 días (Figura 7.2a). Por el contrario, en el influente primario la productividad disminuyó con la carga volumétrica de carbono (CLR) (Figura 7.2c). Este último comportamiento es el que se describe habitualmente en la literatura, principalmente debido a una limitación de sustrato (en este caso, materia orgánica carbonosa) asociado a elevados valores de HRT. Al mismo tiempo, en condiciones de altos HRT y elevada concentración de oxígeno disuelto (> 1 mg/L),

se favorece el crecimiento de protozoos ciliados pedunculados (*Vorticella* sp.), ciliados reptantes (*Euplotes* sp.) y rotíferos (bdelloideos y *Lecane* sp.) (Figuras 7.3c-f), que consumen principalmente bacterias y algas dispersas, y, por tanto, contribuyen a un descenso en la producción de biomasa [12].
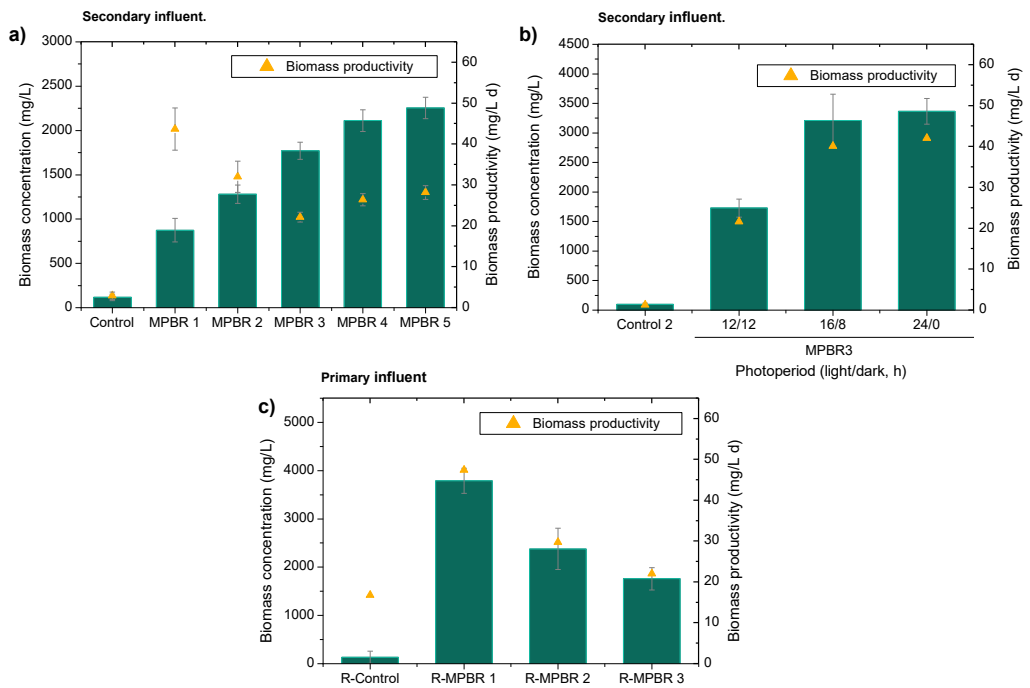
Figura 7.2. Concentración y productividad de biomasa para las condiciones de control y los MPBRs en diferentes HRT, SRT y fotoperiodos. (a) Influente secundario: Control: HRT = 0,75 días, SRT = 40 días; MPBR 1: HRT = 0,75 días, SRT = 20 días; MPBR 2: HRT = 0,75 días, SRT = 40 días; MPBR 3: HRT = 0,75 días, SRT = 80 días; MPBR 4: HRT = 2 días, SRT = 80 días; MPBR 5: HRT = 5 días, SRT = 80 días; (b) Influente secundario. Control 2: HRT = 0,75 días, SRT = 80 días; MPBR 3: HRT = 0,75 días, SRT = 80 días; (c) Influente primario. R-Control: HRT = 2 días, SRT = 80 días; R-MPBR 1: HRT = 2 días, SRT = 80 días; R-MPBR 2: HRT = 5 días, SRT = 80 días; R-MPBR 3: HRT = 3,5 días, SRT = 80 días.

Figura 7.3. Imágenes por microscopio óptico de algunos microorganismos superiores representativos. (a) Paramecio sp. (R-MPBR 1), (b) *Epistylis* sp. (R-MPBR 1); c) *Vorticella* sp. (R-MPBR 2); d) *Euplotes* sp. (R-MPBR 2); (e) rotífero Bdelloid (R-MPBR 2) y (f) *Lecane* sp. (R-MPBR 2).
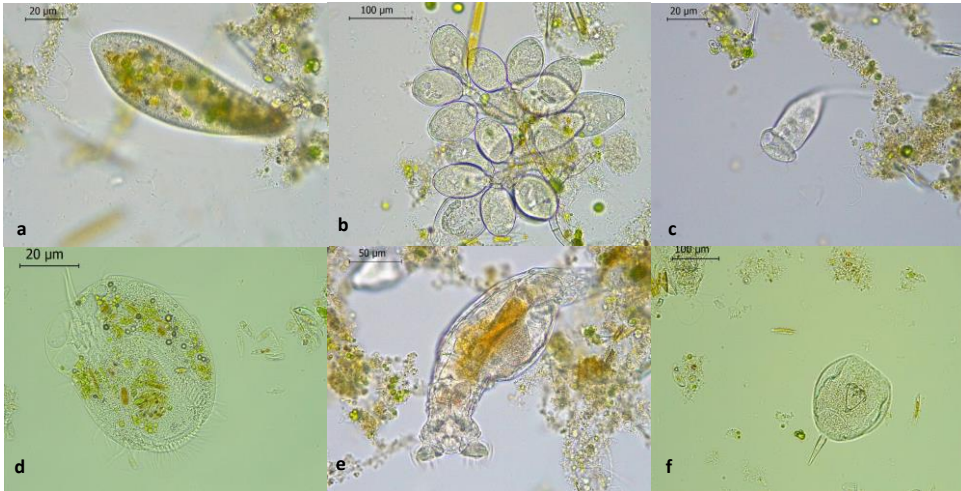
2. Rendimiento de depuración: eliminación de materia orgánica y nutrientes

Al desarrollar un cultivo mixto de bacterias y microalgas, la biomasa resultante es capaz de eliminar de manera conjunta materia orgánica y nutrientes. Esta es una de las principales ventajas de este cultivo mixto frente a un sistema puro de microalgas, que únicamente elimina nutrientes.

En el Capítulo 4, correspondiente al tratamiento de influente secundario—con baja carga orgánica—, se observaron porcentajes de eliminación de materia orgánica (COD) comprendidos entre 23,2 y 44,8%, superiores al 17,8% obtenido en el ensayo control, equivalente a un tratamiento aerobio terciario (Tabla 7.1). Esta mejora es consistente con la existencia de una relación simbiótica entre bacterias y microalgas [13], favoreciendo un mejor rendimiento de depuración. Asimismo, se obtuvieron mayores tasas de eliminación para los nutrientes. En el caso del nitrógeno inorgánico soluble (DIN), los valores estuvieron comprendidos entre 5,6-48,7%, mientras que para el fósforo inorgánico soluble (P-PO$_4^{3-}$) el rango

de eliminación fue de 5,2-34,7%. Aunque se observó una variación importante como consecuencia de las fluctuaciones de las características del influente, de manera general, se puede concluir que es necesario aumentar el HRT hasta valores de 2-5 días para obtener unos rendimientos razonables de eliminación de nutrientes. En estas condiciones, las tasas específicas de eliminación variaron entre 2,0 y 3,4 mg/L·d para el nitrógeno y entre 0,1 y 0,4 mg/L·d para el fósforo; valores que se encuentran dentro del rango típico descrito en otros estudios [14]. Si se analiza el efecto del fotoperiodo, se observa de nuevo un efecto positivo al extender la fase diaria de iluminación hasta 16 h (Figura 7.4), aumentando las tasas específicas hasta 4,71 mg/L·d y 0,67 mg/L·d para el nitrógeno y fósforo, respectivamente. La relación encontrada en la eliminación de nutrientes y la productividad de biomasa sugiere que el mecanismo fundamental de eliminación fue la incorporación de ambos nutrientes en la biomasa, como se describe habitualmente en la literatura [15].

Tabla 7.1. Rendimiento de depuración en el MPBR y en el ensayo control.

Parámetros	MPBR 1 SRT=20 d HRT= 0.75 d	MPBR 2 SRT=40 d HRT= 0.75 d	MPBR 3 SRT=80 d HRT= 0.75 d	MPBR 4 SRT=80 d HRT= 2 d	MPBR 5 SRT=80 d HRT= 5 d	Control SRT=40 d HRT= 0.75 d
COD	50.9±10.1	48.8±10.5	46.9±10.0	34.9±10.3	36.4±10.1	61.9±8.2
NH_4^+-N	0.5±0.1	0.9±0.9	0.4±0.1	0.4±0.1	0.4±0.1	0.6±0.4
TN	8.7±2.5	23.7±7.0	9.9±1.8	7.4±3.5	14.5±2.5	20.4±5.2
$P-PO_4^{3-}$	5.4±2.8	4.8±2.2	5.0±1.7	4.2±1.6	1.5±0.4	4.3±1.5
Eficiencia de eliminación (%)						
COD	23.2±4.3	24.7±14.2	26.7±14.0	35.0±9.7	44.8 ± 14.5	17.8±9.4
$N-NH_4^+$	90.8±3.7	95.7±2.7	92.2±4.1	93.9±2.8	94.9±8.0	95.3±2.2
TN	30.0±12.3	22.2±9.1	5.6±4.9	48.7 ± 13.1	40.6±12.9	4.5±5.9
$P-PO_4^{3-}$	6.4±3.3	14.8±7.2	5.2±3.3	18.5 ± 18.9	34.7±13.4	0.5±1.3

Nota: Datos expresados como media ± desviación estándar.

En el Capítulo 6, correspondiente al tratamiento del influente primario, también se observaron mayores porcentajes de eliminación de COD en el R-MPBR (82,6-85,6%) en relación al ensayo control (78,4-79,5%) (Tabla 7.2). Cabe destacar que, en este caso, las concentraciones de COD en el permeado (50,4-31,0 mg/L) fueron

similares a las encontradas en el influente secundario (50,9-34,9 mg/L), confirmando la elevada capacidad de eliminación de materia orgánica carbonosa de los MPBRs para ambos tipos de influente, en las condiciones de operación utilizadas. No obstante, la similitud de rendimientos de depuración de los MPBRs con los ensayos control revela el papel fundamental de la retención de la membrana en los elevados porcentajes de eliminación obtenidos.
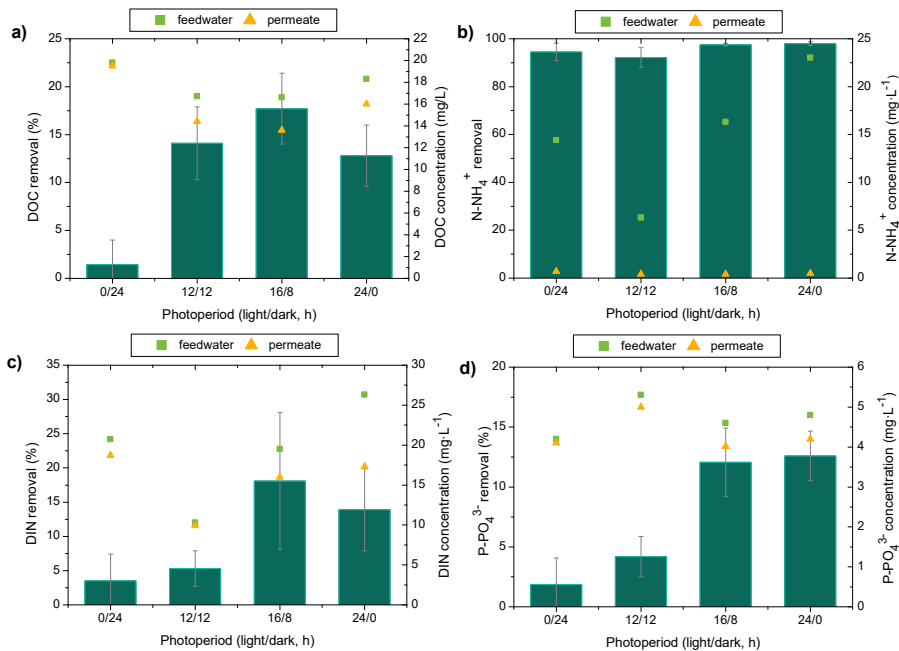
Figura 7.4. Influencia del fotoperiodo en la eliminación de (a) carbono orgánico disuelto (DOC), (b) N-NH^{4+} (c) nitrógeno inorgánico soluble (DIN) (d) y fósforo inorgánico soluble (P-PO$_4^{3-}$).

Asimismo, también se obtuvieron mayores porcentajes de eliminación de los nutrientes respecto al ensayo control. Para unas mismas condiciones de CLR, los valores fueron 2,9 y 3,6 veces superior para el nitrógeno y el fósforo, respectivamente. Cabe destacar la elevada tasa específica de eliminación de nitrógeno (37,2 mg/L·d) alcanzada en el R-MPBR operado a alta carga (R-MPBR 1). Este valor es sensiblemente superior al correspondiente con un mecanismo de incorporación en biomasa (3,8 mg/L·d, asumiendo un 8% de nitrógeno en

biomasa) [16], lo que puede atribuirse a un aparente proceso de nitrificación-desnitrificación simultáneo ocasionado por las condiciones de alta carga orgánica y baja concentración de oxígeno disuelto que se obtuvieron en este experimento. En el resto de las condiciones, las tasas específicas estuvieron dentro de los valores habituales (2,1-4,5 mg/L·d) y son similares a las obtenidas para el influente secundario. De la misma manera, las tasas de eliminación de fósforo fueron las esperadas de un mecanismo de incorporación a la biomasa (0,1-1,6 mg/L·d).

Tabla 7.2. Rendimiento de depuración en el R-MPBR y en el ensayo control.

Parámetros	R-MPBR 1	R-MPBR 2	R-MPBR 3	R-Control
CLR (g DOC·m^{-3}·d^{-1})	36.6	11.4	9.1	36.9
Concentración en el permeado (mg·L^{-1})				
COD	50.4 ± 16.0	43.9±15.4	31.0±15.2	59.9±21.4
DOC	15.2±2.0	10.9±1.7	8.6±1.0	13.7±4.8
N-NH$_4^+$	14.7±12.9	0.6±0.3	0.6±0.6	62.4±8.0
N-NO$_3^-$	0.2±0.3	53.2±9.8	52.8±10.6	0.2±0.2
N-NO$_2^-$	2.6±1.9	2.0±2.2	0.4±0.6	0.3±0.3
TN	17.5±12.9	55.8±8.1	58.8±9.3	62.9±8.0
P-PO$_4^{3-}$	6.8±1.2	6.8±0.7	9.9±1.4	10.4±0.2
Eficiencia de eliminación (%)				
COD	85.6 ± 5.2	84.8±6.8	89.2±5.6	82.6±8.9
DOC	78.4±4.0	73.0±19.1	55.4±1.7	79.5±8.8
N-NH$_4^+$	84.3±14.7	98.8±0.6	99.1 ± 1.2	28.4±14.6
TN	81.2±13.9	20.7±7.9	21.2±10.1	27.9±14.7
P-PO$_4^{3-}$	25.4±12.0	11.0±4.1	12.2±10.6	7.1±4.8

Nota: Datos expresados como media ± desviación estándar.

En función de lo indicado previamente, se puede concluir que el MPBR permite una eliminación elevada de materia carbonosa y moderada de nutrientes para ambos tipos de influentes. En las condiciones óptimas de operación, las concentraciones de nutrientes en el permeado superaron los valores límite para vertido procedentes de instalaciones de tratamiento de aguas residuales urbanas realizados en zonas sensibles establecidos en la normativa de la UE (10-15 mg TN/L and 1-2 mg P/L) [17]. No obstante, la calidad microbiológica (ausencia de *E. coli* y *Legionellla* spp.) y físico-química obtenida (turbidez <0,5 NTU) en el MPBR cumple

con el reciente Reglamento (UE) 2020/741 relativo a los requisitos mínimos para la reutilización del agua [18], por lo que sería apta para ser reutilizada en riego agrícola.

3. Características de la suspensión: biofloculación y acumulación de aglomerados de biopolímeros (BPC)

Como se ha indicado tradicionalmente, una de las principales limitaciones de los procesos de depuración basados en microalgas es la separación de la biomasa, debido a los elevados costes asociados a esta etapa [19]. Esta limitación se debe al pequeño tamaño de las células de microalgas utilizadas normalmente, en el tratamiento de aguas (< 30 μm), con una densidad similar al agua y unas bajas velocidades de sedimentación (generalmente < $3,6\cdot10^{-3}$ m/h) [20]. En este contexto, la biofloculación originada por la agregación de las microalgas a otros microorganismos, como puedan ser bacterias u hongos podría disminuir sensiblemente, los problemas asociados a la separación. En el caso de las bacterias, estas son capaces de acelerar la agregación de células induciendo a las microalgas a la producción de sustancias poliméricas extracelulares (EPS) que actúan como biofloculantes [21].

En el Capítulo 4 se comprobó el efecto positivo del cultivo mixto de microalgas-bacterias sobre el proceso de biofloculación. El análisis de la distribución del tamaño de las partículas mostró un valor medio de 40,2 μm para la condición de control y osciló entre 75,3 y 129,8 μm en el MPBR. Asimismo, el contenido en materia volátil también fue superior (38,3-48,9%) en el MPBR (Tabla 7.3), lo que se puede atribuir a la fijación de CO_2 asociada a la actividad fotosintética. De hecho, las relaciones másicas de C/N obtenidas (5,0-5,9) fueron consistentes con los valores habituales publicados en otros estudios con microalgas [16] y sensiblemente mayores al del ensayo control. Este efecto positivo del cultivo mixto también se observó en el Capítulo 6, durante el tratamiento del influente primario. En este caso, el tamaño de partícula, medido como valores medios de $D_{(0,5)}$, estuvo comprendido entre 61,9 y 92,8 μm en el R- MPBR, con un elevado contenido en materia volátil y una adecuada relación C/N (Tabla 7.4).

Tabla 7.3. Materia volátil y composición elemental en el MPBR y en el ensayo control.

Parámetros	MPBR 1	MPBR 2	MPBR 3	MPBR 4	MPBR 5	Control
	SRT=20 d	SRT=40 d	SRT=80 d	SRT=80 d	SRT=80 d	SRT=40 d
	HRT= 0.75 d	HRT= 0.75 d	HRT= 0.75 d	HRT= 2 d	HRT= 5 d	HRT= 0.75 d
Materia volátil (%wt, base seca)						
	38.3±0.8	38.7±1.5	48.9±1.0	43.6±0.6	48.2±0.4	33.8±2.1
Análisis elemental (%wt, base seca)						
C	22.8±0.8	24.9±1.4	26.4±1.0	26.4±0.3	28.3±0.3	5.8±1.5
H	3.6±0.1	3.7±0.2	4.2±0.6	3.7±0.1	4.4±0.1	0.9±0.2
N	4.5±0.3	4.7±0.7	4.9±0.4	4.5±0.1	5.6±0.2	3.1±0.8

Nota: Datos expresados como media ± desviación estándar.

Tabla 7.4. Principales características de las suspensiones del R-MPBR y del ensayo control.

Parámetros	R-MPBR 1	R-MPBR 2	R-MPBR 3	R-Control
CLR (g DOC·m^{-3}·d^{-1})	36.6	11.4	9.1	36.9
Análisis elemental (%wt, base seca)				
C	36.5±1.2	37.7±0.4	37.8±2.2	37.0±1.8
H	4.4±1.2	5.5±0.1	5.4±0.2	5.7±0.1
N	6.5±0.2	8.2±0.1	8.4±0.2	6.9±0.4
S	0.8±0.3	nd	nd	0.8±0.1
Distribución de tamaño de partículas				
$D_{(0.1)}$ (µm)	17.6±3.0	22.5±4.7	31.4±3.8	13.2±1.2
$D_{(0.5)}$ (µm)	61.9±5.9	70.5± 8.6	92.8 ± 3.0	38.4±5.0
$D_{(0.9)}$ (µm)	162.9±12.1	184.3 ± 20.5	207.9 ± 3.6	81.9±10.9
Sobrenadante				
BPC (mg DOC·L^{-1})	50.0±14.8	24.3±7.4	2.3±0.8	78.2±27.4
(MLSS)s (mg·L^{-1})	317±66	179±21	65±14	994±63
(MLSS)s/MLSS (%)	8.4	7.5	3.7	74.6

Nota: Datos expresados como media ± desviación estándar. nd: no detectado.

Como se ha descrito en la literatura [22], los carbohidratos y las proteínas son los componentes mayoritarios de los EPS. Dado que los carbohidratos facilitan la adhesión celular [23], una proporción consistente de carbohidratos a proteínas

165

puede relacionarse con una adecuada biofloculación. En las Figuras 7.5a y b se muestran los espectros de infrarrojos por transformada de Fourier (FTIR) para el influente secundario y primario, respectivamente. En dichas Figuras se identificaron los picos específicos asignados a los enlaces de carbohidratos (C-O-C) y de proteínas (N-H y C=O). Para ambos influentes, se observó una mayor intensidad en el pico asignado a carbohidratos (1036 cm^{-1}) en las muestras de los MPBRs en relación a las muestras de los ensayos control, lo cual es consistente con las relaciones C/N obtenidas en los análisis elementales. Al comparar ambos influentes, se observó que el primario presentó una mayor intensidad en los picos asociados a proteínas (1542 cm^{-1} y 1650 cm^{-1}).

El análisis de las muestras de biomasa mediante termogravimetría mostró un rango de temperaturas de volatilización comprendido entre 200 y 450 °C (Figuras 7.5c y d). Dentro de este rango es habitual asociar la presencia proteínas a una velocidad máxima de degradación a temperaturas comprendidas entre 275 y 295 °C [24]. Esto es lo que muestran los resultados tanto del ensayo control del influente secundario (Figura 7.5c), como del control y los R-MPBRs para el influente primario (Figura 7.5d), especialmente en las condiciones de baja carga orgánica (R-MPBR 2 y R-MPBR 3). Al comparar ambos influentes, de nuevo se observa un mayor contenido en proteínas en las muestras de MPBRs procedentes del influente primario. En relación a los carbohidratos, en la literatura se describe un intervalo amplio de temperaturas de descomposición de estos compuestos, con valores comprendidos entre 200 y 350 °C, con un pico específico de degradación a 241-261 °C (causado por la degradación de glucosa, maltosa y celobiosa) y otro más pronunciado a 316-353 °C (causado por la degradación de componentes previamente degradados, amilosa y celulosa) [25]. Este segundo pico aparece en las muestras de los MPBRs del efluente secundario (Figura 7.5c), con una mayor intensidad a altos valores de SRT (MPBR 3, MPBR 4 y MPBR 5). Este resultado es coherente con lo observado en los espectros FTIR, donde se encontró una mayor relación de carbohidratos a proteínas en el MPBR respecto al ensayo control.

Los resultados mostrados indican una mejora significativa de la biofloculación en el cultivo mixto de microalgas y bacterias. Se han descrito varios mecanismos de biofloculación, incluida la neutralización de carga y la formación de puentes, ambos debidos a la adsorción de biopolímeros cargados [26]. Por lo tanto, es

razonable asumir una relación entre la concentración de biopolímeros en el sobrenadante de la suspensión y el proceso de biofloculación. De hecho, esto es lo que se desprende de los resultados, donde los agregados de biopolímeros (BPC) se redujeron significativamente en el MPBR, tanto para el influente primario (Tabla 7.4) como para el secundario (Figura 7.6). En el primer caso, se ve un efecto positivo al disminuir la carga orgánica, mientras que, en el segundo, esto se produce al aumentar el SRT a 80 d (MBPR 3-5).
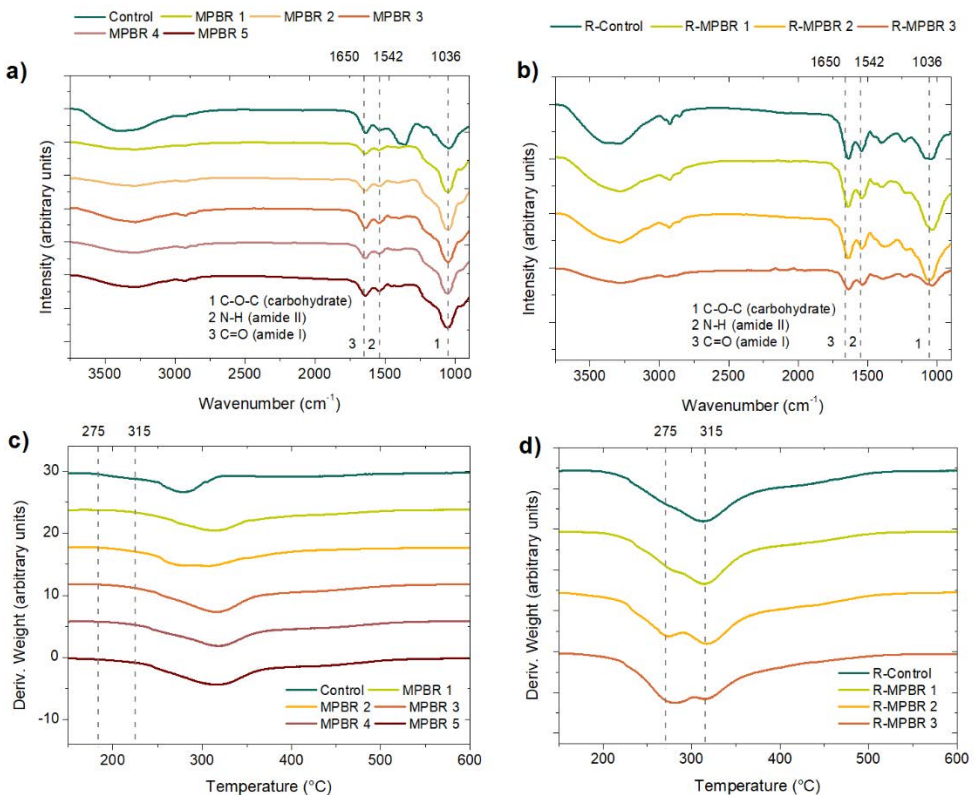

Figura 7.5. Espectros FTIR de las muestras procedentes del MPBR y del ensayo control: (a) influente secundario y (b) influente primario. Se identifican los picos característicos de carbohidratos (1) y proteínas (2 y 3). Termogramas diferenciales procedentes del MPBR y del ensayo control: (c) influente secundario y (d) influente primario. Control: HRT = 0,75 días, SRT = 40 días; MPBR 1: HRT = 0,75 días, SRT = 20 días; MPBR 2: HRT = 0,75 días, SRT = 40 días; MPBR 3: HRT = 0,75 días, SRT = 80 días; MPBR 4: HRT = 2 días, SRT = 80 días; MPBR 5: HRT = 5 días, SRT = 80 días; Influente primario. R-Control: HRT = 2 días, SRT = 80 días; R-MPBR 1: HRT = 2 días, SRT = 80 días; R-MPBR 2: HRT = 5 días, SRT = 80 días; R-MPBR 3: HRT = 3,5 días, SRT = 80 días.
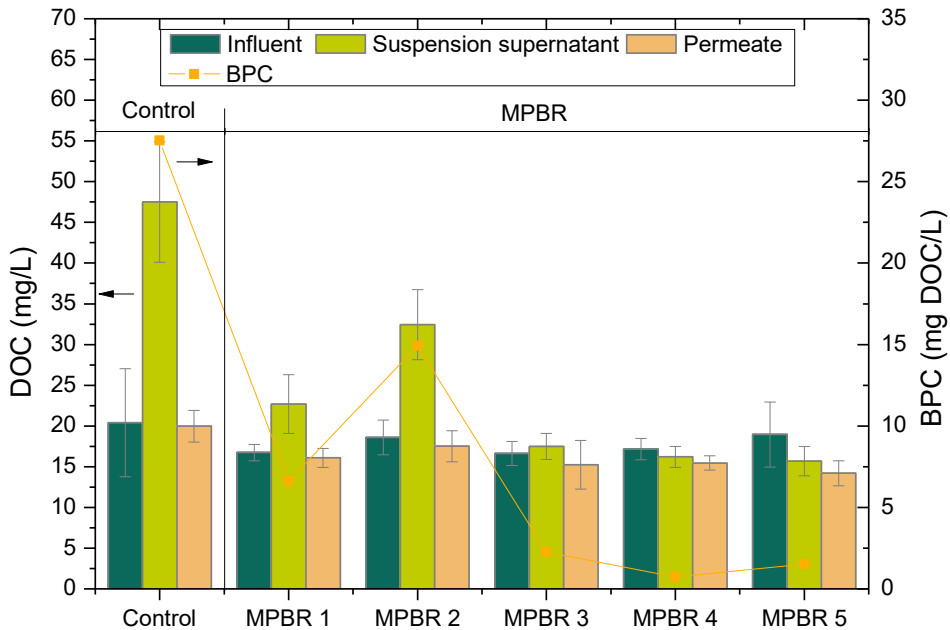
Figura 7.6. Carbono orgánico total en el influente, sobrenadante y permeado, y agregados de biopolímeros (BPC) para las diferentes condiciones. Influente secundario. Control: HRT = 0,75 días, SRT = 40 días; MPBR 1: HRT = 0,75 días, SRT = 20 días; MPBR 2: HRT = 0,75 días, SRT = 40 días; MPBR 3: HRT = 0,75 días, SRT = 80 días; MPBR 4: HRT = 2 días, SRT = 80 días; MPBR 5: HRT = 5 días, SRT = 80 días.

4. Análisis del ensuciamiento de la membrana: optimización de las condiciones de filtración

4.1. Identificación de condiciones para un ensuciamiento mínimo: determinación del flujo umbral

El flujo umbral, relacionado con el concepto teórico de flujo crítico [27], se ha determinado en la presente tesis doctoral mediante el procedimiento de flujo escalonado, que es ampliamente utilizado en la literatura [28]. Este concepto se utiliza para describir el flujo de permeado a partir del cual la velocidad de ensuciamiento reversible (r_f = $dTMP/dt$) aumenta de manera significativa,

haciendo insostenible la operación. En este documento se ha utilizado un valor de referencia de la velocidad r_f de 1 mbar/min, en base a valores operativos de biorreactores de membrana a escala industrial [29].

Los resultados obtenidos en el Capítulo 4, para el influente secundario, mostraron un crecimiento potencial de r_f frente al flujo de permeado (Figura 7.7a). De manera general, las suspensiones generadas en el MPBR produjeron un menor ensuciamiento sobre la membrana en comparación con la condición control. La única excepción fue la condición de SRT de 40 d y HRT de 0,75 d (MPBR 2), cuyo comportamiento podría asociarse con un alto contenido en BPC, mayor incluso que en el ensayo control. Asimismo, se observó un descenso apreciable del ensuciamiento a valores elevados de SRT, incrementándose el valor del flujo umbral desde 22 a 32-40 L/h m^2 cuando se aumentó el SRT desde 20 a 80 d. Cabe indicar, que el rango de valores de SRT generalmente identificado como óptimo en la literatura es de 15-25 d [30,31]. Existe, por tanto, una relación entre el ensuciamiento y el contenido en BPC, de manera similar a lo observado en biorreactores de membrana aerobios [32]. Esta contribución mayoritaria del contenido en biopolímeros también se confirmó mediante los ensayos de filtración realizados con los sobrenadantes de las suspensiones, donde los valores de flujo umbral fueron equivalentes a los obtenidos con las suspensiones (Figura 7.7b).

Al analizar la influencia del fotoperiodo sobre el ensuciamiento en el Capítulo 5, los resultados mostraron un mejor comportamiento para los ciclos de 12/12 y 16/8 h, con valores de flujo umbral de 32 y 22 L/h·m^2, respectivamente, frente a la operación con iluminación continua (24/0 h), donde el flujo umbral descendió a 17,5 L/h·m^2 (Figura 7.7c). De nuevo, se puede relacionar el comportamiento observado en términos de ensuciamiento, con una adecuada biofloculación y, por tanto, con una menor acumulación de BPC.

En el caso del influente primario, si bien los valores de r_f no son directamente comparables al tratarse de otra configuración del módulo de membrana, también se observó un aumento potencial de r_f con el flujo de permeado aplicado (Figura 7.7d). Además, en este caso, se evidenció la mejor filtrabilidad de las suspensiones generadas en R-MPBR frente al experimento control, junto a un efecto positivo de la disminución de la carga orgánica. Se establecieron las mejores condiciones a un valor de 9.1 g DOC/m^3·d (R-MPBR 3), obteniéndose un valor de flujo umbral de 17 L/h·m^2. En relación a la filtrabilidad de los sobrenadantes, se volvió a observar un

comportamiento similar, confirmando su contribución mayoritaria al ensuciamiento de la membrana.
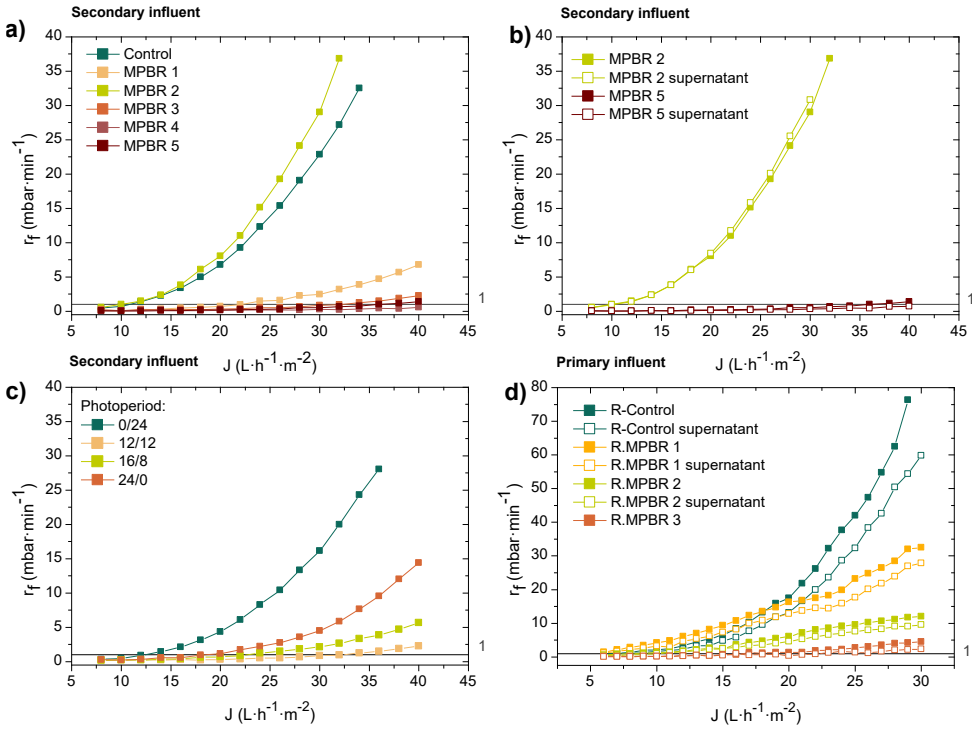

Figura 7.7. Velocidad de ensuciamiento (r_f) frente al flujo de permeado (J) en los ensayos de flujo escalonado para las suspensiones y los sobrenadantes: a) efecto de las condiciones de SRT y HRT en el influente secundario; b) comparativa entre las suspensiones y los sobrenadantes en el influente secundario; c) efecto del fotoperiodo en el influente secundario; y d) efecto de la carga orgánica y comparativa entre suspensiones y sobrenadantes para el influente primario. Control: HRT = 0,75 días, SRT = 40 días; MPBR 1: HRT = 0,75 días, SRT = 20 días; MPBR 2: HRT = 0,75 días, SRT = 40 días; MPBR 3: HRT = 0,75 días, SRT = 80 días; MPBR 4: HRT = 2 días, SRT = 80 días; MPBR 5: HRT = 5 días, SRT = 80 días. R-Control: HRT = 2 días, SRT = 80 días; R-MPBR 1: HRT = 2 días, SRT = 80 días; R-MPBR 2: HRT = 5 días, SRT = 80 días; R-MPBR 3: HRT = 3,5 días, SRT = 80 días.

4.2. Eficacia de diferentes estrategias de limpieza física sobre el control del ensuciamiento residual

Con el objetivo de analizar el ensuciamiento residual de la membrana, se realizaron ensayos de larga duración bajos ciclos consecutivos de filtración y retrolavado. Dado que el ensuciamiento residual es aquel que no se elimina completamente mediante retrovalados, este puede ser cuantificado por la presión inicial de ciclo (TMP_i). Este tipo de ensuciamiento debe estar relacionado con la velocidad de ensuciamiento reversible determinada en los ensayos de flujo escalonado. En la presente tesis doctoral se ha analizado la eficacia de las condiciones de retrolavado aplicadas para limitar el ensuciamiento de dos tipos de módulos de membrana: estático con burbujeo de aire (Capítulos 4 y 5) y rotativo (Capítulo 6). Todos los ensayos se realizaron a un flujo de permeado de 10 L/h·m², que es inferior a los valores de flujo umbral previamente determinados, para garantizar la sostenibilidad de la operación durante los ensayos.

En la Tabla 7.5 se resumen los valores obtenidos tanto para las velocidades de ensuciamiento residual ($dTMP_i/dt$) como reversible (r_f) en el influente secundario (Capítulo 4). Estos resultados muestran que un aumento de SRT hasta 80 d disminuye sensiblemente el ensuciamiento. Además, las condiciones óptimas se encuentran al aumentar el HRT a 5 d. Este comportamiento parece relacionar de nuevo, el contenido en BPC con el ensuciamiento, en este caso, de naturaleza residual. Asimismo, el análisis del aspecto de la membrana al final de los ensayos permitió observar diferencias morfológicas en la biopelícula formada sobre la membrana (Figura 7.8). En las condiciones de alto SRT (MPBR 3-5), esta biopelícula presentó una estructura heterogénea y porosa, consistente con un menor ensuciamiento. Este resultado se puede justificar por el contenido en BPC, debido a que es necesario un recubrimiento orgánico previo por biopolímeros sobre la membrana para el desarrollo de la biopelícula [33]. Esta influencia de los BPC sobre el ensuciamiento se observa claramente en los ensayos correspondientes al estudio de la influencia del fotoperiodo (Capítulo 5). En la Figura 7.9 se puede observar, especialmente en el ensayo control (Figura 7.9a), como las oscilaciones en el contenido de BPC están relacionadas con variaciones en la TMP_i. En relación al efecto del fotoperiodo, se observó una mejora apreciable al aumentar la fase de luz desde un ciclo de 12/12 a 16/8 h. Sin embargo, cuando se aumentó el período de iluminación hasta iluminación completa, el ensuciamiento volvió a aumentar.

Tabla 7.5. Velocidades promedio de ensuciamiento residual y reversible para el control y el MPBR en diferentes condiciones de operación.

Parámetros	MPBR 1	MPBR 2	MPBR 3	MPBR 4	MPBR 5	Control
	SRT=20 d	SRT=40 d	SRT=80 d	SRT=80 d	SRT=80 d	SRT=40 d
	HRT= 0.75 d	HRT= 0.75 d	HRT= 0.75 d	HRT= 2 d	HRT= 5 d	HRT= 0.75 d
$dTMP_i/dt \cdot 10^3$ (kPa/h)	1.5	9.87[a]	2.51	1.58	1.14	1.73
r_f (mbar/min)	1.02	6.90[a]	0.12	0.03	0.01	2.49

[a] Datos obtenidos de las primeras 500 h de operación.

Figura 7.8. Fotografías de las membranas al final de los ensayos de larga duración. Influente secundario. Control: HRT = 0,75 días, SRT = 40 días; MPBR 1: HRT = 0,75 días, SRT = 20 días; MPBR 2: HRT = 0,75 días, SRT = 40 días; MPBR 3: HRT = 0,75 días, SRT = 80 días; MPBR 4: HRT = 2 días, SRT = 80 días; MPBR 5: HRT = 5 días, SRT = 80 días.

Por todo lo indicado, los resultados alcanzados en los Capítulos 4 y 5 para el influente secundario permitieron establecer como condiciones óptimas de operación un SRT de 80 d, un HRT de 5 d y un fotoperiodo de 16/8 h.

En los ensayos realizados con el módulo de membrana rotativo y el influente primario solo se obtuvieron niveles de ensuciamiento operativos (< 0,4 mbar/d; <

$1,7 \cdot 10^{-3}$ kPa/h) en las condiciones de baja carga orgánica (R-MPBR 3) (Figura 7.10d). En estas condiciones, se logró un efectivo control del ensuciamiento, reduciendo la sensibilidad a las fluctuaciones en el influente que se observó en el resto de condiciones aplicadas (Figuras 7.10b y c). Este comportamiento se puede justificar por el bajo contenido de BPC (< 5 mg/L), similar al encontrado para los ensayos con influente secundario a elevados SRT.
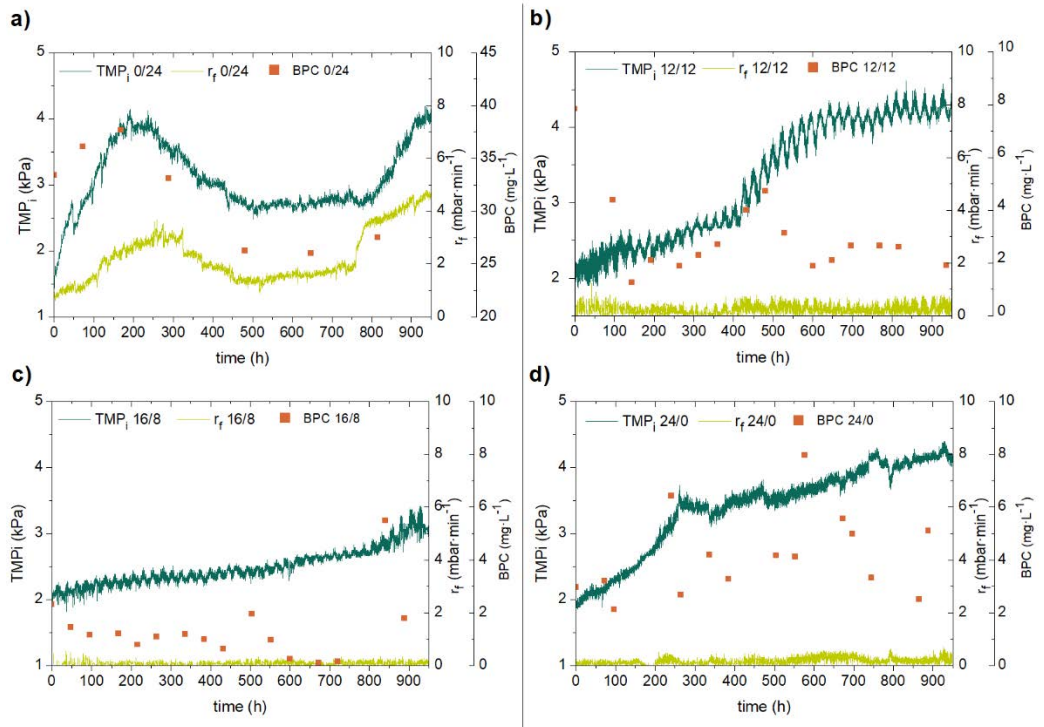

Figura 7.9. Evolución del ensuciamiento durante los ensayos de larga duración: presión transmembrana inicial (TMP_i), velocidad de ensuciamiento reversible (r_f) y BPC para los diferentes fotoperiodos. Influente secundario.
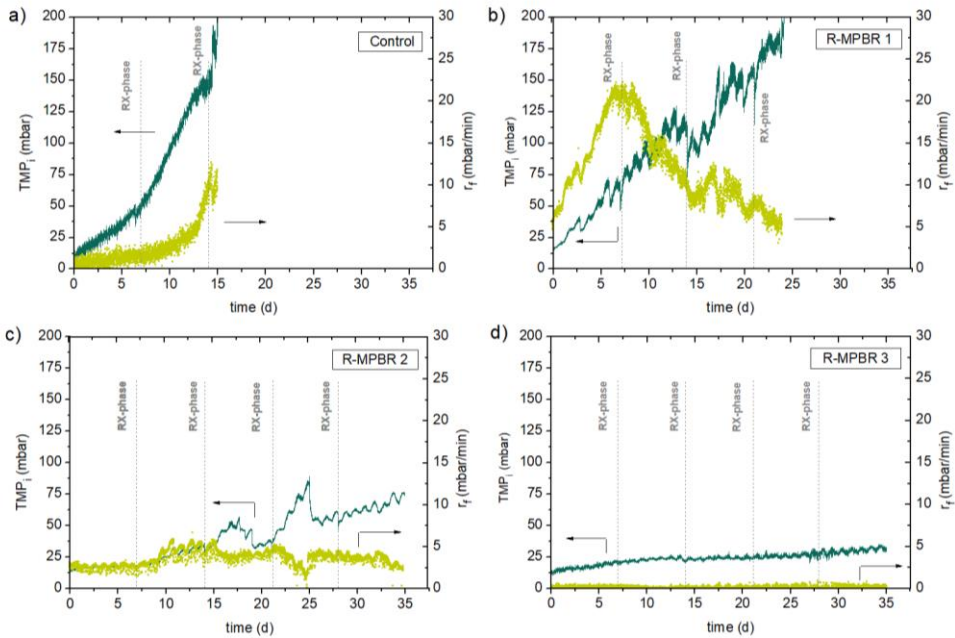
Figura 7.10. Evolución del ensuciamiento durante las pruebas a largo plazo: presión transmembrana inicial (*TMP*i), velocidad de ensuciamiento reversible (r_f) para las diferentes condiciones. Influente primario. R-Control: HRT = 2 días, SRT = 80 días; R-MPBR 1: HRT = 2 días, SRT = 80 días; R-MPBR 2: HRT = 5 días, SRT = 80 días; R-MPBR 3: HRT = 3,5 días, SRT = 80 días.

4.3.   Caracterización del ensuciamiento residual

Al finalizar los ensayos de larga duración se analizó el ensuciamiento residual mediante la metodología de fraccionamiento y se cuantificaron las distintas resistencias hidráulicas. Así, el ensuciamiento residual se separó en tres fracciones principales de ensuciamiento: biopelícula (eliminada por medios físicos: enjuague con agua del grifo), ensuciamiento orgánico (eliminada por un oxidante) y ensuciamiento inorgánico (eliminada por un ácido). En los ensayos con el módulo rotativo, la fracción asociada a la biopelícula se separó en dos tipos: levemente adherida y consolidada.

Para el caso del influente secundario, la mayor parte del ensuciamiento residual se eliminó por medios físicos, lo cual es consistente con el desarrollo significativo de la biopelícula (Figura 7.11). La resistencia hidráulica asociada a esta fracción representó el 62% en la condición de control y aumentó a 70–87% en los MPBRs, probablemente debido a la menor concentración de biomasa en la condición de control. El resto del ensuciamiento se atribuyó mayoritariamente a la fracción orgánica (11-31%) y en menor proporción, a la inorgánica (4-7%).
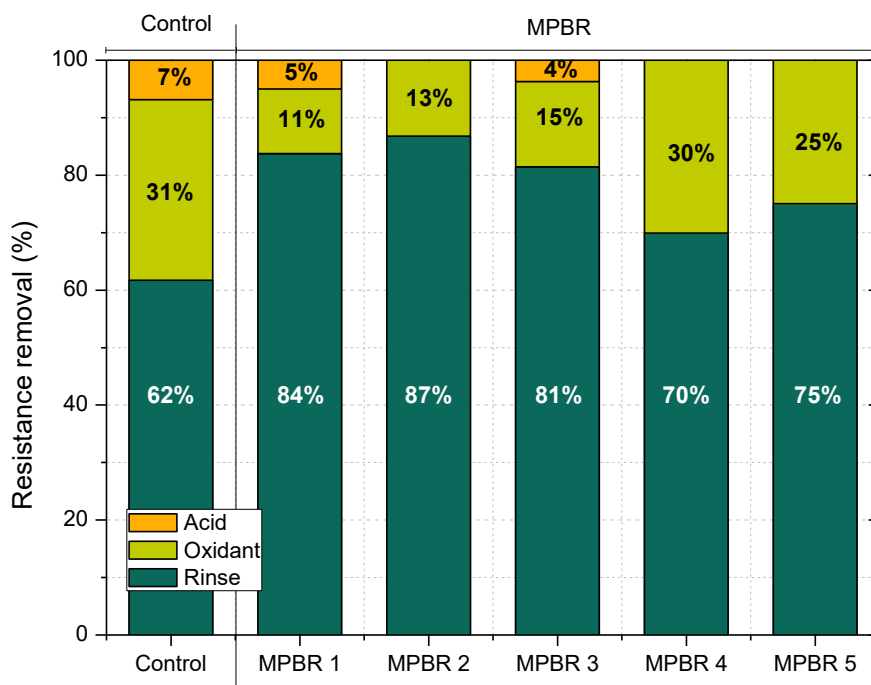

Figura 7.11. Resistencia eliminada por enjuague, oxidante y ácido en diferentes condiciones de operación para MPBR y condición de control. Influente secundario. Control: HRT = 0,75 días, SRT = 40 días; MPBR 1: HRT = 0,75 días, SRT = 20 días; MPBR 2: HRT = 0,75 días, SRT = 40 días; MPBR 3: HRT = 0,75 días, SRT = 80 días; MPBR 4: HRT = 2 días, SRT = 80 días; MPBR 5: HRT = 5 días, SRT = 80 días.

En el caso de influente primario, los resultados fueron similares, encontrándose que la mayor contribución al ensuciamiento de la membrana estaba asociada a la biopelícula. No obstante, se observaron diferencias en los tipos de ensuciamiento según las condiciones experimentales. La fracción levemente adherida tuvo una contribución muy significativa en la condición de alta carga orgánica (R-MPBR 1),

donde alcanzó un valor de 68,7% de la resistencia total. En cambio, esta contribución fue inferior al 12% en las condiciones de baja carga. Para el tipo de biopelícula consolidada, se observó una tendencia decreciente con la carga orgánica, alcanzando valores de 19,6%, 14,2% y 9,1% para R-MPBR 1, R-MPBR 2 y R-MPBR 3, respectivamente. En todos los casos se encontró una influencia menor del material adsorbido (1-4,4%), lo que confirmó que la formación de una biopelícula fue el principal mecanismo de ensuciamiento.

Referencias

[1]   A.L. Gonçalves, J.C.M. Pires, M. Simões, A review on the use of microalgal consortia for wastewater treatment, Algal Res. 24 (2017) 403–415. https://doi.org/10.1016/j.algal.2016.11.008.

[2]   D. García, E. Posadas, S. Blanco, G. Acién, P. García-Encina, S. Bolado, R. Muñoz, Evaluation of the dynamics of microalgae population structure and process performance during piggery wastewater treatment in algal-bacterial photobioreactors, Bioresour. Technol. 248 (2018) 120–126. https://doi.org/10.1016/j.biortech.2017.06.079.

[3]   A. Solmaz, M. Işık, Polishing the secondary effluent and biomass production by microalgae submerged membrane photo bioreactor, Sustain. Energy Technol. Assessments. 34 (2019) 1–8. https://doi.org/10.1016/j.seta.2019.04.002.

[4]   L. Marbelia, M.R. Bilad, I. Passaris, V. Discart, D. Vandamme, A. Beuckels, K. Muylaert, I.F.J. Vankelecom, Membrane photobioreactors for integrated microalgae cultivation and nutrient remediation of membrane bioreactors effluent, Bioresour. Technol. 163 (2014) 228–235. https://doi.org/10.1016/j.biortech.2014.04.012.

[5]   F. Gao, Z.H. Yang, C. Li, G.M. Zeng, D.H. Ma, L. Zhou, A novel algal biofilm membrane photobioreactor for attached microalgae growth and nutrients removal from secondary effluent, Bioresour. Technol. 179 (2015) 8–12. https://doi.org/10.1016/j.biortech.2014.11.108.

[6]   F. Gao, Y.Y. Peng, C. Li, W. Cui, Z.H. Yang, G.M. Zeng, Coupled nutrient removal from secondary effluent and algal biomass production in membrane photobioreactor (MPBR): Effect of HRT and long-term operation, Chem. Eng. J. 335 (2018) 169–175. https://doi.org/10.1016/j.cej.2017.10.151.

[7]   G.H. Chen, M.C.M. van Loosdrecht, G.A. Ekama, D. Brdjanovic, Biological

Wastewater Treatment, 2nd Editio, IWA Publishing, London, UK, 2020.

[8] Y. Luo, P. Le-Clech, R.K. Henderson, Assessment of membrane photobioreactor (MPBR) performance parameters and operating conditions, Water Res. 138 (2018) 169–180. https://doi.org/10.1016/j.watres.2018.03.050.

[9] M. Raeisossadati, N.R. Moheimani, D. Parlevliet, Luminescent solar concentrator panels for increasing the efficiency of mass microalgal production, Renew. Sustain. Energy Rev. 101 (2019) 47–59. https://doi.org/10.1016/j.rser.2018.10.029.

[10] S.K. Parakh, P. Praveen, K.C. Loh, Y.W. Tong, Integrating gravity settler with an algal membrane photobioreactor for in situ biomass concentration and harvesting, Bioresour. Technol. 315 (2020) 123822. https://doi.org/10.1016/j.biortech.2020.123822.

[11] P. Praveen, W. Xiao, B. Lamba, K.C. Loh, Low-retention operation to enhance biomass productivity in an algal membrane photobioreactor, Algal Res. 40 (2019) 101487. https://doi.org/10.1016/j.algal.2019.101487.

[12] V. Montemezzani, I.C. Duggan, I.D. Hogg, R.J. Craggs, Zooplankton community influence on seasonal performance and microalgal dominance in wastewater treatment High Rate Algal Ponds, Algal Res. 17 (2016) 168–184. https://doi.org/10.1016/j.algal.2016.04.014.

[13] R. Mu, Y. Jia, G. Ma, L. Liu, K. Hao, F. Qi, Y. Shao, Advances in the use of microalgal–bacterial consortia for wastewater treatment: Community structures, interactions, economic resource reclamation, and study techniques, Water Environ. Res. 93 (2021) 1217–1230. https://doi.org/10.1002/wer.1496.

[14] A. Solmaz, M. Işık, Optimization of membrane photobioreactor; the effect of hydraulic retention time on biomass production and nutrient removal by mixed microalgae culture, Biomass and Bioenergy. 142 (2020). https://doi.org/10.1016/j.biombioe.2020.105809.

[15] R. Whitton, F. Ometto, M. Pidou, P. Jarvis, R. Villa, B. Jefferson, Microalgae for municipal wastewater nutrient remediation: mechanisms, reactors and outlook for tertiary treatment, Environ. Technol. Rev. 4 (2015) 133–148. https://doi.org/10.1080/21622515.2015.1105308.

[16] P.E.A. Debiagi, M. Trinchera, A. Frassoldati, T. Faravelli, R. Vinu, E. Ranzi, Algae characterization and multistep pyrolysis mechanism, J. Anal. Appl. Pyrolysis. 128 (2017) 423–436. https://doi.org/10.1016/j.jaap.2017.08.007.

[17] Commission Directive 98/15/EC, Commission Directive 98/15/EC of 27 February 1998 amending Council Directive 91/271/EEC, OJ L 67. (1998) 29.

[18] European Parliament and the Council 2020/741, Regulation (EU) 2020/741, Minimum requirements for water reuse, Off. J. Eur. Union. 177/33 (2020) 32–55. https://eur-lex.europa.eu/legal-

content/EN/TXT/PDF/?uri=CELEX:32020R0741&from=EN.

[19]   B. Green, L.S. Bernstone, T.J. Lundquist, W.J. Oswald, Advanced Integrated Wastewater Pond Systems for Nitrogen Removal, Water Sci. Technol. 33 (1996) 207–217.

[20]   D. Hernández, B. Riaño, M. Coca, M. Solana, A. Bertucco, M.C. García-gonzález, Microalgae cultivation in high rate algal ponds using slaughterhouse wastewater for biofuel applications, 285 (2016) 449–458. https://doi.org/10.1016/j.cej.2015.09.072.

[21]   R. Sun, P. Sun, J. Zhang, S. Esquivel-Elizondo, Y. Wu, Microorganisms-based methods for harmful algal blooms control : A review, Bioresour. Technol. 248 (2018) 12–20. https://doi.org/10.1016/j.biortech.2017.07.175.

[22]   A. Fallahi, F. Rezvani, H. Asgharnejad, E. Khorshidi, N. Hajinajaf, B. Higgins, Interactions of microalgae-bacteria consortia for nutrient removal from wastewater: A review, Chemosphere. 272 (2021) 129878. https://doi.org/10.1016/j.chemosphere.2021.129878.

[23]   O. Orgad, Y. Oren, S.L. Walker, M. Herzberg, The role of alginate in Pseudomonas aeruginosa EPS adherence, viscoelastic properties and cell attachment, Biofouling. 27 (2011) 787–798. https://doi.org/10.1080/08927014.2011.603145.

[24]   A. Soria-Verdugo, E. Goos, N. García-Hernando, U. Riedel, Analyzing the pyrolysis kinetics of several microalgae species by various differential and integral isoconversional kinetic methods and the Distributed Activation Energy Model, Algal Res. 32 (2018) 11–29. https://doi.org/10.1016/j.algal.2018.03.005.

[25]   A. Pavlath, K. Gregorski, Atmospheric pyrolysis of carbohydrates with thermogravimetric and mass spectrometric analyses, J. Anal. Appl. Pyrolysis. 8 (1985) 41–48.

[26]   C.H.T. Vu, S.J. Chun, S.H. Seo, Y. Cui, C.Y. Ahn, H.M. Oh, Bacterial community enhances flocculation efficiency of Ettlia sp. by altering extracellular polymeric substances profile, Bioresour. Technol. 281 (2019) 56–65. https://doi.org/10.1016/j.biortech.2019.02.062.

[27]   P. Bacchin, P. Aimar, R.W. Field, Critical and sustainable fluxes: Theory, experiments and applications, J. Memb. Sci. 281 (2006) 42–69. https://doi.org/10.1016/j.memsci.2006.04.014.

[28]   P. Le Clech, B. Jefferson, I.S. Chang, S.J. Judd, Critical flux determination by the flux-step method in a submerged membrane bioreactor, J. Memb. Sci. 227 (2003) 81–93. https://doi.org/10.1016/j.memsci.2003.07.021.

[29]   A. Drews, Membrane fouling in membrane bioreactors-Characterisation, contradictions, cause and cures, J. Memb. Sci. 363 (2010) 1–28. https://doi.org/10.1016/j.memsci.2010.06.046.

[30]   M. Zhang, L. Yao, E. Maleki, B.Q. Liao, H. Lin, Membrane technologies for

microalgal cultivation and dewatering: Recent progress and challenges, Algal Res. 44 (2019) 101686. https://doi.org/10.1016/j.algal.2019.101686.

[31]   Y. Luo, P. Le-Clech, R.K. Henderson, Simultaneous microalgae cultivation and wastewater treatment in submerged membrane photobioreactors: A review, Algal Res. 24 (2017) 425–437. https://doi.org/10.1016/j.algal.2016.10.026.

[32]   O. Díaz, L. Vera, E. González, E. García, J. Rodríguez-Sevilla, Effect of sludge characteristics on membrane fouling during start-up of a tertiary submerged membrane bioreactor, Environ. Sci. Pollut. Res. 23 (2016) 8951–8962. https://doi.org/10.1007/s11356-016-6138-y.

[33]   Y. Liao, A. Bokhary, E. Maleki, B. Liao, A review of membrane fouling and its control in algal-related membrane processes, Bioresour. Technol. 264 (2018) 343–358. https://doi.org/10.1016/j.biortech.2018.06.102.

CONCLUSIONES GENERALES

El desarrollo de la presente Tesis Doctoral ha permitido alcanzar las siguientes conclusiones:

- En general, los fotobiorreactores de membrana (MPBRs) mostraron una mejor operatividad que un biorreactor de membrana (MBR) convencional para tratar aguas residuales domésticas. Se observaron mayores productividades de biomasa y eliminación de nutrientes, así como, una mayor biofloculación.

- Cuando se trató un efluente secundario, incrementar el tiempo de retención de sólidos (SRT) hasta los 80 días en el MPBR mejoró la biofloculación y previno la acumulación de aglomerados biopoliméricos (BPCs) en la suspensión biológica. A pesar de las fluctuaciones del influente, se encontró que el valor óptimo del tiempo de retención hidráulico (HRT) y del fotoperiodo ha de estar comprendido entre los 2 y los 5 días y 16 horas de luz/ 8 horas de oscuridad, respectivamente, para obtener una moderada eliminación de nutrientes.

- Se comprobó la influencia del fotoperiodo en la productividad de la biomasa y en la eliminación de nutrientes de un MPBR alimentado con un efluente secundario. Ambos parámetros aumentaron conforme se incrementaba el periodo de luz en los ciclos ensayados hasta llegar a las 16 horas de luz, a partir de las cuales no se observó mejora.

- El aumento de las horas de luz hasta un fotoperiodo de iluminación continuo produjo una disminución de la biofloculación, del tamaño de partícula e incrementó el contenido de BPCs de las suspensiones, afectando con ello a la filtrabilidad del sistema.

- El MPBR rotatorio demostró su elevada capacidad de tratamiento de un efluente primario bajo oxigenación fotosintética. Se determinó que la carga orgánica al sistema (CLR) determina la concentración de oxígeno disuelto, afectando a la eliminación de nutrientes, a la biofloculación y al ensuciamiento de la membrana.

- El ensuciamiento reversible de las membranas está causado principalmente, por el contenido en BPCs de la suspensión. El ensuciamiento residual estuvo asociado al crecimiento de biopelícula sobre la membrana que se potencia por altos contenidos de BPCs en las suspensiones.

- La filtrabilidad óptima se estableció al operar con un SRT de 80 días y un HRT de 5 días para el tratamiento de un efluente secundario y en valores de SRT y HRT de 80 días y entre 3,5 y 5 días, respectivamente para el tratamiento de un efluente primario.

- Se consiguió el crecimiento de microorganismos indígenas en los MPBR ensayados. Microalgas verdes pertenecientes al género *Chorella* y *Scenedesmus* y diatomeas como *Nitzschia* y *Navicula* fueron encontradas en grandes cantidades en todas las condiciones. En el MPBR rotatorio alimentado con un influente primario, se observó mayor diversidad de especies, identificando, además, cianobacterias como *Oscillatoria* sp. aunque esta especie sólo fue encontrada en aquellos ensayos con mayor CLR.

- En los ensayos con influente primario, sólo cuando la CLR es baja se consiguen identificar ciliados reptantes y pedunculados y rotíferos, cuyo desarrollo parece estar relacionado con una menor concentración de biomasa, en particular con un menor contenido en sólidos en suspensión del sobrenadante.

- El desarrollo de la tecnología MPBR requiere valores adecuados de los parámetros de operación, que pueden maximizar la productividad de la biomasa y la eliminación de nutrientes sin empeorar el rendimiento de la membrana.

ANEXO
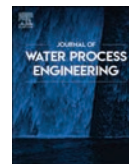
Secondary wastewater effluent treatment by microalgal-bacterial membrane photobioreactor at long solid retention times

E. Segredo-Morales [a], E. González [a,*], C. González-Martín [b], L. Vera [a]

[a] *Departamento de Ingeniería Química y Tecnología Farmacéutica, Universidad de La Laguna, Astrof. Fco. Sanchez s/n, 38200 La Laguna, Spain*
[b] *Instituto Universitario de Enfermedades Tropicales y Salud Pública de Canarias, Universidad de La Laguna, Astrof. Fco. Sanchez s/n, 38200 La Laguna, Spain*

ABSTRACT

Microalgal-bacterial membrane photobioreactors (MPBRs) have recently emerged as a new sustainable technology in wastewater treatment. For advanced treatment of domestic secondary effluents, selecting long solids retention times (SRTs) may be crucial to achieve optimal community structure and therefore, process performance. This study assesses the effects of operating conditions on nutrient removal, biomass productivity, suspension characteristics and membrane fouling. A lab-scale MPBR was run during long-term tests to assess process stability. Indigenous microalgae-bacteria consortia were developed for each condition. Conventional membrane bioreactor was used for tested control condition. Experimental results showed the crucial role of extending SRT to 80 d to enhance bioflocculation, avoid biopolymer clusters accumulation and minimize membrane fouling rates. Despite influent fluctuations, optimal hydraulic retention time value between 2 and 5 d was necessary to achieve moderate nutrient removal (40.6–48.7 % and 18.5–34.7 % for nitrogen and phosphorus, respectively). A mixed microalgal structure of green microalgae, cyanobacteria and diatoms was also achieved.

1. Introduction

Integration of microalgae-bacteria consortia into membrane photobioreactors (MPBRs) has recently been explored as a sustainable technology for nutrient removal from wastewater [1]. The use of microalgae-bacteria systems offers remarkable reductions in nutrient removal costs associated with wastewater treatment [2]. It is well recognized that symbiotic interactions between microalgae and bacteria exhibit better performance with low C/N ratio wastewaters [1,3]. This includes greater nitrifying bacteria population, lower external oxygen demand and direct bioflocculation [4,5]. Consequently, nutrient removal through an algae-bacteria consortium is especially suitable for the treatment of secondary wastewater effluents. Furthermore, the residual biomass produced can be reused for production of bioenergy, animal feedstock or other high-value products [6].

Although the advantages offered by microalgae-bacteria consortia have been demonstrated, there are few studies that have cultured native consortia for real wastewater treatment purposes. Most studies have been performed with inoculated mixed cultures, which may not be representative of native wastewater microbial communities [7]. Another issue to be considered is process stability over long periods with variable wastewater compositions. In this sense, several studies have demonstrated the difficulty to maintain inoculated cultures during wastewater treatment [8,9].

As stated, MPBRs have been considered an emerging option capable of achieving high nutrient removal, complete biomass retention and high-quality permeate [10]. One of the main advantages of the technology is decoupling hydraulic and solid retention times (HRT and SRT, respectively), which allows higher biomass concentration and nutrient load, and thus reduces process footprint [11]. Typical HRT values reported in the literature range between 1 and 5 d, where the optimum mainly depends on nutrient load [12,13]. Another essential parameter that affects process performance is SRT. While short times enhance biomass growth, longer SRTs generally increase microbial diversity, biomass concentration and bioflocculation [1]. Due to self-shading effect and possible nutrient limitation at large biomass concentration, SRT is typically limited to low to moderate values (2–25 d) to avoid microalgae growth inhibition [10,11]. Nevertheless, although studies at longer SRT are limited, some authors have reported an efficient process performance. Sheng et al. observed low biomass productivity (11–17 $mg \cdot L^{-1} \cdot d^{-1}$), which allows higher biomass concentration and nutrient removal (>95 % and >70 %, for nitrogen and phosphorus, respectively) at SRT of 60 d [14]. Another study

showed a considerable productivity (50–167 mg·L^{-1}·d^{-1}) and also optimal nutrient removal at very large SRT (>200 d) [15].

However, a major constraint to this technology's development on a large scale is membrane fouling, which decreases permeate productivity and raises treatment costs [16]. Preliminary cost analysis indicates that fouling control accounts for up to 57 % of operating and maintenance costs [14]. The rate and extent of fouling is influenced by the microbial suspension properties, mainly composed of organic biopolymers, inorganic colloids, cells, cell debris and microbial flocs [17]. In pure microalgae MPBRs, large biopolymers (often associated with algal-derived organic matter, AOM) and small size flocs have been related to severe membrane fouling [18,19]. This can be partially overcome by symbiotic systems, where bacteria can use AOM as carbon source for growth and also promote microalgae aggregation [20]. Membrane fouling is crucially affected by SRT due to its influence over microbial structure, AOM production and bioflocculation. Recent research has shown that increasing SRT from 10 to 30 d decreased membrane fouling as a consequence of changes on the floc size and micromorphology of the microalgal-bacterial flocs [21]. However, as most of MPBR literature is mainly limited to low to moderate SRT values, filtration performance at long SRT is yet to be investigated.

Based on the above considerations, this study prime novelty contribution is the evaluation of the performance of an MPBR operated at long SRT (>20 d). This is higher than that typically adopted, with the aim to define favourable conditions for improving bioflocculation, avoiding biopolymers accumulation and minimizing membrane fouling. Moreover, there are only a few studies that have cultured native consortia from real secondary effluents, which determines the stability of the microbial consortia and therefore, the technical feasibility of the treatment process. Additionally, deep studies assessing membrane fouling, particularly residual fouling during long-term tests, are scarce. This study provides fundamental information of process performance by monitoring nutrient removal efficiency, biomass productivity and main suspension characteristics, microalgae community structure and membrane fouling rates.

2. Materials and methods

2.1. Feedwater

Experimental unit was fed with an effluent from a conventional activated sludge domestic wastewater treatment plant (Santa Cruz de Tenerife, Canary Island, Spain). This plant was designed for only carbon removal forty years ago. Values measured for the different parameters were the chemical oxygen demand (COD), dissolved organic carbon (DOC), ammonium-nitrogen (NH$_4^+$-N), total nitrogen (TN) and phosphate-phosphorus (PO$_4^3$-P): 30–109 mg/L, 12.55–48.10 mg/L, 2.18–39.98 mg/L, 6.82–43.61 mg/L and 0.13–13.59 mg/L, respectively. Finally, it presented an average pH of 8.1 with a medium salinity (1390 μS·cm^{-1}).

2.2. Experimental unit

The laboratory unit consisted of a 3.0 L capacity tank equipped with a ZeeWeed® ZW-1 hollow fiber membrane module (Suez Water Technologies & Solutions, Ontario, ON, Canada) (Fig. 1). ZW-1 was made of PVDF with a nominal pore size of 0.04 μm and a filtration surface of 0.047 m^2. The permeate was extracted by a magnetic drive gear pump (Micropump-GA Series, Stockholm, Sweden) applying a slight vacuum. The experiments were carried out at a constant permeate flux of 10 L·h^{-1}·m^{-2}, measuring the transmembrane pressure (TMP) with a pressure sensor (Sensotech, Barcelona, Spain). This permeate flux value was within the typical range reported in the literature (2.6–15 L·h^{-1}·m^{-2}) [11]. The unit operated with intermittent aeration 10/30 s on/off at 5 NL·min^{-1}. For mixing and to maintain similar aerobic conditions in all the tests, air was supplied at a flow rate of 1 NL·min^{-1} injected at the bottom of the tank. The filtration was conducted under temporized mode, with filtration/backwashing cycles of 450/30 s. The backwash flux was set at 30 L·h^{-1}·m^{-2}. During backwashing, air was continuously applied at 5 NL·min^{-1}. To control the laboratory unit, DAQ Factory software (AzeoTech® Inc., Ashland, OR, USA) was used, which allows the information to be processed for visualization and control filtration variables. The permeate was collected in a tank from which the specific
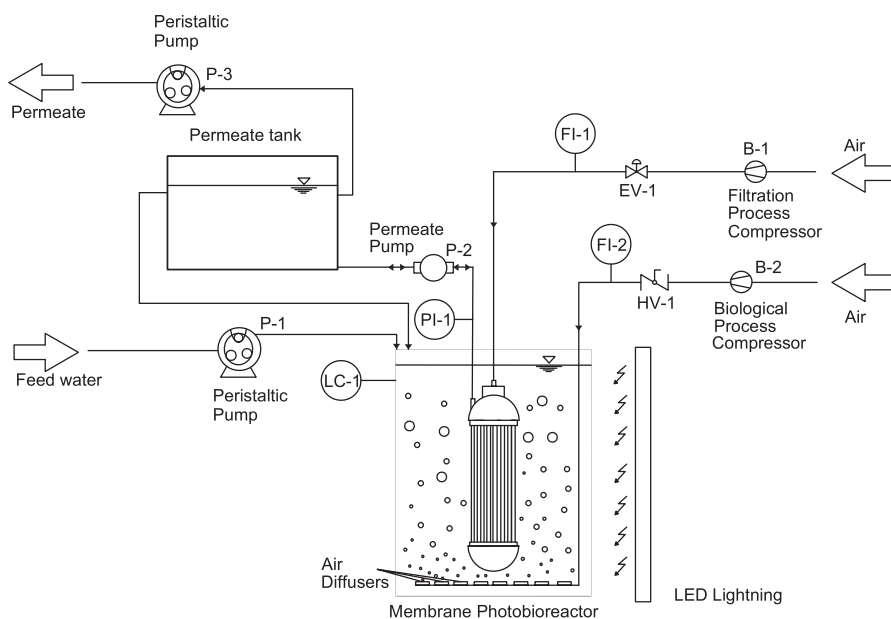

Fig. 1. Experimental setup of the MPBR system.

amount of permeate was extracted by a peristaltic pump (Cole-Parmer Instrument Co., USA) to maintain the HRT at the pre-established values. Tests were carried out at room temperature ($20 \pm 2\,°C$) and the duration of the experimental tests was 1000 h. All experimental tests were carried out under constant irradiation of 300 μmol/m^{2}s measured at the surface of the photobioreactor (PAR irradiance using an irradiance meter, QSP2150A, Biospherical Instrument Inc., USA) in 12/12 h light/dark cycles, except for the control condition in which 0/24 h light/dark was imposed.

2.3. Experimental conditions

As previously stated, values typically adopted for SRT and HRT in the literature are between 5 and 30 d, and between 6 h and 8 d, respectively [10,11]. In accordance with the main objective of the study, longer SRTs were selected (20–80 d), based in a previous study with a conventional MBR treating the same secondary effluent [22]. For each condition, the unit started without any inoculum and the biomass developed from the indigenous microorganisms existing in the influent. Starting (i.e. acclimation) period lasted for a minimum of the design sludge retention times (20, 40 and 80 d), during which the system operated without biomass purge. Then, the amount of suspension necessary to maintain SRT values at the desired levels was periodically purged manually. Biomass concentration reached after each start-up phase was close to that maintained during the tests.

Different combinations of SRTs (20, 40 and 80 d) and HRTs (0.75, 2 and 5 d) were assayed in the MPBR unit: MPBR 1 (HRT = 0.75 d, SRT = 20 d), MPBR 2 (HRT = 0.75 d, SRT = 40 d), MPBR 3 (HRT = 0.75 d, SRT = 80 d), MPBR 4 (HRT = 2 d, SRT = 80 d) and MPBR 5 (HRT = 5 d, SRT = 80 d). As control condition, SRT of 40 d and HRT of 0.75 d were applied. Samples of feedwater, suspension and permeate were withdrawn three times per week. Suspensions were characterized in terms of mixed liquor suspended solid (MLSS), particle size distribution, supernatant DOC, elemental analysis, thermogravimetric analysis (TGA) and Fourier-transform infrared spectroscopy (FTIR).

The biomass productivity was estimated according to Eq. (1):

$$r_x = \frac{MLSS}{SRT} \tag{1}$$

2.4. Short-term flux step trials

Short-term flux step experiments were performed by the flux-step method. Parameters were selected according to previous studies [23]. For these experiments, the flux was increased from 8 L·h^{-1}·m^{-2} to a maximum of 40 L·h^{-1}·m^{-2} in steps of 2 L·h^{-1}·m^{-2}. Each step lasted 15 min. Aeration and backwashing conditions were the same as those applied in the experimental phases. The filtration time was set at 900 s. After each flux-step run, the membrane was chemically cleaned using a 500 mg·L^{-1} sodium hypochlorite solution. The experiments were carried out on all the suspensions of the experimental phases and on the supernatant obtained after 30 min of decantation.

Results were related to reversible fouling rate (r_f), given by the derivative of the transmembrane pressure ($dTMP/dt$).

2.5. Membrane cleaning protocol

After each experimental phase, the membrane was subjected to a cleaning protocol to characterize the fouling produced during the experiments [24]. Firstly, the fouled membrane module was immersed in tap water to measure the transmembrane pressure (TMP_f), then the membrane was rinsed with pressurized water and the transmembrane pressure was measured again with tap water (TMP_{rinse}). After this, the membrane was immersed in a 500 mg·L^{-1} sodium hypochlorite solution for 24 h. Then, the transmembrane pressure was measured again with clean water ($TMP_{oxidant}$). Finally, it was immersed in a 6 g·L^{-1} citric acid

solution for 2 h. The transmembrane pressure measured after this step was called TMP_{acid}. Each of the transmembrane pressure measurements were made after 4 min of filtration. Resistances were calculated from TMP data according to the resistance in a series model (Eq. (2)):

$$TMP_{ci} = J \cdot \mu \cdot (R_m + R_{ci}) \tag{2}$$

where J is the permeate flux, μ is the permeate viscosity, R_m is membrane resistance and TMP_{ci} and R_{ci} are the corresponding post-cleaning step transmembrane pressure and resistance, respectively.

2.6. Membrane fouling characterization

TMP evolution under consecutive cycles of filtration was used to characterize membrane fouling. Reversible fouling was evaluated from the fouling rate data (r_f). Meanwhile, the residual fouling phenomena, which was not removed by backwashing, was measured by the initial transmembrane pressure TMP_i at the beginning of the filtration cycle. Therefore, TMP evolution during the filtration phase can be described by the following equation [23]:

$$TPM = TMP_i + r_f \cdot t \tag{3}$$

where t is the elapsed time.

2.7. Analytical methods

Chemical oxygen demand (COD) and mixed liquor suspended solids (MLSS) were measured by standard methods [25]. Turbidity was measured using a turbidimeter HACH 2100 N (Hach, USA). DOC was measured by a TOC-meter (TOC-5000A, Shimadzu, Japan). The difference in DOC concentration between the filtered supernatant from the suspension (0.45 μm nitrocellulose membrane filter, HA, Millipore, Germany) and the permeate was considered as biopolymer cluster (BPC) concentration. The Nessler method was used for NH$_4^+$-N measurement using a DR-5000 Hach spectrophotometer (Hach, USA). Nitrate-nitrogen (NO$_3^-$-N), nitrite-nitrogen (NO$_2^-$-N), PO$_4^{3-}$-P were measured through ion chromatography using a Compact IC plus 882 device supplied by Metrohm (Metrohm Switzerland). Particle size distribution was measured using a Malvern Mastersizer 2000 instrument (Malvern Instruments Ltd., UK). For elemental analysis, a FLASH EA 1112 Elemental Analyzer (ThermoFisher Scientific, USA) was used. Thermogravimetric analysis (TGA) was performed using a simultaneous thermal analyzer (TG/DSC): Discovery SDT 650 (TA Instruments, USA). A quantity of biomass was loaded in a platinum crucible and heated between 25 and 600 °C at a heating rate of 15 °C/min under a nitrogen flow of 50 mL/min (Alphagaz nitrogen gas, Air Liquid, France). Fourier-transform infrared spectrometry was performed using an IFS 66/S spectrometer (Bruker, USA) equipped with an ATR accessory that measured the transmittance of the samples in a wavelength range between 900 and 4000 cm^{-1}. Dissolved oxygen and temperature in the bioreactor were measured with an on-line Hach HQ40d oximeter (Hach, USA). Microalgae identification and quantification were carried out by optical microscopy (DM750, Leica, Germany), according to Wastewater Organisms Atlas Manual [26].

3. Results and discussion

3.1. Biomass concentration and productivity

Fig. 2 shows biomass concentration and productivity for the control condition, and the MPBR at the different SRTs and HRTs. There was a substantial improvement in biomass productivity (about 11 times) in the MPBR compared with the control one at the same conditions (SRT of 40 d and HRT of 0.75 d). It should be considered that the only difference between both reactors is the lighting regime, therefore, the different productivity should be associated with the presence of microalgae. Due
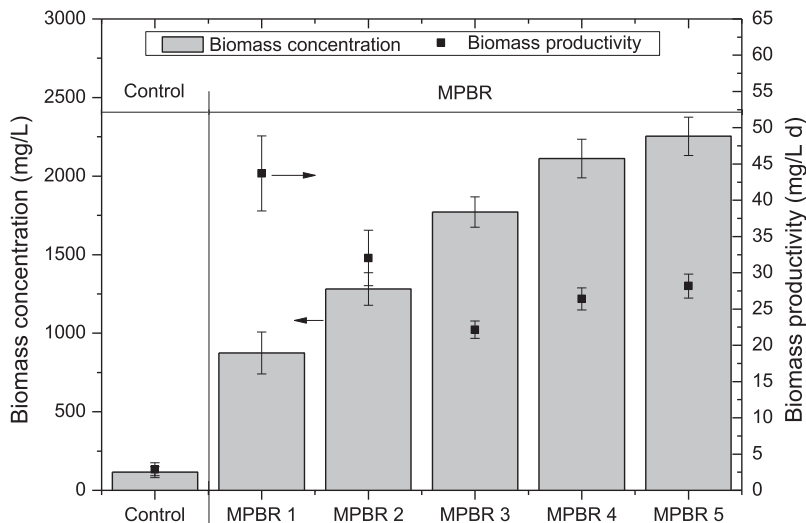
Fig. 2. Biomass concentration and productivity for the control condition and the MPBR at different HRTs and SRTs. Control: HRT = 0.75 d, SRT = 40 d; MPBR 1: HRT = 0.75 d, SRT = 20 d; MPBR 2: HRT = 0.75 d, SRT = 40 d; MPBR 3: HRT = 0.75 d, SRT = 80 d; MPBR 4: HRT = 2 d, SRT = 80 d; MPBR 5: HRT = 5 d, SRT = 80 d.

to the characteristics of the feedwater, characterized by a low C/N ratio, severe organic carbon limitation was imposed. Under this condition, heterotrophic bacteria should preferentially meet their maintenance energy requirements instead of producing additional biomass [27]. This can justify the low biomass productivity in control condition. In the MPBRs, microalgae can fix CO_2 during autotrophic growth while secreting organic carbon, mainly as polysaccharides and proteins, which can be used as a carbon source by the heterotrophs [28]. Accordingly, the synergistic support of bacteria and microalgae enhanced the consortium growth, as previously reported [7].

As can be seen in Fig. 2, both SRT and HRT effectively controlled biomass concentration and productivity in the MPBR. Biomass concentration increased with SRT, since the biomass disposal rate decreased to a greater extent than biomass productivity. The decrease in productivity can be attributed to slight attenuation at high biomass concentrations, as reported in a similar study at moderate SRTs [29]. Nevertheless, productivity values varied between 43.7 and 22.1 $mg \cdot L^{-1} \cdot d^{-1}$, which are comparable with those typically reported in an MPBR at moderate SRTs (4.5–30 d) (20–52 $mg \cdot L^{-1} \cdot d^{-1}$) [29,30] but higher than those observed at SRT of 60 d (10–17 $mg \cdot L^{-1} \cdot d^{-1}$) [14]. Results also showed an increase
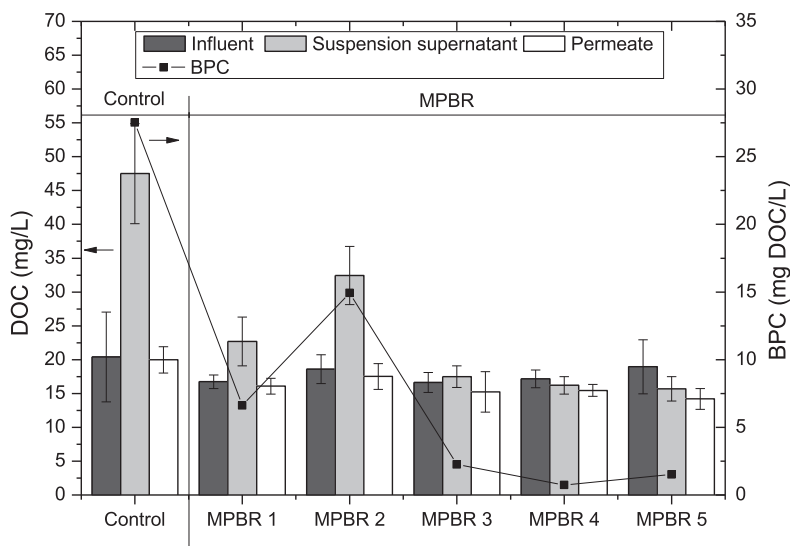

Fig. 3. Dissolved organic carbon (DOC) in feedwater, suspension supernatant and permeate, and biopolymer clusters (BPC) at different operating conditions. Control: HRT = 0.75 d, SRT = 40 d; MPBR 1: HRT = 0.75 d, SRT = 20 d; MPBR 2: HRT = 0.75 d, SRT = 40 d; MPBR 3: HRT = 0.75 d, SRT = 80 d; MPBR 4: HRT = 2 d, SRT = 80 d; MPBR 5: HRT = 5 d, SRT = 80 d.

in biomass concentration and productivity by extending HRT. Specifically, an increase in HRT from 0.75 to 5 d resulted in a productivity increase of 27 %. This trend seems to contradict some previous studies that reported biomass production is inversely proportional to HRT due to nutrient limitation [12,31]. By contrast, other studies have found a positive effect [14] or only slight differences [13]. In the present study, the symbiotic relationship between microalga and bacteria seems to be enhanced at large HRT.

3.2. Biomass characteristics

Many researchers have highlighted the relevance of free-biopolymers secreted by microalgae-bacteria consortia in biomass flocculation [1] and also in membrane fouling [11]. For this reason, DOC was routinely determined in feedwater, suspension supernatant and permeate. The colloidal fraction of the biopolymers (often called biopolymer clusters, BPC) was estimated from the difference between DOC concentration of the supernatant and the permeate. As showed in Fig. 3, there was significant BPC accumulation in the control condition, which was reduced in the MPBR at moderate SRTs (20–40 d) and reached very low concentrations at SRT of 80 d. This clearly indicates that the joint development of microalgae and bacteria enhances the degradation of biopolymers, decreasing the colloidal fraction in the liquid phase. In the range studied, HRT did not have a significant effect. The positive effect microalgae-bacteria consortia in bioflocculation was confirmed by analysis of particle size distribution. Mean value was 40.2 µm for the control condition and ranged between 75.3 and 129.8 µm in the MPBR (Supplementary data, Table S1). Due to the crucial role of BPC and floc size distribution in membrane fouling, the selection of a long SRT will be essential for the sustainable operation of an MPBR.

A basic biomass characterization was also performed by thermogravimetric and elemental analysis. The former has been used to investigate devolatilization process of biomass samples between 150 °C and 600 °C [32]. Analysis of derivative weight curves (Fig. 4) showed significant differences between the samples from the MPBR and the control condition. The curves of the MPBR were wider, covering a range of temperature between 200 and 450 °C, which has been attributed to the

thermal degradation of significant amounts of the three main components of the biomass: carbohydrates, proteins and lipids [32]. However, the curve for the control condition was narrower, with a maximum rate of reaction at approximately 275 °C, which could be due to a higher content of proteins compared to carbohydrates [33]. The elemental analysis also seems to support this approach according to the lower C/N ratio observed in the control condition (Table 1). At the same time, the addition of microalgae to the bacteria community clearly seems to enhance CO_2 fixation, achieving a higher carbon content in the biomass. Consistently, greater volatile matter in the MPBR biomass was obtained (38.3–48.9 %) (Table 1). In general, the volatile content is lower than that typically reported in other studies using a synthetic growth medium, but similar to microalgae biomass cultivated in wastewater [34]. This is probably explained by the characteristics of the feedwater used: a secondary effluent water with a medium saline content (average

Table 1
Volatile matter and elemental composition of MPBR and control condition biomass samples.

Parameters	MPBR 1	MPBR 2	MPBR 3	MPBR 4	MPBR 5	Control
	SRT = 20 d HRT = 0.75 d	SRT = 40 d HRT = 0.75 d	SRT = 80 d HRT = 0.75 d	SRT = 80 d HRT = 2 d	SRT = 80 d HRT = 5 d	SRT = 40 d HRT = 0.75 d
Volatile matter (% wt, dry basis)	38.3 ± 0.8	38.7 ± 1.5	48.9 ± 1.0	43.6 ± 0.6	48.2 ± 0.4	33.8 ± 2.1
Elemental analysis (%wt, dry basis)						
C	22.8 ± 0.8	24.9 ± 1.4	26.4 ± 1.0	26.4 ± 0.3	28.3 ± 0.3	5.8 ± 1.5
H	3.6 ± 0.1	3.7 ± 0.2	4.2 ± 0.6	3.7 ± 0.1	4.4 ± 0.1	0.9 ± 0.2
N	4.5 ± 0.3	4.7 ± 0.7	4.9 ± 0.4	4.5 ± 0.1	5.6 ± 0.2	3.1 ± 0.8

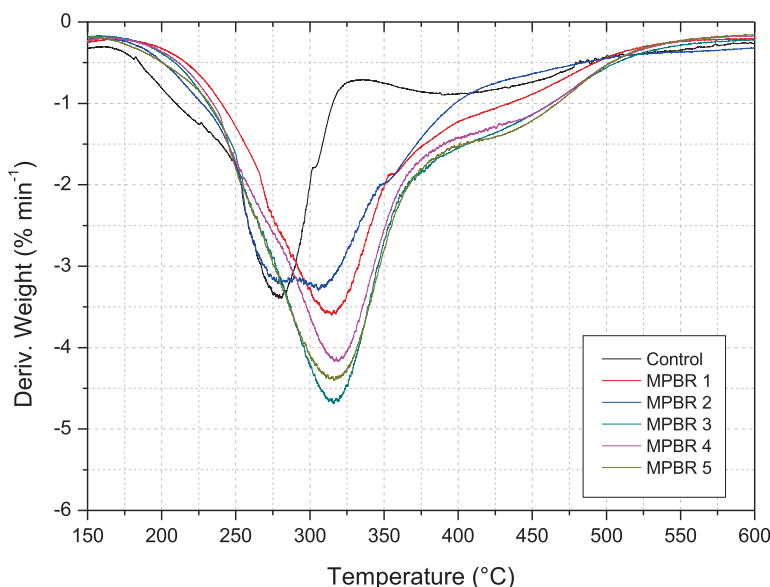Note: The data are expressed as mean ± standard deviation.

Fig. 4. Derivative weight loss curve for the control condition and the MPBR samples. Control: HRT = 0.75 d, SRT = 40 d; MPBR 1: HRT = 0.75 d, SRT = 20 d; MPBR 2: HRT = 0.75 d, SRT = 40 d; MPBR 3: HRT = 0.75 d, SRT = 80 d; MPBR 4: HRT = 2 d, SRT = 80 d; MPBR 5: HRT = 5 d, SRT = 80 d.

electrical conductivity of 1390 μS·cm^{-1}). Therefore, thermal degradation and elemental analysis showed a higher biopolymer content in the MPBR biomass, confirming higher bioflocculation ability, which was enhanced at long SRTs.

Biochemical composition has been also studied by analyzing FTIR spectra of biomass samples from the MPBR and the control condition (Fig. 5). Characteristic bands are observed in all cases, presenting peaks of carbohydrates (980–1174 cm^{-1}), nucleic acids (1072–1099 cm^{-1} and 1191–1356 cm^{-1}), proteins (1357–1709 cm^{-1} and 3029–3639 cm^{-1}) and hydrocarbons from lipids (2809–3012 cm^{-1}), comparable with those reported in the literature [35–37]. In particular, a broad region around a peak at 1052 cm^{-1} can be seen, which is attributed to the υ(C-O-C) stretching of carbohydrates [35]. Nucleic acids also have a specific band in this region (υ_s(>P=O) stretching of phosphodiesters) and another at 1230 cm^{-1} (υ_{as}(>P=O) stretching of phosphodiesters), which can be observed in the spectra of the samples. The presence of proteins was confirmed by peaks at 1643 and 1546 cm^{-1}, representative of υ(C=O) stretching vibrations, and combined δ(N—H) bending and υ(C—N) stretching vibrations, corresponding to protein-associated amides I and II, respectively [36]. Similarly, the characteristic broad band at around 3286 cm^{-1} associated with water υ(O—H) stretching and protein υ(N—H) stretching can also be seen [38]. The proteins have also characteristic bands at 1425–1477 cm^{-1} (δ_{as}(CH$_3$) and δ_{as}(CH$_2$) bending of methyl) and 1357–1423 cm^{-1} (δ_s(CH$_3$) and δ_s(CH$_2$) bending of methyl) [35]. This protein specific pattern appeared in all samples, but band intensities significantly decreased in the MPBR samples compared with the control condition, which was especially obvious at regions around 1400 cm^{-1} and 3286 cm^{-1}. This fact, together with the lower intensity of the carbohydrate-associated band in the control, was probably a result of a higher carbohydrate-to-protein ratio in the MPBR biomass, as previously observed in thermogravimetric and elemental analyses. Finally, a weak peak at 2927 cm^{-1}, assigned to υ_{as}(CH$_2$) and υ_s(CH$_2$) stretching, was observed in all samples, which has been attributed to the presence of lipid-associated hydrocarbons [38].

3.3. Organic matter and nutrient removal

Table 2 shows the organic matter and nutrient removal efficiencies reported in the MPBR at different SRT and HRT conditions. As a result of the nature of the secondary effluent treated, there was a large variation in the concentration of influent pollutants fed to the MPBR under different tested operating conditions. Nevertheless, a significant

Table 2
Biological performance of MPBR and control condition.

Parameters	MPBR 1	MPBR 2	MPBR 3	MPBR 4	MPBR 5	Control
	SRT = 20 d HRT = 0.75 d	SRT = 40 d HRT = 0.75 d	SRT = 80 d HRT = 0.75 d	SRT = 80 d HRT = 2 d	SRT = 80 d HRT = 5 d	SRT = 40 d HRT = 0.75 d
Effluent concentration (mg·L^{-1})						
COD	50.9 ± 10.1	48.8 ± 10.5	46.9 ± 10.0	34.9 ± 10.3	36.4 ± 10.1	61.9 ± 8.2
NH$_4^+$-N	0.5 ± 0.1	0.9 ± 0.9	0.4 ± 0.1	0.4 ± 0.1	0.4 ± 0.1	0.6 ± 0.4
TN	8.7 ± 2.5	23.7 ± 7.0	9.9 ± 1.8	7.4 ± 3.5	14.5 ± 2.5	20.4 ± 5.2
PO$_4^{3-}$-P	5.4 ± 2.8	4.8 ± 2.2	5.0 ± 1.7	4.2 ± 1.6	1.5 ± 0.4	4.3 ± 1.5
Removal efficiency (%)						
COD	23.2 ± 4.3	24.7 ± 14.2	26.7 ± 14.0	35.0 ± 9.7	44.8 ± 14.5	17.8 ± 9.4
NH$_4^+$-N	90.8 ± 3.7	95.7 ± 2.7	92.2 ± 4.1	93.9 ± 2.8	94.9 ± 8.0	95.3 ± 2.2
TN	30.0 ± 12.3	22.2 ± 9.1	5.6 ± 4.9	48.7 ± 13.1	40.6 ± 12.9	4.5 ± 5.9
PO$_4^{3-}$-P	6.4 ± 3.3	14.8 ± 7.2	5.2 ± 3.3	18.5 ± 18.9	34.7 ± 13.4	0.5 ± 1.3

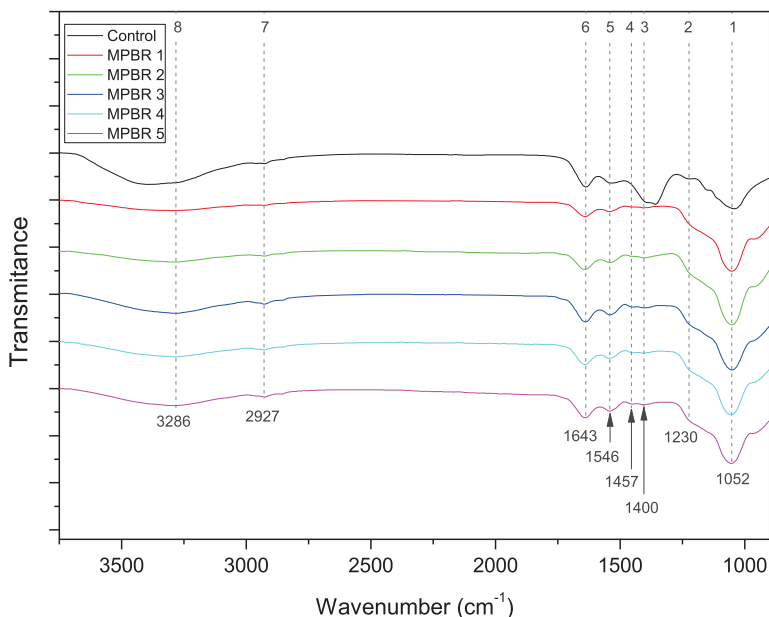Note: The data are expressed as mean ± standard deviation.

Fig. 5. FTIR spectra of biomass samples from the MPBR and the control condition. Characteristics bands were identified from carbohydrates (band 1), nucleic acids (band 2), proteins (bands 3–6 and 8) and lipids (band 7). Control: HRT = 0.75 d, SRT = 40 d; MPBR 1: HRT = 0.75 d, SRT = 20 d; MPBR 2: HRT = 0.75 d, SRT = 40 d; MPBR 3: HRT = 0.75 d, SRT = 80 d; MPBR 4: HRT = 2 d, SRT = 80 d; MPBR 5: HRT = 5 d, SRT = 80 d.

improvement was observed in all parameters with respect to the control condition (i.e. aerobic MBR). Average COD concentrations of 34.9–50.9 mg·L^{-1} and 61.9 mg·L^{-1} were reported in the permeate of the MPBR and of the control condition, leading to COD removals of 23.2–44.8 % and 17.8 %, respectively. Regarding nutrient removal, the MPBR also showed a better performance. A complete nitrification (effluent NH$_4^+$-N < 1 mg·L^{-1}) was also observed in both conditions, but total nitrogen and phosphorus removal increased by 80 % and 97 %, respectively. This is explained by higher biomass growth rate in the MPBR (Fig. 2), where nutrient removal is expected to be mainly achieved through microalgae biomass assimilation [21]. It should be noted that external aeration was supplied for both conditions and dissolved oxygen was always maintained at high levels (9.2 ± 0.7 mg·L^{-1} and 9.1 ± 0.3 mg·L^{-1} for control condition and MPBR, respectively), which prevails over the indirect nitrogen remediation process. An example of the dissolved oxygen profiles is showed in Fig. S1. In addition, similar pH values (8.4–8.6) were recorded for both conditions, reflecting a similar effect of the indirect removal methods of ammonia volatilization and phosphate precipitation [39].

TN removal efficiency decreased with longer SRTs in the MPBR (Table 2), which can be related to lower growth rates. These results are in agreement with other MPBR studies treating synthetic secondary effluents for pure [29] and mixed cultures [21], in which a deterioration was observed of nitrogen removal when increasing SRTs above 20 d. By contrast, no appreciable effect was found on PO$_4^{3-}$-P removal, which ranged between 5.2 and 14.8 % and seems to be very sensitive to influent fluctuation. Therefore, to improve nutrient removal at the optimum SRT of 80 d, HRT was extended for effective bioflocculation. At values of 2 and 5 d, the system increased TN removal efficiencies up to 48.7 and 40.6 %, respectively, while PO$_4^{3-}$-P removal achieved values of 18.5 and 34.7 %, respectively. In these conditions, removal rates varied between 2.0 and 3.4 mg·L^{-1}·d^{-1} for nitrogen and between 0.1 and 0.4 mg·L^{-1}·d^{-1} for phosphorus, which are within the typical range reported in MPBRs [12]. In the present study, despite influent fluctuations, establishing an optimal HRT value between 2 and 5 d seems necessary to achieve moderate nutrient removal, consistent with previous studies [13]. Nevertheless, the system does not meet the legal treatment requirements (10 mg TN·L^{-1} and 1 mg P·L^{-1}, stipulated by EU) [40] (Table 2).

3.4. Membrane fouling

3.4.1. Threshold flux determination

Threshold fluxes were evaluated using the widely used flux-step method [41]. These values are used to describe the permeate flux before reversible fouling (i.e. $r_f = dTMP/dt$) increases to unsustainable rates. Although the selection of sustainable fouling rates is indeed quite subjective, a reference of 1 mbar/min was used in the present study, based on operative values reported in full-scale MBRs [42]. In all cases, a power relationship between the fouling rates and the permeate fluxes was observed, where the MPBR clearly showed better performance than the control condition, excluding for SRT of 40 d and HRT of 0.75 d (MPBR 2) (Fig. 6). It should be noted that under these conditions, the MPBR was characterized by a high level of BCPs, even higher than the control condition. Therefore, there was a significant impact of SRT on the threshold flux, which firstly decreased, reaching a minimum at 40 d, and then sharply increased with increasing SRT. As consequence, compared to value of 20 d, typically adopted in the literature [10], an operation at 80 d increased the threshold flux from 22 to 32–40 L·h^{-1}·m^{-2}. In the tested conditions, there was no significant impact of HRT. Results also showed an evident relationship between reversible fouling rate and BPC content. Similar results were reported in a previous study of an MBR applied to a secondary effluent treatment [22]. In addition, this is consistent with many studies in the literature, which have identified algal organic matter as the main contributor to the membrane fouling in MPBRs [11,17]. This type of fouling is usually associated with gel/cake layer formation on the membrane surface by colloidal and particulate matter. In order to confirm the impact of the colloidal fraction of the biopolymers and fine particles on membrane fouling, results were compared with those obtained under the same conditions by removing sedimentable solids (through 30 min of sedimentation, obtaining suspended solid removal of 71–95 %). Mean characteristics of the supernatants are displayed in Supplementary data, Table S2. Similar behavior was observed (Supplementary data, Fig. S2),
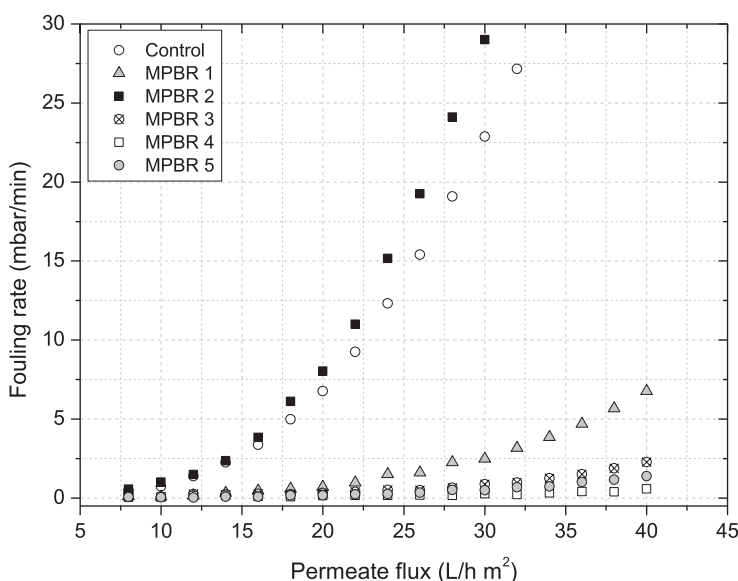

Fig. 6. Fouling rate against permeate flux for MPBR and control condition. Control: HRT = 0.75 d, SRT = 40 d; MPBR 1: HRT = 0.75 d, SRT = 20 d; MPBR 2: HRT = 0.75 d, SRT = 40 d; MPBR 3: HRT = 0.75 d, SRT = 80 d; MPBR 4: HRT = 2 d, SRT = 80 d; MPBR 5: HRT = 5 d, SRT = 80 d.

confirming the crucial role of BPCs. This was probably due to shear conditions in the membrane vicinity due to intermittent air-sparging, which induces back-transport of large suspended solids resulting from shear-induced particle diffusion and inertial lift forces and therefore colloids are selectively deposited [43]. In the present study, optimum conditions involve BPCs below ~5 mg·L^{-1}, which were achieved at SRT of 80 d.

3.4.2. Residual fouling evolution

Fig. 7 shows the TMP_i evolution at the operating conditions, and Table 3 displays average residual and reversible fouling rates.

Since residual fouling refers to the fouling that cannot be removed by frequent physical cleanings (i.e. backwashing) [42], this type of fouling might be related with reversible fouling rates. Therefore, as expected from the flux-steps results, SRT clearly decreased residual fouling rate $dTMP_i/dt$ (Fig. 7d, e, f and Table 3). Furthermore, under these conditions, a significant effect of HRT on both fouling rates were observed, revealing optimal filtration conditions at 5 d. These results are consistent with those reported by Low et al. [19] who reported a decrease in membrane fouling with an increase in HRT in a ceramic MPBR, which was attributed to lower production of supernatant biopolymers. Nevertheless, specific behavior was observed in the MPBR at SRT of 40 d and HRT of 0.75 d (MPBR 2) (Fig. 7c and Table 3), characterized by a sudden TMP_i increase after ~500 h. This sharp increase is commonly observed in MBRs, where different explanations based on pore/area loss, cake-layer porosity decrease and osmotic pressure increase have been provided [44]. All these mechanisms are increased at larger biopolymer content in the supernatant. In addition, once a cake layer (often named biocake in MBRs) is formed, increasing TMP up to a critical value might induce cake compaction, resulting in a higher specific cake resistance and thus requiring further TMP increases to maintain a constant permeate flux [45]. A simple visual inspection of the fouled membranes at the end of the tests showed appreciable biocake development in all cases, but with different structure and heterogeneity. An apparent flat layer was formed in the control condition, while a heterogeneous biocake is observed in the MPBR, that apparently tended to decrease at the higher SRT of 80 d (MPBR 3–5) (Fig. 8). This is consistent with BPC content, since the development of organic coating by biopolymers on the membrane allows the attachment of microalgae and bacteria [17]. Therefore, the notable biocake development together with high

Table 3
Average residual and reversible fouling rates for the control and the MPBR at different operating conditions.

Parameters	MPBR 1	MPBR 2	MPBR 3	MPBR 4	MPBR 5	Control
	SRT = 20 d HRT = 0.75 d	SRT = 40 d HRT = 0.75 d	SRT = 80 d HRT = 0.75 d	SRT = 80 d HRT = 2 d	SRT = 80 d HRT = 5 d	SRT = 40 d HRT = 0.75 d
$dTMP_i/dt \cdot 10^3$ (kPa/h)	1.5	9.87[a]	2.51	1.58	1.14	1.73
r_f (mbar/min)	1.02	6.90[a]	0.12	0.03	0.01	2.49

[a] Data obtained from the first 500 h of operation.

concentrations of biopolymers in the supernatant could explain the sudden TMP increase in MPBR 2.

Regarding r_f, average values followed a similar trend observed for the flux-step trials, though increasing according to the residual fouling development (Table 3). This can be related to a reduction in the available membrane filtration area due to pore/area loss, where the resulting local flux increased [46].

3.4.3. Residual fouling characterization

To investigate biocake organic foulants, samples were collected at the end of the test and analyzed using FTIR (Fig. 9). Characteristic biomass bands were observed, similar to those found in the suspension samples. Nevertheless, specific peaks of carbohydrates (980–1174 cm^{-1}) showed a higher intensity for the MPBR samples at SRT of 80 d (MPBR 3–5) compared to those observed at lower SRTs (MPBR 1 and 2) and the control condition. The opposite trend was found for proteins bands (3–6). It seems that by extending SRT to 80 d, there was a shift in biocake organic composition towards a higher carbohydrate to protein ratio. It was previously reported that carbohydrates represent the main component of the biocake during the slight TMP rise phase, while an increase in protein content is associated with TMP's sharp increase in the MBR [47]. This agrees with the results obtained in the present study for the MPBR 2 condition.

In addition, a fouling resistance analysis was conducted at the end of
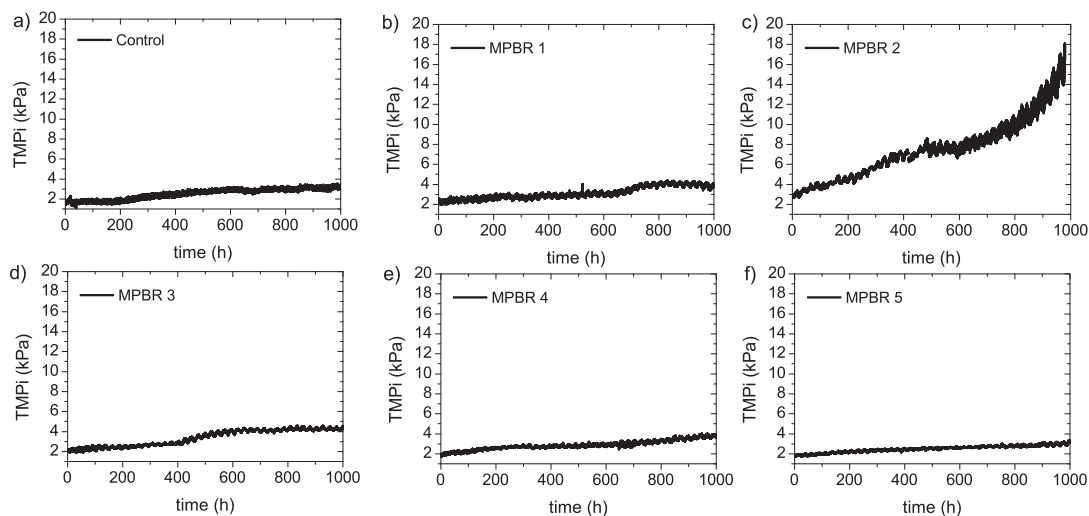

Fig. 7. Initial transmembrane pressure (TMP_i) for MPBR and control condition. Control: HRT = 0.75 d, SRT = 40 d; MPBR 1: HRT = 0.75 d, SRT = 20 d; MPBR 2: HRT = 0.75 d, SRT = 40 d; MPBR 3: HRT = 0.75 d, SRT = 80 d; MPBR 4: HRT = 2 d, SRT = 80 d; MPBR 5: HRT = 5 d, SRT = 80 d.

Fig. 8. Fouled membranes. Control: HRT = 0.75 d, SRT = 40 d; MPBR 1: HRT = 0.75 d, SRT = 20 d; MPBR 2: HRT = 0.75 d, SRT = 40 d; MPBR 3: HRT = 0.75 d, SRT = 80 d; MPBR 4: HRT = 2 d, SRT = 80 d; MPBR 5: HRT = 5 d, SRT = 80 d.
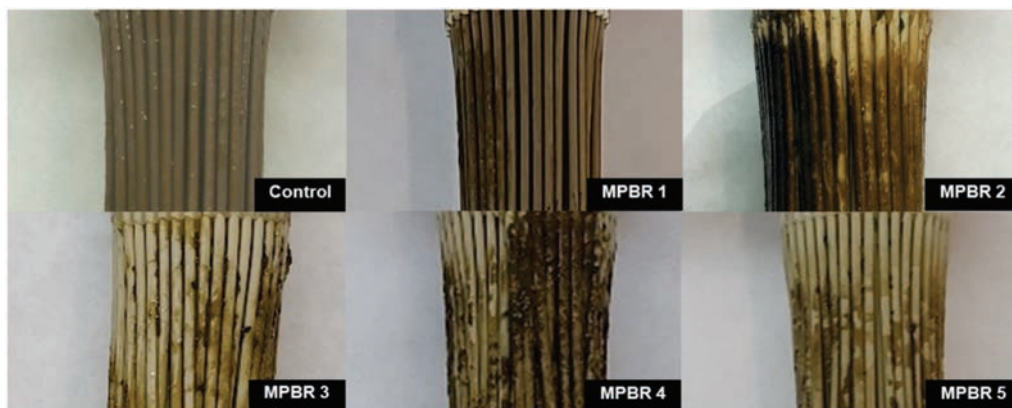

Fig. 9. FTIR spectra of biocake samples from the MPBR and the control condition. Characteristics bands were identified from carbohydrates (band 1), nucleic acids (band 2), proteins (bands 3–6). Control: HRT = 0.75 d, SRT = 40 d; MPBR 1: HRT = 0.75 d, SRT = 20 d; MPBR 2: HRT = 0.75 d, SRT = 40 d; MPBR 3: HRT = 0.75 d, SRT = 80 d; MPBR 4: HRT = 2 d, SRT = 80 d; MPBR 5: HRT = 5 d, SRT = 80 d.
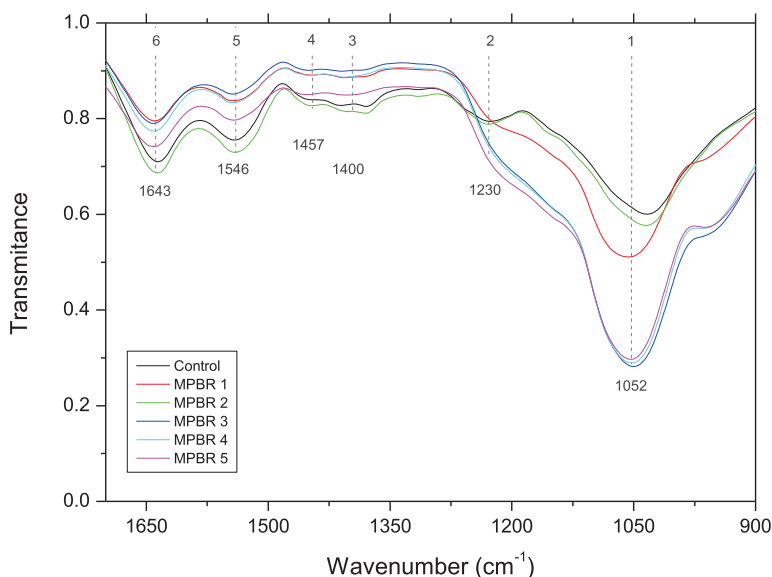
the tests by using a cleaning protocol. Thus, residual fouling was separated into three main types of foulants: biocake (removed by physical means: rinse with tap water), organic fouling (removed by an oxidant) and inorganic fouling (removed by an acid). As can be seen in Fig. 10, in all cases, most of the residual fouling was removed by physical means, which is consistent with the significant biocake development, as previously stated. This resistance removal accounted for 62 % in the control condition and increased to 70–87 % in the MPBR, probably due to the lower biomass concentration in the control condition. The significant role of organic biopolymer fouling was also confirmed by the resistance to removal by the oxidant, while a minor significance was observed for inorganic foulants.

3.5. Microalgal community structure

Indigenous growth of microalgae was successfully achieved in the MPBR under all tested conditions, where a mixed population of green algae, cyanobacteria and diatoms was observed (Table 4). Green microalgae belonging to the genera *Chorella* and *Scenedesmus* and diatoms *Nitzschia* and *Navicula* were observed under all conditions, which confirmed their high productivity and tolerance to secondary effluent pollutants. Nevertheless, the variability in microalgae structure between the different operating conditions revealed the sensitivity of mixed culture to influent fluctuations and the difficulty to maintain a specific microalgae culture over long periods. Dominant species reported here are commonly observed in microalgal consortia applied to wastewater treatment [7,9]. Although less abundant, green microalgae belonging to
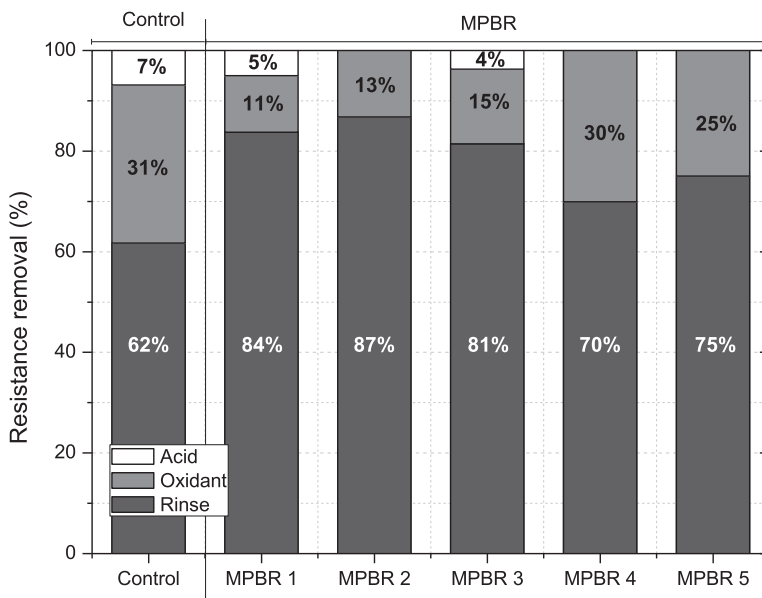
Fig. 10. Resistance removed by rinse, oxidant, and acid at different operating conditions for MPBR and control condition. Control: HRT = 0.75 d, SRT = 40 d; MPBR 1: HRT = 0.75 d, SRT = 20 d; MPBR 2: HRT = 0.75 d, SRT = 40 d; MPBR 3: HRT = 0.75 d, SRT = 80 d; MPBR 4: HRT = 2 d, SRT = 80 d; MPBR 5: HRT = 5 d, SRT = 80 d.

Table 4
Relative abundance of the microalgal community.

Phylum	Family	Genus	MPBR 1	MPBR 2	MPBR 3	MPBR 4	MPBR 5
Chlorophyta	*Trebouxiophyceae*	*Chlorella*	12 %	6 %	28 %	8 %	56 %
	Chlorophyceae	*Scenedesmus*	12 %	39 %	3 %	8 %	39 %
		Chaetophora	1 %	15 %		4 %	1 %
Cyanocbacteria	*Cyanophyceae*	*Oscillatoriales*	7 %		8 %	6 %	
	Microcoleaceae	*Microcoelus*				10 %	
Ochrophyta	*Bacillariaceae*	*Nitzschia*	17 %	9 %	13 %	16 %	1 %
	Naviculaceae	*Navicula*	50 %	32 %	49 %	49 %	4 %

the genus *Chaetophora* were observed, whose presence was significant in MPBR 2 and 4 conditions. This is in agreement with several studies that have reported effective growth of *Chaetophora* sp. in a mixed microalgae culture in an MPBR applied to secondary effluent treatment [9,12]. As stated, the cyanobacteria population was also representative of the mixed culture in several conditions (MPBR 1, 2 and 4), where species belonging to the order *Oscillatoriales* were observed.

4. Conclusions

Microalgal-bacterial membrane photobioreactors (MPBR) for secondary wastewater effluent treatment were investigated. For this purpose, the performance of a MPBR with indigenous microalgae-bacteria consortia was assessed under different SRT and HRT conditions. From this study, the following may be concluded:

- Due to the low C/N ratio in the secondary effluent, the MPBR showed better process performance than a conventional MBR. There was a substantial improvement in biomass productivity, nutrient removal and bioflocculation.
- Extending SRT to 80 d in the MPBR enhanced bioflocculation and effectively prevented biopolymer clusters (BPC) accumulation in the suspension. Despite influent fluctuations, optimal HRT value between 2 and 5 d was necessary to achieve moderate nutrient removal

(40.6–48.7 % and 18.5–34.7 % for nitrogen and phosphorus, respectively).
- Reversible fouling was mainly caused by the supernatant fraction of the suspension, particularly by the BPC content. Residual fouling was associated to a biocake development onto the membrane, which could be enhanced at large BPC concentration. Consequently, optimal filtration conditions were obtained at SRT of 80 d and HRT of 5 d.
- Indigenous growth of microalgae was successfully achieved in the MPBR under all tested conditions. Green microalgae belonging to the genera *Chorella* and *Scenedesmus* and diatoms *Nitzschia* and *Navicula* were identified at high abundance.

CRediT authorship contribution statement

E. Segredo-Morales: Investigation, Data curation, Writing – original draft. **E. González:** Conceptualization, Methodology, Visualization, Writing – review & editing. **C. González-Martín:** Data curation, Writing – review & editing. **L. Vera:** Conceptualization, Funding acquisition, Project administration, Supervision, Writing – review & editing.

Declaration of competing interest

The authors declare that they have no known competing financial

interests or personal relationships that could have appeared to influence the work reported in this paper.

Data availability

Data will be made available on request.

Acknowledgements

Appendix A. Supplementary data

Supplementary data to this article can be found online at https://doi.org/10.1016/j.jwpe.2022.103200.

References

[1] A. Fallahi, F. Rezvani, H. Asgharnejad, E. Khorshidi, N. Hajinajaf, B. Higgins, Interactions of microalgae-bacteria consortia for nutrient removal from wastewater: a review, Chemosphere 272 (2021), 129878, https://doi.org/10.1016/j.chemosphere.2021.129878.

[2] A. Morillas-España, T. Lafarga, A. Sánchez-Zurano, F.G. Acién-Fernández, C. González-López, Microalgae based wastewater treatment coupled to the production of high value agricultural products: current needs and challenges, Chemosphere 291 (2022), https://doi.org/10.1016/j.chemosphere.2021.132968.

[3] S.S. Chan, K.S. Khoo, K.W. Chew, T.C. Ling, P.L. Show, Recent advances biodegradation and biosorption of organic compounds from wastewater: microalgae-bacteria consortium - a review, Bioresour. Technol. 344 (2022), 126159, https://doi.org/10.1016/j.biortech.2021.126159.

[4] S. Li, Y. Chu, P. Xie, Y. Xie, H. Chang, S.H. Ho, Insights into the microalgae-bacteria consortia treating swine wastewater: symbiotic mechanism and resistance genes analysis, Bioresour. Technol. 349 (2022), 126892, https://doi.org/10.1016/j.biortech.2022.126892.

[5] C. Zhang, S. Li, S.H. Ho, Converting nitrogen and phosphorus wastewater into bioenergy using microalgae-bacteria consortia: a critical review, Bioresour. Technol. 342 (2021), 126056, https://doi.org/10.1016/j.biortech.2021.126056.

[6] S. Judd, L.J.P. van den Broeke, M. Shurair, Y. Kuti, H. Znad, Algal remediation of CO2 and nutrient discharges: a review, Water Res. 87 (2015) 356–366, https://doi.org/10.1016/j.watres.2015.08.021.

[7] A.L. Gonçalves, J.C.M. Pires, M. Simões, A review on the use of microalgal consortia for wastewater treatment, Algal Res. 24 (2017) 403–415, https://doi.org/10.1016/j.algal.2016.11.008.

[8] D. García, E. Posadas, S. Blanco, G. Acién, P. García-Encina, S. Bolado, R. Muñoz, Evaluation of the dynamics of microalgae population structure and process performance during piggery wastewater treatment in algal-bacterial photobioreactors, Bioresour. Technol. 248 (2018) 120–126, https://doi.org/10.1016/j.biortech.2017.06.079.

[9] A. Solmaz, M. Işık, Polishing the secondary effluent and biomass production by microalgae submerged membrane photo bioreactor, Sustain. Energy Technol. Assess. 34 (2019) 1–8, https://doi.org/10.1016/j.seta.2019.04.002.

[10] M. Zhang, L. Yao, E. Maleki, B.Q. Liao, H. Lin, Membrane technologies for microalgal cultivation and dewatering: recent progress and challenges, Algal Res. 44 (2019), 101686, https://doi.org/10.1016/j.algal.2019.101686.

[11] Y. Luo, P. Le-Clech, R.K. Henderson, Simultaneous microalgae cultivation and wastewater treatment in submerged membrane photobioreactors: a review, Algal Res. 24 (2017) 425–437, https://doi.org/10.1016/j.algal.2016.10.026.

[12] A. Solmaz, M. Işık, Optimization of membrane photobioreactor; the effect of hydraulic retention time on biomass production and nutrient removal by mixed microalgae culture, Biomass Bioenergy 142 (2020), https://doi.org/10.1016/j.biombioe.2020.105809.

[13] J. González-Camejo, A. Jiménez-Benítez, M.V. Ruano, A. Robles, R. Barat, J. Ferrer, Optimising an outdoor membrane photobioreactor for tertiary sewage treatment, J. Environ. Manag. 245 (2019) 76–85, https://doi.org/10.1016/j.jenvman.2019.05.010.

[14] A.L.K. Sheng, M.R. Bilad, N.B. Osman, N. Arahman, Sequencing batch membrane photobioreactor for real secondary effluent polishing using native microalgae: process performance and full-scale projection, J. Clean. Prod. 168 (2017) 708–715, https://doi.org/10.1016/j.jclepro.2017.09.083.

[15] P. Praveen, Y. Guo, H. Kang, C. Lefebvre, K.C. Loh, Enhancing microalgae cultivation in anaerobic digestate through nitrification, Chem. Eng. J. 354 (2018) 905–912, https://doi.org/10.1016/j.cej.2018.08.099.

[16] Y. Zhang, Q. Fu, Algal fouling of microfiltration and ultrafiltration membranes and control strategies: a review, Sep. Purif. Technol. 203 (2018) 193–208, https://doi.org/10.1016/j.seppur.2018.04.040.

[17] Y. Liao, A. Bokhary, E. Maleki, B. Liao, A review of membrane fouling and its control in algal-related membrane processes, Bioresour. Technol. 264 (2018) 343–358, https://doi.org/10.1016/j.biortech.2018.06.102.

[18] A.F. Novoa, L. Fortunato, Z.U. Rehman, T.O. Leiknes, Evaluating the effect of hydraulic retention time on fouling development and biomass characteristics in an algal membrane photobioreactor treating a secondary wastewater effluent, Bioresour. Technol. 309 (2020), 123348, https://doi.org/10.1016/j.biortech.2020.123348.

[19] S.L. Low, S.L. Ong, H.Y. Ng, Characterization of membrane fouling in submerged ceramic membrane photobioreactors fed with effluent from membrane bioreactors, Chem. Eng. J. 290 (2016) 91–102, https://doi.org/10.1016/j.cej.2016.01.005.

[20] S.-N. Li, C. Zhang, F. Li, N.-Q. Ren, S.-H. Ho, Recent advances of algae-bacteria consortia in aquatic remediation, Crit. Rev. Environ. Sci. Technol. (2022), https://doi.org/10.1080/10643389.2022.2052704.

[21] M. Zhang, K.T. Leung, H. Lin, B. Liao, Effects of solids retention time on the biological performance of a novel microalgal-bacterial membrane photobioreactor for industrial wastewater treatment, J. Environ. Chem. Eng. 9 (2021), 105500, https://doi.org/10.1016/j.jece.2021.105500.

[22] O. Díaz, L. Vera, E. González, E. García, J. Rodríguez-Sevilla, Effect of sludge characteristics on membrane fouling during start-up of a tertiary submerged membrane bioreactor, Environ. Sci. Pollut. Res. 23 (2016) 8951–8962, https://doi.org/10.1007/s11356-016-6138-y.

[23] E. González, O. Díaz, E. Segredo-Morales, L.E. Rodríguez-Gómez, L. Vera, Enhancement of peak flux capacity in membrane bioreactors for wastewater reuse by controlling the backwashing strategy, Ind. Eng. Chem. Res. 58 (2019) 1373–1381, https://doi.org/10.1021/acs.iecr.8b05650.

[24] L. Vera, E. González, O. Díaz, R. Sánchez, R. Bohorque, J. Rodríguez-Sevilla, Fouling analysis of a tertiary submerged membrane bioreactor operated in dead-end mode at high-fluxes, J. Membr. Sci. 493 (2015) 8–18, https://doi.org/10.1016/j.memsci.2015.06.014.

[25] APHA, Standard Methods for the Examination of Water and Wastewater, 21st ed., 2005. Washington, DC, USA.

[26] S.G. Berk, J.H. Gunderson, Wastewater Organisms a Color Atlas, 1st Edition, CRC Press, Florida, USA, 1993.

[27] A. Pollice, G. Laera, D. Saturno, C. Giordano, Effects of sludge retention time on the performance of a membrane bioreactor treating municipal sewage, J. Membr. Sci. 317 (2008) 65–70, https://doi.org/10.1016/j.memsci.2007.08.051.

[28] G. Padmaperuma, R.V. Kapoore, D.J. Gilmour, S. Vaidyanathan, Microbial consortia: a critical look at microalgae co-cultures for enhanced biomanufacturing, Crit. Rev. Biotechnol. 38 (2018) 690–703, https://doi.org/10.1080/07388551.2017.1390728.

[29] Y. Luo, P. Le-Clech, R.K. Henderson, Assessment of membrane photobioreactor (MPBR) performance parameters and operating conditions, Water Res. 138 (2018) 169–180, https://doi.org/10.1016/j.watres.2018.03.050.

[30] A. Viruela, Á. Robles, F. Durán, M.V. Ruano, R. Barat, J. Ferrer, A. Seco, Performance of an outdoor membrane photobioreactor for resource recovery from anaerobically treated sewage, J. Clean. Prod. 178 (2018) 665–674, https://doi.org/10.1016/j.jclepro.2017.12.223.

[31] M. Xu, P. Li, T. Tang, Z. Hu, Roles of SRT and HRT of an algal membrane bioreactor system with a tanks-in-series configuration for secondary wastewater effluent polishing, Ecol. Eng. 85 (2015) 257–264, https://doi.org/10.1016/j.ecoleng.2015.09.064.

[32] Q.V. Bach, W.H. Chen, Pyrolysis characteristics and kinetics of microalgae via thermogravimetric analysis (TGA): a state-of-the-art review, Bioresour. Technol. 246 (2017) 88–100, https://doi.org/10.1016/j.biortech.2017.06.087.

[33] A. Soria-Verdugo, E. Goos, N. García-Hernando, U. Riedel, Analyzing the pyrolysis kinetics of several microalgae species by various differential and integral isoconversional kinetic methods and the distributed activation energy model, Algal Res. 32 (2018) 11–29, https://doi.org/10.1016/j.algal.2018.03.005.

[34] R.B. Carpio, Y. Zhang, C.T. Kuo, W.T. Chen, L.C. Schideman, R.L. de Leon, Characterization and thermal decomposition of demineralized wastewater algae biomass, Algal Res. 38 (2019), 101399, https://doi.org/10.1016/j.algal.2018.101399.

[35] D.Y. Duygu, A.U. Udoh, T. Ozer, A. Akbulut, I. Erkaya, K. Yildz, D. Guler, Fourier transform infrared (FTIR) spectroscopy for identification of Chlorella vulgaris Beijerinck 1890 and Scenedesmus obliquus (Turpin) Kützing 1833, African J. Biotechnol. 11 (2012) 3817–3824, https://doi.org/10.5897/ajb11.1863.

[36] A.P. Dean, M.C. Martin, D.C. Sigee, Resolution of codominant phytoplankton species in a eutrophic lake using synchrotron-based fourier transform infrared spectroscopy, Phycologia 46 (2007) 151–159, https://doi.org/10.2216/06-27.1.

[37] M. Arif, Y. Li, M.M. El-Dalatony, C. Zhang, X. Li, E.S. Salama, A complete characterization of microalgal biomass through FTIR/TGA/CHNS analysis: an approach for biofuel generation and nutrients removal, Renew. Energy 163 (2021) 1973–1982, https://doi.org/10.1016/j.renene.2020.10.066.

[38] Y. Liu, S. Chang, F.M. Defersha, Characterization of the proton binding sites of extracellular polymeric substances in an anaerobic membrane bioreactor, Water Res. 78 (2015) 133–143, https://doi.org/10.1016/j.watres.2015.04.007.

[39] R. Whitton, F. Ometto, M. Pidou, P. Jarvis, R. Villa, B. Jefferson, Microalgae for municipal wastewater nutrient remediation: mechanisms, reactors and outlook for

tertiary treatment, Environ.Technol. Rev. 4 (2015) 133–148, https://doi.org/10.1080/21622515.2015.1105308.

[40] Commission Directive 98/15/EC, Commission Directive 98/15/EC of 27 February 1998 Amending Council Directive 91/271/EEC, OJ L 67 29, 1998.

[41] M.C. Martí-Calatayud, S. Schneider, S. Yüce, M. Wessling, Interplay between physical cleaning, membrane pore size and fluid rheology during the evolution of fouling in membrane bioreactors, Water Res. 147 (2018) 393–402, https://doi.org/10.1016/j.watres.2018.10.017.

[42] A. Drews, Membrane fouling in membrane bioreactors-characterisation, contradictions, cause and cures, J. Membr. Sci. 363 (2010) 1–28, https://doi.org/10.1016/j.memsci.2010.06.046.

[43] L.J. Zeman, A.L. Zydney, Microfiltration and Ultrafiltration: Principles and Applications, 1st Editio, Marcel Dekker, New York, 1996, https://doi.org/10.1201/9780203747223.

[44] Seong-Hoon Yoon, Membrane Bioreactor Processes Principles and Applications, 1st Edition, CRC Press, New York, 2016.

[45] E. Poorasgari, T.V. Bugge, M.L. Christensen, M.K. Jørgensen, Compressibility of fouling layers in membrane bioreactors, J. Membr. Sci. 475 (2015) 65–70, https://doi.org/10.1016/j.memsci.2014.09.056.

[46] P. van der Marel, A. Zwijnenburg, A. Kemperman, M. Wessling, H. Temmink, W. van der Meer, An improved flux-step method to determine the critical flux and the critical flux for irreversibility in a membrane bioreactor, J. Membr. Sci. 332 (2009) 24–29, https://doi.org/10.1016/j.memsci.2009.01.046.

[47] J. Luo, J. Zhang, X. Tan, D. McDougald, G. Zhuang, A.G. Fane, S. Kjelleberg, Y. Cohen, S.A. Rice, The correlation between biofilm biopolymer composition and membrane fouling in submerged membrane bioreactors, Biofouling 30 (2014) 1093–1110, https://doi.org/10.1080/08927014.2014.971238.

PAPER

Check for updates

Evaluation of membrane fouling in a microalgal-bacterial membrane photobioreactor treating secondary wastewater effluent: effect of photoperiod conditions

E. Segredo-Morales, [ID] [a] E. González, [ID] *[a] C. González-Martín[b] and L. Vera [ID] [a]

Microalgal-bacterial membrane photobioreactors (MPBRs) have emerged as a transformative wastewater treatment technology for reducing carbon emissions whilst achieving high quality effluent. However, membrane fouling negatively affects process performance by increasing energy consumption and reducing membrane lifespan. In this study, light/dark photoperiods were varied to optimize treatment performance and biomass properties and reduce membrane fouling. Increasing the length of the light period favored higher production of biomass but decreased bioflocculation. An intermediate photoperiod of 16/8 h achieved high values of biomass concentration (3.21 ± 0.45 g L^{-1}) and nutrient removal rates (4.71 mg N L^{-1} d^{-1} and 0.67 mg P L^{-1} d^{-1}, respectively), while preventing accumulation of biopolymer clusters (≤ 5.5 mg DOC L^{-1}) in the suspension. In addition, short-term fouling—associated with floc deposition forming a cake layer—was minimized at intermediate photoperiods, thus increasing the sustainable (*i.e.*, threshold) permeate flux. Under these sustainable flux conditions, membrane fouling was mainly determined by the biopolymer cluster content, with best performance being attained at 16/8 h. The above results reveal that the photoperiod is a crucial parameter for controlling membrane fouling in microalgal-bacterial membrane photobioreactors.

Water impact

The microalgal-bacterial membrane photobioreactor is a promising approach for sustainable wastewater reclamation. However, its widespread application is limited by the high costs associated with membrane fouling. Due to complex interactions among indigenous consortia, selecting optimal conditions is challenging. This study demonstrated that long-term fouling is minimized at intermediate light/dark photoperiods, which also allows high biomass concentration and effective nutrient removal.

1. Introduction

Progressive decarbonization is prompting the wastewater treatment sector to search for transformative technologies that can increase energy efficiency, recover resources and prevent greenhouse gases emissions.[1,2] Recently, novel treatment technologies, such as photocatalysis,[3] microwave catalysis[4,5] or zero-valent iron nanoparticles[6] have been proposed. Nevertheless, although these are promising technologies, there are several disadvantages that have to be addressed to ensure their safe and effective use in wastewater

treatment. Further investigation on catalysis deactivation, safety hazards due to microwave radiation or release of nanoparticles into the environment, is needed before practical use. Alternatively, a photobioreactor system based on microalgae-bacteria consortia is a promising approach to achieve sustainable wastewater technologies.[7–9] In a symbiotic relationship, microalgae produce dissolved oxygen, which can be used for bacterial respiration (oxidizing organic matter, ammonium and nitrite), reducing operating costs resulting from mechanical aeration. In turn, the carbon dioxide generated is used by the microalgae for carbon anabolism. Additionally, microalgae-bacteria consortia recover nutrients from wastewater through biomass synthesis. Produced biomass can be further valorized into added-value products, such as biogas or agricultural products.[10,11] Likewise, the move to a circular economy needs to be accomplished through the consistent promotion of safe

[a] Departamento de Ingeniería Química y Tecnología Farmacéutica, Universidad de La Laguna, Astrofísico, Fco, Sánchez s/n, 38200 La Laguna, Spain.
E-mail: esegredm@ull.edu.es, eglezc@ull.edu.es, luvera@ull.edu.es
[b] Instituto Universitario de Enfermedades Tropicales y Salud Pública de Canarias, Universidad de La Laguna, Astrofísico, Fco, Sánchez s/n, 38200 La Laguna, Spain.
E-mail: cgonzama@ull.edu.es

Paper

water re-use.[12] Current advanced systems combine biological treatment with microfiltration or ultrafiltration membranes to produce high-quality effluents that are suitable for most industrial applications, including highly demanding agriculture irrigation.[13,14]

A technology now actively being investigated is a microalgal-bacterial membrane photobioreactor (MPBR), which combines suspended biomass with immersed microfiltration or ultrafiltration membranes.[15,16] This technology has demonstrated the capability to efficiently treat municipal wastewaters[17] or secondary effluents.[18,19] Hydraulic and solid retention times (HRT and SRT, respectively) are commonly studied parameters, mainly focused on nutrient removal and biomass productivity.[15,20] Another important factor affecting microalgal-bacterial processes is light availability, mainly determined by light intensity and photoperiods.[21,22] Typically, microalgae activity increases with light intensity up to a saturation point ($\sim$200–540 μmol m^{-2} s^{-1}), which is species dependent, above which the effect becomes insignificant.[23] Indeed, in many species, increasing intensity results in photoinhibition thus reducing microalgae growth rate.[24] A similar behavior has been reported for nitrifying bacteria, particularly nitrite oxidizers, which show significant photoinhibition above 500 μmol m^{-2} s^{-1}.[25] Nevertheless, several strategies can be applied to control light intensity by modifying reactor design (*i.e.* culture depth) or biomass concentration (affecting light shading effect).[8] Regarding the photoperiod, microalgae growth rate is generally enhanced by extending the light period from 12/12 to 24/0 h (continuous illumination),[26,27] but several studies have reported no appreciable effect[28] or even a decrease in the growth rate.[29] These contradictory findings suggest that photoperiod, light intensity and light shading may be interrelated.

A critical constraint of MBPR technology development at an industrial scale is the inherent membrane fouling.[30,31] In general, the extent of fouling is a complex function of biomass characteristics, operating conditions and membrane properties.[20] To alleviate membrane fouling, common practices in MPBRs are the use of moderate permeate fluxes, membrane air scouring, physical cleaning methods (relaxation and backwashing) and chemical cleanings.[19,32] Fouling can be classified into two main categories based on membrane permeability recovery by physical methods. The first is reversible fouling, which can be removed by physical means and is mainly attributed to cake layer development and possibly to pore blocking. The second category is residual fouling (also called physically irreversible fouling), which mainly refers to adsorption of foulants and gel formation, and is only removed by chemical means.[33] These phenomena lead to a loss in membrane permeability, higher energy consumption and more frequent chemical cleanings, which can reduce the membrane's lifespan.[34] Most previous studies assessing membrane fouling in MPBR have focused on biomass characteristics, particularly biomass concentration, particle size distribution and supernatant

biopolymers content.[30,35–39] Main influencing factors assessed in these studies are hydraulic and solid retention times, feedwater characteristics (nitrogen source and ratio of N/P) and alga/activated sludge inoculation ratios. Nevertheless, although light is a key parameter in microalgae-bacteria consortia growth and biomass properties, it has been less studied. In fact, a previous study revealed a trade-off between biomass productivity/nutrient removal and membrane fouling.[40] In this work it is reported that reducing the light path in a photobioreactor (*i.e.* increasing photosynthetic efficiency) significantly increases the membrane fouling rate. Therefore, finding optimal illumination conditions (intensity and/or photoperiod) would considerably improve operational feasibility and reduce the cost of MPBR technology.

This study focuses on assessing the effect of the photoperiod on the performance of a MPBR, particularly on membrane fouling. The assessment was conducted by analyzing treatment performance and main biomass properties, such as concentration, elemental composition, particle size distribution and supernatant biopolymers content. Using a flux-step method, fouling propensity and sustainable flux conditions were investigated. Finally, long-term fouling tests verified sustainable membrane performance by assessing residual fouling evolution.

2. Materials and methods.

2.1. Feedwater

The MPBR unit was fed with a secondary effluent obtained from a conventional activated sludge wastewater treatment plant (Santa Cruz de Tenerife, Canary Island, Spain), which was designed for organic matter removal. Main physical–chemical characteristics are given in Table 1.

2.2. MPBR set-up

The experimental unit consisted of a cylindrical 3.0 L (diameter = 14 cm) MPBR equipped with ZeeWeed® ZW-1 (Suez Water Technologies & Solutions, Ontario, ON, Canada) hollow fiber membranes with a nominal pore size of 0.04 μm and 1.9 mm outer diameter, assembled vertically, which provide 0.047 m^2 of filtering surface area (Fig. 1). ZeeWeed® consists of a woven reinforcing braid on which a PVDF

Table 1 Main physical–chemical characteristics of the feedwater ($n = 55$)

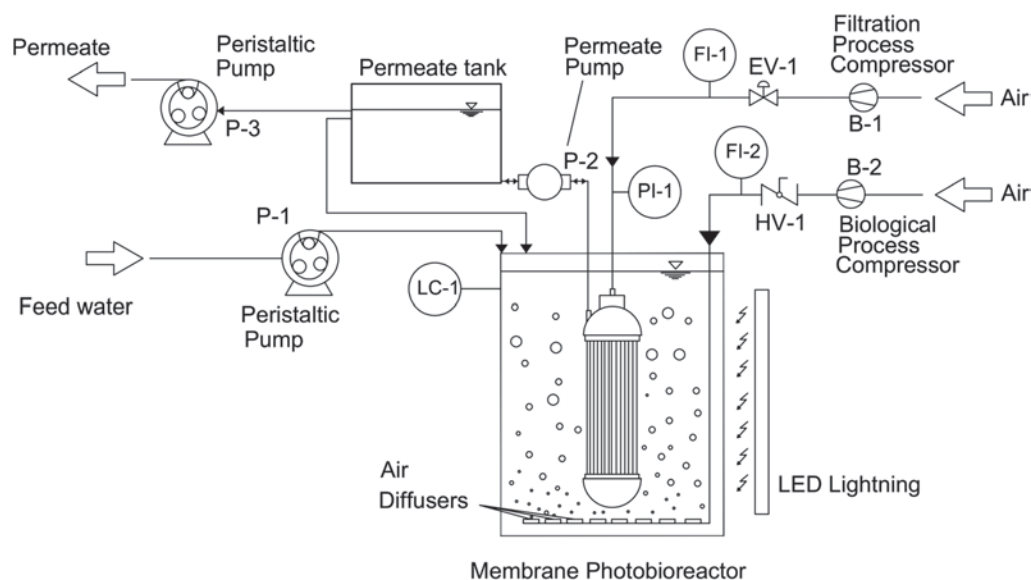| Parameters	Units	Mean	Range
COD	mg L^{-1}	67.2	39–113
DOC	mg L^{-1}	17.9	12.7–45.7
pH	—	8.2	7.9–8.4
N–NH$_4^+$	mg L^{-1}	25.8	2.5–41.9
N–NO$_3^-$	mg L^{-1}	2.0	0–12.9
N–NO$_2^-$	mg L^{-1}	1.7	0–9.5
P–PO$_4^{3-}$	mg L^{-1}	4.1	0.8–7.9
CO$_3^{2-}$	mg L^{-1}	8.5	0–21.6
HCO$_3^-$	mg L^{-1}	552.6	414.0–698.7
Turbidity	NTU	2.0	1.1–5.0
TSS	mg L^{-1}	4.5	0–22

Fig. 1 Schematic diagram of the MPBR system.

membrane is cast. The permeate was extracted by a magnetic drive gear pump (Micropump-GA Series, Stockholm, Sweden) applying a slight vacuum. All the experiments were conducted at a permeate flux (J) of 10 L h^{-1} m^{-2}, measuring transmembrane pressure (TMP) with a pressure sensor (Sensotec, Barcelona, Spain). To prevent severe membrane fouling, the system operated under consecutive filtration/backwashing cycles of 450/30 s combined with intermittent air scouring (10/30 s on/off) at 5 NL min^{-1} during the filtration. The backwash flux was set at 30 L h^{-1} m^{-2} with continuous aeration at 5 NL min^{-1}. DAQ Factory software (AzeoTech® Inc., Ashland, OR, USA) was used for visualization and control of the filtration variables.

Air was also injected at the bottom of the MPBR at 1 NL min^{-1} to provide aerobic conditions and mix the biological suspension. Dissolved oxygen concentration and pH were within the ranges of 6.9–9.6 mg L^{-1} and 8.1–8.9, respectively, throughout all experiments. The system was run at HRT and SRT values of 0.75 d and 80 d, respectively. The former was within the typical range of operating values in MPBRs[41] and the latter was selected according to a previous study on enhancing bioflocculation and avoiding biopolymer cluster accumulation.[42] The effluent was extracted from the permeate tank by a peristaltic pump (Cole-Parmer Instrument Co., USA) according to the selected HRT. To maintain a constant HRT regardless of permeate flux, excess permeate was returned to the MPBR. Experiments were carried out at room temperature (19 ± 1 °C) under constant irradiation of 300 μmol m^{-2} s^{-1} measured at the surface of the photobioreactor (PAR irradiance using an irradiance meter, QSP2150A, Biospherical Instruments Inc., USA). The aim of the experiments was to assess the impact of photoperiods on

the MPBR performance. To do this, four long-term experiments of 900 h were carried out under different light/dark photoperiods (0/24, 12/12, 16/8 and 24/0 h).

Before starting each experiment, the system was initially filled only with feedwater. Then, it was operated at 0.75 d of HRT for a minimum of 80 d without biomass purge. Thus, the system started without inoculum and the biomass developed from indigenous microorganisms. After the acclimation period, the biomass was manually purged to maintain the desired SRT. This procedure allowed the biomass concentration to remain stable during the experiments.

Samples of feedwater, suspension and permeate were analyzed three times per week. Suspensions were characterized by particles size, mixed liquor suspended solids (MLSS), volatile matter, elemental composition (C, N and H), supernatant dissolved organic carbon (DOC) and suspended solids (SS), and Fourier-transform infrared spectroscopy (FTIR). The average biomass productivity (r_x) was estimated following eqn (1):

$$r_x = \frac{MLSS}{SRT} \tag{1}$$

2.3. Short-term flux step trials

A flux-step method with intermediate backwashing cycles was applied.[43] Main parameters were: flux range of 8–40 L h^{-1} m^{-2}, flux increment of 2 L h^{-1} m^{-2} and step duration of 15 min. Air scouring and backwashing conditions were the same as those applied in the long-term experiments. The flux-step trials were carried out with the suspensions and supernatants (obtained after 30 min of decantation and transferred into a clean vessel). Before each run, the membrane was chemically

cleaned using a 500 mg L^{-1} of NaClO for 24 h. Reversible fouling was assessed by the fouling rate (r_f), given by the change in transmembrane pressure with time (dTMP/dt).

2.4. Membrane cleaning protocol

After the long-term fouling tests, the fouled membrane was subjected to a cleaning protocol that included the following steps:[44] (1) rinsing with tap water, (2) chemical cleaning with NaClO (500 mg L^{-1}) for 24 h, and (3) chemical cleaning with citric acid (6 g L^{-1}) for 2 h. After each step, the hydraulic resistance was calculated using a tap water filtration test.

2.5. Membrane fouling characterization

During the long-term tests, TMP evolution with consecutive filtration/backwashing was used to assess membrane fouling. It can be described by the following equation:[43]

$$TMP = TMP_i + r_f \cdot t \tag{2}$$

where TMP_i is the initial transmembrane pressure at the beginning of each filtration cycle, r_f is the reversible fouling rate and t is the elapsed time.

Eqn (2) assumes a constant r_f during the filtration phases, describing an incompressible cake development mechanism on the membrane wall. On the other hand, TMP_i is related to residual fouling, which cannot be removed by physical means. Both parameters have been widely used to describe membrane fouling in conventional membrane bioreactors (MBRs).[33]

2.6. Analytical methods

Dissolved oxygen was measured using an oximeter Hach Lange LDO (USA). Total suspended solids (TSS), mixed liquor suspended solids (MLSS) and chemical oxygen demand (COD) were analyzed according to the standard methods.[45] Nitrogen–ammonium (N–NH$_4^+$) was analyzed by the Nessler method using a DR-5000 Hach spectrophotometer (USA). Nitrogen–nitrite (N–NO$_2^-$), nitrogen–nitrate (N–NO$_3^-$) and phosphorus–phosphate (P–PO$_4^{3-}$) were analyzed by ion chromatography using a Compact IC plus 882 device, supplied by Metrohm. Total dissolved inorganic nitrogen (DIN) was obtained by adding N–NH$_4^+$, N–NO$_2^-$ and N–NO$_3^-$. Dissolved organic carbon (DOC) concentration was measured with a TOC-meter (TOC-5000A, Shimadzu, Japan). The DOC difference between the filtered supernatant (through a filter of glass-fiber with a nominal pore size of 1.2 μm) and the permeate was assigned as biopolymers clusters (BPC) concentration. Particle size distribution was analyzed using Malvern Mastersizer 2000 (UK) laser diffraction particle size analyzer with a detection range of 0.02–2000 μm. FLASH EA 1112 Elemental Analyzer (ThermoFisher Scientific, USA) was used for the elemental analysis. Samples were previously dried in an oven at 100 °C for 1 h. Volatile matter was measured by a thermal analyzer (TG/DSC): Discovery SDT 650 (TA Instruments, USA). Fourier-transform infrared

spectrometry was performed using an IFS 66/S spectrometer (Bruker, USA) equipped with an ATR accessory that measured the transmittance of the samples in a wavelength range between 900 and 4000 cm^{-1}. Microalgae identification was conducted by optical microscopy (DM750, Leica, Germany) according to Wastewater Organisms Atlas Manual.[46] Detection of *Escherichia coli* and *Legionella* spp. was performed in the permeate according to ISO 9308 and ISO 11731, respectively, as recommended by the legislation.

2.7. Statistical analysis

The results were analyzed by OriginPro (OriginLab Corporation, MA, USA). Analysis of variance (one-way ANOVA) and Tukey's test was used to assess differences between photoperiods. Significance was assumed when p-values <0.05.

3. Results and discussion.

3.1. Biomass productivity and characteristics

As shown in Fig. 2a, longer lighting periods significantly influenced biomass concentration and productivity. Maximum biomass concentration (3.21 ± 0.45 g L^{-1}) was obtained at 16/8 h photoperiod (light/dark), which did not increase at continuous illumination ($p > 0.05$). Compared to operation at 0/24 h (control condition), the results revealed a significant growth of microalgae in the mixed consortia (representing approximately a 30-fold increase), which achieved a productivity value of 40.1 mg L^{-1} d^{-1}. Indeed, microalgae belonging to the genera *Scenedesmus* and *Chorella* were identified in abundance. This is consistent with those productivities usually reported for MBPRs operated at long SRTs with secondary effluents (28–41 mg L^{-1} d^{-1}).[22] Nevertheless, the fact that productivity did not increase by extending the photoperiod from 16/8 h to continuous illumination seems to contradict previous results obtained in photo sequencing batch reactors.[27,47] Probably, this behavior can be attributed to an interplay between light penetration and biomass concentration, which may have a relevant role in MPBRs at long SRTs.[48] Therefore, results suggest that it may be difficult to increase biomass concentration up to 3.0–3.5 g L^{-1} due to self-shading effect, as previously reported in MPBR studies.[49,50]

As the nature of the biomass varies with the microbial community, volatile matter and elemental composition were analyzed at the different photoperiods (Fig. 2b). Volatile fraction increased from 25.9 to 37.3% when extending the lighting period from the control condition (0/24 h) to the 16/8 h photoperiod. Again, no further increment was obtained with the continuous illumination ($p > 0.05$). This volatile content was mainly attributed to microalgae growth, where CO$_2$ fixation was expected due to photosynthetic activity. Indeed, consistent C/N mass ratios (5.0–5.4) for microalgae biomass[51] were only detected for the MPBR under lighting conditions (Fig. 2c). Nevertheless, it should be noted that no significant variations were observed in the C/N ratios for the
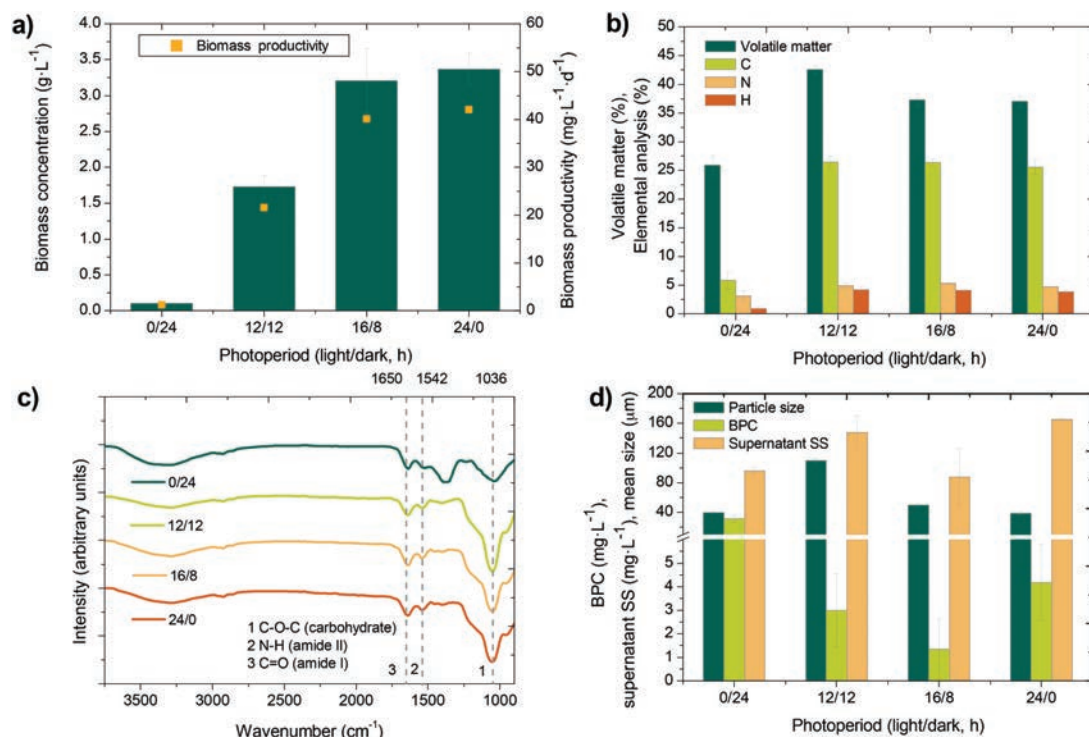
Fig. 2 Effect of the photoperiod on biomass concentration and productivity ($n = 15$) (a), volatile matter and elemental analysis ($n = 3$) (b), FTIR spectra ($n = 3$) (c), and BPC ($n = 15$), supernatant suspended solids (SS) ($n = 3$) and mean particle size ($n = 3$) (d). Elemental analysis data are provided as % wt and dry basis.

different photoperiods, so this parameter could not be related to the ratio of microalgae to bacteria in the biomass. In contrast, the low ratio at 0/24 h can be attributed to low organic carbon in the feedwater (Table 1). Moreover, the ratios of the intensity of the peak assigned to carbohydrate (C–O–C) bonds to the intensity of the specific peaks assigned to proteins (N–H and C=O) in the Fourier transform infrared (FTIR) spectra were probably a result of a higher carbohydrate-to-protein ratio for the MPBR at lighting conditions (Fig. 2c), consistent with the result of the elemental analysis. As reported in the literature, carbohydrates and proteins are major components of the bound extracellular polymeric substances (EPS), which are key in bioflocculation.[8] Since carbohydrate facilitate cell adhesion,[52] a consistent carbohydrate-to-protein ratio can be related to efficient flocculation. This is in accordance with the higher mean particle size obtained in the MPBR under lighting conditions (Fig. 2d). Apparently, microalgal-bacterial consortia enhanced the formation of larger flocs, which agrees with previous studies.[36] However, mean floc size decreased from 104.9 to 38.9 μm while extending the lighting period from 12/12 h to continuous illumination. Particle size distribution has been attributed to microalgae/bacteria proportion, where partial inhibition of microalgae growth

results in larger flocs.[31] In this study, results showed smaller flocs at continuous illumination, which can be justified by the increased microalgae growth (reflected by the higher biomass concentration) associated with the extension of the lighting period.

Due to the biological activity in the MPBR, hydrolysis of EPS and decay products generate soluble microbial products (SMP) and biopolymer clusters (BPC).[53] Due to their larger size, BPC were retained by the membrane and can lead to severe membrane fouling.[38] It was observed that the photoperiod had a significant impact on BPC content (Fig. 2d). Under the control condition, BPC accumulated the most significantly (31.1 ± 6.6 mg L^{-1}), which can be related to the low biomass concentration due to carbon-limited conditions imposed (*i.e.* low influent COD and long HRT). A previous study has demonstrated that endogenous conditions may induce cells lysis and biopolymer release in a MBR fed with a secondary effluent.[54] By contrast, very low BPC contents were found in the MPBR, which achieved a minimum at 16/8 h photoperiod ($p < 0.05$). This is probably due to favorable growth conditions for the microalgal-bacterial consortia, where cells lysis and biopolymers release were minimized. In addition, due to a probable higher abundance of heterotrophic bacteria (see section 3.2),

biopolymers are expected to be degraded into smaller compounds.[38] A similar trend was also observed for supernatant suspended solids, which decreased at the 16/8 h photoperiod ($p < 0.05$).

3.2. Treatment performance

In order to assess treatment performance, feedwater and permeate concentration of dissolved organic carbon (DOC), nitrogen–ammonium (N–NH$_4^+$), total dissolved inorganic nitrogen (DIN) and phosphorus–phosphate (P–PO$_4^{3-}$) were analyzed. Inherent parameter fluctuation in feedwater can be observed, which was particularly evident in the low nitrogen content at 12/12 h photoperiod run (Fig. 3b). As showed in Fig. 3a, DOC removal was significantly increased (approximately 9-fold increase) in the MPBR under lighting conditions, suggesting significant activity of heterotrophic bacteria in the mixed consortia. As stated, this affects process performance positively by decreasing BPC content. In addition, significant DOC permeate concentration has a negative effect on subsequent processes, such as disinfection byproducts.[55]

The ammonium in feedwater varied between 23.0 and 6.3 mg L^{-1} for the different conditions (Fig. 3b). A complete

nitrification was achieved in all cases, obtaining a nitrogen–ammonium content in the permeate below 0.7 mg L^{-1}, where DIN in the permeate was mainly in form of nitrate (>96%), revealing the presence of nitrifying bacteria. In addition, DIN removal significantly increased from 3.5% to 18.1% with increasing photoperiods from control condition (0/24 h) to 16/8 h ($p < 0.05$) (Fig. 3c). However, no further improvement was observed at continuous illumination ($p > 0.05$). At 16/8 h, the average removal rate was 4.71 mg N L^{-1} d^{-1}, consistent with previous studies with similar biomass productivities.[56,57] Since pH was always maintained at similar values (8.1–8.9) under all conditions, the observed increment of nutrient removal was mainly associated with biomass assimilation. As recently reviewed,[58] feedwater ammonium leads to microalgae-nitrifying bacteria competition, which negatively affects nitrogen removal rate. To overcome this issue, operation at short to moderate SRTs has been proposed.[16,37] Nevertheless, a lower SRT would lead to significantly lower biomass concentration and thus increase harvest costs.[8] In addition, long SRTs can decrease BPC and therefore, minimize membrane fouling.[42]

The phosphate concentration in the feedwater and the permeate are showed in Fig. 3d. A similar trend as that
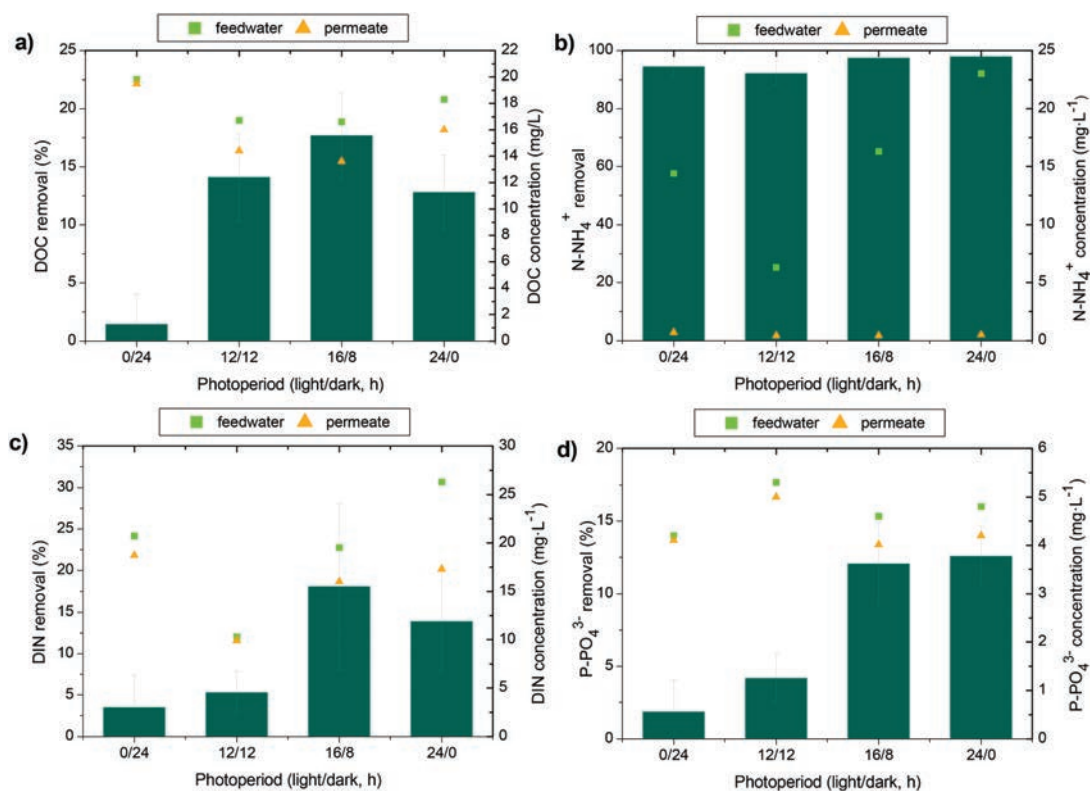

Fig. 3 Influence of the photoperiod on the removal of DOC (a), N–NH$_4^+$ (b), DIN (c) and P–PO$_4^{3-}$ (d). Error bars represent the standard deviation (n = 15).

observed for nitrogen removal was found, where photoperiod increased the phosphate removal. A maximum value of 12.1% was obtained for 16/8 h photoperiod, which did not significantly increase at continuous illumination ($p > 0.05$). This can be attributed to a higher biomass productivity when compared with the control condition or the 12/12 h photoperiod. The calculated phosphate removal rate was 0.67 mg L^{-1} d^{-1}, comparable with those reported in previous studies.[48,57]

Finally, it is important to note that the membrane provided a high quality effluent in terms of microbial (absence of *E. coli* and *Legionella* spp.) and physical (turbidity <0.5 NTU) parameters, which complied with the new European regulation of minimum requirements for the use of reclaimed water quality for agricultural irrigation.[59]

In summary, results demonstrate consistent organic matter and nutrient removal rates in MPBR under lighting conditions. Removal rates were influenced by the photoperiod, where maximum values were obtained at 16/8 h, mainly due to greater biomass productivity. No further improvement was attained at continuous illumination, probably due to self-shading caused by the high biomass concentration at long SRTs. Therefore, future work should focus on improving MPBR design to optimize light utilization by reducing culture depth and allow biomass productivities

and nutrient removal rates comparable to those obtained at short SRTs.

3.3. Membrane fouling

3.3.1. Reversible fouling characterization: flux step experiments. The effect of the photoperiod on fouling propensity was investigated by conducting the flux-step method,[43] using the reversible fouling rate ($r_f = $ dTMP/dt) as the fouling parameter (Fig. 4). It should be noted that applying lab-scale results to full-scale plant operation may be limited due to certain differences in hydrodynamics.[60] Nevertheless, despite these limitations, lab-scale experiments are useful for elucidating fouling propensity for the different conditions tested, mainly based on the effect of different light/dark photoperiods on biomass properties and biopolymer accumulation. Given the importance of dispersed cells and BPC in the fouling process,[61] the results were compared, under the same experimental conditions, with those obtained while filtering the non-settleable fraction of the suspension. It should be noted that there was no appreciable sedimentation in the control suspension, therefore fractionation could not be carried out. In all cases, an exponential relationship was observed, in accordance with most studies of fouling rate trends in MBRs.[62,63] Therefore, a
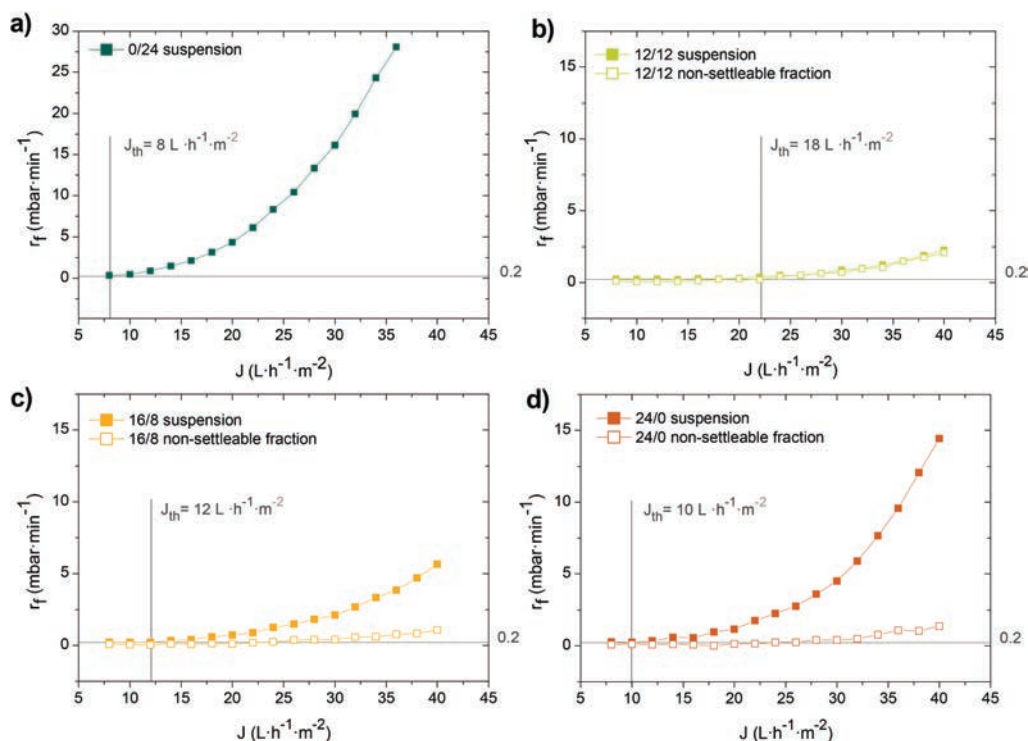

Fig. 4 Fouling characterization by flux stepping experiments. Reversible fouling rate (r_f) of the suspension and non-settleable fraction against permeate flux (J) for the different photoperiods: a) 0/24 h; b) 12/12 h; c) 16/8 h and d) 24/0 h. Threshold fluxes (J_{th}) are determined at each condition.

threshold flux (J_{th}) that separates low and high fouling regions can be identified.[64] A reference value for the fouling rate of 0.2 mbar min^{-1} was assumed which is within the typical range (0.1–1 mbar min^{-1}) reported for reversible fouling rates occurring in full-scale MBRs.[33] Results did not show a linear correlation between the photoperiod and J_{th}, which varied within the range of 8–18 L h^{-1} m^{-2}. Such variation can be explained by the different suspension characteristics. Many previous studies have emphasized the importance of biomass concentration, supernatant biopolymers content and floc size distribution on fouling propensity in MPBRs.[30,35–37,65] Consistently, the lower J_{th} obtained for the control condition (0/24 h) may be attributed to significant BPC accumulation (Fig. 2d). Under lighting conditions, due to lower BPC content, the non-settleable fraction showed a low fouling propensity in all cases (Fig. 4b–d). Therefore, differences in J_{th} may be related to the variations in settleable solid concentration and size. In the case of the suspension at 12/12 h photoperiod, due to its lower biomass concentration, the contribution of settleable solids was negligible and the r_f curve was similar to that obtained for the non-settleable fraction (Fig. 4b). Consequently, the highest J_{th} was attained. This can be explained by the effect of shear conditions associated with air scouring in preventing solids deposition onto the membrane.[66] However, this efficiency declines with

increasing solids concentration, resulting in cake layer development.[63] This may explain the relevant contribution of settleable solids at fluxes above the J_{th} and photoperiods of 16/8 and 24/0 h. The increasing trend of fouling rates with the permeate flux also supports the cake development mechanism.[67] Therefore, due to the similar biomass concentrations of the 16/8 and 24/0 h photoperiods, lower fouling rates at the former were consistent with the higher mean floc size. In accordance with previous studies,[31,39] these results suggest that although there is a positive effect of microalgae growth in the mixed culture bioflocculation (BPC decrease and floc size increase), an excessive microalgae/bacteria proportion led to a floc size decrease and higher fouling propensity.

3.3.2. Long-term fouling evolution. To assess residual fouling evolution, long-term tests were conducted under temporized filtration/backwashing cycles (Fig. 5). As previously reported, the residual fouling was characterized by the transmembrane pressure after each backwashing.[43] A permeate flux of 10 L h^{-1} m^{-2} was selected, which according to previously determined threshold values, appeared reasonable to achieve long-term sustainable conditions.[64] This value was comparable with those typically reported in MPBR studies, generally in the range 1.5–17 L h^{-1} m^{-2}.[31,35,39]

Throughout the assays, TMP$_i$ increases as a consequence of residual fouling, regardless of the low permeate flux
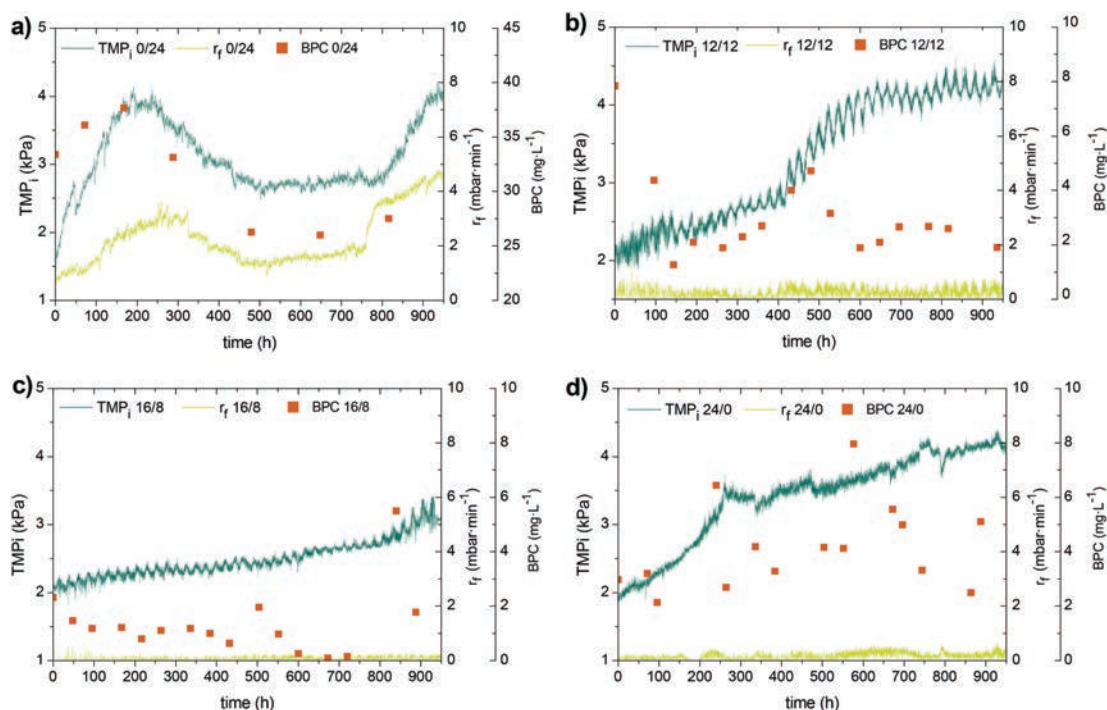

Fig. 5 Fouling evolution during long-term tests. Initial transmembrane pressure (TMP$_i$), reversible fouling rate (r_f) and BPC for the different photoperiods: a) 0/24 h; b) 12/12 h; c) 16/8 h and d) 24/0 h.

applied (below the threshold one for 12/12, 16/8 and 24/0 h photoperiods). As expected, the high fouling rates obtained for the control condition (0.6–4.8 mbar min^{-1}) led to rapid residual fouling development (Fig. 4a). However, values higher than 4.3 kPa were not reached, observing some fluctuations that seem to correspond to variations in BPC over experimentation time. This reflects an effective control of residual fouling due to the physical cleaning applied. By contrast, under lighting conditions, TMP$_i$ tended to increase continuously at a low rate (0.9×10^{-3}–2.2×10^{-3} kPa h^{-1}, equivalent to 1.5×10^{-4}–3.7×10^{-4} mbar min^{-1}), consistent with the very low fouling rates observed (0.1–0.3 mbar min^{-1}) and BPC content. Optimal performance was achieved at 16/8 h photoperiod, corresponding to the minimal BPC accumulation. Again, results suggest that excessive light irradiation may negatively affect filtration performance.

In addition, membrane recovery by physical and cleaning methods was analysed. Most residual fouling was removed by physical means (rinsing with tap water), revealing external biocake development (Fig. 6a). This was supported by images of the membrane (Fig. 6b–e), in which significant differences in biocake morphology were observed. A dense and compact layer was found for the control condition (Fig. 6b) in contrast to the porous and heterogeneous biocake formed under lighting conditions (Fig. 6c–e). As reported in previous studies, slight biocake formation is inevitable regardless of the physical cleaning (i.e. air scouring and backwashing) applied.[31,32] Nevertheless, the results obtained in this study showed a less attached and non-homogeneous biocake layer for the MPBR under lighting conditions, probably due to low BPC accumulation in the supernatant at the tested conditions. Generally, it is reported that biofouling development begins after the formation of an organic conditioning layer on the support.[68] This is corroborated by the hydraulic resistances obtained after rising, which declined when cleaning with an oxidant (Fig. 6a). Also, this organic film was clearly observed in membrane images (Fig. 6f–i), which disappeared after cleaning (Fig. 6j–m). In addition, some level of inorganic fouling was obtained, but the membrane was completely recovered by the acid cleaning (Fig. 6a).

4. Conclusions

This study has demonstrated the significant effect of photoperiod on the performance of a microalgal-bacterial membrane photobioreactor (MPBR) treating real secondary wastewater effluent. Under the long SRT applied (80 d), biomass productivity and nutrient removal increased with the length of the light period up to a saturation point at 16/8 h (light/dark), above which the effect became insignificant. Subsequently, increasing illumination above saturation deteriorated bioflocculation, decreasing particle size and increasing biopolymer cluster content. This negatively impacted membrane performance by decreasing the sustainable (i.e., threshold) permeate flux and enhancing biocake layer growth during long-term operation.

Development of MPBR technology requires appropriate values of operating parameters, which can maximize biomass productivity and nutrient removal without worsening membrane performance. This work has revealed that the photoperiod is a crucial parameter to be considered.

Author contributions

Segredo-Morales, E.: investigation, data curation, writing – original draft. González, E.: conceptualization, methodology, visualization, funding acquisition, project administration,
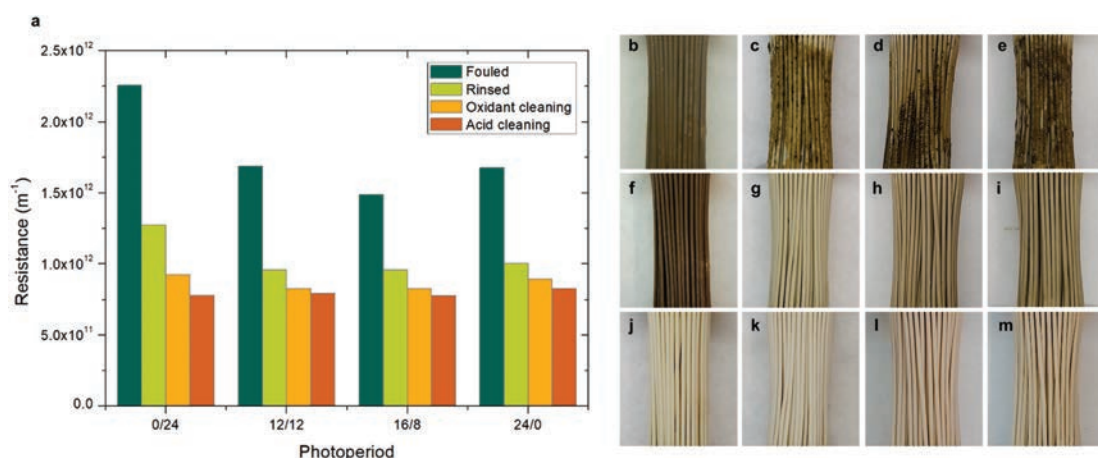

Fig. 6 (a) Recovery of long-term fouled membranes after cleaning protocol: hydraulic resistances of fouled, rinsed and chemical cleaned (oxidant and acid) membranes for the different photoperiods. Images of the fouled membranes for 0/24 h (b), 12/12 h (c), 16/8 h (d) and 24/0 h (e); after rising for 0/24 h (f), 12/12 h (g), 16/8 h (h) and 24/0 h (i); and after cleaning with an oxidant for 0/24 h (j), 12/12 h (k), 16/8 h (l) and 24/0 h (m).

writing-review & editing. González-Martín, C.: data curation, writing-review & editing. Vera, L.: conceptualization, methodology, funding acquisition, project administration, supervision, writing-review & editing.

Conflicts of interest

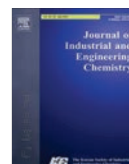There are no conflicts to declare.

Acknowledgements

References

1 Z. J. Ren and K. Pagilla, *Pathway to water sector decarbonization, carbon capture and utilization*, IWA Publishing, London, UK, 2022.

2 A. Soares, *Environ. Sci. Ecotechnology*, 2020, **2**, 100030.

3 N. Liu, Y. Dang, B. Hu, M. Tian, H. Jiang, G. Quan, R. Qiao, J. Lei and X. Zhang, *Surf. Interfaces*, 2022, **35**, 102472.

4 H. Li, J. Yu, Y. Gong, N. Lin, Q. Yang, X. Zhang and Y. Wang, *Sep. Purif. Technol.*, 2023, **307**, 122716.

5 J. Yu, H. Li, N. Lin, Y. Gong, H. Jiang, J. Chen, Y. Wang and X. Zhang, *Catalysts*, 2023, **13**, 148.

6 Y. Wang, Y. Gong, N. Lin, L. Yu, B. Du and X. Zhang, *J. Colloid Interface Sci.*, 2022, **606**, 941–952.

7 J. J. Y. Yong, K. W. Chew, K. S. Khoo, P. L. Show and J. S. Chang, *Biotechnol. Adv.*, 2021, **47**, 107684.

8 A. Fallahi, F. Rezvani, H. Asgharnejad, E. Khorshidi, N. Hajinajaf and B. Higgins, *Chemosphere*, 2021, **272**, 129878.

9 R. Mu, Y. Jia, G. Ma, L. Liu, K. Hao, F. Qi and Y. Shao, *Water Environ. Res.*, 2021, **93**, 1217–1230.

10 A. Morillas-España, T. Lafarga, A. Sánchez-Zurano, F. G. Acién-Fernández and C. González-López, *Chemosphere*, 2022, **291**, 132968.

11 C. Zhang, S. Li and S. H. Ho, *Bioresour. Technol.*, 2021, **342**, 126056.

12 G. Mannina, H. Gulhan and B. J. Ni, *Bioresour. Technol.*, 2022, **363**, 127951.

13 J. R. Werber, C. O. Osuji and M. Elimelech, *Nat. Rev. Mater.*, 2016, **1**, 16018.

14 P. Kehrein, M. Jafari, M. Slagt, E. Cornelissen, P. Osseweijer, J. Posada and M. van Loosdrecht, *Water Reuse*, 2021, **11**, 705–725.

15 M. Zhang, L. Yao, E. Maleki, B. Q. Liao and H. Lin, *Algal Res.*, 2019, **44**, 101686.

16 J. González-Camejo, P. Montero, S. Aparicio, M. V. Ruano, L. Borrás, A. Seco and R. Barat, *Water Res.*, 2020, **172**, 115499.

17 M. Zhang, K. T. Leung, H. Lin and B. Liao, *Chemosphere*, 2020, **261**, 128199.

18 A. F. Novoa, L. Fortunato, Z. U. Rehman and T. O. Leiknes, *Bioresour. Technol.*, 2020, **309**, 123348.

19 E. González, O. Díaz, I. Ruigómez, C. R. de Vera, L. E. Rodríguez-Gómez, J. Rodríguez-Sevilla and L. Vera, *Bioresour. Technol.*, 2017, **239**, 528–532.

20 Y. Liao, A. Bokhary, E. Maleki and B. Liao, *Bioresour. Technol.*, 2018, **264**, 343–358.

21 K. Li, Q. Liu, F. Fang, R. Luo, Q. Lu, W. Zhou, S. Huo, P. Cheng, J. Liu, M. Addy, P. Chen, D. Chen and R. Ruan, *Bioresour. Technol.*, 2019, **291**, 121934.

22 Y. Luo, P. Le-Clech and R. K. Henderson, *Water Res.*, 2018, **138**, 169–180.

23 M. Wang, R. Keeley, N. Zalivina, T. Halfhide, K. Scott, Q. Zhang, P. van der Steen and S. J. Ergas, *J. Environ. Manage.*, 2018, **217**, 845–857.

24 M. Raeisossadati, N. R. Moheimani and D. Parlevliet, *Renewable Sustainable Energy Rev.*, 2019, **101**, 47–59.

25 C. Vergara, R. Muñoz, J. L. Campos, M. Seeger and D. Jeison, *Int. Biodeterior. Biodegrad.*, 2016, **114**, 116–121.

26 M. M. Maroneze, S. F. Siqueira, R. G. Vendruscolo, R. Wagner, C. R. de Menezes, L. Q. Zepka and E. Jacob-Lopes, *Bioresour. Technol.*, 2016, **219**, 493–499.

27 H. Jia and Q. Yuan, *J. Water Process. Eng.*, 2018, **26**, 108–115.

28 J. González-Camejo, A. Viruela, M. V. Ruano, R. Barat, A. Seco and J. Ferrer, *Algal Res.*, 2019, **40**, 101511.

29 M. Atta, A. Idris, A. Bukhari and S. Wahidin, *Bioresour. Technol.*, 2013, **148**, 373–378.

30 J. González-Camejo, A. Jiménez-Benítez, M. V. Ruano, A. Robles, R. Barat and J. Ferrer, *J. Environ. Manage.*, 2019, **245**, 76–85.

31 M. Zhang, K. T. Leung, H. Lin and B. Liao, *Chemosphere*, 2021, **282**, 131015.

32 L. Fortunato, A. F. Lamprea and T. O. Leiknes, *Sci. Total Environ.*, 2020, **708**, 134548.

33 A. Drews, *J. Membr. Sci.*, 2010, **363**, 1–28.

34 A. L. K. Sheng, M. R. Bilad, N. B. Osman and N. Arahman, *J. Cleaner Prod.*, 2017, **168**, 708–715.

35 S. L. Low, S. L. Ong and H. Y. Ng, *Chem. Eng. J.*, 2016, **290**, 91–102.

36 M. Zhang, K. T. Leung, H. Lin and B. Liao, *J. Environ. Chem. Eng.*, 2021, **9**, 105500.

37 Y. Luo, P. Le-Clech and R. K. Henderson, *Algal Res.*, 2020, **50**, 102013.

38 Y. Luo, R. K. Henderson and P. Le-Clech, *Algal Res.*, 2019, **44**, 101682.

39 L. Sun, Y. Tian, J. Zhang, H. Li, C. Tang and J. Li, *Chem. Eng. J.*, 2018, **343**, 455–459.

40 J. González-Camejo, S. Aparicio, A. Jiménez-Benítez, M. Pachés, M. V. Ruano, L. Borrás, R. Barat and A. Seco, *Water Res.*, 2020, **172**, 115518.

41 Y. Luo, P. Le-Clech and R. K. Henderson, *Algal Res.*, 2017, **24**, 425–437.

42 E. Segredo-Morales, E. González, C. González-Martín and L. Vera, *J. Water Process. Eng.*, 2022, **49**, 103200.

43 E. González, O. Díaz, E. Segredo-Morales, L. E. Rodríguez-Gómez and L. Vera, *Ind. Eng. Chem. Res.*, 2019, **58**, 1373–1381.

44 L. Vera, E. González, O. Díaz, R. Sánchez, R. Bohorque and J. Rodríguez-Sevilla, *J. Membr. Sci.*, 2015, **493**, 8–18.

45 APHA, *Standard Methods for the Examination of Water and Wastewater*, Washington, DC, USA, 21st edn, 2005.

46 S. G. Berk and J. H. Gunderson, *Wastewater Organisms A Color Atlas*, CRC Press, Florida, USA, 1st edn, 1993.

47 C. S. Lee, H. S. Oh, H. M. Oh, H. S. Kim and C. Y. Ahn, *Bioresour. Technol.*, 2016, **200**, 867–875.

48 A. Solmaz and M. Işik, *BioEnergy Res.*, 2019, **12**, 197–204.

49 S. K. Parakh, P. Praveen, K. C. Loh and Y. W. Tong, *Bioresour. Technol.*, 2020, **315**, 123822.

50 P. Praveen, W. Xiao, B. Lamba and K. C. Loh, *Algal Res.*, 2019, **40**, 101487.

51 P. E. A. Debiagi, M. Trinchera, A. Frassoldati, T. Faravelli, R. Vinu and E. Ranzi, *J. Anal. Appl. Pyrolysis*, 2017, **128**, 423–436.

52 O. Orgad, Y. Oren, S. L. Walker and M. Herzberg, *Biofouling*, 2011, **27**, 787–798.

53 Y. Shi, J. Huang, G. Zeng, Y. Gu, Y. Hu, B. Tang, J. Zhou, Y. Yang and L. Shi, *Rev. Environ. Sci. Biotechnol.*, 2018, **17**, 71–85.

54 O. Díaz, L. Vera, E. González, E. García and J. Rodríguez-Sevilla, *Environ. Sci. Pollut. Res.*, 2016, **23**, 8951–8962.

55 H. Y. He, W. Qiu, Y. L. Liu, H. R. Yu, L. Wang and J. Ma, *Water Res.*, 2021, **190**, 116690.

56 A. Solmaz and M. Işik, *Sustain. Energy Technol. Assess.*, 2019, **34**, 1–8.

57 A. Solmaz and M. Işik, *Biomass Bioenergy*, 2020, **142**, 105809.

58 J. González-Camejo, S. Aparicio, M. Pachés, L. Borrás and A. Seco, *Algal Res.*, 2022, **61**, 102563.

59 European Parliament and the Council 2020/741, *Off. J. Eur. Union*, 2020, **177**(33), 32–55.

60 M. Kraume, D. Wedi, J. Schaller, V. Iversen and A. Drews, *Desalination*, 2009, **236**, 94–103.

61 Y. Zhang and Q. Fu, *Sep. Purif. Technol.*, 2018, **203**, 193–208.

62 P. Buzatu, H. Qiblawey, A. Odai, J. Jamaleddin, M. Nasser and S. J. Judd, *Water Res.*, 2018, **144**, 46–54.

63 A. Robles, M. V. Ruano, J. Ribes, A. Seco and J. Ferrer, *J. Membr. Sci.*, 2013, **444**, 139–147.

64 R. W. Field and G. K. Pearce, *Adv. Colloid Interface Sci.*, 2011, **164**, 38–44.

65 L. Sun, Y. Tian, J. Zhang, L. Li, J. Zhang and J. Li, *Bioresour. Technol.*, 2018, **251**, 311–319.

66 M. Bagheri and S. A. Mirbagheri, *Bioresour. Technol.*, 2018, **258**, 318–334.

67 Y. Jang, H. S. Kim, J. H. Lee, S. Y. Ham, J. H. Park and H. D. Park, *Chemosphere*, 2021, **280**, 130763.

68 C. Thobie, W. Blel, C. Dupré, H. Marec, J. Pruvost and C. Gentric, *Chem. Eng. Process.*, 2022, **175**, 108899.

Performance of a novel rotating membrane photobioreactor based on indigenous microalgae-bacteria consortia for wastewater reclamation

Check for updates

E. Segredo-Morales [a], C. González-Martín [b], L. Vera [a], E. González [a],*

[a] Departamento de Ingeniería Química y Tecnología Farmacéutica, Universidad de La Laguna, Astrofísico. Fco. Sánchez s/n, 38200 La Laguna, Spain
[b] Instituto Universitario de Enfermedades Tropicales y Salud Pública de Canarias, Universidad de La Laguna, Astrofísico. Fco. Sánchez s/n, 38200 La Laguna, Spain

ABSTRACT

Performance of a novel a rotating membrane photobioreactor (R-MPBR) for wastewater reclamation under photosynthetic oxygenation was investigated. The unit was operated in dead-end mode with an alternative physical cleaning strategy based in membrane module rotation. It was found that the carbon loading rate applied (CLR) (9.1–36.6 g $DOC \cdot m^{-3} \cdot d^{-1}$) determined the dissolved oxygen concentration, affecting nutrient removal, bioflocculation and membrane fouling. Indigenous microalgae-bacteria consortia were effectively developed under each condition. At high CLR values, the dissolved inorganic nitrogen removal was significantly enhanced (81.2 ± 13.9 %), probably due to a simultaneous nitrification–denitrification process as a result of the negligible dissolved oxygen concentration. Decreasing CLR from 36.6 to 9.1 g $DOC \cdot m^{-3} \cdot d^{-1}$, increased particle size ($D_{(0.5)}$ from 61.9 to 92.8 μm) and decreased biopolymer clusters content (from 50.0 to 2.3 mg $DOC \cdot L^{-1}$). It also revealed that membrane rotation does not compromise bioflocculation. Cake filtration model showed that fouling was associated to the supernatant fraction, particularly to the biopolymer clusters. Sustainable long-term operation was achieved at a permeate flux of 10 $L \cdot h^{-1} \cdot m^{-2}$ and CLR ≤ 11.4 g $DOC \cdot m^{-3} \cdot d^{-1}$. The proposed configuration effectively controlled membrane fouling, allowing to further process optimization.

© 2022 The Author(s). Published by Elsevier B.V. on behalf of The Korean Society of Industrial and Engineering Chemistry. This is an open access article under the CC BY license (http://creativecommons.org/licenses/by/4.0/).

Introduction

Climate change is pushing the water sector towards a new paradigm of circular water economy, where the focus is on water reuse, carbon neutral operations, resource recovery and system level planning [1]. For wastewater treatment and reuse, there is a need for technologies that promote process intensification, low energy consumption and reduced chemical demand. Among such technologies, the use of photobiological systems, particularly microalgal-bacterial based processes, have emerged as efficient technologies for combined carbon and nutrient removal from wastewater. These systems also assimilate ambient CO_2 to provide residual biomass that can be further converted into added-value products [2]. The ongoing technology evolution to overcome challenges (i.e. poor biomass settling and harvesting limitations) and strict legislation affecting reclaimed wastewater reuse has led to the incorporation of micro- or ultrafiltration membranes, resulting in the membrane photobioreactor (MPBR) concept [3,4].

Several configurations of the MPBR technology have been proposed, generally including a closed or semi-closed photobioreactor (bubble columns, flat panel and tubular reactors) combined with a submerged or side stream membrane (hollow fibre or flat sheet modules) [5]. As described in the literature, the MPBR has demonstrated its treatment capabilities for synthetic or real secondary effluents [6–8]. In addition, MPBRs are also capable of removing organics and nutrients from high organic loading influents, such as anaerobically digested wastewater and primary settled wastewater, although these applications have been less studied [5]. These influents promote microalgae-bacteria consortia to remove simultaneously carbon and nutrients, which can reduce the carbon footprint of the overall wastewater treatment process [1]. Nevertheless, as these consortia are easily affected by several factors such as light restriction, dissolved oxygen and influent characteristics, operating conditions should be carefully selected for avoiding negative impacts on the community structure [3]. Hydraulic retention time (HRT) is a crucial parameter affecting MPBR performance, and while short values typically enhance microbial growth, long HRTs improve nutrient removal efficiency [3]. In addition, HRT (i.e. organic and ammonia loading rates) regulates dissolved oxygen concentration due to the balance between

aerobic bacteria consumption and photosynthetic oxygen production by microalgae [9]. Another widely studied parameter is solid retention time (SRT), which can be decoupled from the HRT in MBPRs, and therefore represents a significant advantage over conventional photobioreactors [5]. SRT is related to biomass concentration, growth rate and microbial community. Among these, biomass concentration is critical, since high values can induce photolimitation due to shelf-shading, which negatively impacts on microalgae growth [10]. Typical values reported in the literature for HRTs and SRTs are 0.25–8 d and 5–25 d, respectively [3,5]. Nevertheless, these values are mainly based on studies with pure microalgae cultures and synthetic wastewater, which may not be representative of native microalgae-bacteria consortia performance applied to real wastewater treatment [11].

For all membrane processes, membrane fouling is a major challenge limiting their wide application [5,12–14]. Fouling is caused by specific chemical and physical interactions between the membrane and the microbial components of the suspension, which lead to decreases in membrane permeability. Similar to conventional membrane bioreactors, several mechanisms have been proposed to describe this complex phenomenon, including pore clogging, foulant adsorption and gel o cake layer formation [4]. According to many MPBR studies, extracellular organic matter and small suspension particles have been identified as the main foulants [8,10,15]. Additionally, the rate of fouling is not only governed by membrane characteristics and suspension foulants, but also by permeate flux, hydrodynamic conditions and any physical–chemical cleaning strategies applied [16–18]. Based on its reversibility by physical means (i.e. backwashing or relaxation), fouling can be classified into two main categories: reversible and residual fouling. The former is generally associated with an external cake deposit which can be removed by physical cleaning. Residual fouling (also called physically irreversible fouling) refers to the fouling that can be only removed by chemical cleaning and is related to gel formation, adsorption and probably to consolidated cake layer [16].

Alleviating membrane fouling by modifying hydrodynamic conditions has been extensively proven as an efficient means of promoting foulant back-transport from the cake layer by inducing shear stress [4]. In submerged MPBRs, intermittent air scouring is generally applied to produce a wall shear rate [6]. However, this operation strategy becomes energy intensive, exceeding 50 % of overall O&M costs [19]. Therefore, alternative operation modes with lower energy demands are required. Dead-end filtration (i.e. without shear conditions during the filtration phase) can be an attractive option, and it has been widely used in direct membrane filtration of secondary effluents [20]. However, higher suspended solids in microbial suspension of MPBRs can lead to lower permeate fluxes and more efficient physical cleaning to maintain operative fouling rates is needed. In this sense, to enhance cleaning efficiency, dynamic shear-enhanced membranes, which create a high shear rate by a moving part such as vibrating or rotating systems, are a promising approach. Disc membranes (vibrating or rotating) and vibrating hollow fibre membranes have been extensively applied for the filtration of very concentrated suspensions [21]. More recently, the concept of a rotating hollow fibre module in the submerged configuration has been developed [22]. With the aim of decreasing energy demand for less concentrated matrices, subsequent studies have demonstrated its effectiveness in combination with traditional physical cleaning techniques (i.e. relaxation and backwashing) at dead-end filtration mode [23]. Considering the great concern of membrane fouling in MPBRs, it is hypothesized that the rotating module may enhance backwashing efficiency, achieving a sustainable operation with a low energy demand.

In this study, the performance of a rotating membrane photobioreactor (R-MPBR) with indigenous microalgae-bacteria consortia was investigated for wastewater reclamation. Performance was assessed in terms of treatment capability, biomass characteristics, microalgae community and long-term fouling control as a function of several organic carbon loadings applied in order to optimise operating conditions.

Materials and methods

Feedwater

The lab-scale unit was fed with primary settled wastewater collected from a municipal wastewater treatment plant (Valle de Guerra, Canary Islands, Spain). Average and standard deviation values for dissolved organic carbon (DOC), chemical oxygen demand (COD), total suspended solids (TSS), ammonium-nitrogen (NH_4^+-N), dissolved inorganic nitrogen (DIN) and phosphate-phosphorus (PO_4^{3-}-P) were: 59.0 ± 26.3 mg·L^{-1}, 331 ± 135 mg·L^{-1}, 65.2 ± 35.6 mg·L^{-1}, 75.5 ± 13.8 mg·L^{-1}, 75.6 ± 13.7 mg·L^{-1} and 8.5 ± 2.4 mg·L^{-1}, respectively. As can be seen, the primary effluent was characterized by a low COD/N mass ratio (4.5) and low organic particulate content (COD/SST = 4.8) [24]. Also, average N/P ratio was 9.0, which was within the typical range reported for adequate microalgae growth [11]. Likewise, it presented an average pH of 8.1 with high alkalinity (12.7 meq·L^{-1}).

Experimental unit

The photobioreactor consisted of a tubular tank of 3.0 L made of acrylic plastic illuminated by a LED lamp (20 W, Aquatlantis Easy LED, Portugal) at 300 µmol·m^{-2}·s^{-1} measured at the outer surface of the photobioreactor, in the area closest to the source (PAR irradiance using QSP2150A, Biospherical Instrument Inc., USA) (Fig. 1). A photoperiod of 12/12 h light/dark was applied, except for the control condition, which operated without illumination. A PVDF ultrafiltration hollow fibre (Zeeweed® ZW-1, SUEZ Water Technologies and Solutions, Ontario, ON, Canada) with an average pore size of 0.04 µm and a nominal membrane surface area of 0.047 m^2 was used. A magnetic drive pump (Micropump-GA Series, AxFlow, Stockholm, Sweden) was used to withdraw permeate from the module. Membrane fouling was monitored by an increase in the transmembrane pressure which was measured by a pressure sensor (Sensotech, Barcelona, Spain). A mechanical stirrer (Heidolph-RZR2020, Heidolph Instruments GmbH & CO., Schwabach, Germany) connected to the permeate line, acted as the impeller of membrane rotation and provided turbulence. During the long-term tests (35 days), the unit operated at dead-mode (i.e. without membrane rotation during the filtration phase) with a filtration flux of 10 L·h^{-1}·m^{-2} at filtration/backwashing cycles of 450/30 s. During the backwashing phase, backwashing flux was fixed at 30 L·h^{-1}·m^{-2} and membrane rotation was applied at 260 rpm in order to improve cleaning effectiveness. Additional physical cleanings were applied once a week by conducting a relaxation phase (i.e. ceasing filtration) during 5 min with continuous module rotation at 260 rpm. The system was equipped with on-line sensors of temperature and dissolved oxygen for process performance monitoring (Hach HQ40d oximeter, Hach, USA). The control system was integrated using a personal computer which allowed implementing programs (DAQ Factory software, AzeoTech®, Inc., Ashland, OR, USA) to control the process and collate data. Further details can be found in a previous study [22]. A level controller HSE-20987 (Aeman, Spain) and two peristaltic pumps Masterflex Easy-Load L/S 7518–00 (Cole-Parmer Instrument Co., USA) controlled influent and permeate flow rates to achieve the selected carbon loading rates (CLR). To maintain a CLR independent of the filtration flux, a fraction of the permeate was returned to the tank.
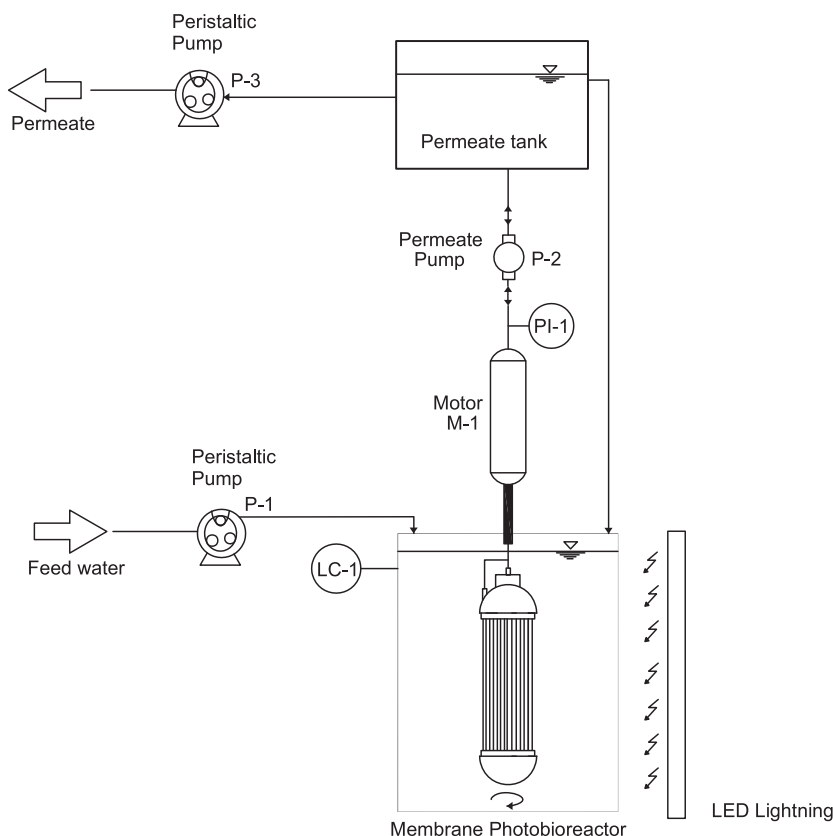
Fig. 1. Experimental setup of the R-MPBR system.

Experimental conditions

The unit started without any inoculum, thus, the biomass developed from the indigenous microorganisms existing in the influent. Acclimation period lasted the equivalent of the solids retention time, during which the system operated without biomass purge. Then, the microbial suspension was periodically and manually purged to maintain the selected SRT, which was 80 d in all the tests. The selection of this value was based on a previous study, where an effective fouling control was achieved [25]. Three experiments were conducted to assess the effect of the CLR on the R-MPBR performance: R-MPBR 1 at 36.6 ± 9.5, R-MPBR 2 at 11.4 ± 3.1, and R-MPBR 3 at 9.1 ± 2.1 g DOC·m^{-3}·d^{-1}, while operating at HRT of 2, 5 and 3.5 days, respectively. An additional test, with the filtration unit operating under control conditions (i.e. without illumination), was conducted at CLR of 36.9 ± 13.7 DOC·m^{-3}·d^{-1} (HRT = 2 d). Suspension was characterized according to mixed liquor suspended solid (MLSS), supernatant dissolved organic matter (DOC) and suspended solids (MLSS)$_s$, particle size distribution, elemental analysis, thermogravimetric analysis (TGA) and Fourier-transform infrared spectroscopy (FTIR). The biomass productivity was estimated according to Eq. (1):

$$r_x = \frac{MLSS}{SRT} \qquad (1)$$

Short-term flux step trials

After each acclimation period, flux-steps trials were conducted to assess reversible fouling tendency and to establish sustainable conditions for conducting long-term tests, according to previous studies [23]. Selected parameters were a filtration flux range of 6–30 L·h^{-1}·m^{-2}, flux step increment of 1 L·h^{-1}·m^{-2}, step duration of 15 min, backwashing flux of 30 L·h^{-1}·m^{-2} and backwashing duration of 30 s. Also, membrane rotation at 260 rpm was applied during backwashing.

Membrane cleaning protocol

After each long-term test, the membrane was cleaned according to a specific "ex situ" protocol, which included three steps: (1) extended rotation, (2) rinsing with tap water and (3) chemical cleaning with sodium hypochlorite (500 mg·L^{-1}) for 24 h [26]. At the beginning of the protocol and after each step, a tap water filtration test was conducted to determine the remaining hydraulic resistance.

Membrane fouling characterization

Transmembrane pressure (*TMP*) evolution under consecutive cycles of filtration/backwashing was used to characterize membrane fouling. Reversible fouling rate (r_f) was evaluated using the

slope of the straight line TMP against filtration time (t). Meanwhile, the residual fouling phenomena, which was not removed by backwashing, was measured by the initial transmembrane pressure TMP_0 at the beginning of the filtration cycle. Therefore, TMP evolution during the filtration phase can be described by the following equation:

$$TMP = TMP_0 + r_f \cdot t \qquad (2)$$

Analytical methods

Total suspended solids (TSS), mixed liquor suspended solids (MLSS) and chemical oxygen demand (COD) were analyzed according to the Standard Methods [27]. Turbidity was measured using a turbidimeter HACH 2100 N (Hach, USA). Ammonium-nitrogen (NH_4^+-N) was analyzed by the Nessler method using a DR-5000 Hach spectrophotometer (USA). Nitrite-nitrogen (NO_2^--N), nitrate-nitrogen (NO_3^--N) and phosphate-phosphorus (PO_4^{3-}-P) were analyzed by ion chromatography using a Compact IC plus 882 device, supplied by Metrohm. Total dissolved inorganic nitrogen (DIN) was obtained by adding NH_4^+-N, NO_2^--N and NO_3^--N. Dissolved organic carbon (DOC) concentration was measured with a TOC-meter (TOC-5000A, Shimadzu, Japan). The DOC difference between the filtered supernatant (through a filter of glass-fiber with a nominal pore size of 1.2 μm) and the permeate was assigned as biopolymer cluster (BPC) concentration [28]. Microbial floc size distribution was measured using a Malvern Mastersizer 2000 instrument (UK) with a detection range of 0.02–2000 μm. For the elemental analysis, a FLASH EA 1112 Elemental Analyzer (ThermoFisher Scientific, USA) was used. Thermogravimetric analysis (TGA) was performed using a simultaneous thermal analyzer (TG/DSC): Discovery SDT 650 (TA Instruments, USA). A quantity of biomass was loaded in a platinum crucible and heated between 25 and 600 °C at a heating rate of 15 °C/min under a nitrogen flow of 50 mL/min (Alphagaz nitrogen gas, Air Liquid, France). Fourier-transform infrared spectrometry was performed using an IFS 66/S spectrometer (Bruker, USA) equipped with an ATR accessory that measured the transmittance of the samples in a wavelength range between 900 and 4000 cm^{-1}. Microscopic observation of microalgae community and grazers was done following a protocol previously described by Madoni, with modifications [29]. Briefly, three preparations of each sample were analyzed using an aliquot (100 μl) of each one deposited in a glass slide after a gentle homogenization. After covering with a coverslip, they were visualized with an optical microscopy (DM750, Leica, Germany) using objectives 10x, 40x and 100x. Microorganisms were identified according to Wastewater Organisms Atlas Manual [30]. Microalgae community and grazers counts were obtained as the average value of 10 counts per preparation.

Detection of *Escherichia coli* and *Legionella* spp. was performed in the permeate according to ISO 9308 and ISO 11731, respectively, as recommended by the legislation. These methodologies are based in the filtration of the water using 0.45 μm pore size nitrocellulose filters that are placed on specific culture media. After the incubation period at 36 ± 2 °C (21 ± 3 h for E. *coli* and 7–10 days for *Legionella* spp.), bacteria can be identified and quantify, if needed, and results expressed as CFU (Colony Forming Units) per 100 ml (E. *coli*) or 1 L (*Legionella* spp.).

Results and discussion

Treatment performance and biomass productivity

Table 1 shows the removal efficiencies of the main pollutants. Comparable organic matter removal was achieved for the R-

MPBR 1 and the control condition, operated at similar CLR. Average concentrations ranging from 50.4 to 59.9 mg COD·L^{-1}, and from 13.7 to 15.2 mg DOC·L^{-1} were observed in the permeate of both systems, resulting in removal efficiencies of 82.6–85.6 % and 78.4–79.5 %, respectively. It should be noted that the observed variability was mainly due to the inherent fluctuation of the feedwater. The high efficiencies achieved might be explained by the membrane retention, since no appreciable biological degradation is expected in the control condition. In fact, these results are in agreement with those previously reported in a direct membrane ultrafiltration process applied to the same feedwater [23]. In addition, decreasing CLR in the R-MPBR below 11.4 g DOC·m^{-3}·d^{-1} (57.7 g COD·m^{-3}·d^{-1}) caused a significant increment of dissolved oxygen concentration (DO), as can be seen in Fig. 2, revealing that photosynthetic oxygenation potential was enough to provide aerobic conditions below this CLR. It should be noted that average ammonia loading at this condition was 10.2 g N·m^{-3}·d^{-1}, which might increase the theoretical oxygen demand in 46.6 g O_2·m^{-3}·d^{-1} (assuming 4.57 g O_2·g^{-1}N for complete nitrification [24]), resulting in a global theoretical value of oxygen demand of 104.3 g O_2·m^{-3}·d^{-1}. This oxygenation potential was comparable with that reported in a previous study of degradation of piggery wastewater (116 to 133 g O_2·m^{-3}·d^{-1}) [9]. Nevertheless, despite the aerobic conditions achieved, no further organic matter removal was obtained (Table 1), which confirmed the main role of membrane retention.

Table 1 also shows biomass concentration and productivity under the different conditions. By comparing the results obtained for the R-MPBR 1 and the control condition, it is evident that the introduction of microalgae significantly increased (2.8 times) biomass productivity. Previous studies have reported the influence of organic matter, more than other environmental factors, on microalgae population in mixed consortia, enhancing the dominance of species with a high tolerance [31]. Nevertheless, very high organic carbon concentrations (>231 mg DOC·L^{-1}) were found to inhibit the growth of microalgae due to a competitive interaction with heterotrophic bacteria, as noted by He et al. [32]. Consistently, the obtained results confirmed the effective growth of native microalgae species in the tested conditions. In this sense, several microalgae, such as *Chlorella* and *Scenedesmus*, have demonstrated their tolerance and/or ability to acclimatize to primary settled wastewater [33]. This is in agreement with a synergistic support between microalgae and bacteria, where microalgae can provide photosynthetic dissolved oxygen and extracellular metabolites and bacteria can release inorganic carbon, vitamins or other substances that can enhance the growth of microalgae in return [2,34]. In fact, biomass productivities reported here are comparable to those typically found in MPBRs applied to secondary effluents treatment (10–60 mg·L^{-1}·d^{-1}) [35]. Additionally, decreasing CLR should decrease bacterial growth due to lower organic substrate loading. Also, low CLRs promote zooplankton grazers, which mainly consume dispersed bacteria and microalgae [36]. Consistently, biomass productivity decreased from 47.4 ± 3.3 mg·L^{-1}·d^{-1} to 22.0 ± 2.9 mg·L^{-1}·d^{-1}.

Regarding nutrient removal, significant differences were found between the R-MPBR 1 and the control condition (Table 1). At similar CLR, average nitrogen and phosphorus removal efficiencies increased 2.9 and 3.6 times, respectively. This might be attributed to the presence of microalgae growth and the associated nutrient needs, as previously stated. Concentrations of 17.5 ± 12.9 mg DIN·L^{-1} and 6.8 ± 1.2 mg PO_4^{3-}-P·L^{-1} were recorded in the R-MBPR permeate. Calculated removal rates were 37.2 mg·L^{-1}·d^{-1} and 1.6 mg·L^{-1}·d^{-1} for nitrogen and phosphorus, respectively. The DIN removal rate was much higher than those typically found (1.6–12.5 mg·L^{-1}·d^{-1}) in other MPBR studies [10,37]. Also, much more than expected by biomass assimilation (3.8 mg·L^{-1}·d^{-1},

Table 1
Biological performance of MPBR and control condition.

Parameters	R-MPBR 1	R-MPBR 2	R-MPBR 3	Control
CLR (g DOC·m^{-3}·d^{-1})	36.6	11.4	9.1	36.9
Permeate concentration (mg·L^{-1})				
COD	50.4 ± 16.0	43.9 ± 15.4	31.0 ± 15.2	59.9 ± 21.4
DOC	15.2 ± 2.0	10.9 ± 1.7	8.6 ± 1.0	13.7 ± 4.8
NH$_4^+$-N	14.7 ± 12.9	0.6 ± 0.3	0.6 ± 0.6	62.4 ± 8.0
NO$_3^-$-N	0.2 ± 0.3	53.2 ± 9.8	52.8 ± 10.6	0.2 ± 0.2
NO$_2^-$-N	2.6 ± 1.9	2.0 ± 2.2	0.4 ± 0.6	0.3 ± 0.3
DIN	17.5 ± 12.9	55.8 ± 8.1	58.8 ± 9.3	62.9 ± 8.0
PO$_4^{3-}$-P	6.8 ± 1.2	6.8 ± 0.7	9.9 ± 1.4	10.4 ± 0.2
Removal efficiency (%)				
COD	85.6 ± 5.2	84.8 ± 6.8	89.2 ± 5.6	82.6 ± 8.9
DOC	78.4 ± 4.0	73.0 ± 19.1	55.4 ± 1.7	79.5 ± 8.8
NH$_4^+$-N	84.3 ± 14.7	98.8 ± 0.6	99.1 ± 1.2	28.4 ± 14.6
DIN	81.2 ± 13.9	20.7 ± 7.9	21.2 ± 10.1	27.9 ± 14.7
PO$_4^{3-}$-P	25.4 ± 12.0	11.0 ± 4.1	12.2 ± 10.6	7.1 ± 4.8
Biomass concentration (mg·L^{-1})	3788 ± 261	2378 ± 427	1759 ± 232	1333 ± 125
Biomass productivity (mg·L^{-1}·d^{-1})	47.4 ± 3.3	29.7 ± 5.3	22.0 ± 2.9	16.7 ± 3.3

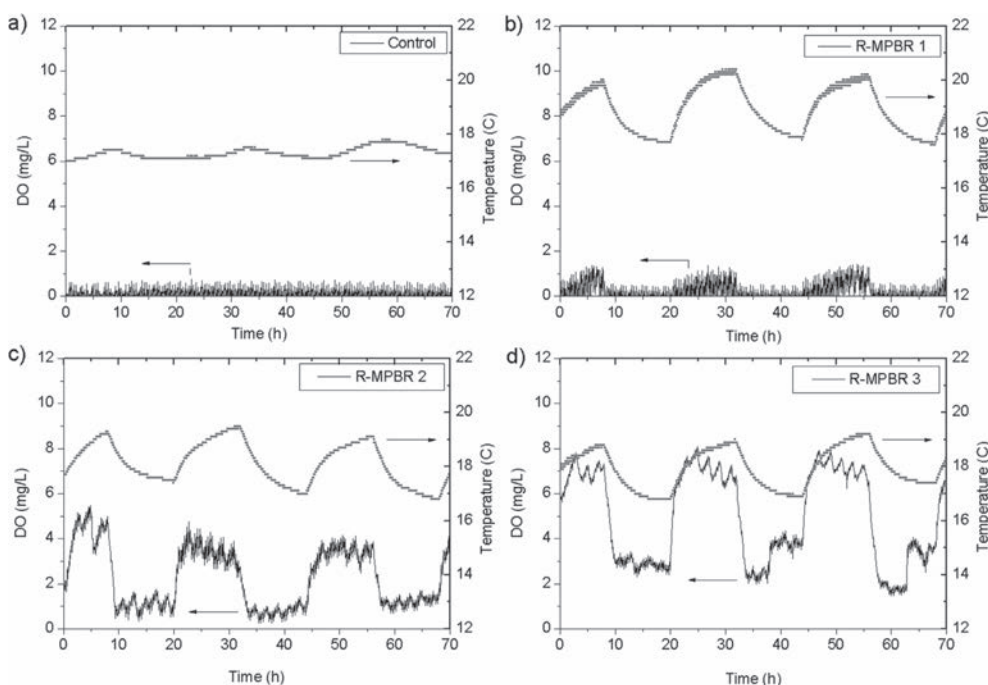Note: The data are expressed as mean ± standard deviation.

Fig. 2. Dissolved oxygen (DO) and temperature profiles of (a) control condition, (b) R-MPBR 1, (c) R-MPBR 2 and (d)R-MPBR 3.

assuming a ratio of nitrogen to increased biomass of 8 % [38]), which suggest an additional removal mechanism. It should be noted that recorded pH values (7.8 ± 0.1) made ammonia volatilization negligible. In addition, a slight NO$_2^-$-N concentration was also detected (Table 1), revealing an apparent simultaneous nitrification–denitrification process, consistent with the slightly aerobic conditions (Fig. 2b) and the significant nitrogen removal decrease observed at lower CLR (Table 1). This removal mechanism has also been reported in a previous study of a photosequencing batch reactor [39]. Regarding phosphorus removal, the obtained rate (1.2 mg·L^{-1}·d^{-1}) was consistent with a biomass assimilation mechanism [40].

Different performance was obtained at CLR bellow 11.4 g DOC·m^{-3}·d^{-1}, since the photosynthetic oxygenation rate was sufficient to provide aerobic conditions, which prevented the denitrification process. Dissolved oxygen profiles showed average values of about 3.5/0.8 mg·L^{-1} and 7/3 mg·L^{-1} during the light/dark periods, for 11.4 and 9.1 g DOC·m^{-3}·d^{-1}, respectively (Fig. 2c and d). Consequently, nitrogen removal was mainly due to biomass assimilation. Removal efficiencies decreased to 20.7 ± 7.9 % and 21.2 ± 10.1 % corresponding to DIN concentrations of 55.8 ± 8.1 mg·L^{-1} and 58.8 ± 9.3 mg·L^{-1} in the permeate, mainly in the form of nitrate-nitrogen, for CLR of 11.4 and 9.1 g DOC·m^{-3}·d^{-1}, respectively (Table 1). Calculated DIN removal rates were 2.1 and 4.5 mg·L^{-}

$^1 \cdot d^{-1}$, respectively. Additionally, phosphorus removal rates were also lower (0.1 and 0.3 $mg \cdot L^{-1} \cdot d^{-1}$, respectively) than those obtained at CLR of 36.6 g $DOC \cdot m^{-3} \cdot d^{-1}$, consistent with a lower biomass productivity.

Finally, microbial (absence of *E. coli* and *Legionella spp.*) and physical (turbidity < 0.5 NTU) quality of the permeate generated in the R-MPBRs complied with the new European regulation of reclaimed water quality for agricultural irrigation [41].

Biomass suspension characteristics

FTIR spectra of the biomass samples showed the typical biochemical composition, with the presence of specific peaks of carbohydrates, nucleic acids, proteins and lipids [42] (Fig. 3). Nevertheless, thermogravimetric analysis revealed different proportions of components according to devolatilization profiles (Fig. 4). Control and R-MPBR 1 samples showed a narrow degradation profile with a main peak at about 315 °C (Fig. 4a). However, while decreasing the CLR applied (from R-MPBR 2 to R-MPBR 3), the peak intensity progressively decreased and an additional peak appeared at around 275 °C, revealing a wider degradation profile. This could be due to higher protein content, which typically decomposes at a lower temperature than carbohydrates and lipids. Indeed, it has been reported main degradation peaks in the range 275–295 °C for some high-protein microalgae [43].Therefore, it seems that decreasing CLR may induce a more complex biomass structure, which can be related to higher bioflocculation. Nevertheless, no significant differences of total biomass volatile matter were found (57.7–61.8 %) (Fig. 4b), whose values were within the typical range reported for microalgae biomass cultured in wastewater [44]. Additionally, elemental analysis showed that all biomass samples had carbon, hydrogen, nitrogen and sulfur content of 36.5–37.8 %, 4.4–5.7 %, 6.5–8.4 % and 0–0.8 %, respectively (Table 2). These values are comparable to those reported for microalgal biomass [38]. In agreement with the thermogravimetric analysis, N

content increased with decreasing CLR in R-MPBRs, consistent with higher amounts of protein.

Due to its impact on membrane performance, bioflocculation has been assessed by analyzing particle size distribution and biopolymer cluster content in the supernatant (Table 2). A significant increase in floc size was observed in the R-MPBR samples, revealing efficient bioflocculation by the microalgae-bacteria consortium. In R-MPBR 1, medium-size flocs were observed ($D_{(0.5)}$ = 61.9 ± 5.9 μm) with narrow distribution (spread index of 1.17 ± 0.04). Also, decreasing CLR to 11.4 and 9.1 $DOC \cdot m^{-3} \cdot d^{-1}$ increased the median value up to 70.5 ± 8.6 μm (1.15 ± 0.03) and 92.8 ± 3.0 μm (0.95 ± 0.03), respectively. These values are higher than those reported in a microalgal-bacterial MPBR treating a secondary effluent [35], confirming the efficient flocculation achieved in the test conditions. It should be noted that an increase in floc size (with a narrow distribution) may reduce membrane fouling due to formation of a porous cake layer with low filtration resistance. On the other hand, previous studies have highlighted the role of extracellular polymeric substances (EPS) released by the microalgae and bacteria on the bioflocculation [2]. Several bioflocculation mechanisms have been reported, including charge neutralization and bridging, both due to the adsorption of charged biopolymers [45]. Therefore, it is expected that supernatant biopolymers may be related to the bioflocculation process. This is consistent with the current study, where the biopolymer clusters (BPC), which represented the colloidal fraction of biopolymers, was significantly reduced in the R-MPBR (Table 2). In addition, it has been argued that BPC, which are apparently formed by affinity clustering of soluble EPS, can be degraded by heterotrophic bacteria [46]. This can justify the lower BPC content in the R-MPBR when decreasing the CLR, which, as already indicated, enhances aerobic degradation. It should be noted the impact of BPC in membrane fouling, which can reduce cake layer porosity, and thus enhance floc attachment to the membrane [47]. The enhancement of bioflocculation at low CLR was also confirmed by the low values of suspended solids
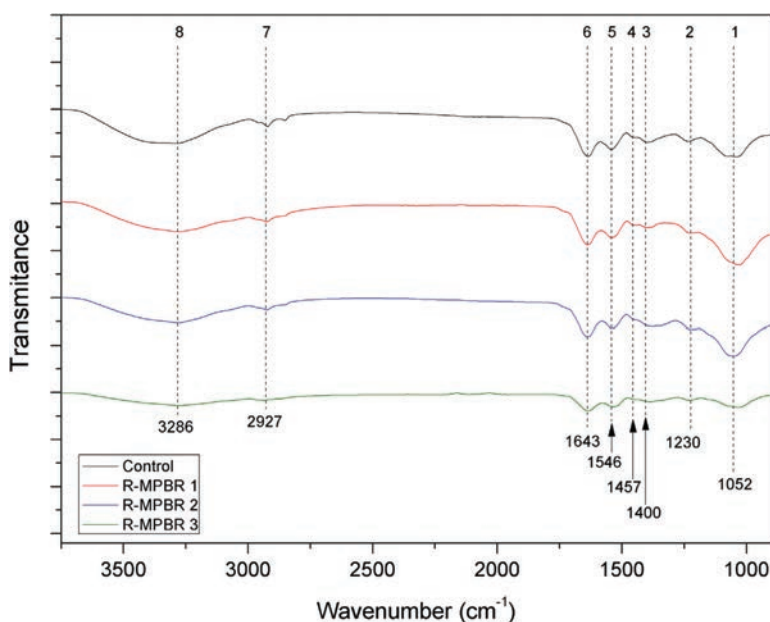

Fig. 3. FTIR spectra of biomass samples from the R-MPBRs and the control one. Characteristics bands were identified from carbohydrates (band 1), nucleic acids (band 2), proteins (bands 3–6 and 8) and lipids (band 7).
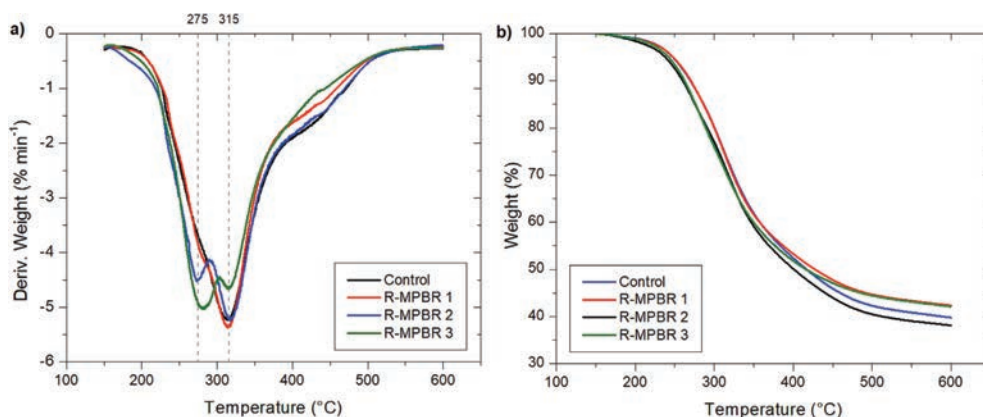
Fig. 4. Differential thermogravimetric (DTG) (a) and thermogravimetric analysis (TGA) (b) dataset of the control condition and the R-MPBR samples.

Table 2
Main suspension characteristics of the MPBR and the control condition.

Parameters	R-MPBR 1	R-MPBR 2	R-MPBR 3	Control
CLR (g DOC·m^{-3}·d^{-1})	36.6	11.4	9.1	36.9
Elemental analysis (%wt, dry basis)				
C	36.5 ± 1.2	37.7 ± 0.4	37.8 ± 2.2	37.0 ± 1.8
H	4.4 ± 1.2	5.5 ± 0.1	5.4 ± 0.2	5.7 ± 0.1
N	6.5 ± 0.2	8.2 ± 0.1	8.4 ± 0.2	6.9 ± 0.4
S	0.8 ± 0.3	nd	nd	0.8 ± 0.1
Particle size distribution				
D$_{(0.1)}$ (µm)	17.6 ± 3.0	22.5 ± 4.7	31.4 ± 3.8	13.2 ± 1.2
D$_{(0.5)}$ (µm)	61.9 ± 5.9	70.5 ± 8.6	92.8 ± 3.0	38.4 ± 5.0
D$_{(0.9)}$ (µm)	162.9 ± 12.1	184.3 ± 20.5	207.9 ± 3.6	81.9 ± 10.9
Supernatant				
BPC (mg DOC·L^{-1})	50.0 ± 14.8	24.3 ± 7.4	2.3 ± 0.8	78.2 ± 27.4
(MLSS)$_s$ (mg·L^{-1})	317 ± 66	179 ± 21	65 ± 14	994 ± 63
(MLSS)$_s$/MLSS (%)	8.4	7.5	3.7	74.6

Note: The data are expressed as mean ± standard deviation. nd: not-detected.

in the supernatant (MLSS)$_s$ and the corresponding ratios to the solid concentration in the suspension (MLSS)$_s$/MLSS (Table 2).

Membrane fouling

Analysis of reversible fouling rate in flux-steps trials

As stated, many MPBR studies have reported similarities in the fouling mechanisms with those typically observed in MBRs [3,4]. Therefore, flux-step trials have been conducted to assess the effect of the suspension characteristics on fouling rates (r_f) under different permeate flux (J) conditions. Additionally, the results were compared to those achieved with the corresponding supernatants, which were obtained by removing sedimentable solids from the suspension (see main characteristics in Table 2). For all the experiments performed, r_f continuously increased with J (Fig. 5a). Nevertheless, the control condition and the R-MPBRs behaved differently. In the former, a sharp increase of r_f was observed at moderate fluxes. Specifically, r_f increased from 1.0 to 76.3 mbar·min^{-1} when increasing J from 6 to 29 L·h^{-1}·m^{-2}. By contrast, the fouling trend of the R-MPBR under the same conditions (R-MPBR 1) followed a linear increase. In this case, r_f values were between 1.5 and 32.5 mbar·min^{-1}, which was a substantially lower fouling sensitivity. In addition, an evident effect of decreasing CLR was also observed in R-MPBR 2 and R-MPBR 3, where the r_f ranges were 0.6–12.1 mbar·min^{-1} and 0.2–4.5 mbar·min^{-1}, respectively. Regarding supernatant fractions, similar behaviours were

observed, where only slightly lower fouling rates were achieved compared with those obtained by the suspensions. Consequently, results showed that the fouling was mainly determined by supernatant fractions for all the tested conditions.

The results were analysed using the cake filtration model, where the fouling rate is expressed in terms of solvent viscosity (μ), specific cake resistance (α), cake concentration (ω) and permeate flux, as showed in Eq. (3):

$$r_f = \mu \cdot \alpha \cdot \omega \cdot J^2 \tag{3}$$

According to the model, the product $\alpha\omega$ depends on the cake properties and, consequently, on suspension characteristics. Calculated values for the control condition showed two different regions above and below a critical flux (J^*) of 11 L·h^{-1}·m^{-2}. At subcritical fluxes, constant $\alpha\omega$ was achieved (4.9·10^{14} ± 5.2·10^{13} m^{-2}). By increasing flux above J^*, $\alpha\omega$ linearly increased (4.9·10^{14} + 6.6·10^{13}· (J - J^*), R^2 = 0.98). Provided that ω is proportional to the solids concentration in the suspension, then α should increase with J at supra-critical conditions. For dead-end filtration, the existence of a critical flux has been related to a consolidation of the cake layer [28]. It is expected that in the control condition, characterized by a high BPC content, the internal void spaces of the cake layer become clogged with the biopolymers, reaching an "overclogging situation" [47], where cake porosity substantially decreased. According to the Carman-Kozeny equation, α gradually increases with decreasing cake layer porosity until a threshold
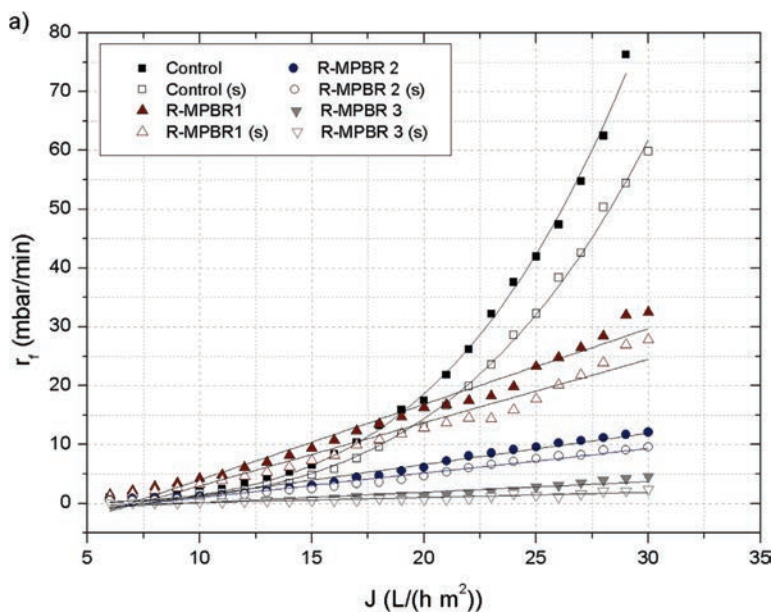
Fig. 5. Fouling rate (a) against permeate flux during the flux-step trials and calculated $\alpha\omega$ values (b) for the suspension and supernatant (s) of the control condition and the R-MPBRs. For the R-MPBRs, $\alpha\omega$ is expressed as average and standard deviation values at the flux range 6–30 L·h^{-1}·m^{-2}.
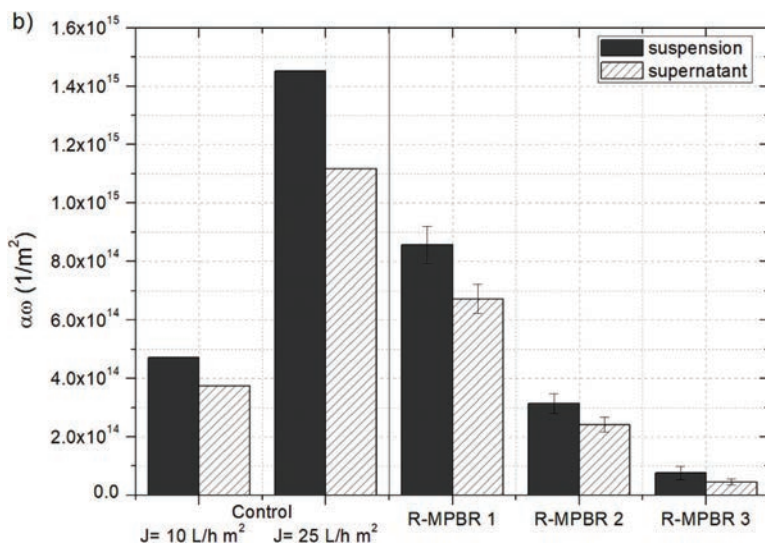

Fig. 5 (*continued*)

value is achieved, from which it increases abruptly [48]. The impact of BPCs was confirmed when filtering the supernatant of the control condition, where the $\alpha\omega$ values accounted for 75 ± 6 % of that obtained for the suspension (Fig. 5b).

As stated, R-MPBRs followed a different behaviour. Fig. 5b shows nearly constant $\alpha\omega$ values of $8.6 \cdot 10^{14} \pm 6.3 \cdot 10^{13}$ m^{-2}, $3.1 \cdot 10^{14} \pm 3.4 \cdot 10^{13}$ m^{-2} and $7.8 \cdot 10^{13} \pm 2.2 \cdot 10^{13}$ m^{-2} for R-MPBR 1, R-MPBR 2 and R-MPBR 3, respectively. In addition to the effect

of the solid concentration, results also showed that $\alpha\omega$ decreased with increasing particle size and decreasing BPCs. This is consistent with the crucial role of both parameters in regulating cake porosity. Also, these results are in agreement with those reported in previous MPBR studies culturing *C. Vulgaris*, where significant supernatant biopolymer retention by membrane and a large fraction of smaller particles were found to induce severe fouling [8,15]. Similar to that observed for the control condition, the filtra-

tion tests with the supernatants resulted in $\alpha\omega$ values comparable to those obtained for the suspensions (79 %, 77 % and 59 % for R-MPBR 1, R-MPBR 2 and R-MPBR 3, respectively).

Effect of the physical cleaning strategy on residual and reversible fouling during long term operation

Process sustainability was analysed by assessing the cleaning efficiency of the proposed strategy. The permeate flux was fixed at 10 $L \cdot h^{-1} \cdot m^{-2}$ to achieve reasonable process productivity, in agreement with most MPBR studies, where operating fluxes are typically within the range of 2.6–15 $L \cdot h^{-1} \cdot m^{-2}$ [3]. In addition, according to the previous flux-steps trials (Fig. 5a), this flux should avoid initial non-operative fouling rates (<5 mbar·min^{-1}) for the tested suspensions [6]. Also, additional physical cleanings were applied once a week by conducting a relaxation (RX) phase with continuous module rotation, as described in section 2.

Fig. 6 shows the residual fouling evolution, described by the initial transmembrane pressure (TMP_0) at the beginning of the filtration cycles, for the control condition and the R-MPBRs. The results showed the pattern predicted by the flux-steps tests, revealing the relationship between reversible and residual fouling. As physical cleaning cannot completely remove fouling, residual fouling progressively grows with the operation time. For the control condition, TMP_0 increased at a slow rate of 5.9 mbar·d^{-1} for the first 8 days, but then sharply increased up to 200 mbar by day 15. This profile is commonly observed in submerged MBRs and has been mainly associated to a cake layer compaction which accelerates fouling rate [48]. Therefore, similarities can be observed with the effect of increasing permeate flux in the flux-step trials conducted for the control condition. During long-term operation, due to the low flux applied, fouling rates were initially maintained at low values, but some residual fouling was observed (Fig. 6a). With increasing operating time, this residual fouling may decrease the available membrane filtration area, leading to a progressive increase of the actual flux, which finally results in a cake layer consolidation. In

addition, consolidated cakes are reported to be less reversible by backwashing [49] and probably contributed to the rapid residual fouling (i.e. TMP_0) increase observed. Low fouling reversibility can also be observed in the inefficiency of the relaxing phases conducted after 7 and 14 days (Fig. 6a). Moreover, a recent work by Vroman et al. [50] has introduced the critical inter cake-membrane concept (i.e. minimal pressure force to detach the cake), which links both cake and membrane hydraulic resistances to the critical backwashing pressure to achieve maximal cleaning efficiency.

A different fouling behaviour was observed for the R-MPBRs. In all cases, a roughly linear TMP_0 increase was found, whose rate of increase declined with CRL (from R-MPBR 1 to R-MPBR 3) (Fig. 6-b-d). In agreement with a previous MPBR study [7], a noticeable effect of light pattern on TMP_0 profile can be observed, where a reduction of residual fouling was typically recorded during light hours. This can be attributed to the temperature profile (from 17 to 20 °C) and its effect on permeate viscosity. When operated at the same conditions of the control test (R-MPBR 1), TMP_0 continuously increased at an average rate of 6.66 ± 0.02 mbar·d^{-1} (R^2 = 0.95), reaching 200 mbar on day 25. An evident improvement of the filtration performance was achieved as a consequence of avoiding the cake consolidation, but the large r_f values reached throughout the test (>5 mbar·min^{-1}) (Fig. 6b) induced a non-operative residual fouling rate. As stated, this is related to a larger proportion of small flocs and higher BPC obtained at these conditions. Additionally, significant fouling sensitivity (within the range of 5–22 mbar·min^{-1}) to influent fluctuations, particularly the nitrogen organic load and the resulting variable ammonia removal rates (see Table 1) were observed. This positive effect of ammonia nitrification is frequently reported in many MBR studies [51]. Regarding the cleaning efficiency of the relaxation phases, an instantaneous TMP_0 decrease was observed after each event, although it rapidly increased until reaching the previous values. This behaviour suggests that cleaning parameters (mainly back-
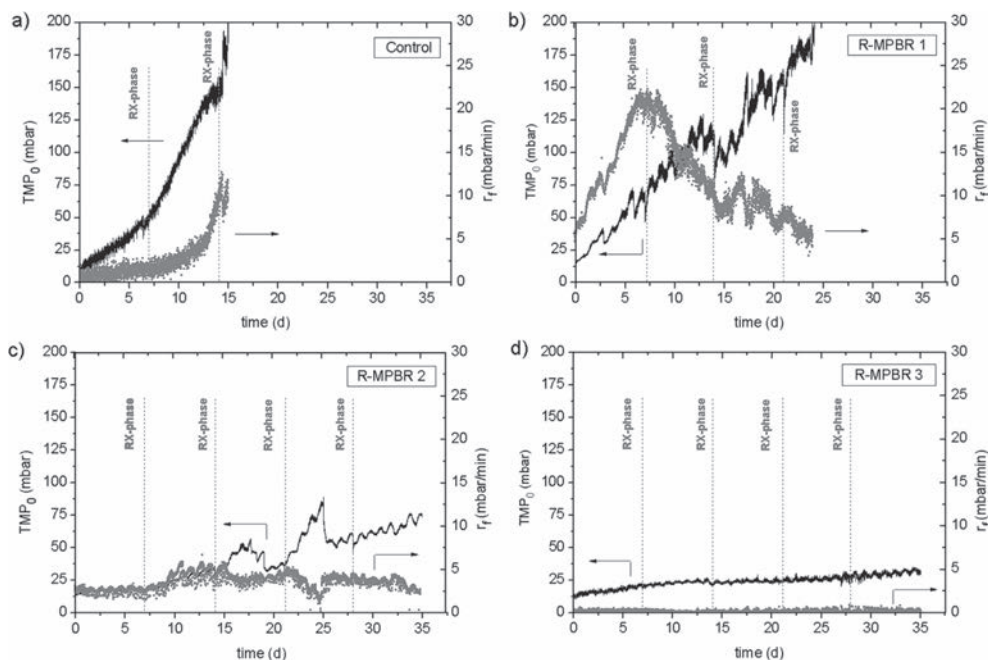

Fig. 6. Initial transmembrane pressure (TMP_0) and reversible fouling rate (r_f) evolution of (a) control condition, (b) R-MPBR 1, (c) R-MPBR 2 and (d) R-MPBR 3.

washing duration) can be improved to achieve better residual fouling control. Hence, although non-operative residual fouling rates were found in R-MPBR 1, the results also revealed the reversibility of a significant part of this type of fouling in contrast with the behaviour obtained in the control condition.

Sustainable operation can be maintained in R-MPBR 2 and R-MPBR 3, where TMP_0 increased at rates of 1.80 ± 0.01 mbar·d^{-1} ($R^2 = 0.88$) and 0.42 ± 0.01 mbar·d^{-1} ($R^2 = 0.86$), respectively (Fig. 6c and d). Comparable values have been reported for full-scale MBRs [16]. This behaviour can be attributed to the low and stable fouling rates achieved through the tests (3.63 ± 0.90 mbar·min^{-1} and 0.16 ± 0.13 mbar·min^{-1} for R-MPBR 2 and R-MPBR 3, respectively). Compared with the corresponding values found during the flux-steps trials (Fig. 5a) at the same flux (10 L·h^{-1}·m^{-2}) with a clean membrane, r_f increased about 3 times in R-MPBR 2 and remained at the same value in R-MPBR 3, consistent with the residual fouling trends for each condition. In addition, due to the low fouling loads at these conditions, relaxation phases did not induce significant fouling removal, revealing that the cleaning parameters were optimal.

In summary, the long-term behaviour revealed the efficiency of the proposed cleaning strategy at moderate CLR, suggesting that the system can be operated during long periods. Nevertheless, fur-

ther studies should focus on improving process productivity by increasing permeate flux.

After the long-term tests, a simplified analysis of the residual fouling layer was conducted. A specific "ex situ" cleaning protocol (described in section 2) separated the layers in three main fractions: loose cake (removed by extended rotation), consolidated cake (removed by rinsing in tap water) and adsorbed material (removed by NaClO). Assessing the individual contribution of each layer in terms of resistance, the loose cake accounted for 0 %, 68.7 %, 11.8 % and 1.1 % of total fouling resistance, for the control condition, R-MPBR 1, R-MPBR 2 and R-MPBR 3, respectively. As expected, these results are consistent with those obtained by conducting relaxation events in the filtration tests. An opposite trend was found for consolidated cake, achieving values of 98 %, 19.6 %, 14.2 % and 9.1 %, respectively. A minor influence of adsorbed material (1–4.4 %) was found in all cases, confirming that the cake filtration is the main fouling mechanism.

Microalgal composition and zooplankton grazers in the R-MPBRs

As stated, the R-MPBR was started-up without inoculum and the feedwater was used to fill the photobioreactor the first day. After the corresponding acclimation period at each condition, a
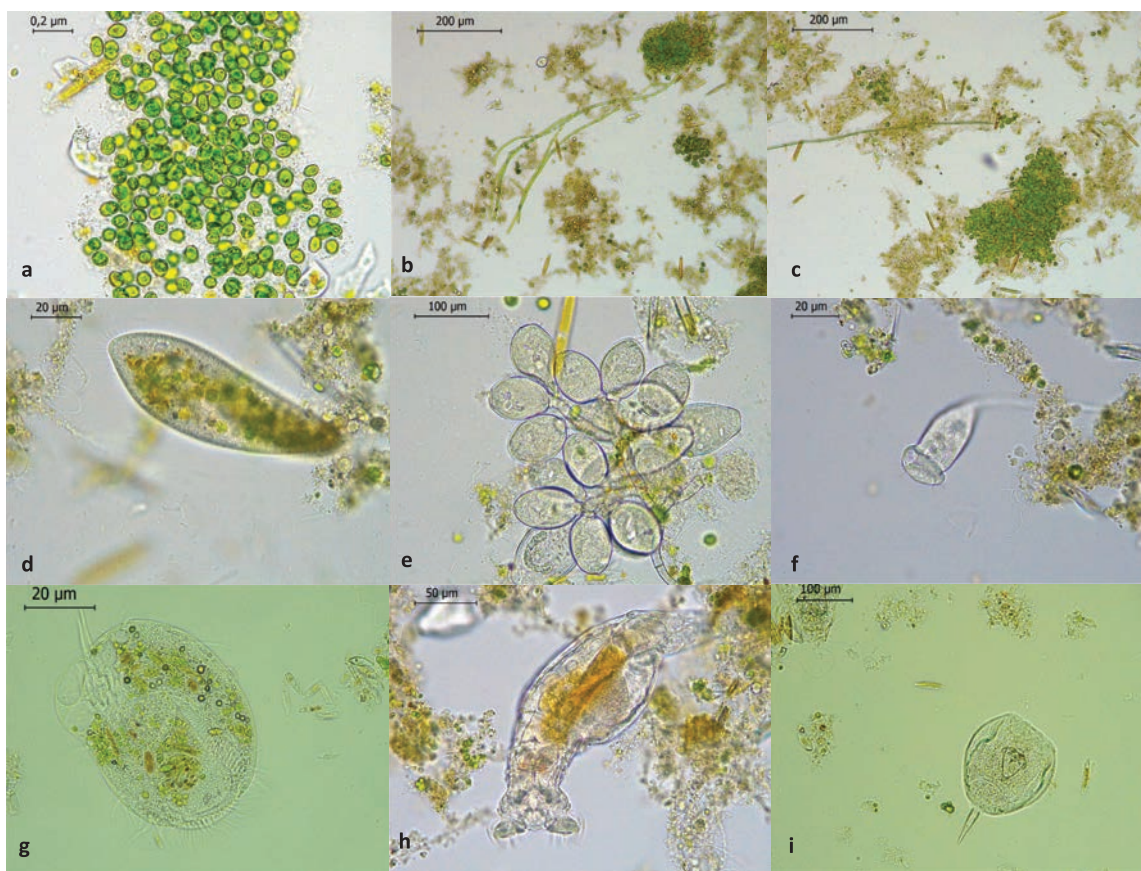

Fig. 7. Representative microscopic view of microalgae community and zooplankton grazers developed. (a) *Chlorella* sp. (R-MPBR 1); (b) *Chlorella* sp., *Chaetophora* sp. and *Nitzshia* sp. (R-MPBR 1); (c) *Chlorella* sp., *Oscillatoria* sp. and *Nitzshia* sp. (R-MPBR 1); (d) *Paramecium* sp. (R-MPBR 1), (e) *Epistylis* sp. (R-MPBR 1); (f) *Vorticella* sp. (R-MPBR 2); (g) *Euplotes* sp. (R-MPBR 2); (h) Bdelloid rotifer (R-MPBR 2) and (i) *Lecane* sp. (R-MPBR 2).

combination of species belonging to *Chlorella* genera embedded in dense flocs and diatoms (*Nitzschia* and *Navicula* genera) were observed in all conditions (Fig. 7a-c). Due to their versatility and tolerance to a wide range of environmental conditions, these species are commonly observed in microalgal consortia applied to wastewater treatment [11]. In fact, species of *Chlorella* developed at high COD concentration, probably due to its dual phototrophic and heterotrophic metabolism [52]. However, filamentous species of microalgae (*Chaetophora* sp.) and cyanobacteria (*Oscillatoria* sp.) were only found at higher CRL (Fig. 7b and c). Although less studied, *Chaetophora* sp. has been previously observed in MPBRs treating secondary effluents [53]. Moreover, species of *Oscillatoria* were reported as organic pollution-tolerant [54]. Additionally, the development of cyanobacteria can be related to the negligible dissolved oxygen concentration at higher CLR, as reported in a PBR fed with a synthetic wastewater operated at comparable CLR (44.5 g DOC·m^{-3}·d^{-1}), where simultaneous nitrification–denitrification process was also achieved [55].

Microscopic examination also showed several species of ciliates (*Vorticella* sp., *Epistylis* sp., *Paramecium* sp., *Euplotes* sp., *Aspidisca* sp., *Coleps* sp.) (representative species are showed in Fig. 7d-g). These protozoan microbes have been frequently recorded in biological wastewater treatments [56], and have a crucial role in bioflocculation by consuming dispersed bacteria and microalgae [36]. In this regard, free-swimming ciliates predominated in all conditions. Additionally, a change in species structure from attached to crawling ciliates (Fig. 7e-g) was observed with decreasing CLR, in accordance with previous studies [56]. Moreover, apart from testate amoebae and ciliates, metazoans were also observed. Large nematodes were found in all conditions. By contrast, rotifers (Bdelloidea Order and *Lecane* sp.) were only observed at low CLR (Fig. 7h and i). This situation was probably due to the oxygen depletion at high CLR, which has been identified as a significant factor limiting rotifers growth [57]. This seems to be related to the observed trend of decreasing biomass concentration and, particularly, suspended solids in supernatant, with decreasing CLR. Furthermore, it has been stated that bdelloid rotifers enhance bioflocculation due to secreted substances [58], which is consistent with what was observed in the present study. Hence, results showed that the density and diversity of grazers, mainly crawling ciliates and rotifers, seems to be related to better R-MPBR performance.

Conclusions

The rotating membrane photobioreactor with indigenous microalgae-bacteria consortia demonstrated its capability in the treatment of primary settled wastewater under photosynthetic oxygenation. It was observed that the carbon loading rates (CLR) determined the dissolved oxygen concentration, affecting nutrient removal, bioflocculation and membrane fouling. At the higher value (36.6 g DOC·m^{-3}·d^{-1}), dissolved inorganic nitrogen removal was significantly enhanced (81.2 ± 13.9 %), which was about 2.5–2.6 times of those obtained at lower CLRs, revealing a simultaneous nitrification–denitrification process. Decreasing CLR from 36.6 to 9.1 g DOC·m^{-3}·d^{-1} led to complete nitrification, increased particle size (D$_{(0.5)}$ from 61.9 to 92.8 μm) and decreased biopolymer clusters content (from 50.0 to 2.3 mg DOC·L^{-1}). Cake filtration model showed that the fouling was mainly caused by the supernatant fraction of the suspension, particularly by the biopolymer clusters content. Consequently, optimal filtration conditions were obtained at low to moderate CLRs ($\leq$11.4 g DOC·m^{-3}·d^{-1}), where a sustainable long-term operation at a filtration flux of 10 L·h^{-1}·m^{-2} was observed. Microalgae species belonging to the genera *Chlorella* and diatoms (*Nitzschia* and *Navicula* genera) were identified in all

conditions, while filamentous microalgae (*Chaetophora* sp.) and cyanobacteria (*Oscillatoria* sp.) were only found at high CLR. Meanwhile, crawling ciliates and rotifers were only observed at low CLR, which seems to be related to the lower biomass concentration and, particularly, suspended solids in the supernatant. The new proposed configuration effectively controlled membrane fouling, allowing to further process optimization.

CRediT authorship contribution statement

E. Segredo-Morales: Investigation, Data curation, Writing – original draft. **C. González-Martín:** Data curation, Writing – review & editing. **L. Vera:** Conceptualization, Funding acquisition, Project administration, Supervision, Writing – review & editing. **E. González:** Conceptualization, Methodology, Visualization, Funding acquisition, Project administration, Writing – review & editing.

Declaration of Competing Interest

The authors declare that they have no known competing financial interests or personal relationships that could have appeared to influence the work reported in this paper.

References

[1] , IWA Publishing, London, UK, 2022.
[2] A. Fallahi, F. Rezvani, H. Asgharnejad, E. Khorshidi, N. Hajinajaf, B. Higgins, Chemosphere 272 (2021), https://doi.org/10.1016/j.chemosphere.2021.129878.
[3] Y. Luo, P. Le-Clech, R.K. Henderson, Algal Res. 24 (2017) 425–437, https://doi.org/10.1016/j.algal.2016.10.026.
[4] Y. Liao, A. Bokhary, E. Maleki, B. Liao, Bioresour. Technol. 264 (2018) 343–358, https://doi.org/10.1016/j.biortech.2018.06.102.
[5] M. Zhang, L. Yao, E. Maleki, B.Q. Liao, H. Lin, Algal Res. 44 (2019), https://doi.org/10.1016/j.algal.2019.101686.
[6] J. González-Camejo, A. Jiménez-Benítez, M.V. Ruano, A. Robles, R. Barat, J. Ferrer, J. Environ. Manage. 245 (2019) 76–85, https://doi.org/10.1016/j.jenvman.2019.05.010.
[7] E. González, O. Díaz, I. Ruigómez, C.R. de Vera, L.E. Rodríguez-Gómez, J. Rodríguez-Sevilla, L. Vera, Bioresour. Technol. 239 (2017), https://doi.org/10.1016/j.biortech.2017.05.042.
[8] A.F. Novoa, L. Fortunato, Z.U. Rehman, T.O. Leiknes, Bioresour. Technol. 309 (2020), https://doi.org/10.1016/j.biortech.2020.123348.
[9] I. de Godos, V.A. Vargas, S. Blanco, M.C.G. González, R. Soto, P.A. García-Encina, E. Becares, R. Muñoz, Bioresour. Technol. 101 (2010) 5150–5158, https://doi.org/10.1016/j.biortech.2010.02.010.
[10] M. Zhang, K.T. Leung, H. Lin, B. Liao, J. Environ. Chem. Eng. 9 (2021), https://doi.org/10.1016/j.jece.2021.105500.
[11] A.L. Gonçalves, J.C.M. Pires, M. Simões, Algal Res. 24 (2017) 403–415, https://doi.org/10.1016/j.algal.2016.11.008.
[12] M. Wu, Y. Chen, H. Lin, L. Zhao, L. Shen, R. Li, Y. Xu, H. Hong, Y. He, Water Res. 181 (2020), https://doi.org/10.1016/j.watres.2020.115932.
[13] Y. Long, G. Yu, L. Dong, Y. Xu, H. Lin, Y. Deng, X. You, L. Yang, B.Q. Liao, Water Res. 189 (2021), https://doi.org/10.1016/j.watres.2020.116665.
[14] J. Teng, M. Zhang, K.T. Leung, J. Chen, H. Hong, H. Lin, B.Q. Liao, Water Res. 149 (2019) 477–487, https://doi.org/10.1016/j.watres.2018.11.043.
[15] S.L. Low, S.L. Ong, H.Y. Ng, Chem. Eng. J. 290 (2016) 91–102, https://doi.org/10.1016/j.cej.2016.01.005.

[16] A. Drews, J. Memb. Sci. 363 (2010) 1–28, https://doi.org/10.1016/j.memsci.2010.06.046.

[17] H. Lin, M. Zhang, F. Wang, F. Meng, B.Q. Liao, H. Hong, J. Chen, W. Gao, J. Memb. Sci. 460 (2014) 110–125, https://doi.org/10.1016/j.memsci.2014.02.034.

[18] H. Lin, W. Peng, M. Zhang, J. Chen, H. Hong, Y. Zhang, Desalination 314 (2013) 169–188, https://doi.org/10.1016/j.desal.2013.01.019.

[19] A.L.K. Sheng, M.R. Bilad, N.B. Osman, N. Arahman, J. Clean. Prod. 168 (2017) 708–715, https://doi.org/10.1016/j.jclepro.2017.09.083.

[20] , 1st editio., Metcalf & Eddy, 2007.

[21] T. Zsirai, H. Qiblawey, M.J. A-Marri, S. Judd, J. Memb. Sci. 516 (2016) 56–63, https://doi.org/10.1016/j.memsci.2016.06.010.

[22] I. Ruigómez, L. Vera, E. González, G. González, J. Rodríguez-Sevilla, J. Memb. Sci. 501 (2016), https://doi.org/10.1016/j.memsci.2015.12.011.

[23] I. Ruigómez, E. González, L. Rodríguez-Gómez, L. Vera, Chem. Eng. J. 436 (2022), https://doi.org/10.1016/j.cej.2022.135161.

[24] , 2nd Editio., IWA Publishing, London, UK, 2020.

[25] E. Segredo-Morales, E. González, C. González-Martín, L. Vera, J. Water Process Eng. 49 (2022), https://doi.org/10.1016/j.jwpe.2022.103200.

[26] L. Vera, E. González, O. Díaz, R. Sánchez, R. Bohorque, J. Rodríguez-Sevilla, J. Memb. Sci. 493 (2015) 8–18, https://doi.org/10.1016/j.memsci.2015.06.014.

[27] APHA, 21st ed., Washington, DC, USA, 2005.

[28] O. Díaz, E. González, L. Vera, J.J. Macías-Hernández, J. Rodríguez-Sevilla, J. Memb. Sci. 525 (2017) 368–377, https://doi.org/10.1016/j.memsci.2016.12.014.

[29] P. Madoni, Water Res. 28 (1994) 67–75, https://doi.org/10.1016/0043-1354(94)90120-1.

[30] , 1st Editio., CRC Press, Florida, USA, 1993.

[31] D. García, E. Posadas, S. Blanco, G. Acién, P. García-Encina, S. Bolado, R. Muñoz, Bioresour. Technol. 248 (2018) 120–126, https://doi.org/10.1016/j.biortech.2017.06.079.

[32] P.J. He, B. Mao, F. L-., L.M. Shao, D.J. Lee, J.S. Chang, Bioresour. Technol. 146 (2013) 562–568. https://doi.org/10.1016/j.biortech.2013.07.111

[33] P. Bohutskyi, D.C. Kligerman, N. Byers, L.K. Nasr, C. Cua, S. Chow, C. Su, Y. Tang, M.J. Betenbaugh, E.J. Bouwer, Algal Res. 19 (2016) 278–290, https://doi.org/10.1016/j.algal.2016.09.010.

[34] R. Mu, Y. Jia, G. Ma, L. Liu, K. Hao, F. Qi, Y. Shao, Water Environ. Res. 93 (2021) 1217–1230, https://doi.org/10.1002/wer.1496.

[35] Y. Luo, P. Le-Clech, R.K. Henderson, Water Res. 138 (2018) 169–180, https://doi.org/10.1016/j.watres.2018.03.050.

[36] V. Montemezzani, I.C. Duggan, I.D. Hogg, R.J. Craggs, Algal Res. 11 (2015) 211–226, https://doi.org/10.1016/j.algal.2015.06.024.

[37] J. González-Camejo, R. Barat, M.V. Ruano, A. Seco, J. Ferrer, Water Sci. Technol. 78 (2018) 195–206, https://doi.org/10.2166/wst.2018.259.

[38] P.E.A. Debiagi, M. Trinchera, A. Frassoldati, T. Faravelli, R. Vinu, E. Ranzi, J. Anal. Appl. Pyrolysis 128 (2017) 423–436, https://doi.org/10.1016/j.jaap.2017.08.007.

[39] M. Wang, H. Yang, S.J. Ergas, P. van der Steen, Water Res. 87 (2015) 38–48, https://doi.org/10.1016/j.watres.2015.09.016.

[40] N. Powell, A. Shilton, Y. Chisti, S. Pratt, Water Res. 43 (2009) 4207–4213, https://doi.org/10.1016/j.watres.2009.06.011.

[41] The European Parliament and the Council, Regulation (EU) 2020/741, Off. J. Eur. Union. 177/33 (2020) 32–55. https://eur-lex.europa.eu/legal-content/EN/TXT/PDF/?uri=CELEX:32020R0741&from=EN

[42] D.Y. Duygu, A.U. Udoh, T. Ozer, A. Akbulut, I. Erkaya, K. Yildiz, D. Guler, J. Biotechnol. 11 (2012) 3817–3824, https://doi.org/10.5897/ajb11.1863.

[43] C. Gai, Y. Zhang, W.T. Chen, P. Zhang, Y. Dong, Bioresour. Technol. 150 (2013) 139–148, https://doi.org/10.1016/j.biortech.2013.09.137.

[44] R.B. Carpio, Y. Zhang, C.T. Kuo, W.T. Chen, L.C. Schideman, R.L. de Leon, Algal Res. 38 (2019), https://doi.org/10.1016/j.algal.2018.101399.

[45] C.H.T. Vu, S.J. Chun, S.H. Seo, Y. Cui, C.Y. Ahn, H.M. Oh, Bioresour. Technol. 281 (2019) 56–65, https://doi.org/10.1016/j.biortech.2019.02.062.

[46] D.J. Barker, D.C. Stuckey, Water Res. 33 (1999) 3063–3082, https://doi.org/10.1016/S0043-1354(99)00022-6.

[47] A. Charfi, Y. Yang, J. Harmand, N. Ben Amar, M. Heran, A. Grasmick, J. Memb. Sci. 475 (2015) 156–166, https://doi.org/10.1016/j.memsci.2014.09.059.

[48] Seong-Hoon Yoon, 1st Editio, CRC Press, New York, 2016

[49] D. Jeison, J.B. van Lier, Sep. Purif. Technol. 56 (2007) 71–78, https://doi.org/10.1016/j.seppur.2007.01.022.

[50] T. Vroman, F. Beaume, V. Armanges, E. Gout, J.C. Remigy, J. Memb. Sci. 620 (2021), https://doi.org/10.1016/j.memsci.2020.118836.

[51] A. Sepehri, M.H. Sarrafzadeh, Chem. Eng. Process. - Process Intensif. 128 (2018) 10–18, https://doi.org/10.1016/j.cep.2018.04.006.

[52] E. Spennati, S. Mirizadeh, A.A. Casazza, C. Solisio, A. Converti, Algal Res. 60 (2021), https://doi.org/10.1016/j.algal.2021.102519.

[53] A. Solmaz, M. Işık, Biomass and Bioenergy 142 (2020), https://doi.org/10.1016/j.biombioe.2020.105809.

[54] H.O. Tighiri, E.A. Erkurt, Bioresour. Technol. 286 (2019), https://doi.org/10.1016/j.biortech.2019.121396.

[55] I. de Godos, V.A. Vargas, H.O. Guzmán, R. Soto, B. García, P.A. García, R. Muñoz, Water Res. 61 (2014) 77–85, https://doi.org/10.1016/j.watres.2014.04.050.

[56] P. Madoni, Ital. J. Zool. 78 (2011) 3–11, https://doi.org/10.1080/11250000903373797.

[57] B. Deruyck, K.H. Thi Nguyen, E. Decaestecker, K. Muylaert, Algal Res. 38 (2019), https://doi.org/10.1016/j.algal.2018.101398.

[58] G. Ding, X. Li, W. Lin, Y. Kimochi, R. Sudo, Water Res. 112 (2017) 208–216, https://doi.org/10.1016/j.watres.2017.01.044.